EVALUATION OF DEEP WASTE DISPOSAL COLD LAKE AREA, ALBERTA AND SASKATCHEWAN: LOCAL EFFECTS

OPEN FILE REPORT 1996 - 2A

Prepared by
Basin Analysis Group
Alberta Geological Survey
Alberta Research Council
(Project Manager: Dr. Stefan Bachu)

Project jointly funded by
Alberta Research Council
and
Alberta Environment

1988 - 08 - 31

DISCLAIMER

This report was prepared as an account of work sponsored by Alberta Environment and the Alberta Research Council (ARC). Every possible effort was made to ensure that the work conforms to accepted scientific practice. However, neither Alberta Environment nor te ARC, nor any of their employees, makes any warranty, expressed or implied, or assumes any legal liability or responsibility for the accuracy, completeness, or usefulness of any information, product, or process disclosed, or represents that its use would not infringe privately owned rights. Reference herein to any specific commercial product, process, or service by trade name, trademark, manufacturer, or otherwise, does not necessarily constitute or imply its endorsement, recommendation, or favoring by Alberta Environment or the ARC. The views and opinions of the authors expressed herein do not necessarily state or reflect those of Alberta Environment or the ARC.

Alberta Research Council
Edmonton, Alberta, Canada

1988-08-31

TABLE OF CONTENTS

	Page
Executive summary	x
Introduction	1
Analysis of the geothermal regime (Stefan Bachu)	3
Introduction	3
Effects of fluid flow on geothermal regime	4
Data capture and processing	6
Temperature distributions	11
Geothermal gradients	22
Conclusions	27
Geochemical effects (Ernie Perkins and Brian Hitchon)	28
Introduction	28
Selection of representative formation waters	31
Basal Cambrian aquifer	31
Beaverhill Lake aquifer system	31
McMurray aquifer	35
Clearwater aquifer	35
Mannville aquifer	35
Injection aquifer mineralogy	38
Basal Cambrian sandstone	38
Cooking Lake and Beaverhill Lake Formations	39
McMurray Formation	39
Clearwater Formation	41
Grand Rapids Formation	41
Correction of formation water analyses	41
Injection water composition	43
Calculation of potential water-rock interactions	45
Basal Cambrian aquifer	46
Cooking Lake aquifer	48
McMurray aquifer	51
Clearwater aquifer	55
Mannville aquifer	58
Conclusions	62

Page

Evaluation of hydrofracturing thresholds during sustained subsurface injection of liquid wastes (Claude M. Sauveplane) 67
Introduction 67
In situ stress regime and failure criteria 71
Classical evaluation of breakdown pressures 77
Discussion 78
Derivation of a new equation 79
Estimation of the required parameters and variables 81
Poisson's ratio 81
Overburden stress and initial pore pressure 84
Constants α and K 88
Critical hydraulic head buildups 88
Conclusions 93
Numerical simulation of local effects of injection (Stefan Bachu) 94
Introduction 94
Local hydraulic parameters 94
Numerical modelling 98
Local simulations of injection 103
Conclusions 113
Transport processes as a result of deep waste disposal (Stefan Bachu) 115
Conclusions 119
References 122

Figures

Figure 1 Temperature distribution at the top of the Precambrian (base of Basal Cambrian sandstone) (isotherms 5°C interval) 13

Figure 2 Temperature distribution in the Contact Rapids Formation (isotherms 5°C interval) 14

Page

Figure 3 Temperature distribution at the top of the Elk Point Group (isotherms 5°C interval) 15

Figure 4 Temperature distribution in the Beaverhill Lake Group (isotherms 5°C interval) 17

Figure 5 Temperature distribution in the Ireton Formation (isotherms 5°C interval) 18

Figure 6 Temperature distribution in the Grosmont Formation (isotherms 5°C interval) 19

Figure 7 Temperature distribution in the Camrose Tongue Dolomite (isotherms 5°C interval) 20

Figure 8 Temperature distribution in the Winterburn Group (isotherms 5°C interval) 21

Figure 9 Temperature distribution in the McMurray aquifer (isotherms 5°C interval) 23

Figure 10 Temperature distribution in the Mannville aquifer (isotherms 5°C interval) 24

Figure 11 Distribution of the integral geothermal gradient at the top of the Precambrian (base of Basal Cambrian sandstone) (contour intervals 2°C/km) 26

Figure 12 Injection sites, salinity isoconcentration contours (mg/L) and locations of representative formation waters for five injection aquifers in the Cold Lake region. A. Basal Cambrian aquifer; B. Beaverhill Lake aquifer system; C. McMurray aquifer; D. Clearwater aquifer; E. Mannville aquifer 32

Page

Figure 13 Saturation indices of selected minerals for mixtures of formation water and injection waters, Basal Cambrian aquifer 47

Figure 14 Saturation indices of selected minerals for mixtures of formation water and injection waters, Cooking Lake aquifer 49

Figure 15 Saturation indices of selected minerals for mixtures of formation water and injection waters, McMurray aquifer 52

Figure 16 Saturation indices of selected minerals for mixtures of formation water and injection waters, Clearwater aquifer 56

Figure 17 Saturation indices of selected minerals for mixtures of formation water and injection waters, Mannville aquifer 59

Figure 18 Total volume of minerals (cm^3) precipitated/dissolved per litre of injection fluid as a function of time 65

Figure 19 A. Schematic section of a hydraulic (vertical) fracture and B. example of pressure variation during hydrofracturing 69

Figure 20 Variation of fracturing gradient with depth 70

Figure 21 Example of acoustic and density logs used in this study 85

Page

Figure 22 Plan view of the finite element grids used for local simulation of effects of injection in the Cold Lake area: A. Lower Paleozoic, northern area; B. Post-Prairie, north-central area; C. Post-Prairie, south-central area; and D. Post-Prairie, southern area 99

Figure 23 Effects of injection in Lower Paleozoic (Cambrian) aquifers at Dome (10-5-67-4-W4) and BP (10-8-66-5-W4) sites: A. spread of hydraulic head buildup (the contour represents the 10 m isoline of hydraulic head increase after 30 a); B. hydraulic head increase at Dome site and C. hydraulic head increase at BP site 105

Figure 24 Effects of injection in Post-Prairie aquifers at Dome (10-5-67-4-W4) and BP (8-7-66-5-W4) sites: A. spread of hydraulic head buildup (the contour represents the 10 m isoline of hydraulic head increase after 30 a); B. hydraulic head increase at Dome site and C. hydraulic head increase at BP site 107

Figure 25 Hydraulic head increase at Suncor sites as a result of injection: A. in Cummings Member at 6-28-61-4-W4; and B. in Clearwater Formation at 5-28-61-4-W4 109

Figure 26 Spread of hydraulic head buildup at Suncor sites as a result of injection: A. in Cummings Member at 6-28-61-4-W4; and B. in Clearwater Formation at 5-28-61-4-W4 (the contour represents the 10 m isoline of hydraulic head increase after 30 a) 110

Figure 27 Hydraulic head increases at Murphy site (5-13-58-5-W4) as a result of injection in: A. Cooking Lake Formation; and B. Lower Grand Rapids Formation 111

Page

Figure 28 Spread of hydraulic head buildup at Murphy site (5-13-58-5-W4) as a result of injection in: A. Cooking Lake Formation; and B. Lower Grand Rapids Formation (the contour represents the 10 m isoline of hydraulic head increase after 30 a) 112

Figure 29 Effects of injection at Westmin site (11-1-55-5-W4) in Lloydminster sandstone: A. spread of hydraulic head buildup (the contour represents the 10 m isoline of hydraulic head increase after 30 a); and B. hydraulic head increase 114

Tables

Table 1 Chemical composition (mg/L), physical properties and production data for formation waters from injection aquifers, Cold Lake area, Alberta and Saskatchewan 30

Table 2 Comparison of major components in formation waters from the Basal Cambrian aquifer 33

Table 3 Comparison of major components in formation waters from the Beaverhill Lake aquifer system 34

Table 4 Comparison of major components in formation waters from the McMurray aquifer 36

Table 5 Comparison of major components in formation waters from the Clearwater aquifer 37

Table 6 Bulk mineral composition (%) of the Beaverhill Lake Formation, Cold Lake area, Alberta 40

Page

Table 7 Adjustments made to the formation water analyses in table 1 to account for missing values for Al and SiO_2, and lost of CO_2 44

Table 8 Range of variation of the tensile strength T (MPa), after Lama and Vutukuri (1978) 74

Table 9 Geomechanical parameters suggested by Dusseault and Simons (1982) for the Cold Lake area 83

Table 10 Estimation of Poisson's ratio for rocks at selected injection sites 86

Table 11 Estimation of overburden stress at selected injection sites 87

Table 12 Estimation of breakdown pressures (P_b in MPa) for rocks at selected injection sites 89

Table 13 Evaluation of fracturing thresholds using equation 33: maximum hydraulic head buildups to preclude fracturing (in equivalent freshwater head, m) 90

Table 14 An example of the use of breakdown pressure estimations BP/Lower Paleozoic aquifer system: Theis analytical model 92

Table 15 Local versus regional values of hydraulic parameters used in simulation of effects of injection in the Cold Lake area 97

Table 16 Characteristics of the finite element grids and CPU time used for local simulation of deep waste disposal at selected sites in the Cold Lake area 102

Page

Table 17 Projected injection rates for the period 1985-2015 at selected deep well disposal sites in the Cold Lake area, Alberta 104

EXECUTIVE SUMMARY

The local effects of injecting waste water from in situ oil sands pilots have been evaluated in a suite of cases representative of the injection aquifers and conditions of injection in the Cold Lake oil sands deposit, Alberta. Although water-rock reactions will take place between the injected fluid, formation water and minerals in the injection aquifer, only reactions involving quartz and calcite are significant. Based on calculations of the amounts of these minerals precipitated or dissolved, the most important change that should be made to waste water before injection is softening or the removal of carbon dioxide. Fracturing thresholds were evaluated by several methods and pressure buildups simulated at representative sites. These results show that vertical fracturing will occur close to the injection well at selected sites but overlying strata are expected to prevent propagation to the top of the bedrock. Thermal effects of injection are shown to be negligible, except close to the injection well, and the transport of contaminants contained in the injected water can be neglected once outside the radius of influence of each injection well -- generally of the order of a few hundred metres. Thus, as a general observation, the effects of injection of waste waters in the Cold Lake area are felt only in the near field, close to the injection well.

INTRODUCTION

This report represents the results of the second year of a two-year jointly funded contract between the Alberta Research Council and Alberta Environment. In the report of the results of the first year (Basin Analysis Group, 1987) the regional geology and natural fluid flow regime were described for an area defined as Tp 50-70, R 15 W3 Mer to R 17 W4 Mer (60 000 km^2), together with numerical simulation of the regional effects of deep waste injection at 27 sites using rates projected to the year 2015.

Not included in the above regional study was the geothermal regime in the study area, and this topic is, therefore, covered first in the present report. It completes the analysis of all natural regional aspects of the study area and provides the basis for evaluation of thermal effects of deep waste disposal.

The major part of this report is concerned with what may be termed local effects of injection. Specifically, they relate to potential water-rock interactions as these affect permeability reduction due to mineral precipitation, the onset of induced fractures during sustained injection of liquid wastes, and the pressure buildup adjacent to the injection well. The geochemical effects of deep waste disposal in the Cold Lake area are presented first, in order to evaluate possible changes in the porosity of the host aquifer as a result of mineral precipitation/dissolution. Significant changes in porosity affect the hydraulic characteristics (permeability, specific storage), therefore influencing the pressure buildups resulting from injection. Given that deep waste disposal is generally a safe operation except for possible vertical migration through conduits such as fractures in the confining formations, it is important to know at what stage in the injection process fracturing will be initiated. Thus, an evaluation of fracturing thresholds for rocks at sites in the Cold Lake area is presented before the numerical simulations of hydraulic head (pressure) buildups. A brief evaluation of transport processes related to deep waste disposal is presented at the end.

The local effects were evaluated at a limited number of sites which were chosen based on representativeness of the injection aquifer with respect to stratigraphy (Basal Cambrian, Cooking Lake, McMurray, Clearwater and Grand Rapids aquifers), areal distribution of wells injecting into these aquifers, data availability and, when appropriate, closeness to injection sites. Based on all these studies it is concluded that the injection of waste waters in the Cold Lake area has only limited local effects close to the injection wells.

ANALYSIS OF THE GEOTHERMAL REGIME

Stefan Bachu

INTRODUCTION

Information on the geothermal regime of the subsurface environment is important in hydrogeological and environmental studies for several reasons. The flow of fluids and heat flow are coupled phenomena, influencing each other in different ways; for example, the convective transport of heat can become important in the case of strong fluid flow driven by hydraulic head differences. On the other hand, natural convection of fluids can occur as a result of significant temperature differences. The thermal field also plays a significant role in water-rock processes, because many reactions are temperature dependent. Knowledge of the geothermal field is important when the variations in fluid density due to temperature changes are no longer negligible. Inclusion of the analysis of the geothermal regime in the study is motivated by the fact that it provides the baseline temperature distributions in the Phanerozoic succession and an assessment of the relative importance of heat transfer mechanisms, both of which are important in the evaluation of geochemical and transport processes associated with deep waste disposal in the Cold Lake area.

There is a basic difference between the flow of fluids and/or contaminants and the flow of heat in the subsurface environment. While the fluid can flow and thereby transport contaminants only through the porous and/or fractured space, the heat flows through both the solid and fluid phases of the porous medium. This aspect is very important when considering the effects of man's activity related to oil recovery or deep waste disposal. Strata separated from the exploitation/disposal sites by impervious layers can be affected by changes in the natural geothermal regime, as well as changes induced by heat sources created by human activity (for example, EOR steam chambers).

In a previous report (Basin Analysis Group, 1985), the geothermal regime in the Cold Lake area was analysed for a region in Alberta defined by Tp 55-69, R 1-17, W4. In this report the analysis is extended to a larger region, defined by Tp 50-70, R 15 W3 to R 17 W4. Moreover, the

previous analysis was based on 1244 temperature values from the ERCB Pool Data Base and 515 temperature values from drillstem test reports, while this study is based on 19 218 bottom hole temperature (BHT) values.

EFFECTS OF FLUID FLOW ON GEOTHERMAL REGIME

As pointed out by Bachu (1988), in the case of sedimentary basins with complex hydrostratigraphic successions it is difficult to assess the importance of convective versus conductive heat flow using numerical modelling, or using detailed quantitative descriptions of each parameter and variable involved. The problem is compounded in cases like the Cold Lake area, where the amount of the available data and information requires automatic processing. In such cases, dimensional analysis provides a tool for assessing the effects of fluid flow on the geothermal regime.

In the case of gravity-driven fluid flow in sedimentary basins, a measure of the intensity of convective heat transfer versus conductive heat transfer is given by the Peclet number. The Peclet number is not characterized by the existence of a critical value below which the system is conductive, as in the case of the critical Rayleigh number in natural convection. However, for Peclet numbers much less than unity, the system is conduction dominated, while for values significantly greater than unity the system is convection dominated. An order of magnitude of one for the Peclet number indicates a conductive-convective system.

The expression of the Peclet number is obtained by applying dimensional analysis to the equation of heat transfer in porous media (Bachu, 1985), and is given by:

$$Pe = \gamma v_o l / \kappa_m \qquad (1)$$

where:

$$(\rho c)_m = n\rho_f c_f + (1-n)\rho_s c_s, \qquad (2)$$

$$\lambda_m = n\lambda_f + (1-n)\lambda_s, \qquad (3)$$

and $\gamma = n\rho_f c_f / (\rho c)_m$ is the ratio of the heat capacity of the fluid

fraction to the heat capacity of the fluid saturated porous medium, n is porosity, ρ is density, c is specific heat, v_o is a characteristic velocity of fluid flow, l is a characteristic length to be discussed later, λ is thermal conductivity and $\kappa=\lambda/\rho c$ is thermal diffusivity. The subscripts f, s and m refer, respectively, to fluid, solid and saturated porous media. The expressions 2 and 3 are derived through analysis of heat transfer processes and averaging at the pore scale (Cheng, 1978; Bear and Bachmat, 1986).

In the computation of the values of the Peclet number it is crucial to define, properly, the characteristic velocity v_o and the characteristic length l. In the case of a complex hydrostratigraphic succession as in the Cold Lake area, it is not possible to define equivalent characteristic velocity and characteristic length for the entire sedimentary block. The analysis of the relative importance of convective versus conductive heat transfer has to be done by hydrostratigraphic units. In this case, the average thickness D of each unit is the characteristic length (Bachu, 1988), and the characteristic velocity is given by:

$$\bar{v}_o = K\bar{\nabla}H \qquad (4)$$

where K is the characteristic hydraulic conductivity and $\bar{\nabla}H$ is the average hydraulic gradient in each hydrostratigraphic unit.

Values for the thermal conductivity of the saturated porous medium were computed according to equation 3, using the following values for the thermal conductivity (W/m°C) of the rocks: sandstone 3.1, limestone 2.4, dolomite 3.1, shale 1.4, anhydrite 5.8, salt 5.7 (Beach, 1985). Standard values at the respective temperature were used for the thermal conductivity and heat capacity of the water (Haar et al., 1984). The geometric and hydraulic characteristics (gradient, conductivity, porosity) of various hydrostratigraphic units were defined based on the hydrogeological analysis of the Cold Lake area (Basin Analysis Group, 1987). For units where data were not available for all parameters needed in the dimensional analysis, characteristic values were inferred based on literature values (e.g. shale porosity), or similarity with adjacent strata (e.g. density of formation waters). For the purpose of this analysis the implicit error of these approximations is of no consequence

because here we are interested in the order of magnitude of Pe, and not in its exact value.

The values of Peclet number for the hydrostratigraphic units in the Cold Lake area vary between 10^{-5} (Clearwater shale) and 10^{-2} (Basal Cambrian sandstone), with values mostly around 10^{-3}. It follows that the convective heat transfer in the sedimentary rocks is negligible throughout the Cold Lake area and that the main mechanism for heat transport from the basement to the ground surface is thermal conduction through the sedimentary column. Therefore, in the absence of tectonic processes, the heat flux crossing the sedimentary basin produces a vertical temperature distribution and a geothermal gradient depending ultimately on the geometry and lithology of the strata (Bachu, 1985).

DATA CAPTURE AND PROCESSING

Bottomhole temperatures (BHT) obtained from routine geophysical logs comprise, for good reasons, a little used data set in geothermal and heat flow studies. The bottomhole temperatures required for heat flow determinations and reasonable interpretation of temperature data are unattainable with confidence from routine geophysical logs of the wells taken soon after the completion of drilling. Even if accurate temperature measurements are made (which generally is unnecessary in well logging), temperatures in and around wells are perturbed by the drilling process, principally by the circulation of mud at a temperature that differs from in situ conditions. There is seldom sufficient information to make accurate corrections for the perturbation. Thus, spatial variations in thermal gradients deduced from BHTs may be either spurious because of errors in the temperature data or, in the case of the gradients being fortuitously correct, the ambiguity in interpreting gradient patterns in terms of tectonic hydrologic processes, or conductivity variations will be unresolved.

Despite these difficulties it is possible, especially upon application of temperature corrections, to obtain useful information from BHT data (Chapman et al., 1984). Given the large number of wells in the Cold Lake area (approximately 14 800) it was decided to use BHTs as the primary source of information in the analysis of the geothermal pattern.

A total of 19 218 BHT values at 10 467 wells in the Cold Lake area were manually read from logs on microfiche (ERCB data) and entered into a computer data base. From these, 432 readings had to be rejected upon immediate examination because of missing or incorrect information (e.g. same time of measurement given for different temperature values recorded at the same depth in the same well).

Because of several factors, primarily fluid circulation before logging, BHTs from well logs are lower than static formation temperatures. The Horner technique is a method commonly used to correct these temperatures. The technique involves plotting the BHT in a given well versus time according to the equation:

$$T_B(t_e) = T_B(\infty) + A \log \left(\frac{t_c + t_e}{t_e}\right) \qquad (5)$$

where t_c is the circulation time, t_e is the time elapsed since circulation, and $T_B(t_e)$ is the time-dependent BHT. By plotting $\log[(t_c+t_e)/t_e]$ against T, one can estimate $T_B(\infty)$ the true formation temperature, as the ordinate intercept. Because the circulation time that corresponds to a BHT measurement is generally unknown, a standard circulation time of 4 h was used (Chapman et al., 1984). The correction for drilling disturbances requires multiple BHT measurements at successive times in order to extrapolate to an equilibrium temperature, as well as the elapsed time since cessation of circulation. Out of the 10 467 wells with BHT data, 3968 have only one temperature reading, with the elapsed time t_e given for only 2370 of them. Of the remaining 6499 wells, 4885 have only two BHT values, and the rest of the 1614 wells have between three and six temperature measurements.

By automatically performing the Horner analysis on the 6499 sets of multiple BHT measurements, 31 cases were differentiated as having a positive slope, 4659 cases with zero slope, and 1809 cases with negative slope. The cases with positive slope were rejected as bad data (the resulting formation temperature would be lower than the BHT measurements themselves). A zero slope means that the same temperature value is recorded for several log runs. Usually these cases are rejected also, based on the belief that a temperature was measured on one log run only

and simply recorded on later logs (Chapman et al., 1984). Obviously it is very difficult to check this assumption, and in the Cold Lake area that would mean the rejection of an additional 4659 cases. However, examination of the data in these cases revealed that the range of temperature variation is 20°C to 30°C for depths of up to 1200 m. This observation lead to the hypothesis that the temperature of the drilling fluid was very close to the formation temperature, therefore producing a quite small disturbance followed by a quick temperature recovery. In this case, the successive identical temperature readings could be correct, giving the actual formation temperature. Based on this hypothesis particular to the Cold Lake area, it was decided to consider the 4659 cases with zero Horner slope.

Out of the total of 6468 cases of multiple BHT measurements, only 534 have more than two values which are nonidentical at the same time. For these cases the formation temperature was automatically computed by linear regression techniques applied to the multiple BHT readings. The square of the correlation coefficient was used as a measure of the fit through the data points. Based on this analysis, an additional 39 cases were rejected because of poor data. Another 51 cases were rejected due to extrapolation errors, leaving a total of 6378 cases for which the formation temperature was derived from multiple BHT data.

Most of the time, the data at wells with insufficient information (single BHTs; or no elapsed time) are neglected (Chapman et al., 1984). However, by applying different types of corrections to the data at wells with missing information, all the available data can be used. Willett and Chapman (1986) apply a correction ΔT as a function of the depth z, or as a function of depth and elapsed time when t_e is given, to the data at wells with single BHT readings. The method used by them actually amounts to rewriting equation 5 as:

$$\Delta T \equiv T_B(\infty) - T_B(t_e) = F(z) \log \left(\frac{t_c + t_e}{t_e}\right) \qquad (6)$$

where F(z) is a polynomial in z. The dependence of temperature correction on depth is obvious. As the depth increases, the formation temperature is

higher, therefore the disturbance created by the drilling fluid is larger. On the other hand, as the elapsed time since cessation of circulation becomes larger the formation tends to recover its initial temperature and the correction ΔT becomes smaller. Assuming that at the surface ($z=0$) there is no temperature disturbance, ($\Delta T=0$), it follows that $F(z)$ is a polynomial without a free term.

A modified version of this type of correction with depth is used here in order to eliminate the first order dependence of ΔT on z. If $F(z)$ is an nth order polynomial in z, it can always be expressed as:

$$F(z) = (az+b)G(z) \tag{7}$$

where $G(z)$ is a polynomial of the order $n-2$. The expression $(az+b)$ is of the same type as the usual linear geothermal gradient giving the temperature $T(z)$ at the depth z, such that one can actually write:

$$F(z) = T(z)\ H(z) \tag{8}$$

where $H(z)$ is an $(n-2)$ order polynomial with no free term. Substituting relation 8 back into relation 6, a relative temperature correction can be written as:

$$\Delta T_r \equiv \frac{T_B(\infty)-T_B(t_e)}{T_B(t_e)} = H(z)\ \log\left(\frac{t_c+t_e}{t_e}\right) \tag{9}$$

The correction ΔT_r was computed individually for each BHT measurement of the 6378 cases with multiple BHT values for a total of 14 470 values.

Automatic examination of the relative corrections ΔT_r pointed to cases with excessive high corrections (e.g. more than 50%). These cases were checked again, revealing additional cases of data errors. A total of 6207 cases with 14 090 BHT values were left at the end of the data cleaning process. This set was first correlated with depth, to obtain an expression for the correction of 1598 cases with a single BHT value and no elapsed time given; and then with depth and with $\log[(t_c+t_e)/t_e]$ to obtain the correction for the 2370 cases with a single BHT value associated with the elapsed time since circulation.

The coefficients of the polynomial H(z) in z were computed by regression techniques. Because the degree n of the polynomial was unknown to start with, several cases were considered: m=1, m=2, m=3 and m=4. If all 14 090 data points are included in the analysis, a low coefficient of correlation (less than 0.45) is obtained for the dependence of ΔT_r on z. Closer examination of the whole data sample offered an obvious explanation for this low correlation. A total of 13 905 BHT values were recorded for depths less than 1 km, and only 185 values for depths between 1 km and 2 km. Given the fact that for most of the readings in the "shallower" depth (lower temperature range) the correction ΔT_r is zero, the shear number of these data concentrated at one end of the range skewed the statistics. A solution to this problem of the imbalance of the data sample is to divide all the data at depths less than 1 km into given depth intervals and replace the large number of individual values at each depth interval by their average for use in the regression analysis. The limits of each depth interval were determined by computing the correlation coefficient for different depth increments (in this case from 0.5 m to 300 m) for different degrees (m=1,2,3,4) of the polynomial H. The proper depth interval was determined to be Δz=1 m, and the best correlation was found for a third degree (m=3) polynomial in z (correlation coefficient 0.62). As a result, the bottom hole temperatures at wells in the Cold Lake area with single readings were corrected according to the relations:

$$\Delta T_r = 2.558z + 5.34z^2 - 4.035z^3 \qquad (10)$$

when the elapsed time t_e is not given; and

$$\Delta T_r = (9.505z+42.84z^2-27.459z^3)\ \log\left(\frac{t_c+t_e}{t_e}\right)+ (-17.172z-54.348z^2+35.080z^3)\ \log^2\left(\frac{t_c+t_e}{t_e}\right) \qquad (11)$$

when the elapsed time t_e is given.

In the above relations z is in km, t_c and t_e in h and ΔT_r in percent. It must be stressed here that these relations for temperature corrections are valid only in the Cold Lake area for depths of up to 1.8 km. These relations were applied to correct the 3968 single BHT data. When dealing

with such an amount of data covering a large area (60 000 km^2), a question arises if there is any areal dependence of the BHT corrections, besides the dependence on depth and on elapsed time. Such a dependence could be explained, among other things, by thermal conductivity variations due to lithological changes, or by significant areal variations in the heat flux. This possibility was checked using statistical methods, but no correlation was found between the relative correction of BHTs and their areal distribution.

As a result of this process of correcting BHTs, a total of 10 175 formation temperature data were retained and used to characterize the geothermal regime in the Cold Lake area.

TEMPERATURE DISTRIBUTIONS

The temperature distribution in the Cold Lake area is presented by hydrostratigraphic units, although it was shown previously that the convection of heat by the flow of formation waters is negligible. The range of temperature variation is between 12°C and 70°C, for depths ranging from 125 m at the top of the bedrock to 1997 m at the top of the Precambrian basement in the southwest of the study area. The distribution of BHTs in the stratigraphic/hydrostratigraphic succession is very uneven, with most of the data in the Mannville Group (5363), and at the top of the Paleozoic (4446), the explanation probably being that the drilling was stopped once past the Cretaceous oil sands and heavy oil deposits. However, 47 wells record BHTs at the top of the Precambrian, and there are some temperature measurements between the Precambrian and the Beaverhill Lake Group, to allow characterization of the thermal regime in this interval. As a general comment, the temperature distributions in each unit show a strong correlation with the stratigraphic dip (general temperature decrease updip from southwest to northeast), which points out again to a strong conductive regime. This is the direction also of the flow of formation waters in the regional system. If the fluid flow had been strong enough to convect heat significantly, then the temperatures would be higher downstream, toward the discharge areas in the northeast.

Measured temperatures at the top of the Precambrian (base of Basal Cambrian sandstone) vary between 24°C at a depth of 746 m in the northeast

and 70°C at a depth of 1997 m in the southwest. The temperatures decrease generally along the basement in an updip direction (figure 1). However, a few features alter this general pattern. In the southeast corner there is an increase in temperatures, as well as in the area around the Alberta-Saskatchewan border in the northern part of the area. In the western third of the area the isotherms are crowded, while in the rest, particularly in the centre, they are widely spaced. These features in the temperature distribution at the top of the Precambrian can be linked with changes in stratigraphy and lithology as it will be shown later.

There are only 10 BHT measurements in the Basal Cambrian sandstone, mainly in the north, and another 10 measurements in the rest of the thick Cambrian section, mainly in the Saskatchewan portion of the study area. Values range between 21°C and 47°C at depths between 867 m and 1501 m. Because these data are scattered over the entire thickness of the Cambrian, two-dimensional representation of the three-dimensional distribution was considered meaningless.

Nineteen BHTs were measured in the Saskatchewan portion of the Contact Rapids Formation (figure 2). The values range between 19°C and 33°C for depths between 350 m and 1045 m. There is a southwest to northeast decrease in temperature, although there is apparently a temperature increase from the centre toward the north (figure 2). This temperature anomaly is dictated by a single data point (Tp 65, R 22, W3), and is not seen in other temperature distributions higher up in the succession, therefore, this feature should be viewed critically.

Nine BHT values are recorded in the Prairie Formation, most of them clustered in the southwest corner of the study area. Temperatures range between 24°C at 566 m depth in the north-centre of the study area, and 40°C at 1325 m depth in the southwest.

Measured temperature values at the top of the Elk Point Group above the Prairie Formation vary between 20°C at 600 m in the northeast and 48°C at 1280 m in the southwest. The 26 values scattered over the entire area produce a temperature distribution correlated with the stratigraphic dip (figure 3).

The Beaverhill Lake aquifer system lies immediately above the Elk Point Group throughout the Cold Lake area. In the eastern two-thirds of the Cold Lake area the Beaverhill Lake Group is unconformably overlain by

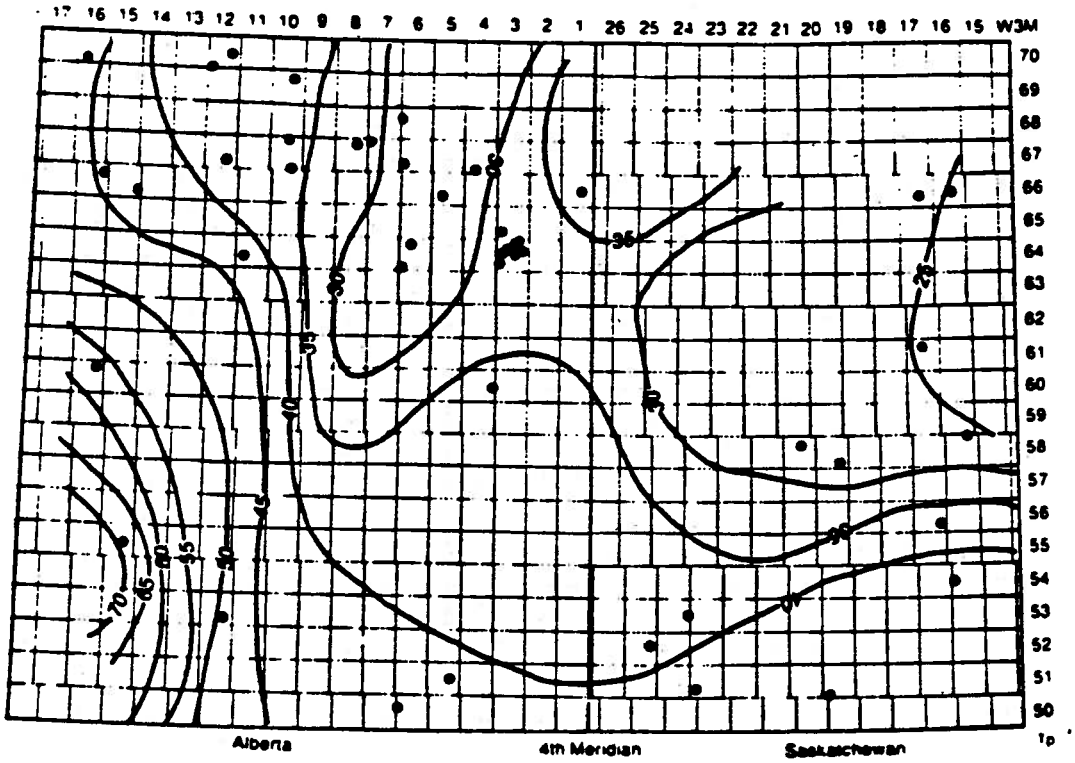

Figure 1 Temperature distribution at the top of the Precambrian (base of Basal Cambrian sandstone) (isotherms 5°C interval)

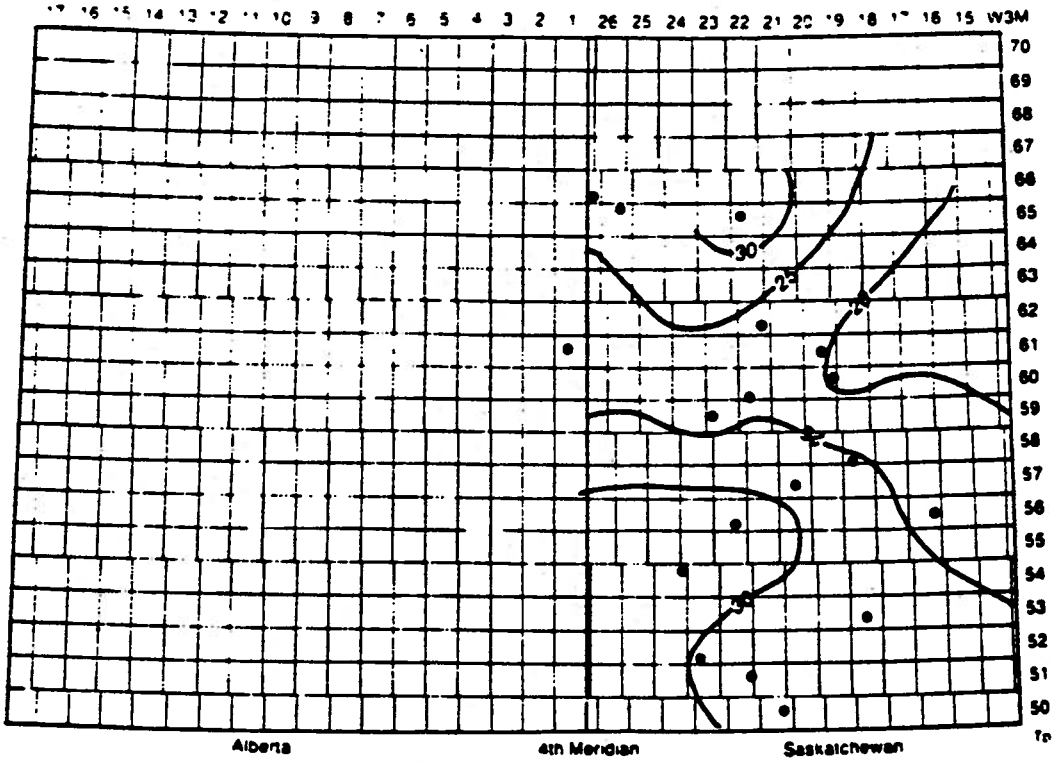

Figure 2 Temperature distribution in the Contact Rapids Formation (isotherms 5°C interval)

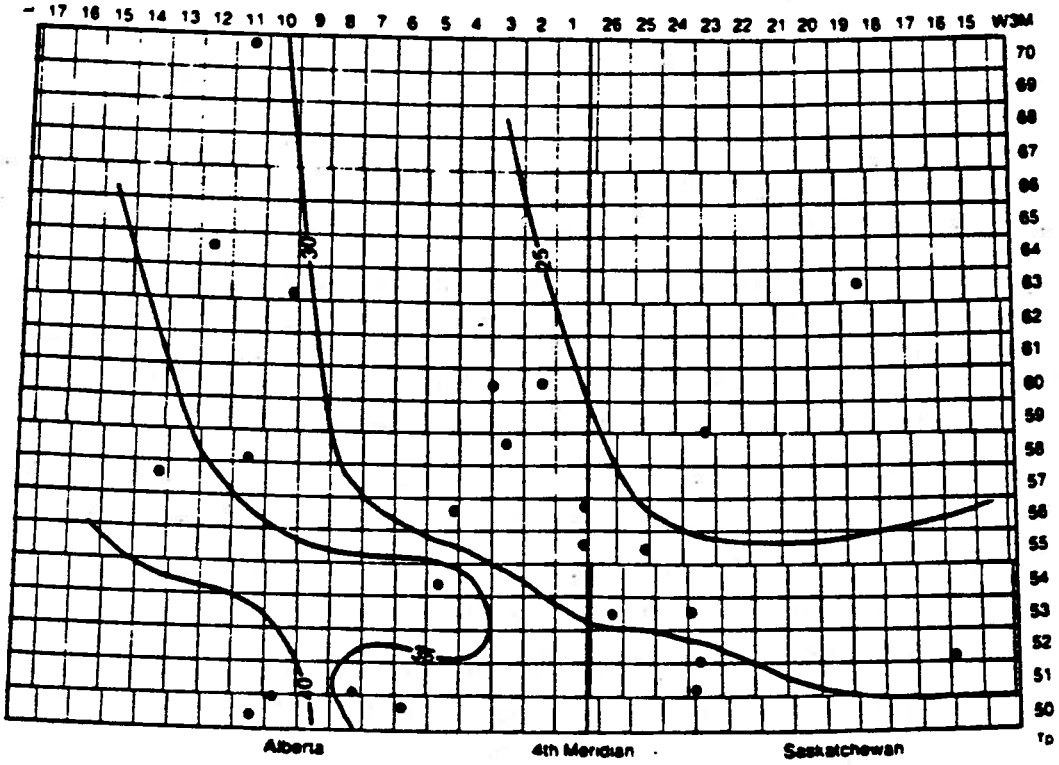

Figure 3 Temperature distribution at the top of the Elk Point Group (isotherms 5°C interval)

Cretaceous strata, whereas in the western third it is overlain conformably by the Ireton Formation. There are 1221 BHTs measured in this unit, most of them in the uppermost part of the group in the central third of the area, generally right underneath the oil sands and heavy oil deposits. Figure 4 presents isotherms generally at the top of the Beaverhill Lake Group. The northeast-southwest trend of increasing temperatures is again consistent with the dip of the unit, especially in the western third of the study area where the Beaverhill Lake Group is uneroded. In the eroded part, the 25°C isotherm follows the erosional features at the top of the Beaverhill Lake Group, the "higher" temperatures being in the subsurface valley which delineates the collapse of Beaverhill Lake Group strata due to salt dissolution of the underlying Prairie Formation.

In the western third of the study area, the Ireton Formation lies immediately below the Cretaceous, except for the northwest corner where the Grosmont reef platform replaces the Ireton shales. More than 3050 wells which penetrate the top of the Ireton Formation record BHTs, which range between 19°C at a depth of 190 m, and 45°C at a depth of 1230 m The general trend of temperature increase follows the stratigraphic dip from northeast to southwest (figure 5). Only in the northwest corner of the area is this pattern altered by the presence of Grosmont carbonates, which are characterized by higher thermal conductivity.

The temperatures in the Grosmont Formation (118 values) vary in a narrow range, most being around 25°C (figure 6). No clear trend with dip can be distinguished in this temperature distribution. The Camrose Tongue Dolomite in the southwest corner of the area, near the top of the Ireton Formation, shows a southwest-northeast decrease in temperature, along the dip of the unit (figure 7). This temperature distribution is defined by 131 BHT values. Finally, the Winterburn Group present only along the western edge of the study area at the top of the Paleozoic succession, shows a dip increase in temperature (figure 8) consistent with the general pattern.

Cretaceous rocks have a shallower dip toward southwest than the underlying Paleozoic strata, and as a result the isotherms in the Cretaceous units do not show such a clear similarity with the dip as do the deeper units. Moreover, the porous medium is less homogeneous with respect to the solid matrix, fluid content and saturation, therefore

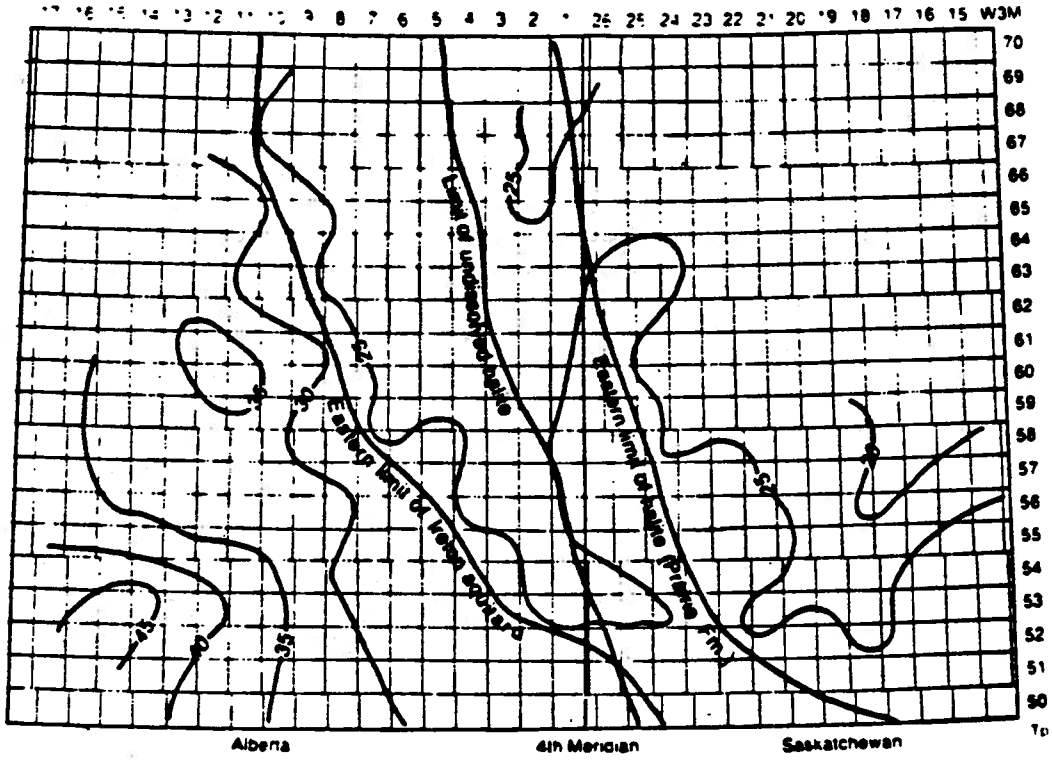

Figure 4 Temperature distribution in the Beaverhill Lake Group (isotherms 5°C interval)

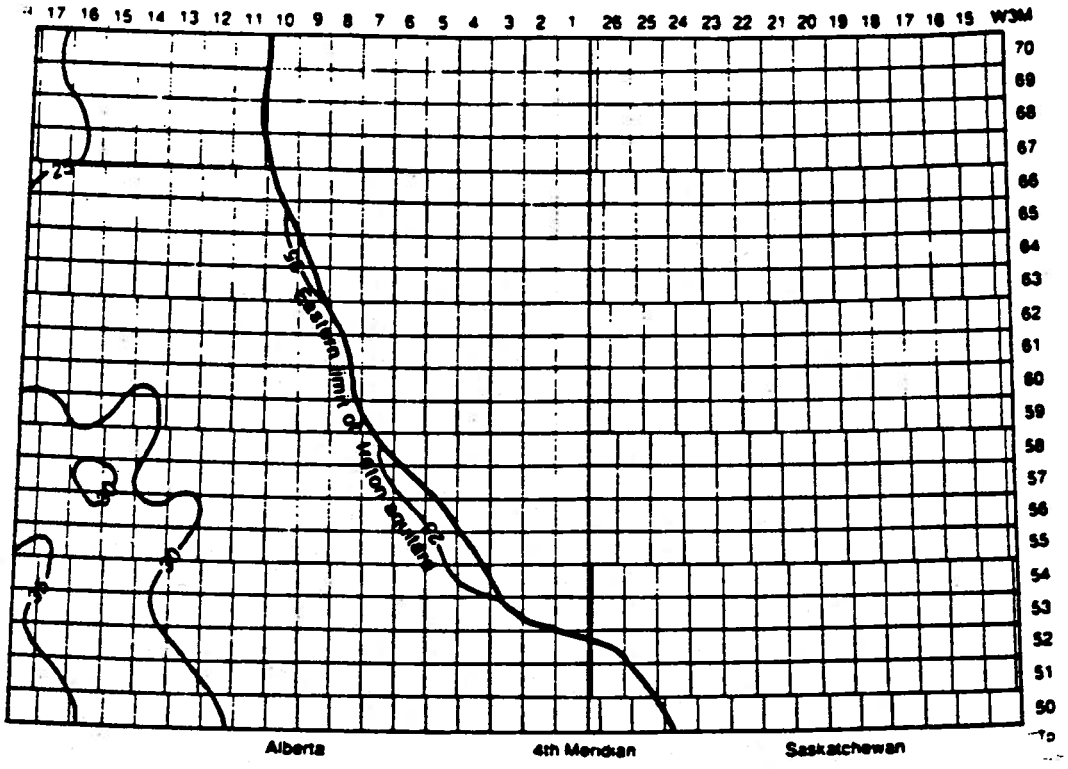

Figure 5 Temperature distribution in the Ireton Formation (isotherms 5°C interval)

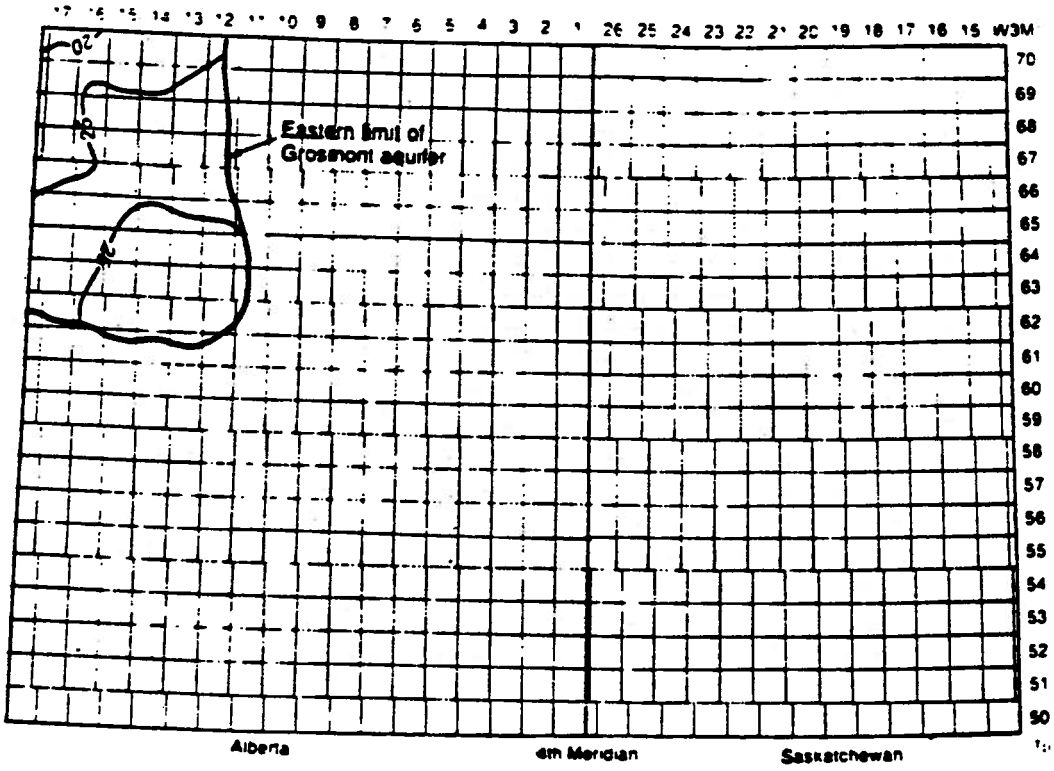

Figure 6 Temperature distribution in the Grosmont Formation (isotherms 5°C interval)

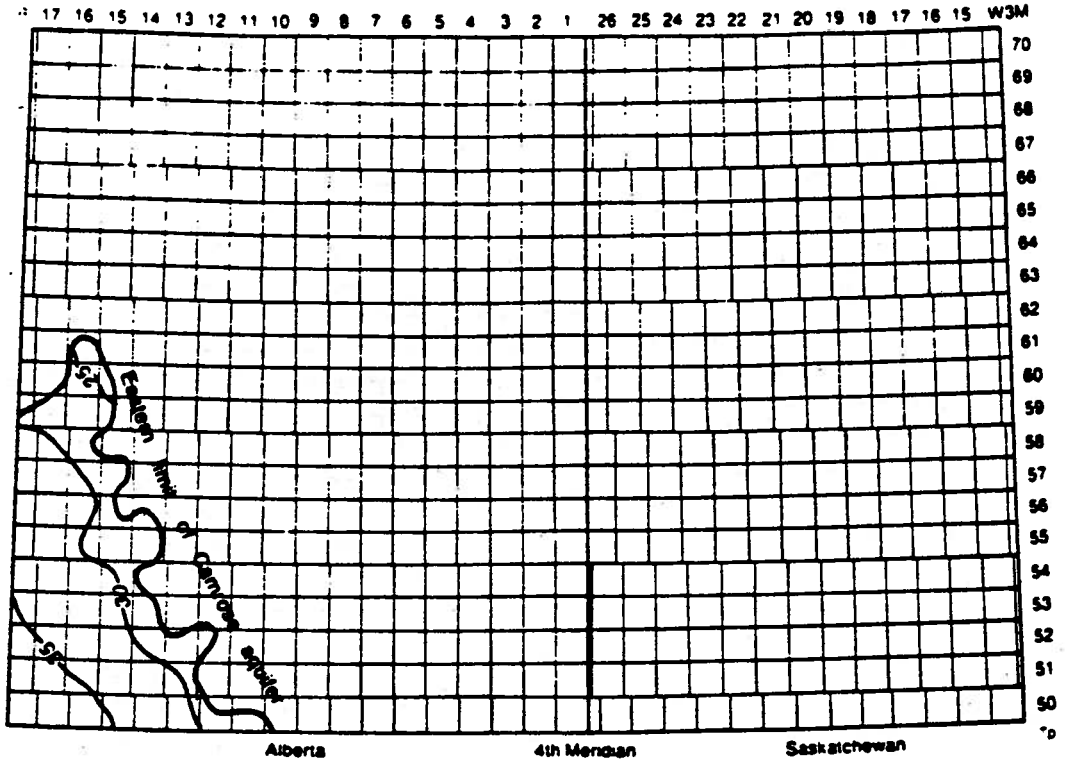

Figure 7 Temperature distribution in the Camrose Tongue Dolomite (isotherms 5°C interval)

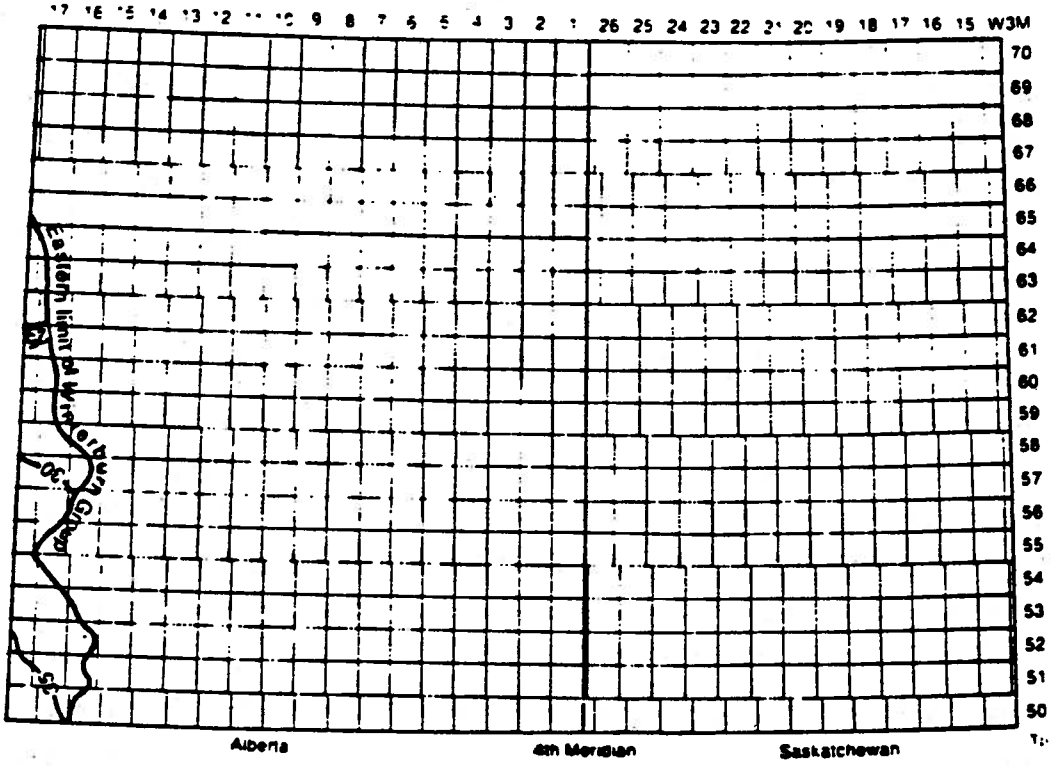

Figure 8 Temperature distribution in the Winterburn Group (isotherms 5°C interval)

influencing the temperature distributions through local variations in thermal conductivity.

The measured temperatures in the McMurray aquifer (745 values) vary between 15°C at a depth of 430 m and 36°C at a depth of 720 m. A general trend can be discerned in the temperature distribution, with decreasing values from southwest to northeast (figure 9).

In the lower Clearwater shale, in the Clearwater sandstone and in the upper Clearwater shale there are 46, 71 and 65 BHT values, respectively, but they are mostly so clustered that no trend analysis could be performed. The BHTs vary in range between 18°C and 31°C, for depths between 400 m and 715 m.

Finally, 4436 BHT values characterize the Upper Mannville, varying between 12°C at 275 m and 40°C at 1025 m. The temperature distribution shows a general decrease updip (figure 10), with some variations around 25°C in the large band between the southwest and northeast corners. It is believed that this pattern is caused by thermal conductivity variations due to the existence of oil sands and heavy oil deposits.

Only 61 temperature measurements are recorded between the top of the Mannville Group and the top of the bedrock, with values ranging from 15°C at 133 m depth to 34°C at 770 m depth in the southwest. Because these values were measured at different depths in the thick Colorado Group, no two-dimensional trend analysis could be performed. Another ten temperature values were measured right at the top of the bedrock, at depths varying between 125 m and 270 m, with a distribution precluding a meaningful analysis.

GEOTHERMAL GRADIENTS

Although there are a great many BHT measurements in the study area, they are unevenly distributed both areally and with depth, such that it is very difficult to define individual geothermal gradients characterizing the stratigraphic or hydrostratigraphic units. However, the heat flow in the Cold Lake area can be characterized by the distribution of the integral geothermal gradient $\bar{G}$, which is defined (Bachu, 1988) as the weighted average of the individual geothermal gradients over the sedimentary column above the Precambrian basement:

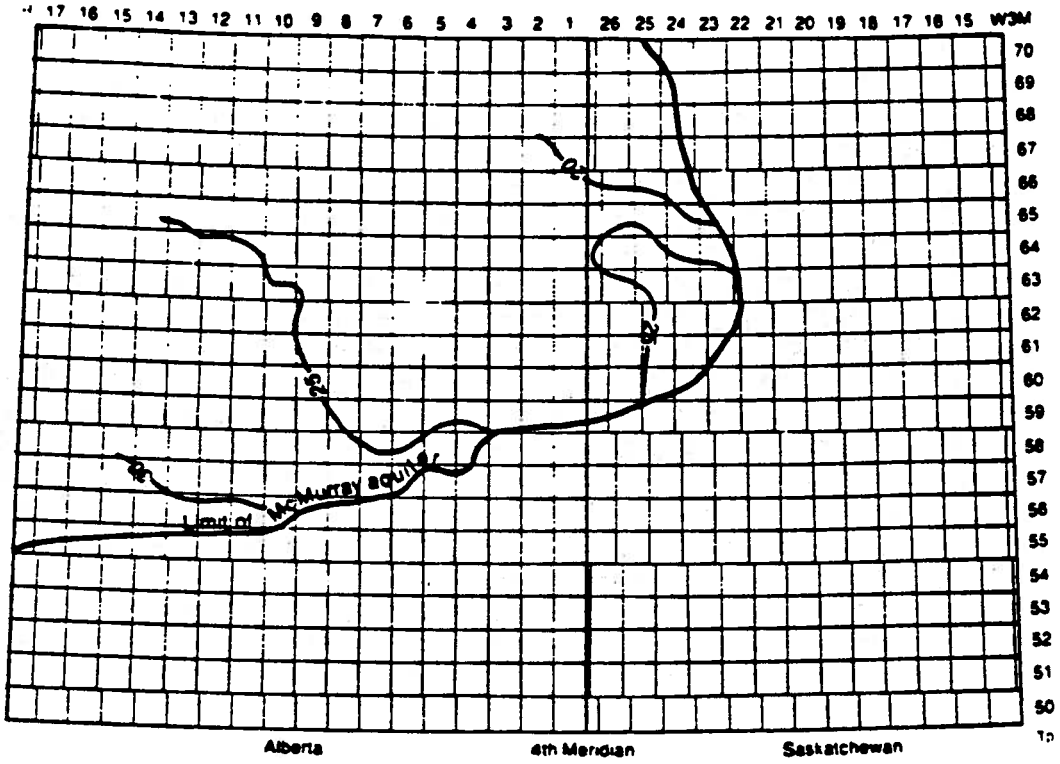

Figure 9 Temperature distribution in the McMurray aquifer (isotherms 5°C interval)

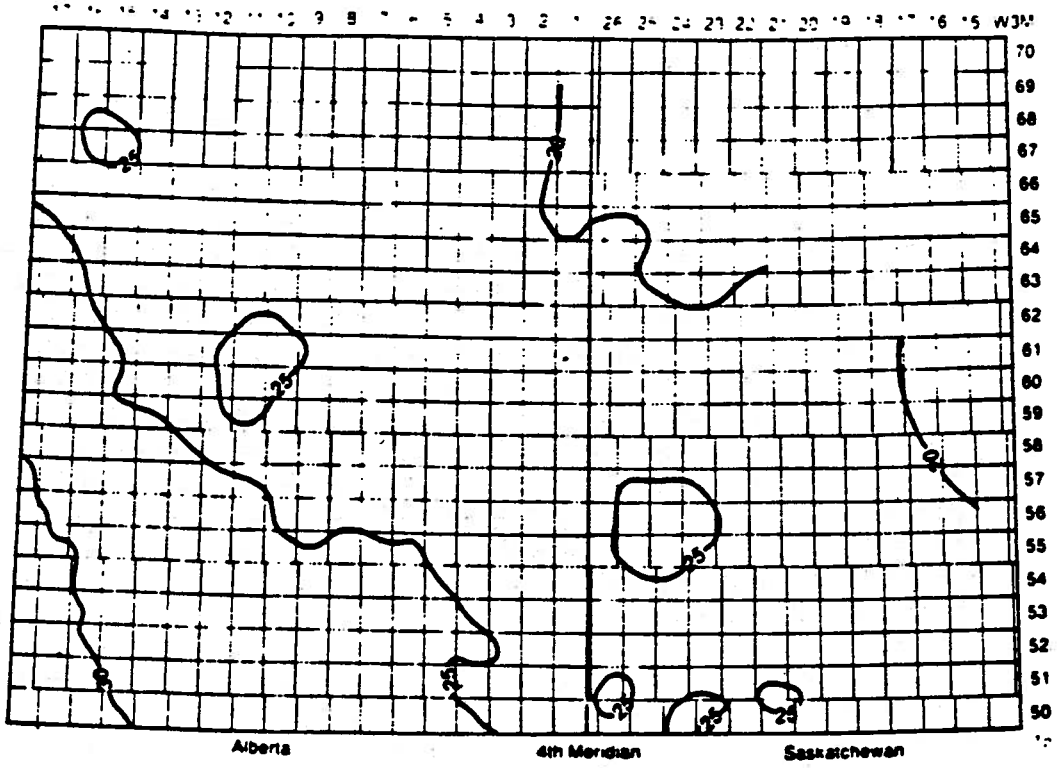

Figure 10 Temperature distribution in the Mannville aquifer (isotherms 5°C interval)

$$\bar{G} = (T_b - T_o)/Z \equiv Q/\bar{\lambda} \qquad (12)$$

where T_b and T_o are the temperatures at the bottom and top of the sedimentary column, Z is the thickness of the sediments, Q is the heat flux and $\bar{\lambda}$ is the average thermal conductivity of the sediments. The integral geothermal gradient is computed as the temperature difference between bottom and top versus the total depth. The temperature of 6°C at the top is given by the mean annual temperature, considering a ground temperature of 0°C whenever air temperatures dip below zero (Environment Canada, 1982). Figure 11 shows the distribution of the integral geothermal gradient in the Cold Lake area. In the absence of convective effects due to the flow of formation waters, and assuming a constant heat flux at the bottom of the sedimentary rocks (Bachu, 1988), the distribution of the integral geothermal gradients is controlled by the geometry and lithology of the strata above the basement (Bachu, 1985). Indeed, the distribution of the integral geothermal gradients (figure 11) and of temperatures at the top of the Precambrian (base of Basal Cambrian sandstone; figure 1) can be explained in terms of stratigraphic and lithological variations in the sedimentary rocks.

For a given constant heat flux at the top of the Precambrian basement, the integral geothermal gradient is dependent on the average thermal conductivity of the rocks. The average thermal conductivity is lowest in the southwest corner of the Cold Lake area due to the highest ratio of shale in the sedimentary column (up to 200 m of uneroded Ireton Formation present), with resulting "high" geothermal gradients (up to 30°C/km). The average thermal conductivity increases eastward and northward due to the thinning of Ireton shales through erosion at the Pre-Cretaceous unconformity, resulting in lower integral geothermal gradients. The effect of the Grosmont Formation carbonates replacing Ireton shales explains the pattern in the northwest corner of the study area. The average thermal conductivity is highest in the central part of the Cold Lake area, due to the absence of Ireton shales (lowest thermal conductivity) and presence of salt and anhydrite (highest thermal conductivity) in the Prairie, Cold Lake and Lotsberg Formations. As a result, the integral geothermal gradient is lowest in this area (as low as 17°C/km). The geothermal gradient increases again toward the northeast,

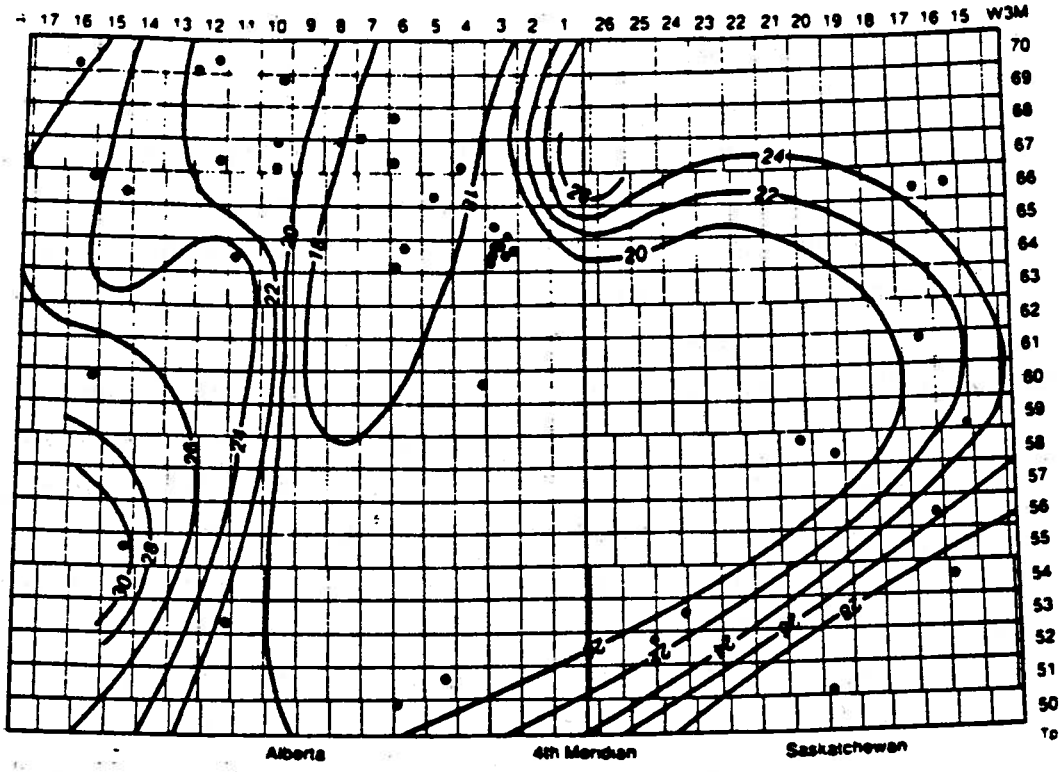

Figure 11 Distribution of the integral geothermal gradient at the top of the Precambrian (base of Basal Cambrian sandstone) (contour intervals 2°C/km)

which can be explained by a decrease in the average thermal conductivity due to salt dissolution (Prairie Formation). However, the increase is somehow higher than expected. Because this feature is determined by a single data point (Tp 66, R 1 W4 Mer), more information is needed to verify and explain this trend. The average geothermal conductivity decreases again at the eastern margin and in the southeast corner of the area due to the absence of halite and anhydrite formations (Prairie, Cold Lake, Lotsberg). As a result, higher integral geothermal gradients are present along the eastern edge and in the southeast corner of the Cold Lake area (up to 29°C/km). The variations in the average thermal conductivity of the sedimentary column explain also the temperature distribution at the top of the Precambrian (figure 1). Given the fact that the ground relief is relatively flat in the Cold Lake area, the isotherms at the top of the Precambrian should show the same southwest-northeast regular distribution as the structure contours (Basin Analysis Group, 1987, figure 3A), if it were not for these changes in thermal conductivity due to lithological changes. The temperature at the bottom of the sedimentary rocks has to vary according to the variations in thermal conductivity in order to accommodate the heat flux coming from the bottom and being transferred to the atmosphere at a constant-temperature top. For this reason there is a certain similarity between the distributions of temperatures and integral geothermal gradients at the top of the Precambrian basement (figures 1 and 11, respectively).

CONCLUSIONS

The heat transfer in the Phanerozoic sediments in the Cold Lake area is a conduction dominated process, due to the very low permeability of the rocks. As a result, the natural geothermal regime (temperature distribution) is governed by the lithology of the various units in the stratigraphic succession. The implication for deep waste disposal and EOR activity is that heat introduced by artificial sources, such as steam or warm water, will dissipate basically through conduction, unless there is fast movement of warm (hot) fluids through very permeable conduits such as fractures, microannuli and channels in the cement sheath resulting from poor well completion practices, and improperly abandoned wells.

GEOCHEMICAL EFFECTS

Ernie Perkins and Brian Hitchon

INTRODUCTION

Geochemical effects of deep waste disposal are important on a local scale due to the potential for mineral precipitation or solution as a result of water-rock interaction between the injected waters and the formation fluids and rocks. The hydraulic characteristics of the rocks around the injection zone may be modified because of these geochemical effects, thus influencing the movement of injected water and the pressure buildup during the lifetime of the operation. The potential for mineral precipitation and solution can be determined by a variety of techniques which range from laboratory experiments on representative cores using actual injection waters to computer codes designed to determine individual mineral saturations for given mixtures of injection waters and formation waters. The latter route was chosen in this study.

Water-rock interaction computer codes generally require, as input, complete analyses of both the injection water and the formation water, together with knowledge of the mineralogy of the injection aquifer. Most are designed to calculate reactions at equilibrium conditions and kinetic effects are usually not evaluated. However, based on knowledge of the rates of reaction for some mineral transformations the possibility of precipitation or solution taking place can be indicated.

With respect to potential water-rock interaction during deep waste injection in the Cold Lake region there were three major limiting factors, namely: (1) the lack of complete analyses of formation waters at any of the injection sites, (2) only restricted information on the composition of the injected waters, which vary in composition as in situ recovery processes evolve, and (3) limited data on the mineralogy of the injection aquifers at the injection sites. Each of these limiting factors was addressed and evaluated prior to determining potential reactions resulting from injection.

The computer code SOLMNEQF (Aggarwal et al., 1986) requires detailed analyses of the waters under investigation, and specifically of both

formation waters and injected waters if interactions between the injected waters and the disposal aquifer (rock matrix plus formation water) are to be modelled. Information on the composition of the injected waters is given by Gunter et al. (1986), and the mineralogy of the rock matrix of selected aquifers is provided elsewhere in this report. All formation water analyses used in the regional evaluation of the hydrogeology of the Cold Lake area (Basin Analysis Group, 1987) originated from the files of the Energy Resources Conservation Board (ERCB). The limitations of these analyses are described in Hitchon et al. (1987) and the methods of data processing in Bachu et al. (1987). None of these analyses are suitable for water-rock interaction studies, for a variety of reasons.

In the early 1970s, a suite of about one thousand formation waters were collected across Alberta through a cooperative program with the ERCB. All were from drillstem tests of then currently drilled wells, and the produced formation waters were subsampled for the Alberta Research Council. In addition to selected major element determinations by the ERCB, the samples were sent to the Alberta Research Council, filtered and preserved, and selected minor and trace elements determined by a variety of techniques. Bearing in mind the vicissitudes of drillstem tests and the need for appropriate field procedures if reliable formation water composition is to be achieved, it is believed that the analyses resulting from the cooperative program with the ERCB are reasonably representative of in situ formation water composition; certainly, they are more representative than conventional standard analyses but not as representative as if sampled and preserved in the field. With this caveat in mind the analysis file from the cooperative program was searched for data from the Cold Lake study area. A selection was made of data from appropriate injection aquifers and areally as close as possible to, or representative of the major formation water composition at, the 27 injection sites in the model area.

In the following sections of the report each injection aquifer will be considered in sequence and, if appropriate formation water analyses are available, the analytical data are presented in table 1.

Table 1.
Chemical composition (mg/L), physical properties and production data for formation waters from injection aquifers, Cold Lake area, Alberta and Saskatchewan

Sample number	-	W13-RCA-765	RCAH 72-475A	RCAH 51-275A	RCAH 1-875B
Stratigraphic Unit	Basal Cambrian	Cooking Lake Fm.	McMurray Fm.	Clearwater Fm.	Glauconitic Ss.
Location	12-30-49-27-W3	9-29-57-19-W4	11-12-67-16-W4	11-26-63-12-W4	11-20-55-6-W4
Depth (m)	1634-1685	1120.1-1122.0	534.6-538.3	527.9-530.4	615.7-629.7
Source	Injectivity test	Wellhead, perf.	DST 1	DST 5	DST 1
Recovery	-	Pumping	27.4 m SW, gas 1.23 MCF/D	163 m SW, 18.3 m m SW	61 m SW, gas 1.043 MMcf/d
Li	-	20	4.4	7.6	6.2
Na	112 645	47 100	10 600	10 900	19 000
K	1 289	840	90	117	84
Mg	1220	2980	222	322	975
Ca	1920	8440	450	484	1430
Sr	-	300	31	41	112
Ba	0.8	-	11	10	35
Cu	2.3	0.49	*	*	*
Ag	-	-	0.3	*	0.3
Zn	0.84	2.12	*	*	5.8
Pb	0.94	-	0.6	0.4	0.3
Fe	29	0.19	0.2	*	0.2
Mn	1.2	0.7	*	*	0.2
Al	-	-	*	0.01	*
H_2AsO_3	0.008	-	*	2	1.3
H_3BO_3	-	189	64	58	58
PO_4	-	-	3.7	5.5	2.3
NH_3	-	-	-	-	41
SiO_2	29.7	-	8.9	14	2.9
F	-	-	1.1	1.7	0.13
Cl	188 000	99 900	16 900	20 600	35 500
Br	-	296	52	55	120
I	-	15	8	9	11
SO_4	3 180	790	17	47	37
HCO_3	80	139	942	760	220
CO_3	0.0	0.0	0.0	0.0	0.0
Cations (anal., meq/L)	5130.0 (25°C)	2766.3 (25°C)	505.6 (25°C)	529.9 (25°C)	982.8 (25°C)
Anions (anal., meq/L)	5370.3 (25°C)	2836.5 (25°C)	492.7 (25°C)	594.8 (25°C)	1005.8 (25°C)
Cations (calc., meq/L)	4529.9 (30°C)	2568.1 (40°C)	491.3 (30°C)	513.7 (22.8°C)	948.9 (28.2°C)
Anions (calc., meq/L)	4741.5 (30°C)	2634.1 (40°C)	477.5 (30°C)	578.6 (22.8°C)	969.4 (28.2°C)
TDS (calc.)	308 399	161 205 (40°C)	29 306 (30°C)	33 385 (22.8°C)	57 500 (28.2°C)
TDS (110°C)	-	178 700	-	33 300	60 300
TDS (ignition)	-	153 600	-	31 580	55 370
pH (laboratory)	6.2 (25°C)	6.78 (25°C)	7.3 (25°C)	7.9 (20°C)	7.61 (25°C)
pH (calc.)	6.18 (30°C)	6.66 (40°C)	7.26 (30°C)	7.86 (22.8°C)	7.45 (28.2°C)
Density	1.286 (15°C)	1.1095 (25°C)	1.0212 (15.56°C)	1.026 (15.56°C)	1.0346 (15.56°C)
Refractive Index	1.373 (25°C)	1.3595 (25°C)	1.3372 (21°C)	1.3388 (25°C)	1.3430 (25°C)
Resistivity (ohm m) (25°C)	0.031	0.0551	0.241	0.195	-

- = not determined
* = below detection

SELECTION OF REPRESENTATIVE FORMATION WATERS

Basal Cambrian Aquifer

Detailed analyses of formation waters are not available in the Cold Lake study area. The Basin Analysis Group has carried out contract work for Husky Oil Operations Ltd. at their Bi-provincial Upgrader site near Lloydminster, immediately south of the study area. With the permission of the client, an analysis of formation water from the Basal Cambrian Table 1 sandstone at well Husky Lloyd SWD B12-30-49-27-W3M is given in table 1. Based on extrapolation of the formation water composition maps (33 to 39) in the Atlas accompanying the report by the Basin Analysis Group (1987), the analysis from the Husky well is close to the regional averages for all components mapped (figure 12A, table 2). Comparison with the local averages for mapped components near the four injection sites (table 2), shows that the formation waters near the injection sites have lower salinities, and correspondingly lower contents of Cl, Ca and Mg, but increased amounts of HCO_3 and, especially, SO_4.

Beaverhill Lake Aquifer System

Detailed analyses of formation waters in the Beaverhill Lake aquifer system are not available in the Cold Lake study area. The nearest detailed analysis is from the Skaro field, which produces oil from the Cooking Lake Formation at 9-29-57-19-W4. The analysis is given in table 1 (from Hitchon et al., 1971). Injection sites for disposal into the Cooking Lake Formation of the Beaverhill Lake aquifer system lie in a general N-S line, with salinities of the formation waters ranging from less than 40 000 mg/L to close to 125 000 mg/L (figure 12B, table 3). Based on the formation water composition maps (60 to 66) in the Atlas accompanying the report by the Basin Analysis Group (1987) the corresponding values for other major components are given in table 3. From the point of view of modelling water-rock interaction the two injection sites at Tp 56 R 6 and Tp 55 R 6 were selected for study because the extrapolated regional compositional trends in this area most closely compare with the analysis from the Skaro field.

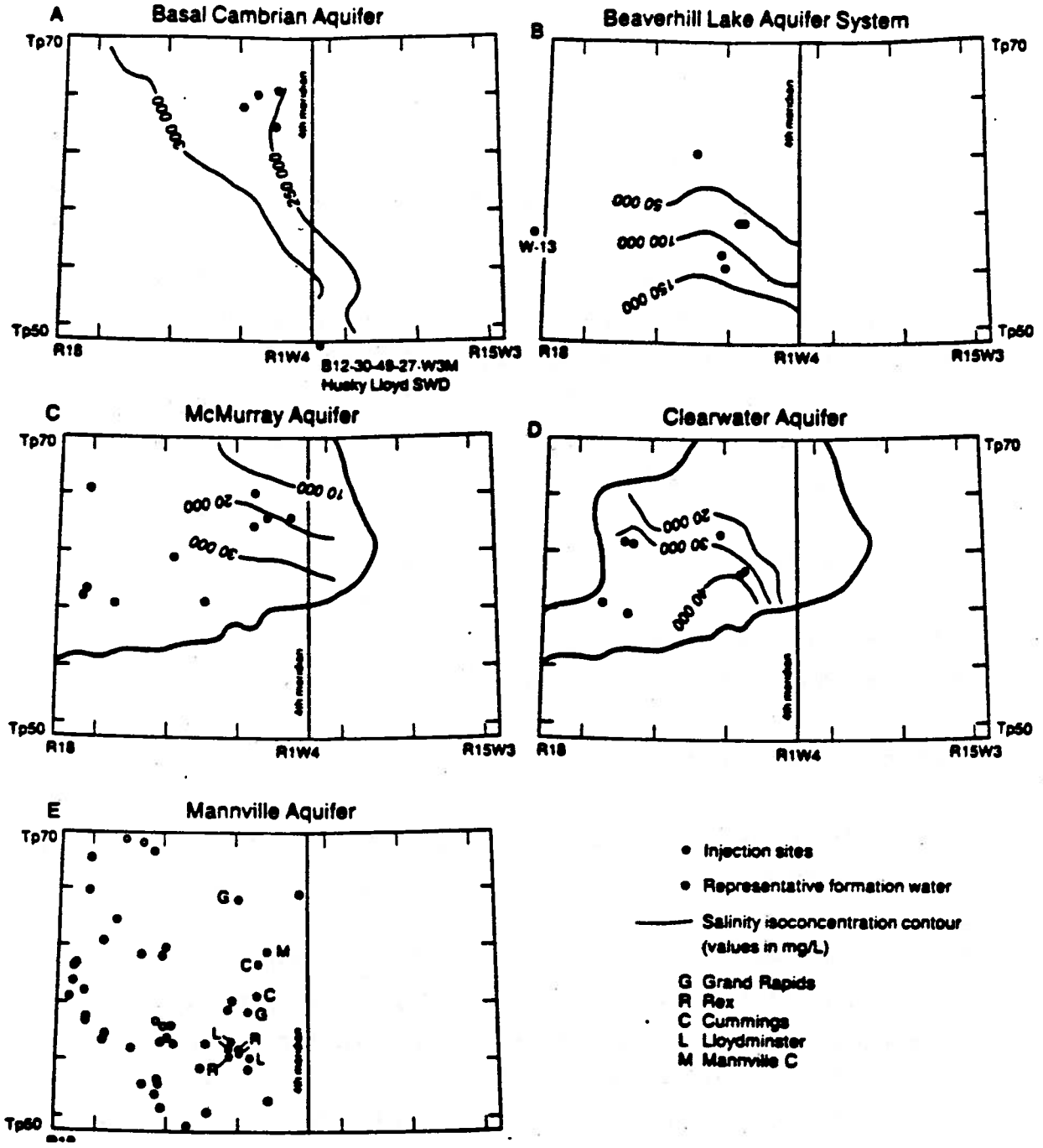

Figure 12 Injection sites, salinity isoconcentration contours (mg/L) and locations of representative formation waters for five injection aquifers in the Cold Lake region. A. Basal Cambrian aquifer; B. Beaverhill Lake aquifer system; C. McMurray aquifer; D. Clearwater aquifer; E. Mannville aquifer

Table 2.
Comparison of major components in formation waters from the Basal Cambrian aquifer

	Husky Lloyd SWD B12-30-49-27-W3M	Regional average 50-27-W3M	Average around injection sites (66-4-W4M)
Salinity	308 400	300 000	260 000
Cl	188 000	175 000	150 000
Ca	1 920	3 000	1 500
Mg	1 220	1 250	500
HCO_3	80	150	260
SO_4	3 180	2 000	6 000
Density	1.286	1.190	1.165

Table 3.
Comparison of major components in formation waters from the Beaverhill Lake aquifer system

	W13-RCA-765 9-29-57-19-W4	Regional averages around injection sites 63-8-W4	58-4/5	56-6,55-6
Salinity	161 205	40 000	75 000	125 000
Cl	99 900	20 000	50 000	75 000
Ca	8 440	1 000	2 500	6 000
Mg	2 980	500	1 250	2 000
HCO_3	139	300	200	200
SO_4	790	1600	300	400
Density	1.1095	1.030	1.060	1.090

McMurray Aquifer

Regional salinity gradients in the McMurray aquifer are oriented E-W, with salinities decreasing from 60 000 mg/L in the south to 10 000 mg/L in the north (Basin Analysis Group, 1987, figure 37). In the area of the four sites designated for injection into the McMurray aquifer the regional salinity is 20 000 mg/L (figure 12C). Because of the strong compositional gradients of the regional salinity pattern for formation waters in the McMurray aquifer in the Cold Lake area and the relative distribution of injection sites and locations of detailed formation water analyses (figure 12C), only one detailed analysis is comparable (table 4) to the regional salinity around the injection sites; the analysis of this sample (table 1) is used in the water-rock modelling study.

Clearwater Aquifer

Three sites are designated for injection into the Clearwater aquifer (figure 12D). Four detailed analyses of formation waters are available in the Cold Lake area, none of which are close to the injection sites (figure 12D). However, comparison (table 5) of the regional average formation water composition values around the two groups of injection sites (based on Basin Analysis Group, 1987, accompanying Atlas maps 99 to 105) with the detailed analysis RCAH 51-275A in table 1 indicates that it is suitable for use in water-rock modelling studies.

Mannville Aquifer

More than 40 detailed analyses of formation waters are available for the Cold Lake study area (figure 12E). For the purpose of water-rock interaction modelling, one analysis (table 1, RCAH 1-875B) has been selected from the Lindberg area; it formed part of the data base used to compile the regional maps in the Atlas accompanying the report by the Basin Analysis Group (1987, maps 107 to 113).

Table 4.
Comparison of major components in formation waters from the McMurray aquifer

	RCAH 72-475A 11-12-67-16-W4	Regional average 65-4
Salinity	29 306	20 000
Cl	16 900	12 000
Ca	450	200
Mg	222	100
HCO_3	942	800
SO_4	17	50
Density	1.0212	1.013

Table 5.
Comparison of major components in formation waters from the Clearwater aquifer

	RCAH 51-275A 11-26-63-12-W4	Regional averages around injection sites 64-6	61-4
Salinity	33 385	27 000	35 000
Cl	20 600	16 000	21 000
Ca	484	400	700
Mg	322	200	100
HCO_3	760	450	300
SO_4	47	25	20
Density	1.026	1.019	1.026

INJECTION AQUIFER MINERALOGY

The selected representative formation water analyses, while better than 'standard' formation water analyses, are nevertheless incomplete, lacking determinations for Al and SiO_2 in some cases. The analyses can be corrected and modified provided the mineralogy of the injection aquifer is known and assuming that the formation waters are in equilibrium with the minerals in the aquifers. Formations currently undergoing diagenetic reactions will not be in total equilibrium with the formation waters; however, they will buffer the water composition to values relatively near an equilibrium value. The formation mineralogy has been determined for most of the aquifers except for the Beaverhill Lake aquifer system. Accordingly, a combination of x-ray diffraction (Co K-alpha radiation at 50 kV and 20 mA; scan rate 1 degree 2 θ/min; chart speed 500 mm/h), and visual and thin section examination was made of selected cores from the Beaverhill Lake aquifer system.

Basal Cambrian Sandstone

In general, the Basal Cambrian sandstones are fine- to coarse-grained, sub- to well-rounded, and poorly sorted (Pugh, 1973; MacDonald, 1987). Pebble beds and shaly laminae are locally common. Sedimentary features are commonly well developed but many have been destroyed by bioturbation.

As of 1986, there were only seven wells with preserved core from the Basal Cambrian sandstones in the study area. As part of an M.Sc. project, MacDonald (1987) examined core from six wells and thin sections from five wells in the Basal Cambrian sandstone. The visual examination of core from Esso 83 SWD at Ethel Lake (11-22-64-3-W4) for the interval between 1214.38 to 1227.58 m indicated a dark red sandstone, poorly sorted and intercalated with red and green shale. Bioturbation is rare. For the interval between 1227.58 to 1251.63 m, this unit consisted of poorly sorted sandstones (green, yellow and red) interbedded with 0.5 to 5 cm bands of red and green shales. Unfortunately, no thin section or x-ray work was done on this well.

The nearest well to Cold Lake that was examined by MacDonald (1987) in thin section was the Imperial Willingdon No. 1 well (14-14-55-15W5) at a depth of 1955.75 m. In thin section, the sample comprised 94% quartz, 3% chlorite, 1% feldspar, 1% kaolinite, with trace amounts of zircon and magnetite. Illite occurred as a minor pore-filling cement.

Comparison of these thin section examinations, x-ray diffractions and core examinations indicates that there are only small differences in the minerals present in small/trace amounts when compared to the Basal Cambrian sandstone elsewhere in the province. The differences include the presence/absence of calcite, the presence/absence of anhydrite, the presence of dolomite (but not calcite) in one sample, and the replacement of magnetite by hematite.

Cooking Lake and Beaverhill Lake Formations

Literature data on the mineralogical composition of the Cooking Lake and Beaverhill Lake Formations is sparse, and they are generally described as "carbonate rocks". This is insufficient for modelling purposes, and thus an x-ray diffraction (XRD) study of nine whole-rock samples was carried out. Three samples (at different depths) were taken from the BA Corbett site, three from the Arco Heart Lake site, one from the Odd Coral, Arco Heart Lake site and two from the Rothwell Frog Lake site.

The samples were not chemically treated prior to XRD. Representative portions of the samples were ground to less than 20 μ and packed into aluminum sample holders. This procedure produces a randomly oriented distribution of particles in the sample.

The mineralogical data are presented in table 6. These rocks are predominantly calcite and dolomite, with between 1 and 30% quartz. No other phases are consistently present. Illite, kaolinite and chlorite were the only clay minerals observed; smectite is not present. Pyrite, plagioclase and potassium feldspar are also present in trace amounts.

McMurray Formation

The McMurray Formation is predominantly composed of quartz (93%), feldspar (5%) and minor chert/rock fragments (2%). Trace amounts of calcite, dolomite, siderite, pyrite, and clay minerals may be present but

Table 6.
Bulk mineral composition (%) of the Beaverhill Lake Group, Cold Lake area, Alberta

Well Name Depth (m)	Calcite	Dolomite	Quartz	Illite	Kaolinite	Chlorite	Plagioclase	K-feldspar	Pyrite
Rothwell Frog Lake 9-6-56-2-W4									
603.2	63	13	19	2	1	t	t	t	1
605.0	98	-	2	-	-	-	-	-	-
BA Corbetts 5-12-63-10-W4									
714.3	86	6	8	-	-	-	-	-	-
718.6	24	35	30	4	2	2	2	1	-
799.4	77	2	1	-	t	-	-	-	-
Arco Heart Lake 11-26-69-10-W4									
647.6	86	3	11	t	-	-	-	-	-
658.3	82	16	2	-	-	-	-	-	-
660.7	70	4	20	3	2	t	t	-	-
665.2	81	13	4	-	-	-	-	-	2

t = trace

their amounts are small and variable. When present, the dominant clay mineral is usually kaolinite (Mossop et al., 1982; James and Oliver, 1977).

Clearwater Formation

The Clearwater Formation is extremely complex and variable in its mineralogy. It can be considered to be chemically immature and still undergoing diagenesis. The grain-forming mineralogy of the Clearwater Formation in the Cold Lake area comprises quartz (21%), feldspar (28%), volcanic rock fragments (23%), chert (20%), and other sedimentary and metamorphic rock fragments (8%). The fine fraction (approximately 1 to 5% in general, but locally it can be much higher) is composed of illite (43%), smectite (14%), mixed layer smectite/illite (12%), kaolinite (16%) and chlorite (15%) (Visser et al., 1985; Harrison et al., 1982).

Grand Rapids Formation

Mineralogically, the Grand Rapids Formation is very similar to the Clearwater Formation, but differs primarily in the modal amounts of the minerals. Rock fragments and chert account for much less of the total rock volume, with a corresponding increase in the modal amount of quartz. The dominant clay is kaolinite, although illite and smectite are still present in significant amounts (Harrison et al., 1982). It, too, is currently undergoing diagenesis.

CORRECTION OF FORMATION WATER ANALYSES

The selected formation water analyses are not complete; values for Al are missing for all except the sample from the Clearwater aquifer and a value for dissolved silica is missing for the sample from the Cooking Lake aquifer. Various other cations and anions are missing in some of the analyses, but none are critical. No analyses had the Eh or redox potential directly measured, thus no computations involving any element with more than one redox state (Fe, Cu, etc.) can be made without a number of assumptions. In addition, all of the formation waters except that from

the Basal Cambrian aquifer were supersaturated with respect to calcite. As discussed below, this indicates that there is analytical error in both the TIC measurement and the pH measurement.

The XRD study of the cores from the Cooking Lake Formation indicated that quartz was present in all the sections studied. It is reasonable to assume that some of the quartz has dissolved into the formation water, but the actual amount is unknown. Examination of the other formation water analyses shows that their silica values range from 2.9 to 29.7 mg/L. Some of the highest values for silica are from formations currently undergoing diagenesis, which generally have rock fragments and significant amounts of other silicate minerals. The Cooking Lake Formation has small amounts of quartz present, but there is no evidence of rock fragments, chert or amorphous silica. For this reason, the estimated value of silica should be close to quartz saturation and not significantly higher. A reasonable assumption is that the fluid is in equilibrium with quartz, thus a value of 3 mg/L was used for total dissolved silica in solution in the formation water from the Cooking Lake aquifer.

Aluminum is missing from all of the formation water analyses except that from the Clearwater aquifer. This cation is very difficult to measure because it is typically present in fractions of a part per billion, a value much below the detection limit of all analytical equipment. In general, only in waters with very low or high pH will its value exceed the detection limit of the instruments. Because all clay minerals, and most of the silicate minerals except quartz and the other silica polymorphs, contain significant amounts of Al, some value must be obtained for modelling purposes.

By assuming that the formation water is in equilibrium with the dominant clay mineral present in the formation, a value for Al can be calculated. The values used in this report are of the order of 0.00002 mg/L and were obtained by assuming that the water was in equilibrium with either kaolinite or illite. This procedure is similar to that which was used to obtain a value for silica but there is a much higher uncertainty. Assumed values for silica can be directly compared to silica analyses in waters derived from various geological formations, thus validating the assumption. The low values of calculated Al in a formation water make this comparison nearly impossible for normal formation waters.

Those formation waters with analyses for Al are generally derived from either a high(er) temperature environment, a formation actively undergoing chemical diagenesis and thus are not in equilibrium, or have very high or low pH. "Normal" formation waters with reported Al analyses have a potentially high analytical error caused by the inclusion of extremely fine particulate material (for example) and a low precision because of the inherent difficulty of analyses in the ppb range.

The formation water analysis from the Clearwater aquifer has an Al value three orders of magnitude higher than the value assumed for the other aquifers. When this value is used to calculate the saturation indices (SI) for various alumino-silicate minerals (e.g. kaolinite, illite, smectite) SI values are four to five units supersaturated. Some supersaturation is to be expected in a formation undergoing chemical reactions, but this value does appear high. However, in the absence of other information, this value will be used.

Many comprehensive studies have indicated that in any groundwater flow system in the presence of calcite, the maximum that the water is supersaturated with respect to calcite is less than 0.1 SI units. If the SI of calcite is greater than this value, CO_2 has been lost from the solution before the laboratory analysis. With the exception of the formation waters from the Basal Cambrian aquifer, all of the formation waters are supersaturated with respect to calcite. Carbon dioxide has presumably been lost from each of the formation waters before analysis, thus it is necessary to add CO_2 to the analytical value until calcite saturation is reached.

All of the above modifications to the formation water analyses have been taken into account, and the adjustments shown in table 7.

INJECTION WATER COMPOSITION

The composition of waste water from an enhanced oil recovery operation is primarily dependent on the composition of the production water, but is modified by treatment, by the length of storage time, by the temperature during storage, and by mixing with surface water/shallow aquifer water before disposal to reduce the total dissolved solids. The composition of production water from enhanced oil recovery pilots is the result of the

Table 7.
Adjustments made to the formation water analyses in table 1 to account for missing for Al and SiO_2, and loss of CO_2

Stratigraphic unit	Component	Analysed value	Calculated value (mg/L
Basal Cambrian sandstone	Al^{+3}	-	0.00001
Cooking Lake Formation	Al^{+3}	-	0.00001
	HCO_3^{-1}	139	80.9
	SiO_2 (aq)	-	3.0
	pH	6.78	6.35
McMurray Formation	Al^{+3}	-	0.00001
	HCO_3^{-1}	942	722.3
	pH	7.3	6.51
Clearwater Formation	HCO_3^{-1}	760	785.7
	pH	7.9	6.54
Glauconitic sandstone	Al^{+3}	-	0.00001
	HCO_3^{-1}	220	228.2
	pH	7.61	6.72

interaction of the injection water and steam with the reservoir minerals, the formation water, the formation gases (if present) and the heavy oil/ bitumen. For the purpose of modelling water-rock interactions, the initial composition is important, as are the formation temperature and pressure, the steam quality, and the length of time that the injection fluid has to react. It is clear that the composition of the produced water will vary significantly over a production cycle and that, in principle, all of the chemical reactions occurring during production could be inferred from this process.

Because of the variation in waste water composition with respect to time, it is impossible to establish a typical composition for any given pilot. For this reason, approximately 20 different waste waters from pilots in the Cold Lake area were used in the modelling. A number of the waste waters came from the same pilot, but were measured at different times during the production cycle. For reasons of confidentiality, the waste waters cannot be identified with a specific pilot. Typical composition are given in Gunter et al. (1986).

CALCULATION OF POTENTIAL WATER-ROCK INTERACTIONS

Using the computer code SOLMNEQF (Aggarwal et al., 1986) each of the 20 waste waters were mixed with the formation water from each of the aquifers, and the saturation indices for every mineral which can possibly be saturated, were calculated and plotted. The saturation index (SI) is a measure of the ability of a mineral to precipitate or dissolve. The SI is defined as the logarithm to the base ten of the ratio of the activity quotient for the hydrolysis reaction of a mineral to the equilibrium constant for the same reaction. If the SI is less than 0.0, the mineral (phase) should dissolve into the fluid; if the SI is greater than 0.0 the phase should precipitate from the fluid; if SI is 0.0 the phase is in equilibrium with the fluid. This calculation is strictly an equilibrium calculation. If the fluid is supersaturated with respect to a mineral, the mineral may not precipitate because of kinetic considerations. However, the greater the supersaturation, the more likely it will precipitate.

Because of the large number of waste waters considered, individual mixing curves for each waste water/formation water pair could not be plotted. Instead, the area where all of the curves fall is shaded. If any of the curves are significantly different than the others, they are plotted as a separate line or region. Individual curves which fall below the rest of the SI curves correspond to waste waters which were formed from production waters early in a cyclic process.

All of the figures have the same abscissa, with values ranging from 0 to 1. A value of 0 indicates that the fluid composition used in calculating the SI values is formation water, while a value of 1 indicates that the fluid composition is that of the waste water. Data between 0 and 1 represent various mixtures of formation water and waste water. On all of the figures, the ordinate axis is the saturation index (SI) of the mineral; the range of ordinate values varies from figure to figure, but always includes a value of 0.0 because this value corresponds to saturation.

Basal Cambrian Aquifer

Figure 13 illustrates the effects of mixing the formation water from the Basal Cambrian aquifer with the various waste waters.

The results can be summarized as follows. Quartz is supersaturated in the formation water with an SI of approximately 1. The injection waters and their mixtures with the formation water have a range of SI values which vary from 0.8 SI units below that in the formation water to approximately 0.6 SI units above that in the formation water. The average value is, therefore, the same as or slightly above that in the formation, but not significantly so. The SI values for the other silica phases (amorphous silica and chalcedony) are lower than that for quartz and the shape of their SI curves is similar. Because the change in SI for quartz is not extreme, in view of the assumptions made, quartz is not expected to precipitate in significant amounts. All of the carbonate minerals are undersaturated in the formation water but some of the waste waters and their mixtures have SI values greater than zero. The average SI value for all of the carbonates is less than zero, thus in these waters precipitation of calcite should not be a problem. The sheet silicates and

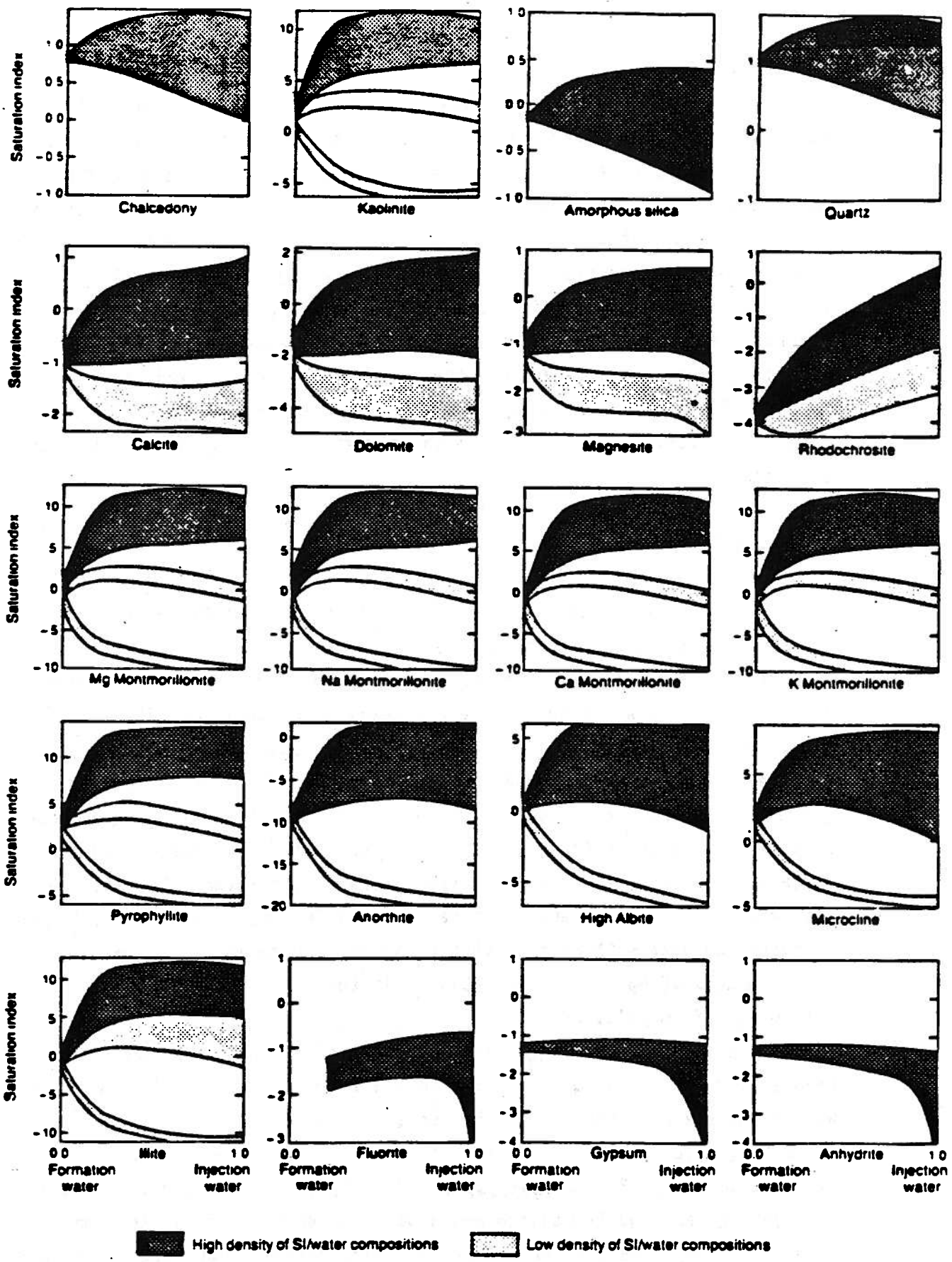

Figure 13 Saturation indices of selected minerals for mixtures of formation water and injection waters, Basal Cambrian aquifer

clays (kaolinite, illite, pyrophyllite, K-montmorillonite, Ca-montmorillonite, Na-montmorillonite, and Mg-montmorillonite) are all saturated (SI approximately zero) in the formation water. In the waste waters and their mixtures, the SI values increase rapidly to a maximum of approximately 12. These are highly supersaturated, and indicate that one or more of these phases will precipitate from solution. The SI values of the feldspars (plagioclase, microcline and albite) increase as the proportion of waste water increases. Only albite and microcline are supersaturated, however. Because they share the same elements as the clay minerals, it is anticipated that the clay minerals will precipitate instead of them. Gypsum, anhydrite and fluorite are undersaturated in the formation waters, waste waters and their mixtures, and will not cause any problems.

Cooking Lake Aquifer

Figure 14 illustrates the effects of mixing the formation water from the Cooking Lake aquifer with the various waste waters.

The dominant mineral in the formation is calcite, thus the SI values for all the carbonate minerals are extremely important. Calcite and dolomite are saturated in the formation water. Some of the waste waters and their mixtures are undersaturated with respect to calcite and dolomite, but most are slightly saturated. An exception is the manganese carbonate, rhodochrosite, which is almost completely undersaturated. Trace amounts of Mn would be expected in calcite, however. Dolomite has extremely slow kinetics when compared to calcite, and thus if the solution is supersaturated with respect to the carbonate minerals, calcite (with minor amounts of Mg, Mn and probably Fe in the structure) would precipitate from solution.

Quartz is the second most important mineral in the formation and has been assumed to be in equilibrium with the formation water. In the waste waters and their mixtures with the formation waters, quartz is increasingly supersaturated, and in some waste waters reaches an SI value of approximately 1.3. The average trend of SI values is also up, thus in the Cooking Lake aquifer silica would be expected to precipitate from solution. The SI values for the other silica phases (amorphous silica and

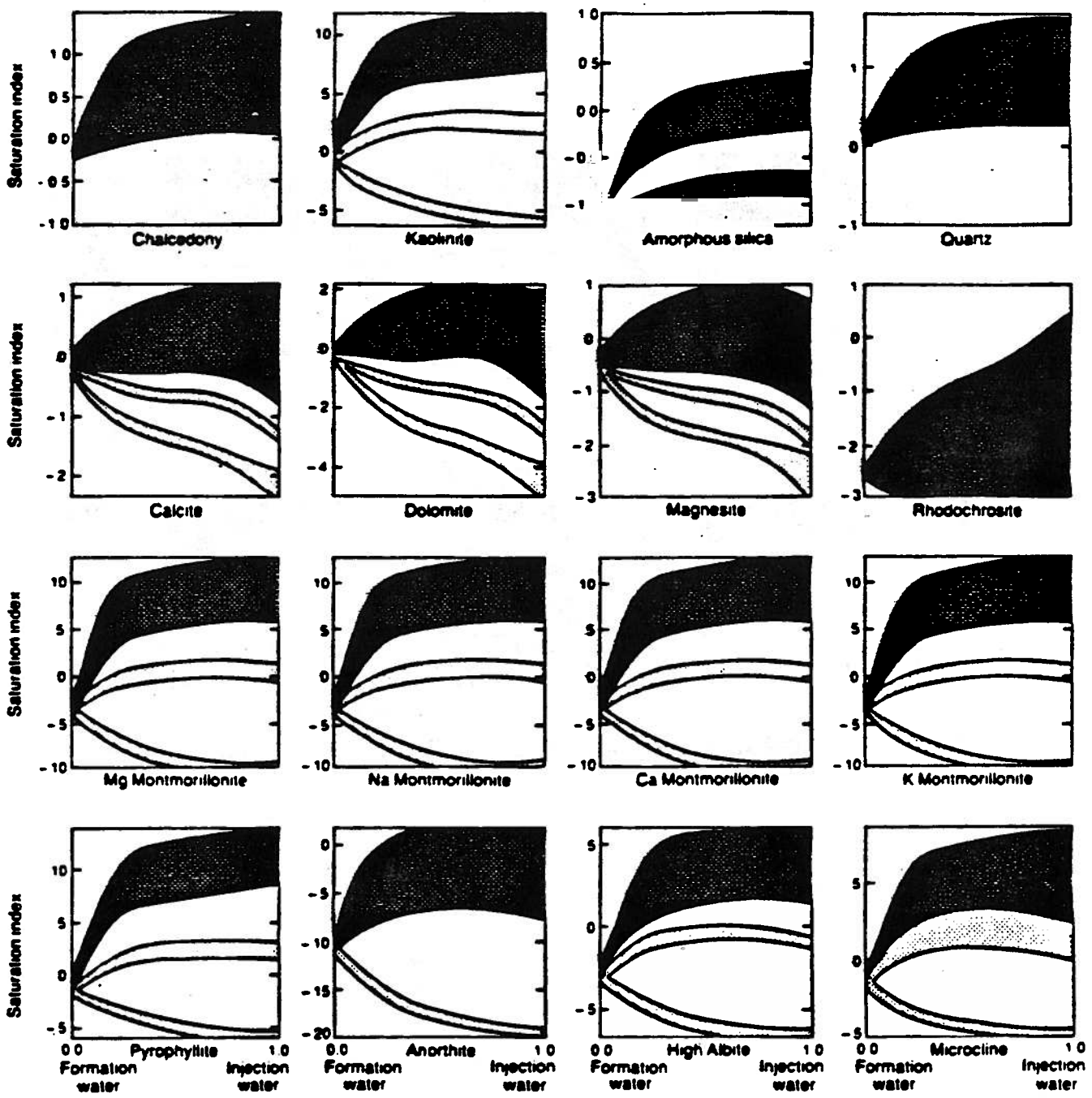

Figure 14 Saturation indices of selected minerals for mixtures of formation water and injection waters, Cooking Lake aquifer

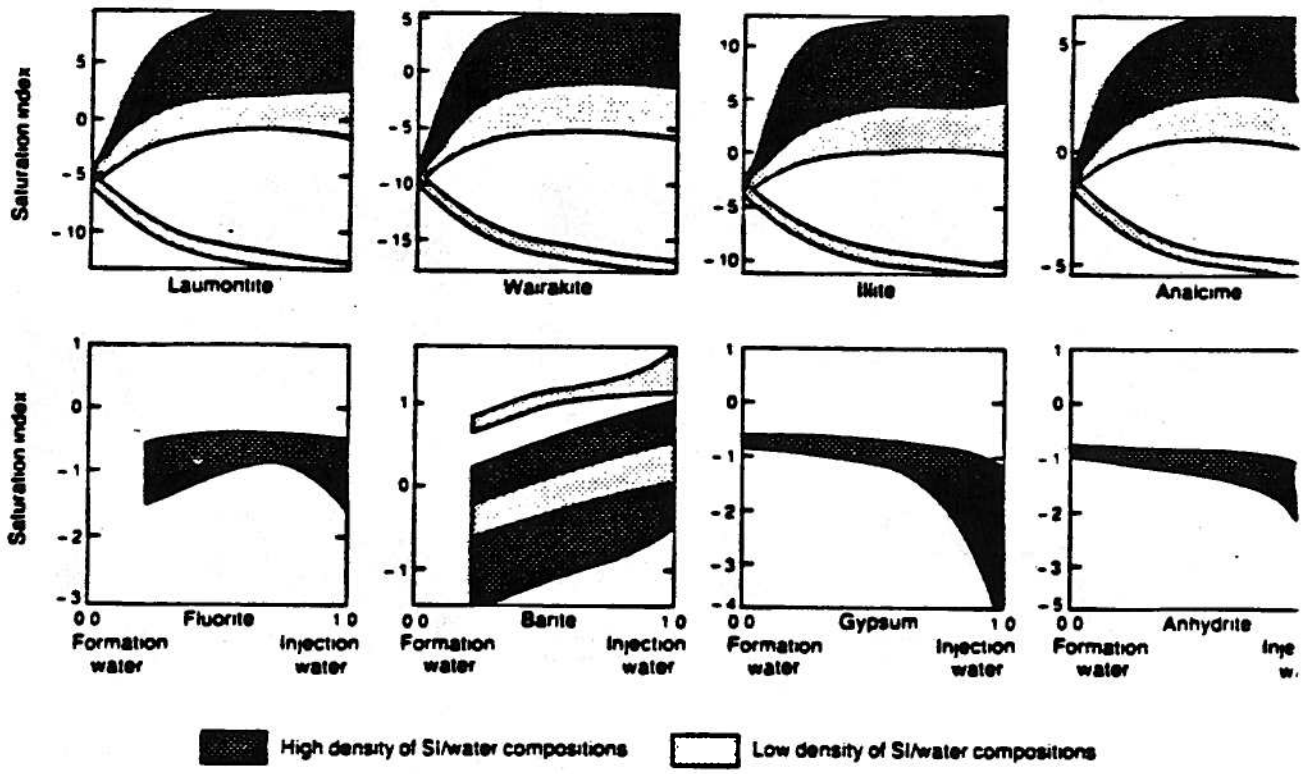

Figure 14. Continued

chalcedony) are lower than that for quartz but the shape of their SI curves are similar to the quartz SI curve.

The sheet silicates and clays, (kaolinite, illite, pyrophyllite, K-montmorillonite, Ca-montmorillonite, Na-montmorillonite, and Mg-montmorillonite) are all undersaturated (SI less than zero) in the aquifer. In the waste waters and their mixtures, their SI values increase by up to 12 units. These phases are highly supersaturated and certainly one or more will precipitate from solution. The SI values of the feldspars (plagioclase, microcline and albite) are initially less than zero, but increase rapidly above zero as the proportion of waste water increases (with the exception of plagioclase where only a few of the solutions have SI values greater than zero). Only albite and microcline are supersaturated to any degree. Because the feldspars have some of the same elements as the clays and because the clays precipitate much faster from solution, it is anticipated that the clays will form instead of the feldspars. Fluorite, anhydrite and gypsum are undersaturated in the formation waters, waste waters and their mixtures, and will not cause any problems. Barite is supersaturated in the formation waters, the waste waters and their mixtures, and precipitation of this mineral may cause some formation damage. The zeolite laumontite is undersaturated in the formation water but most of the mixtures with the waste waters, as well as the waste waters themselves, are supersaturated. The zeolite wairakite is also undersaturated in the formation water, and in approximately half of the waste waters and their mixtures. Analcime is supersaturated in almost all of the waters considered, with only the formation water and one waste water/formation water mixing curve having SI values below zero. Zeolites form in low temperature environments, thus it is possible that analcime or laumontite may form. Because these zeolites will be competing for the same ions as the clays, only one of the two should form in significant amounts.

McMurray Aquifer

Figure 15 illustrates the effects of mixing the formation water from the McMurray aquifer with the various waste waters.

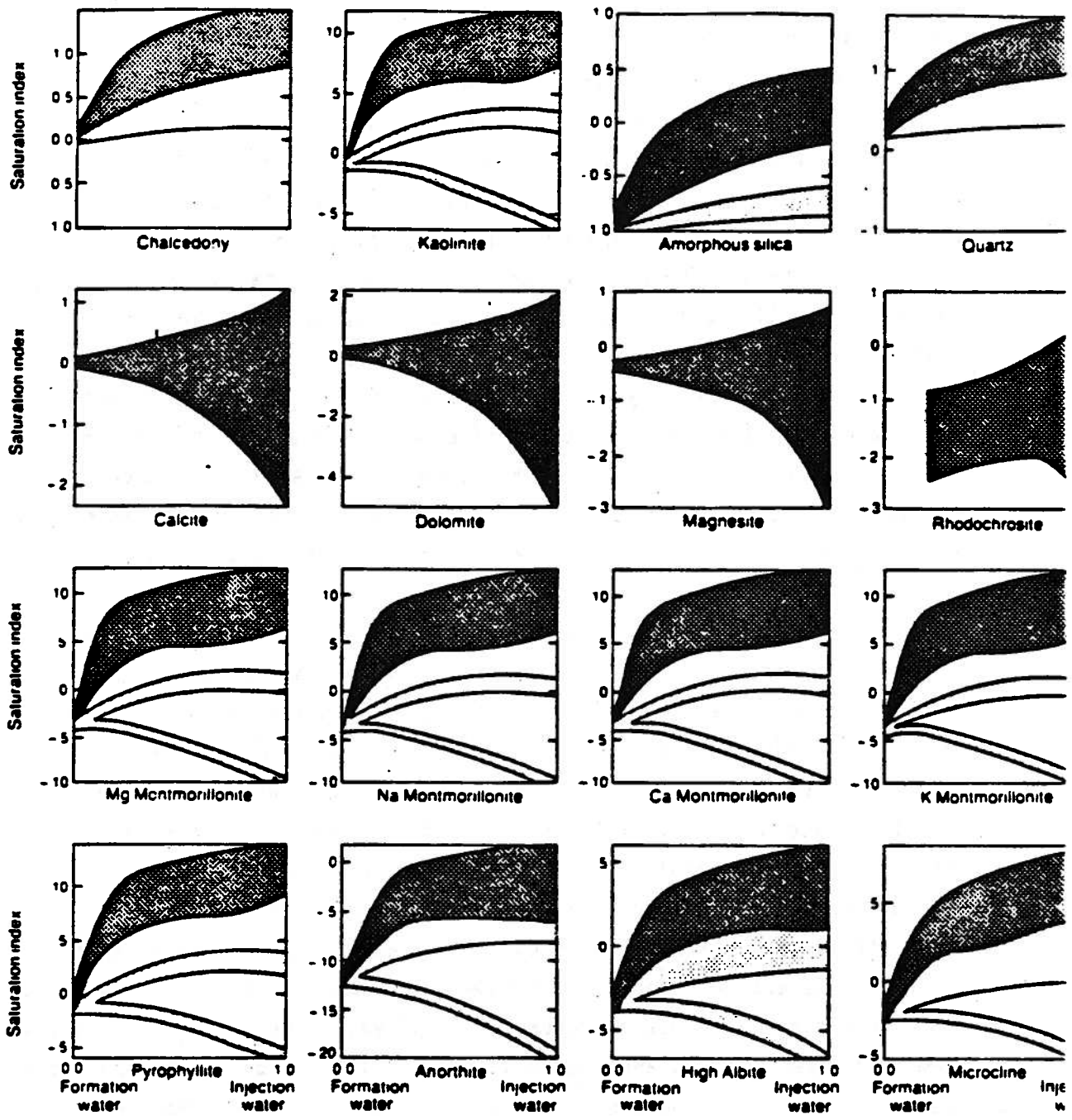

Figure 15 Saturation indices of selected minerals for mixtures of formation water and injection waters, McMurray aquifer

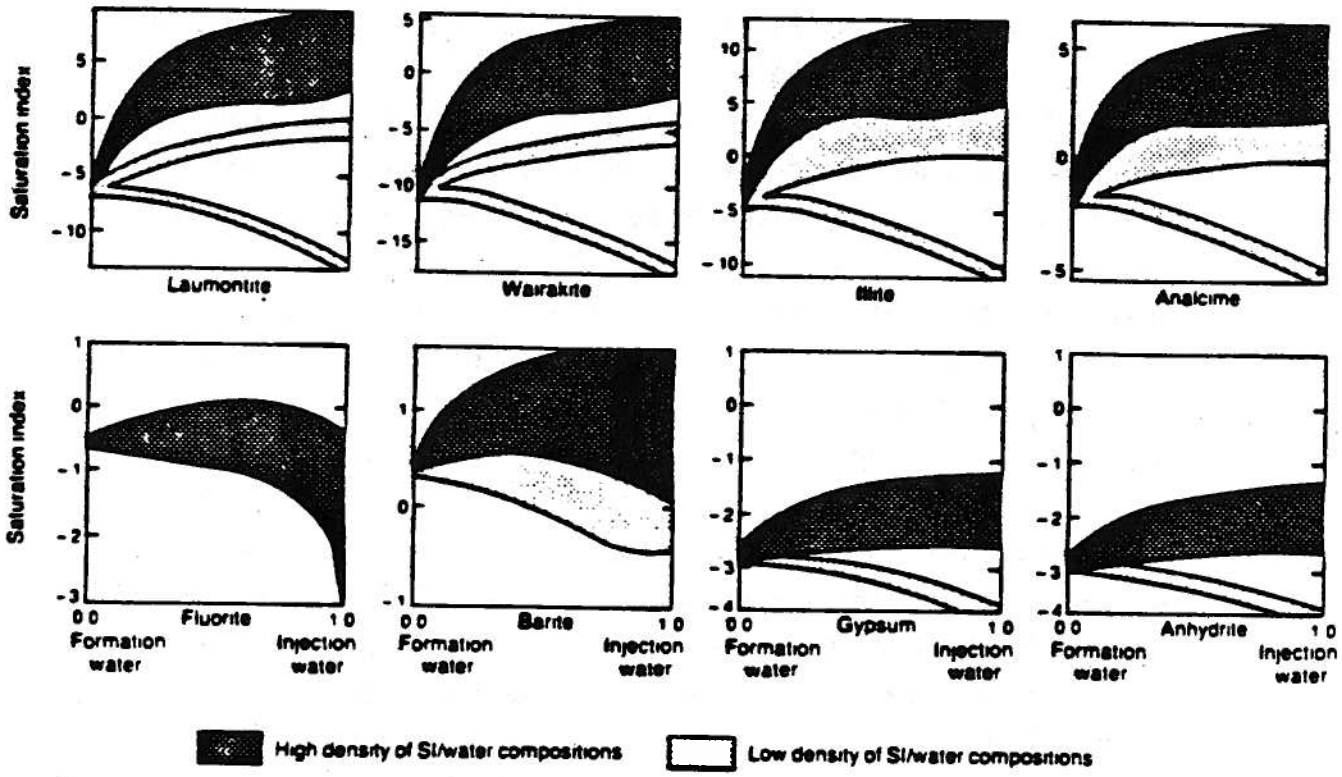

Figure 15. Continued

The dominant formation mineral is quartz, which is slightly supersaturated with respect to the formation water, but is supersaturated in all of the waste waters and their mixtures with a maximum value of approximately 1.65 SI units. The average trend of the SI values is up, thus indicating that it is extremely likely that quartz will precipitate from the waste waters and their mixtures. The SI values for the other silica phases (amorphous silica and chalcedony) are lower than that for quartz but the shape of their SI curves are similar. The formation waters in the McMurray aquifer are in equilibrium with both calcite and dolomite. The waste waters and their mixtures have SI values evenly distributed about an SI of zero, and although not significant the trend is to slightly negative values. The maximum SI value for calcite is about 1.2 while the minimum is approximately -2.4. The range of dolomite values are approximately twice as large. Because of kinetic constraints, dolomite precipitates much slower than calcite and, therefore, calcite precipitates preferentially. Trace amounts of Mn and Mg will be included in the calcite structure. The sheet silicates and clays, (kaolinite, illite, pyrophyllite, K-montmorillonite, Ca-montmorillonite, Na-montmorillonite, and Mg-montmorillonite) are all undersaturated (SI less than zero) in the aquifer. In the waste waters and their mixtures, their SI values increase to 13 SI units. These phases are highly supersaturated, and certainly one or more will precipitate from solution. The SI values of the feldspars (plagioclase, microcline and albite) are initially less than zero, but rapidly increase above zero as the proportion of waste water increases (with the exception of plagioclase where only a few of the waste waters have SI values greater than zero). Only albite and microcline are supersaturated to any degree. Because the feldspars share common elements with the clays and because clays precipitate much faster from solution, it is anticipated that the clays will form instead of the feldspars. Fluorite, anhydrite and gypsum are undersaturated in the formation water, waste waters and their mixtures, and will not cause any problems. Barite is supersaturated in the formation water, the waste waters and their mixtures and, therefore, precipitation of this mineral may cause some formation damage. The zeolite laumontite is undersaturated in the formation water but most of the mixtures with the waste waters, as well as the waste waters themselves, show supersaturation. The zeolite wairakite

is also undersaturated in the formation water and in approximately three-quarters of the waste waters and their mixtures. Analcime is supersaturated in many of the waters with only the formation water and several waste water/formation water mixtures having SI values less than zero. The zeolites form in low temperature environments, thus it is possible that analcime or laumontite may form. Because these zeolites will be competing for the same ions as the clays, only one of the two should form in significant amounts.

Clearwater Aquifer

Figure 16 illustrates the effects of mixing the formation water from the Clearwater aquifer with the various waste waters. The results can be summarized as follows. Quartz is supersaturated in the formation water with an SI of approximately 0.40. The waste waters and their mixtures with the formation water have a range of SI values, which vary from the same SI as the formation water to approximately 1.7 SI units above that of the formation water. The average value increases significantly. The SI values for the other silica phases (amorphous silica and chalcedony) are lower than that of quartz and the shape of their SI curves are similar. Because of the change in the SI for quartz with increasing proportions of waste water, quartz has a significant potential for precipitation. All of the carbonate minerals are saturated in the formation water (a result of the initial assumptions) with the exception of Mn carbonate; this is probably because there is no analytical value for Mn in the formation water. The waste waters and their mixtures have SI values which fall above and below the value for the formation water in an approximately equal distribution. The potential for precipitation of carbonates in some of the injection fluids is relatively high, whereas others have significant potential for dissolution if they are present in the Clearwater Formation. The problem of carbonate precipitation is thus totally dependent on the specific waste water and cannot be generalized.

The sheet silicates and clay minerals (kaolinite, illite, pyrophyllite, K-montmorillonite, Ca-montmorillonite, Na-montmorillonite and Mg-montmorillonite) all are supersaturated (SI significantly greater than zero) in the formation water. In the waste waters and their

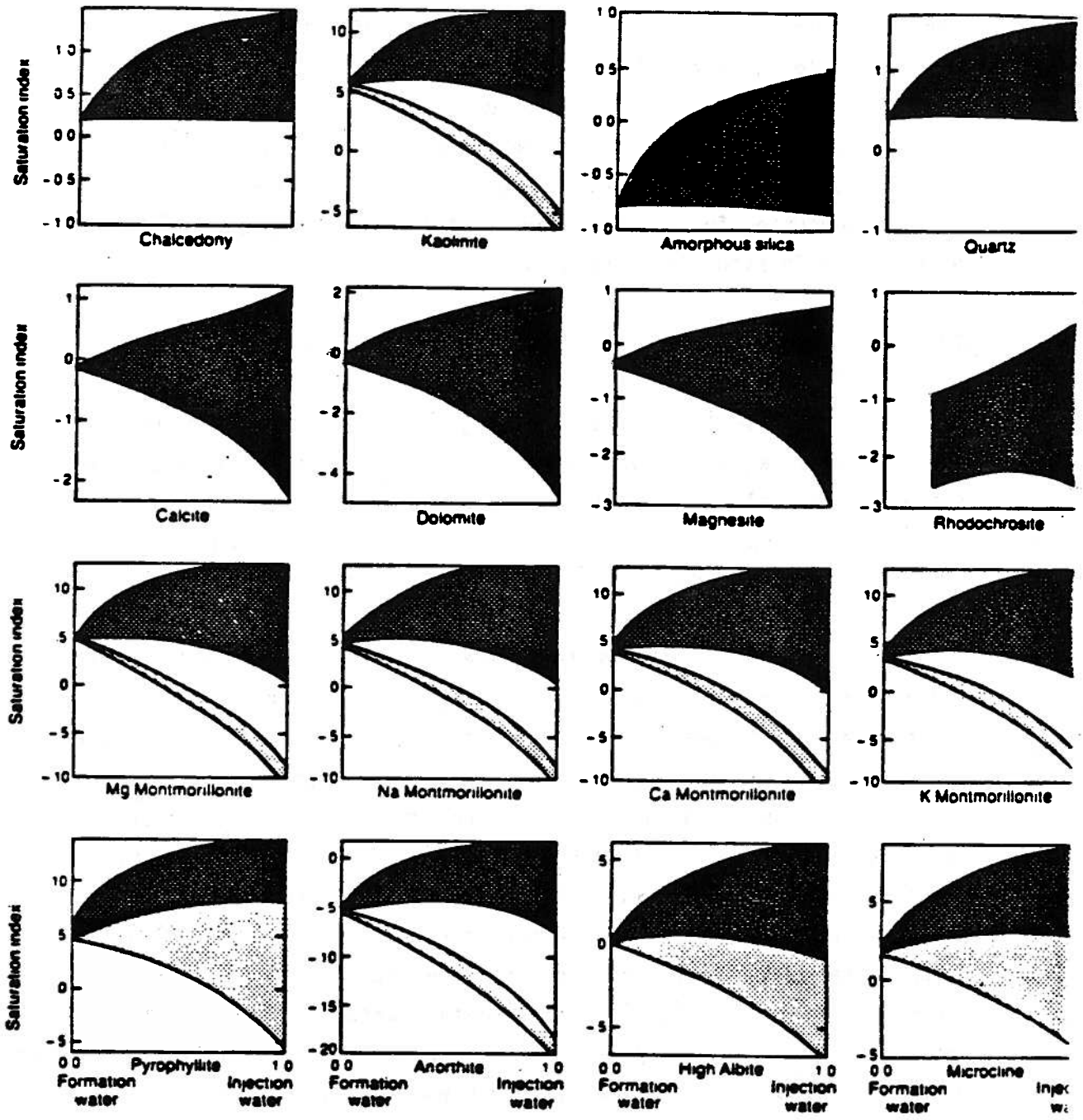

Figure 16 Saturation indices of selected minerals for mixtures of formation water and injection waters, Clearwater aquifer

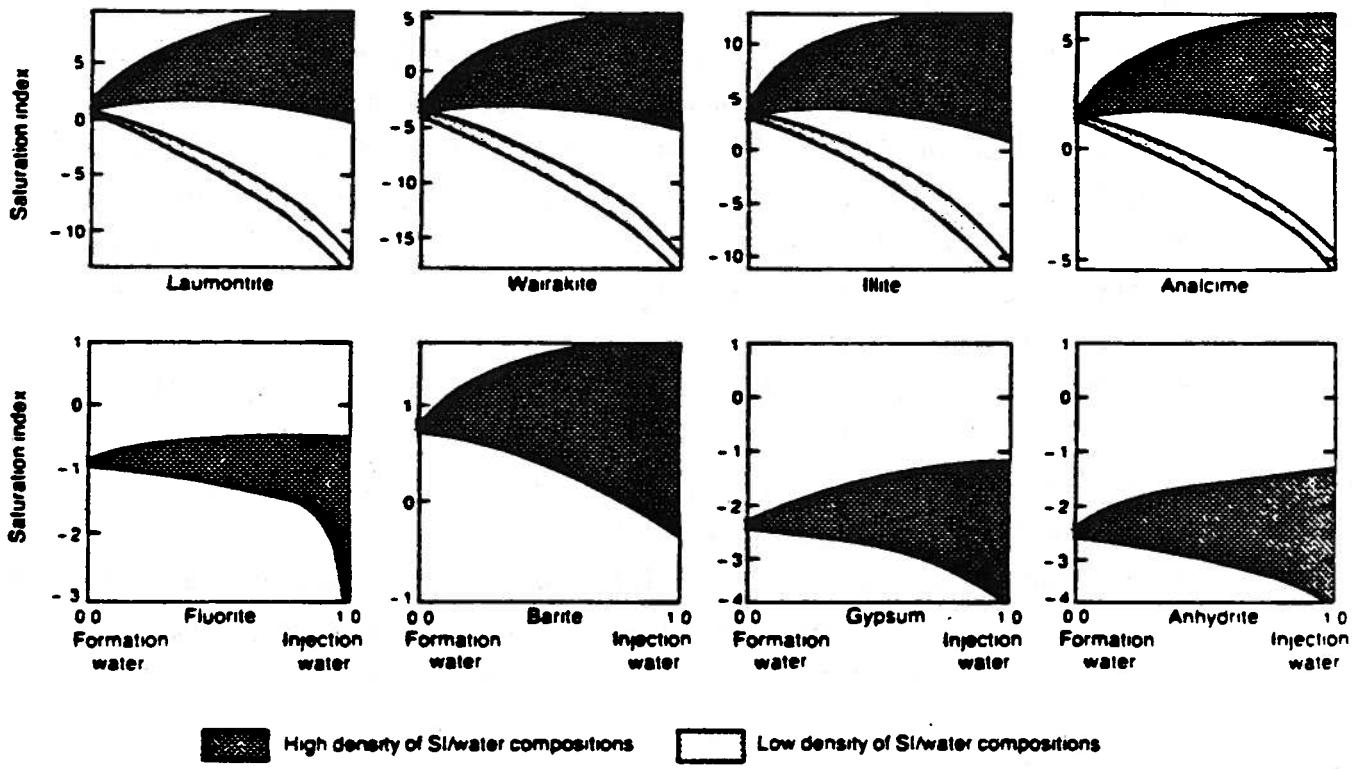

Figure 16. Continued

mixtures, their SI values increase an average of approximately four units. These phases are highly supersaturated and certainly one or more will precipitate from solution. The SI values of the feldspars (plagioclase, microcline and albite) increase as the proportion of waste water increases. Only albite and microcline are supersaturated to any degree, and because the feldspars share similar elements with the clay minerals and because clay precipitates much faster from solution, it is anticipated that the clay minerals will precipitate instead of them. Gypsum, anhydrite and fluorite are undersaturated in the formation water, waste waters and their mixtures, and will not cause any problems. Barite is supersaturated in the formation water, the waste waters and their mixtures and, therefore, the precipitation of this mineral may cause some formation damage. The zeolite laumontite is only slightly supersaturated in the formation water but most of the mixtures with the waste waters, as well as the waste waters themselves, are supersaturated. The zeolite wairakite is undersaturated in the formation water, and many of the waste waters and their mixtures. Analcime is supersaturated in almost all of the waters considered, with only one waste water/formation water mixing curve having SI values below zero. The zeolites form in low temperature environments, thus it is possible that analcime or laumontite may form. Because these zeolites will be competing for the same ions as the clays, only one of the two should form in significant amounts.

Mannville Aquifer

Figure 17 illustrates the effects of mixing the formation water from the Mannville aquifer with the various waste waters.

The dominant formation mineral is quartz, which is slightly undersaturated in the formation waters; this is a function of the initial assumptions. Quartz is supersaturated in all of the waste waters and their mixtures with a maximum value of approximately 1.7 SI units. The average trend of the SI values is up, thus indicating that it is extremely likely that quartz will precipitate from the waste waters and their mixtures. The SI values for the other silica phases (amorphous silica and chalcedony) are lower than that for quartz but the shape of their SI curves is similar. The formation water of the Mannville aquifer is in

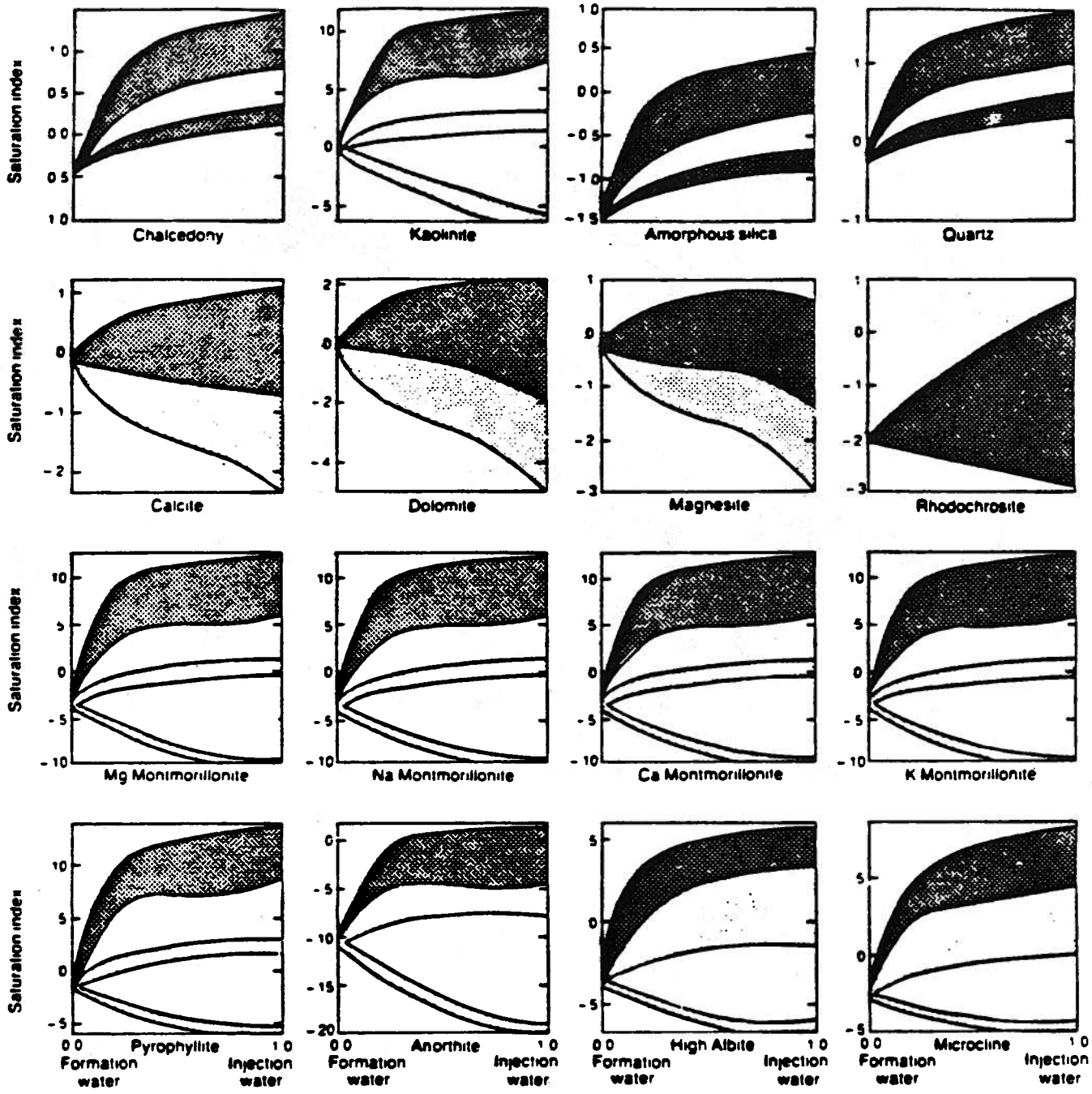

Figure 17 Saturation indices of selected minerals for mixtures of formation water and injection waters, Mannville aquifer

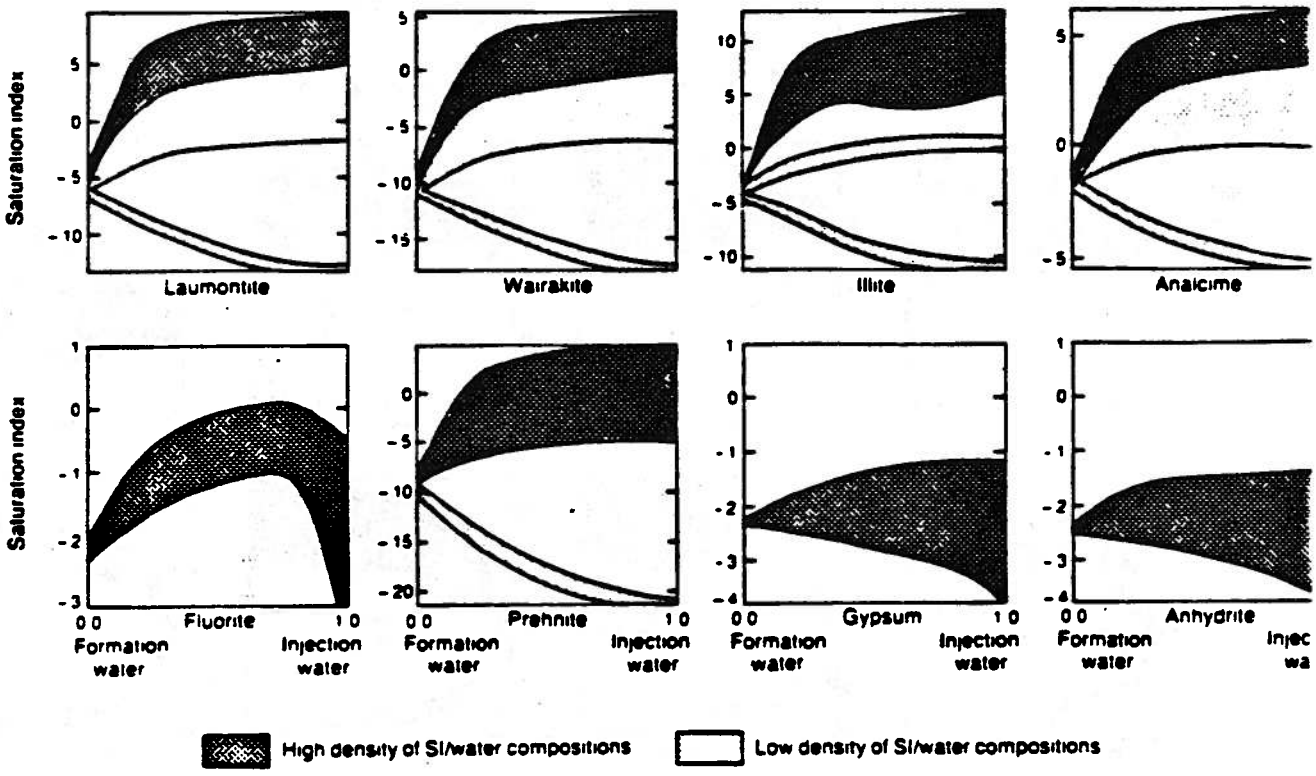

Figure 17. Continued

equilibrium with both calcite and dolomite, in part a result of the initial assumptions. The waste waters and their mixtures have SI values evenly distributed about an SI of zero, although not significantly so, with a trend to slightly positive values. The maximum SI value for calcite is about 1.2 while the minimum is approximately -2.4. The range of dolomite values is approximately twice as great. Because of kinetic constraints, dolomite precipitate more slowly than calcite and hence calcite will precipitate first. Trace amounts of Mn and Mg will be included in the calcite structure. The sheet silicates and clay minerals (kaolinite, illite, pyrophyllite, K-montmorillonite, Ca-montmorillonite, Na-montmorillonite, and Mg-montmorillonite) are all undersaturated (SI less than zero) in the aquifer. In the waste waters and their mixtures, their SI values increase up to 13 SI units. These phases are highly supersaturated and certainly one or more will precipitate from solution. The SI values of the feldspars (plagioclase, microcline and albite) are initially less than zero but increase rapidly to above zero as the proportion of waste water increases, with the exception of plagioclase where only a few of the waste waters have SI values greater than zero. Only albite and microcline are supersaturated to any degree, and because the feldspars share elements with the clay minerals and because clay minerals precipitate much faster from solution, it is anticipated that the clay minerals will form instead of the feldspars. Fluorite, anhydrite and gypsum are undersaturated in the formation water, waste waters and their mixtures, and will not cause any problems. The zeolite laumontite is undersaturated in the formation water but most of the mixtures with the waste waters, as well as the waste waters themselves, are supersaturated. The zeolite wairakite is also undersaturated in the formation water and in approximately three-quarters of the waste waters and their mixtures. Analcime is supersaturated in almost all of the waters considered, with only the formation water and one waste water/formation water mixing curve having SI values below zero. Prehnite is generally undersaturated, but some values are supersaturated. The zeolites form in low temperature environments, thus it is possible that analcime or laumontite may form. Because these zeolites will be competing for the same ions as the clays, only one of the two should form in significant amounts.

CONCLUSIONS

All of the formation waters are either at (or near) equilibrium with the minerals observed in the formation, or are significantly undersaturated with respect to them. This is partially a result of the assumptions made with respect to the amount of SiO_2 and Al in solution, and the assumption about loss of CO_2 from the water analyses. The apparent undersaturation of the clay minerals is a result of the assumed Al values and because the natural clay mineral stability fields are considerably larger than those calculated due to solid solution effects. This close agreement between the fluid chemistry and the mineralogy does illustrate a very important point. Given sufficient time, the formation mineralogy will control the fluid chemistry.

In the waste waters and their mixtures with the formation waters, quartz, the clay and sheet silicate minerals, feldspars and zeolites are almost always supersaturated. This cannot be avoided and is a result of the EOR process. The produced fluids have come to equilibrium with the reservoir mineralogy at temperatures typically in excess of 100°C, where the solubility of SiO_2 and Al is much higher. But because of (1) their short residence time in the production equipment, (2) the lack of a suitable substrate for minerals to precipitate on to, and (3) the lack of appropriate treatment, they will probably remain supersaturated until injected into an aquifer. The supersaturation is most significant when the trend of SI values increase above the SI value in the aquifer.

Although not shown on the figures, when phosphate is present in the waste water the fluid is typically supersaturated with the phosphate minerals, chlor-apatite, fluor-apatite, and hydroxal apatite. As mentioned previously, there may be Fe minerals with SI values significantly above zero, but in the absence of information about the redox state of Fe this cannot be calculated.

The amount and identity of the minerals which will precipitate in any system with more than one supersaturated phase is currently impossible to predict. However, various constraints can be used to indicate the maximum amount of a mineral that will precipitate. Consider first the clay minerals which are typically 10 orders of magnitude supersaturated. Because of this and the presence of clay minerals in all aquifers, we

would expect their precipitation to be rapid. However, the total amount of Al in waste water is very small, typically of the order of 0.05 mg/L or less. Even if all the Al is used in clay formation, the number of moles of clay that can be formed per litre of solution is of the order of 10^{-6} to 10^{-7}. This amount is trivial and can be ignored. The local solid-solid reactions between Al-bearing phases will be far more important than this. The maximum amount of any Al-bearing mineral which can be precipitated is of a similar order of magnitude, thus the feldspars and zeolites can be ignored.

The most significant minerals which can precipitate from or dissolve into the fluid are quartz and calcite (dolomite is excluded because its rate of precipitation is orders of magnitude slower than calcite). If the solution has an SI value for quartz of approximately 1, then approximately 10^{-3} moles can precipitate per litre of solution. If the solution has an SI value for calcite of approximately 1, then approximately 10^{-4} moles per litre of calcite can precipitate.

These values are not precise because they depend totally on the pH, the amount of each of the individual aqueous species in the fluid, and how they change during the reaction. If more than one mineral is dissolving into or precipitating from solution at one time, then they will all be affected by the rates of each reaction. These values should only serve as a guide, but they do indicate an approximate maximum amount of mineral which can be precipitated per litre of waste water.

Values of 10^{-3} moles per litre of fluid can be important when integrated over large volumes of fluid over a long time, and if precipitated quickly enough can affect the fluid flow. Using the rates of precipitation measured for quartz at high temperatures, and extrapolating them to 25°C, the amount of silica precipitated from solution over the life time of injection can be calculated. Over a period of 30 a, if a solution is supersaturated with respect to quartz, approximately 20% of the available silica will precipitate from solution. Approximately 50% will have precipitated after 95 a. Many formation waters are currently supersaturated with respect to quartz and probably have been for millennia, indicating these calculations should be considered conservative.

If a solution is undersaturated with respect to calcite, approximately

50% of the amount of calcite which can dissolve, will do so in 3 to 4 d. Over a period of 30 a, all of the calcite which can dissolve into solution must be considered to have done so. The rapid rate of dissolution and precipitation is confirmed by the lack of natural groundwaters which are supersaturated or undersaturated with respect to calcite when calcite is present in the formation. The rates of precipitation of calcite from a solution supersaturated with respect to calcite is very similar to the dissolution rates.

Multiple waste water samples were taken from several of the pilots at different times, with the calcite saturation index generally undersaturated but not for all of the samples. This is consistant with the SI plots for calcite for all of the waste waters, which indicate that more than 60% of the waste waters are undersaturated with respect to calcite. Because the average saturation index of calcite is negative, dissolution of calcite from the aquifer would be expected, resulting in an increase in the local porosity and permeability. With the exception of the Cooking Lake/Beaverhill Lake Formation which may consist of up to 98% calcite, the total change in porosity and permeability is expected to be small because calcite is present only in trace amounts. Due to the rapid kinetic properties of calcite, all of the calcite in the near well region will be expected to be dissolved. Figure 18 presents the variation with time of the total volume of minerals which will precipitate/dissolve per litre of injected fluid.

These results are indicative of the maximum volume change of the minerals in the formation due to precipitation and dissolution, and have been calculated using average values for the saturation indices of quartz and calcite. Variation of waste water compositions over the production cycle could modify the results. However, quartz is the most significant precipitant (by volume) and is not expected to precipitate as quickly in the formation as was assumed for the calculations. Thus, it is unlikely that the decrease in porosity and permeability will be as rapid as shown.

The rate at which both calcite and quartz precipitate from solution is dependent on a large number of factors including the effective surface area for growth and the presence/absence of nucleation sites. These parameters are largely unknown in natural systems, and add to the uncertainty of the above figures. However, the relative rate at which

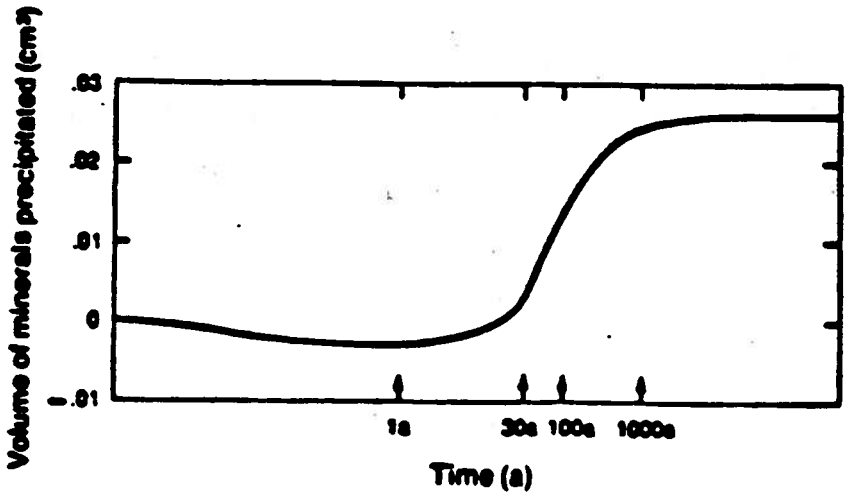

Figure 18 Total volume of minerals (cm^3) precipitated/dissolved per litre of injection fluid as a function of time. Negative values indicate dissolution

calcite and quartz precipitate will be similar. For this reason, if treatment of waste waters is to be considered, the most important change that can be made is to reduce the SI of calcite. This can be accomplished by softening of the water, removing CO_2, modifying the pH, or increasing the residence time in a holding tank.

Many of the mineral reactions which will occur during the interaction of the waste water and the minerals in the formation are endothermic, a few are exothermic. Because of (1) the relatively long time over which these reactions occur, (2) the small amount of material involved per litre of fluid, and (3) the large thermal mass of fluid and rock, they will not affect the local temperature. The thermal effects of reaction can thus be ignored.

EVALUATION OF HYDROFRACTURING THRESHOLDS DURING SUSTAINED SUBSURFACE INJECTION OF LIQUID WASTES

Claude M. Sauveplane

INTRODUCTION

Compared to other waste disposal methods, deep waste disposal is considered to have the advantages of isolating wastes in a confined aquifer well below the horizon of human activity and potable groundwater resources. Most injected wastes move laterally in the injection zone; however, vertical migration is possible through permeable vertical conduits such as fractures and improperly abandoned wells. Of particular concern is the fracturing associated with the injection operation itself. If vertical fractures propagate all the way up to the shallow aquifers used as a source of water, then contaminant migration becomes a very real possibility. Thus, in assessing the local effects of deep waste injection in the Cold Lake area, it is necessary to evaluate the fracturing thresholds of various rocks and subsequently to compare them with predicted pressure (hydraulic head) buildups.

In reservoir engineering, hydraulic fracturing is a current practice; its objective is to increase the value of near-wellbore hydraulic parameters. It is environmentally acceptable when carried out in a controlled manner and at a relatively localized scale. It has been proposed and experimented some forty years ago. Because it is an important operation in the exploitation of oil and gas reservoirs, much research has been conducted to improve its efficiency, for example, with regard to the use of special fracturing fluids and propping agents that keep the fracture open once the pressure stimulus has ceased. The technology is well summarized in Howard and Fast (1970).

For the purpose of this study, the problem is that massive hydraulic fracturing may result from long-term, constant-rate injections that induce pressure buildups above the breakdown (or fracture) pressures of the injection zones (large scale hydrofracturing). Potential upward conduits for undesirable substances may then develop in the overlying strata damaging their integrity and modifying the flow conditions.

Hydraulic fractures are most frequently vertical. As shown on figure 19A, the length L, the width W and the height H are the geometric characteristics of a vertical hydraulic fracture. The variations of pressure with time for a typical fracturing operation are shown schematically in figure 19B, although it is common to experience differences with this trend of pressure variations.

The breakdown pressure (P_b) is the reference measurement in most low-volume hydraulic fracturing experiments ("Mini-Frac"): it is the only parameter that can be easily measured and permits comparisons between predictions and reality. Whenever they can be measured, a combination of P_b and ISIP allows the evaluation of in situ horizontal stresses around the wellbore under reasonable assumptions. Risks are high in the method of hydraulic fracturing: only half of the operations occur as planned and even when the fractures develop as predicted, the operation is not necessarily beneficial to hydrocarbon recovery. This, together with the costs involved, explains why results of frac tests are not more commonly available (executed and reported in the public domain).

Figure 20 is a classical plot of the fracturing gradient FG (kPa/m) with depth based on many measurements in the U.S.A. Figure 20 also shows that the variation of FG with depth changes at about 600-800 m, beyond which it usually remains less than 23 kPa/m, and commonly around 16 kPa/m. This can be interpreted using a model of tension failure. This interpretation has not been verified at depths greater than 4 km. A fracture that develops vertically may cross rocks of different lithology; its behaviour at the interface depends typically on the depth. At shallow depth, one may find a "sliding" of the fracture at the interface and no further vertical propagation. This mechanism does not occur at intermediate to greater depths, where the fracture propagates beyond the interface.

In addition to this brief overview, two points are worth noting:

1. the hydraulic properties of the host injection zones are usually such that subsurface disposal wells are completed in formations of greater permeability than the usual "recipients" of hydrofracturing in oil and gas production;

A.

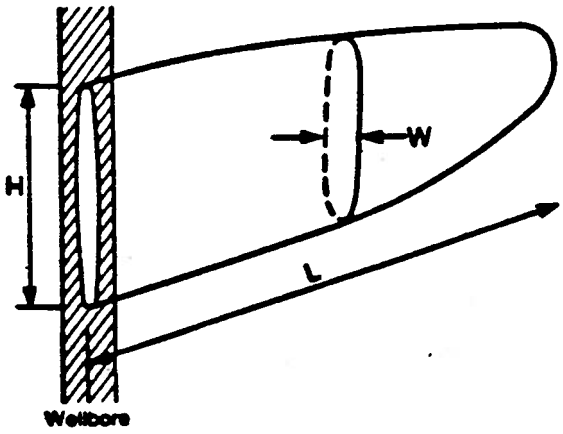

B.

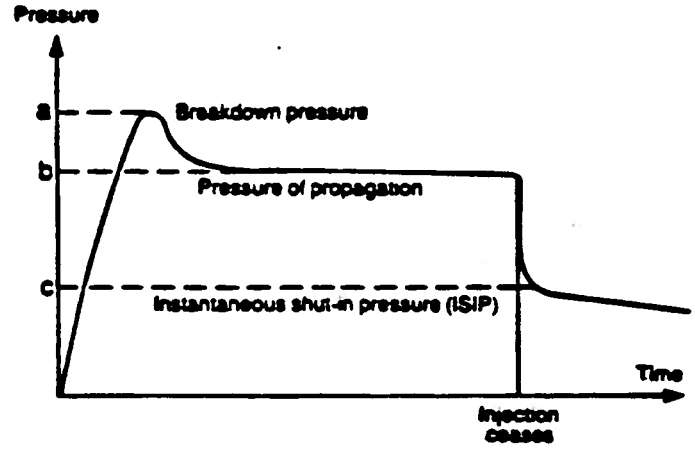

a. The pressure peak that defines the breakdown pressure P_b may not be apparent;
b. The pressure of propagation is not constant: it tends to fluctuate slightly;
c. ISIP or "closing pressure" may be difficult to determine with sufficient accuracy.

Figure 19 A. Schematic section of a hydraulic (vertical) fracture.
B. Example of pressure variation during hydrofracturing

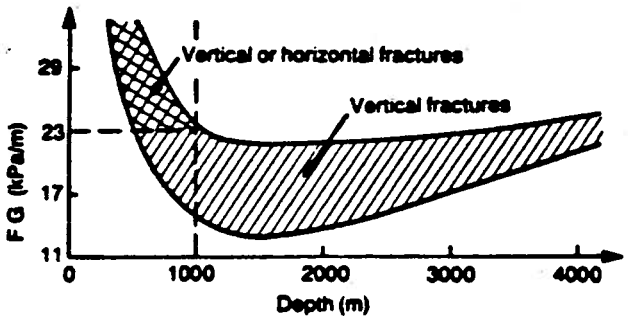

F G :the fracturing gradient indicates the variation of breakdown pressure with depth

Figure 20 Variation of fracturing gradient with depth

2. in spite of the impressive amount of knowledge developed concerning hydrofracturing, much remains to be understood in the conceptual and predictive aspects. It remains a fairly complex process and a highly non-linear mathematical problem. Both fracture initiation and propagation are difficult to predict accurately, mostly because of the unavailability of in situ measurements of some key geomechanical properties and initial stress regime.

The objective of this section is to assess (and eventually develop) techniques for evaluating, as accurately as possible, breakdown pressures for twelve injection zones that have been selected for local evaluation in the Cold Lake area. Only publicly available data are used and this is a constraint that should be kept in mind.

The problem belongs to the general class of "coupled problems" in earth sciences (coupling of fluid flow components with stress/strain relations) and thus requires a multidisciplinary approach (geology, hydrogeology and geomechanics). Because the problem is not commonly considered by hydrogeologists studying subsurface injection of liquid wastes, this section contains all the necessary details to be fully comprehensive, especially in the area of geomechanics.

IN SITU STRESS REGIME AND FAILURE CRITERIA

Because of the crucial lack of in situ measurements of the stress regimes, classical theories for evaluating breakdown pressures assume that:

i) one of the principal stresses is vertical,
ii) the horizontal field of stress is isotropic,
iii) stress increases linearly with depth.

Following the work of Haimson (1968), it is possible to interpret fracturing pressure charts of low-volume hydrofracturing operations ("Mini-Frac" tests) and these analyses reveal that while assumption i) is still satisfactory, in practice assumptions ii) and iii) are rarely verified: stress may vary by a few hundred kilopascals from one stratum to another at a given site, and horizontal stresses are rarely isotropic.

In a purely elastic model, the overburden stress (which equals the weight of the overlying rocks above a given point) generates horizontal stresses in a simplistic fashion that does not take into account the geological history and nature of the stratum from the tectonic, lithologic (diagenetic) and even anthropogenic points of view (Warpinski et al., 1985).

In terms of tension failure, hydrofracturing implies that the fracture develops perpendicular to the lesser principal stress; this lesser stress is most frequently in the horizontal plane and this explains the common generation of a vertical fracture.

The compressive stress regime in a sedimentary basin can be resolved into three orthogonal stresses applied at any point of the basin; the maximum stress S_1, the intermediate stress S_2, and the minimum stress S_3. Stress is pressure, force per unit area, and always acts normal to a selected plane. In the Cold Lake area, and at the local scale of the injection sites, one can assume the following conditions: the strata are horizontal; the topography is flat; and horizontal strains are small and negligible. If, in addition, the elastic theory is applicable, then the maximum principal stress S_1 is vertical and equal to the weight of the overlying rocks or:

$$S_1 = S_v = g\int_0^D \rho_b\,(z)\,dz \qquad (13)$$

where ρ_b is the bulk density of rocks, g is the gravity acceleration, D is the depth from ground surface to the point of interest, and z is a dummy variable of integration. It is presently accepted that the minimum principal stress in the horizontal plane has a determining influence on the height of the vertical fracture. Also, its upward propagation would be more confined by overstress zones than by a change of geomechanical properties at the interface with the overlying stratum.

The type of relevant geomechanical properties for the injection zone and "confining" layer depend on the mechanical model used in the evaluation of fracture propagation. The most commonly used theory is limited to an elastic, brittle failure, and a linear process operating in isothermal conditions. Therefore, the rocks are characterized by:

- Young modulus E
- Poisson's ratio μ
- a failure criterion usually related to the minimum energy required to create a fracture plane.

Often, one considers the shear modulus G related to E and μ by:

$$2G = E/(1 + \mu) \qquad (14)$$

For the failure criterion, one should distinguish the first phase of hydrofracturing, which consists of rupture of the rock around the injection well followed by initiation of a fracture, from the second phase that is concerned with fracture propagation. The first phase is governed by the tensile strength of the rock which has to be overcome in the failure criterion; considerations of energy balance are to be used for the second phase of fracture propagation but this is beyond the scope of the present study. Tensile strength is defined as the maximum possible stress supported by a solid in simple tension. In non-fractured but fragile rocks (e.g. a poorly consolidated sandstone) this stress corresponds to a decohesive failure along a plane perpendicular to the applied tension. If the rock is naturally fractured (this includes the presence of joints and/or micro-fractures) tensile strength cannot be adequately defined because of the superposition of propagation along existing cracks, in addition to the decohesive process. This explains why laboratory measurements of tensile strength show wide variations. The "Brazilian test" (indirect tensile testing), however, gives the closest values when measuring decohesive failure. Different ranges can be obtained when other laboratory methods are used. Analysis of data given by Lama and Vutukuri (1978) for the tensile strength T (MPa) is presented in table 8. Where the "Brazilian test" data only are considered, one can use:

Table 8.
Range of variation of the tensile strength T (MPa), after Lama and Vutukuri (1978)

Material	No. determinations	Tensile Strength		
		Minimum	Average	Maximum
Sandstone	94	0	10	28
Limestone	84	3.4	13	22.5
Dolomite	6	2.6	6	10
Siltstone	17	0	14	28
Shale	26	0	5.5	12
Salt/Gypsum	12	0	1.5	2

Consolidated sandstone	$3 \leq \bar{T} \leq 5$
Massive limestone	$10 \leq \bar{T} \leq 15$
"Soft" limestone	$1 \leq \bar{T} \leq 1.5$

The rocks considered in the present study have a matrix porosity and contain pressured fluids; in these conditions it is necessary to define the total stress S_{ij} which would be transmitted by the dry rock, the pore pressure P_f and the effective stress σ_{ij}. In an elastic medium, total and effective stresses are related by (Biot, 1941):

$$\sigma_{ij} = S_{ij} - \alpha P_f \delta_{ij} \qquad (15)$$

where $\alpha = 1 - C_r/C_b$ and C_r = rock compressibility, C_b = bulk compressibility. The coefficient α is often called "Biot's poroelastic constant" because it increases with the rock porosity. It is commonly assumed to be 1 for aquifers and zero in non-porous rocks. In equation 15, δ_{ij} is the Kronecker delta, S_{ij} represents the total stress tensor acting on an element of the fluid-filled porous medium (i face, j direction).

Let us substitute for the real medium an elastic medium which is infinite, homogeneous and isotropic, with a Poisson's ratio μ and a homogeneous, two-dimensional, but anisotropic stress regime ($S_{H\,max}$, $S_{H\,min}$). Let us assume that this elastic medium has a circular opening (the well). If the centre of the coordinates is at the well axis and the abscissa axis is coincident with the $S_{H\,max}$ direction, one may identify a point of the medium by its polar coordinates (r,θ).

If P is the fluid pressure at the wall of the wellbore, it can be verified that :

$$S_r = P$$
$$S_\theta = S_{H\,max} + S_{H\,min} - 2\,(S_{H\,max} - S_{H\,min})\cos 2\theta - P \qquad (16)$$

in an impermeable medium with S_θ minimum for $\theta = 0$, and:

$$\sigma_r = 0$$
$$\sigma_\theta = \sigma_{H\,max} + \sigma_{H\,min} - 2(\sigma_{H\,max} - \sigma_{H\,min})\cos 2\theta - (1+\mu)(P-P_f) \qquad (17)$$

in a permeable medium with σ_θ minimum again for $\theta=0$. The effective principal (horizontal) stresses "at infinity" are $\sigma_{H\ max}$ and $\sigma_{H\ min}$. Their values are therefore independent of time and can be expressed by :

$$\begin{aligned} \sigma_{H\ max} &= S_{H\ max} - P_f \\ \sigma_{H\ min} &= S_{H\ min} - P_f \end{aligned} \qquad (18)$$

assuming $\alpha=1$.

Using the elastic theory, and assuming that the criterion of tensile strength is a valid one for fracture initiation, the fracture direction is perpendicular to the maximum tension, that is, to the minimum in situ stress in this case.

If failure occurs when the minimum tangential stress S_θ is such that $(S_\theta)_{min} + T = 0$ for $P = P_b$, then:

$$P_b \geq (3\ S_{H\ min} - S_{H\ max} + T) \qquad (19)$$

for an impermeable medium, and:

$$(P_b - P_f) \geq (3\sigma_{H\ min} - \sigma_{H\ max} + T)/(1 + \mu) \qquad (20)$$

for a permeable medium.

Equation 19 is the same as that derived by Hubbert and Willis (1957) and later used by Bredehoeft et al. (1976). It assumes "a non-penetrating fluid in a tectonically relaxed area having reasonably gentle topography, where it can be assumed that the maximum principal stress is vertical and collinear with the axis of the borehole" (Bredehoeft et al., 1976, p. 251).

According to Haimson and Fairhurst (1969), when α is different from unity but not nil, the denominator of equation 20 is:

$$2 - \alpha\ \frac{1 - 2\mu}{1 - \mu}$$

which yields $1/(1 - \mu)$ rather than $(1 + \mu)$ when $\alpha = 1$. Only when μ is small, are the two expressions approximately equivalent.

Assuming that $\sigma_{H\ min}$ = ISIP, which is not a unanimously accepted hypothesis (Nolte, 1984), then equation 20 can be used to determine the effective horizontal stress field from the data of a "Mini-Frac" test:

$$\sigma_{H\ min} = ISIP$$
$$\sigma_{H\ max} = 3\ \sigma_{H\ min} - (1 + \mu)(P_b - P_f) + T \qquad (21)$$

where $(P_b - P_f)$ is the pressure measured at the wellhead at failure if the well loss are neglected. Equation 21 also suggests that $\sigma_{H\ max}$ will not be as accurately determined as $\sigma_{H\ min}$ because of the assumptions that have to be made on the values of μ and T for the tested interval.

Equation 19 represents the usual basic equation for evaluating breakdown (or fracture) pressures.

CLASSICAL EVALUATION OF BREAKDOWN PRESSURES

Examination of equations 19 or 20 reveals that, even with assumptions on the values of the intrinsic properties μ and T, the evaluation of P_b requires knowledge of the horizontal principal stress field. In the absence of "Mini-Frac" test results, and for the purpose of this study, additional assumptions have to be made in order to arrive at a working method to evaluate P_b.

The most common assumption is to impose a horizontal constraint, that is, the strains in x and y directions are equal and nil. In this case, Biot's stress/strain relations can be solved, noticing that $\mu=\lambda/2(G+\lambda)$ where λ is the Lame constant and assuming a horizontal isotropic stress field, yielding:

$$\sigma_{H\ min} = \sigma_{Hmax} = \frac{\mu}{(1 - \mu)}\ \sigma_v \qquad (22)$$

where σ_v is the vertical effective stress.

Denoting the total vertical stress by S_v as in equation 13, and assuming $\alpha = 1$, Eaton (1969) combined equations 22 and 19 to first obtain:

$$S_{H\ min} = \frac{\mu}{(1 - \mu)}\ (S_v - P_f) + P_f \qquad (23)$$

and then:

$$P_b \geq \frac{\mu}{1 - \mu} (S_v - P_f) + P_f \qquad (24)$$

The derivation of equation 24 assumes that $T = 0$ and that the failure criterion is simply $P_b \geq S_{H\ min}$ and not what equation 19 would yield with $T = 0$, which is $P_b \geq 2S_{H\ min}$. Using $\mu = 1/4$ in equation 24 yields the equation recommended by Hubbert and Willis (1957):

$$P_b \geq (S_v + 2\ P_f)/3 \qquad (25)$$

Anderson et al. (1973) have proposed another equation for the Gulf Coast area noticing that, for weakly cemented sandstones, the formation cannot withstand a positive strain in the tangential direction of the borehole. This means that the nil effective tangential stress in Biot's sense (α not equal to 1 or 0) is the failure criterion, which corresponds to $T + \alpha P_f = 0$. Combining equation 15, 19 and 22 and rearranging, it is easy to prove that:

$$P_b \geq \frac{2\mu}{1 - \mu} S_v + \frac{1 - 3\mu}{1 - \mu} \alpha P_f \qquad (26)$$

is another form of the same failure criterion. Anderson et al. (1973) recommend the use of $\alpha \simeq \phi_D$ where ϕ_D is the porosity from density logs; for μ, they suggest the use of an area-dependent linear relation between μ and a "shale index" defined by $(\phi_s - \phi_D)/\phi_s$, where ϕ_s is the sonic log porosity. The coefficients of this linear relation require data from "Mini-Frac" tests.

Discussion

Equation 26, although more accurate than equation 24, is often criticized for the suggested evaluations of α and μ, which are viewed as unrealistic. Equation 24, Eaton's equation, is not based on a realistic failure criterion and is more empirical than equation 26. Both

equations assume an isotropic horizontal stress field. In spite of these limitations, both equations are commonly used. They make use of the relation expressed by equation 22 which clearly stipulates that the weight of the overlying rocks is the only source of stress and the horizontal elongations are nil. According to Jaeger and Cook (1976), it is reasonable to assume that even in the absence of tectonic structures and seismicity, a region must be subject to some tectonic stress; they suggest the existence of a superposed horizontal stress S_t increasing uniformly with depth or σ_v. It has been demonstrated that reverse faulting must occur when the horizontal effective stress becomes about three times greater than the vertical effective stress (Hubbert, 1945). If there is no superposed tectonic stress, then the relation of equation 22 may accurately represent a minimum horizontal effective stress $\sigma_{H\ min}$. It is, therefore, legitimate to define S_t as:

$$0 \leq S_t < 3\sigma_v - \frac{\mu}{1-\mu}\sigma_v = \frac{3-4\mu}{1-\mu}\sigma_v \qquad (27)$$

Actual estimation of in situ tensile strengths is very difficult, if not impossible, but one can make the assumption that any interval of sedimentary rock is intersected by natural discontinuities (joints and partings) across which the tensile strength T is effectively zero. However, this is not a very accurate assumption except for some specific zones or lithologies. Stress release at borehole walls occurring during the drilling process is a well documented phenomenon which generates microcracks and supports this concept of a zero tensile strength.

As a result of this discussion, one may derive a new equation which simultaneously accounts for a nonzero tectonic stress, a horizontal anisotropy of the principal stress regime, and a zero tensile strength.

DERIVATION OF A NEW EQUATION

Starting with the simplest case of a non-penetrating fluid and using the sign convention that tension is positive, one may write a failure criterion as:

$$P_b - P_f \geq S_t + 3\,\sigma_{H\,min} - \sigma_{H\,max} \qquad (28)$$

From a previous argument, $S_t/\sigma_v = K$, a constant that one may determine from a frac test or better from a series of frac tests in a given area. Bell and Babcock (1986) suggest that:

$$S_{H\,max} \simeq 1.5\,S_{H\,min} \qquad (29)$$

in the Alberta portion of the Western Canada Sedimentary Basin. An amazingly similar result is obtained for another sedimentary basin by Bredehoeft et al. (1976). Finally, from the definition of α, we have evaluated the ratio C_r/C_b for the limestone of the Beaverhill Lake aquifer as 3×10^{-5} and for the poorly consolidated sandstones of the Mannville, Clearwater or McMurray aquifers as 1.6×10^{-4}. Therefore, for the Cold Lake study area and the considered injection aquifers of this study, it is legitimate from equation 15 to take $\alpha = 1$. Consequently, one may use the equations 18 for effective stress and rewrite 28 after obvious manipulations as:

$$P_b \geq P_f + K\,\sigma_v + 1.5\,\sigma_{H\,min} - 0.5\,P_f \qquad (30)$$

Assuming horizontal constraint of deformation, one may use equation 22 for a relation between $\sigma_{H\,min}$ and σ_v and after collecting terms, equation 30 becomes:

$$P_b \geq \left[K + \frac{3\mu}{2(1-\mu)}\right]\sigma_v + 0.5\,P_f \qquad (31)$$

otherwise:

$$P_b \geq \left[K + \frac{3\mu}{2(1-\mu)}\right](S_v - P_f) + 0.5\,P_f \qquad (32)$$

It is convenient to write equation 32 as:

$$P_b \geq A\,S_v + B\,P_f \qquad (33)$$

where $A = \left[K + 1.5\ (\mu/1-\mu) \right]$ and $B = (0.5 - A)$

With this formulation, it is easier to compare equation 33 with equation 26 of Anderson et al. (1973). In equation 26, the coefficients for S_v and P_f are $(2\mu/1-\mu)$ and $\alpha\ (1-3\mu)/(1-\mu)$, respectively. Eaton's equation 24 gives $(\mu/1-\mu)$ for the coefficient of S_v, and $(1-2\mu)/(1-\mu)$ for the coefficient of P_f.

ESTIMATION OF THE REQUIRED PARAMETERS AND VARIABLES

This section describes how the above-defined components can be evaluated on the basis of the existing curves of density and sonic logs for the injection intervals considered in this study. An original method is proposed here for a critical parameter, Poisson's ratio.

Poisson's Ratio

In the laboratory, Poisson's ratio is measured under static conditions (uniaxial compression or tension) and by dynamic methods (resonance, ultrasonic testing). Static and dynamic results indicate that the ratio (μ dynamic)/(μ static) varies typically between 1.1 and 1.8 (Balmer, 1953). Although closer to in situ values because of accounting for zones of weaknesses and anisotropies, the dynamic values of Poisson's ratio obtained with laboratory methods on cores are usually less reliable than with acoustic-log derived methods.

The classical approach (Schlumberger's Mechanical Properties Log (MPL)) to evaluate Poisson's ratio from acoustic logs is to use the empirical relation between Δt_p and Δt_s proposed by Pickett (1963) for typical lithologies, where Δt_p is the transit time for compressional wave velocity measured with the acoustic log, and Δt_s is the transit time for shear wave velocity. When Δt_s is deducted from Δt_p with Pickett's proposed relations, then Poisson's ratio is calculated with:

$$\mu = \frac{1-2R^2}{2(1-R)^2} \qquad (34)$$

where $R = (\Delta t_p / \Delta t_s)$.

One should be aware that this method can be seriously inaccurate because the recognition of shear wave arrivals in most sedimentary sections is generally impossible. Pickett's relations can induce significant errors in the evaluation of μ (McLennan et al. 1982) and this is a weak link in the procedure.

In the Cold Lake area, there are insufficient "Mini-Frac" test results and/or MPL data to evaluate in situ values of Poisson's ratio for the injection intervals. Yet, the error introduced in the evaluation of breakdown pressures can be significant as shown below for typical values of Poisson's ratio:

$\mu = 0.10$	$\mu = 0.20$	$\mu = 0.30$
$P_b = 5.73$ MPa	$P_b = 7.40$ MPa	$P_b = 9.54$ MPa

These values of P_b are calculated using equation 33 and $S_v = 12$ MPa, $P_f = 4$ MPa and $K = 0.3$. Similar discrepancies can be obtained with equations 24 or 26. Dusseault and Simmons (1982) discuss properties of the material that constitute the bulk of the injection aquifers in the Cold Lake area and suggest the (reasonable) values shown in table 9.

Application of the above MPL technique for a sandstone would give a value of $\mu = 0.15$ with a typical compressional transit time of $\Delta t_p = 200$ μs/m, which is an important underestimation of the above values for μ.

Alternately, if the pairs of geomechanical parameters suggested by Dusseault and Simmons (1982) are approximately correct for the studied injection aquifers, one may devise another method for evaluating Poisson's ratio.

Starting from the well-established relation (Lama and Vutukuri, 1978, vol. II, p. 196):

$$\rho_b / (\Delta t_p)^2 = E \frac{(1 - \mu)}{(1 + \mu)\ (1 - 2\mu)} \qquad (35)$$

where ρ_b is the bulk density, one may combine data from digitized density and acoustic logs of the injection intervals to compute the left hand side

Table 9.
Geomechanical parameters suggested by Dusseault and Simons (1982) for the Cold Lake area.

Aquifer	Poisson's ratio μ	Dynamic Young's modulus E (GPa)
Mannville	0.35	6.8
Clearwater	0.35	7.1
McMurray	0.32	11.0
Beaverhill Lake	0.25	34.7

of equation 35 and then use a reasonable value (or a range of values) for E to solve equation 35 for μ. This new method has been applied using the data given by Dusseault and Simmons (1982): $6 \leq E \leq 11$ GPa for the poorly consolidated sandstones of the Mannville, Clearwater and McMurray aquifers, and $15 \leq E \leq 25$ GPa for the limestone of the Beaverhill Lake aquifer. An example of density and acoustic curves used in this analysis is presented in figure 21. In the absence of available geophysical logs for the Lower Paleozoic aquifer system, literature values of the static Poisson's ratio have been used; it is felt that the error introduced should be minimal for a well-consolidated sandstone at the greater depths of injection in this aquifer.

Poisson's ratio was automatically calculated using this method, applied to the actual intervals, or to equivalent intervals when no log was available at the specific injection well. The numerical values and the range of Poisson's ratio are summarized in table 10 which also contains an average value recommended for the injection interval.

Overburden Stress and Initial Pore Pressure

Calculation of the definite integral of equation 13 is done automatically on the basis of either actual density/depth curve or users' supplied average values for missing intervals. Average values are obtained from neighbouring wells at equivalent elevations. The overburden stress S_v is calculated at the midpoint of the injection interval. The results of the calculations are summarized in table 11. It can be verified that these results are substantially less than the predictions obtained with the commonly used average lithostatic gradient of 22.62 kPa/m (1 psi/ft) or even with a more experimental regression relation based on the data of Bell and Babcock (1986) given in column (B) of table 11.

Pore pressures are back-calculated from either measured or computed values of hydraulic heads at the site as a result of the previous part of the hydrogeological study (Basin Analysis Group, 1987).

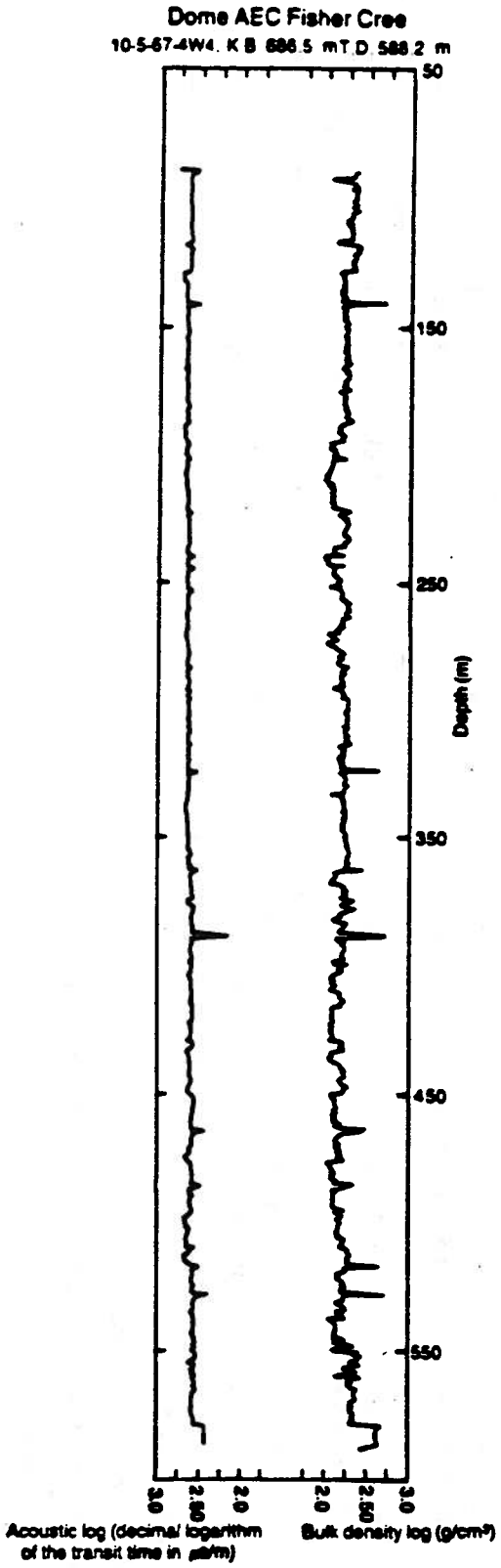

Figure 21 Example of acoustic and density logs used in this study

Table 10.
Estimation of Poisson's ratio for rocks at selected injection sites

Operator Name/ Injection Aquifer	Location	Interval Depths (m) and Dominant Lithology	Mean "Static (Laboratory) Poisson's Ratio"	Standard Deviation for "Static (Laboratory) Poisson Ratio"	"Dynamic Poisson's Ratio"		Recommended "Dynamic Poisson Ratio"
					For E=6GPa*	For E=11GPa*	
Westmin/Mannville (A)	11-1-55-5-W4	512-524 (L.SS.)	0.19 (117)	0.10	0.424	0.326	0.375
Westmin/Mannville (B)	11-1-55-5-W4	558-567 (L.SS.)	0.19 (117)	0.10	0.426	0.327	0.376
Westmin/Beaverhill Lake	3-13-55-6-W4	634-700 (LIME.)	0.24 (152)	0.07	0.391**	0.262***	0.322
Murphy/Mannville	6-13-50-5-W4	609.4-611.7 (L.SS.)	0.19 (117)	0.10	0.404	0.261	0.328
Murphy/Beaverhill Lake	6-13-50-5-W4	684.1-696.6 (LIME.)	0.24 (152)	0.07	0.391**	0.262***	0.322
Suncor/Clearwater	6-28-61-4-W4	412-458 (L.SS.)	0.19 (117)	0.10	0.394(4)	0.205(4)	0.299
Suncor/McMurray (A)	6A-28-61-4-W4	443.8-462.3 (L.SS.)	0.19 (117)	0.10	0.397(4)	0.219(4)	0.308
Suncor/McMurray (B)	6A-28-61-4-W4	499.6-502.6 (L.SS.)	0.19 (117)	0.10	0.403(4)	0.242(4)	0.322
BP/Mannville	8-7-66-5-W4	422.5-440.7 (L.SS.)	0.19 (117)	0.10	0.400(10)	0.230(10)	0.315
BP/Lower Paleozoic	10-8-66-5-W4	1321-1329 (SS.)	0.19 (117)	0.10	[0.29]	[0.09]	[0.19]
Dome/McMurray	10-5-67-4-W4	468.5-487.0 (L.SS.)	0.19 (117)	0.10	0.402	0.243	0.323
Dome/Lower Paleozoic	10-5-67-4-W4	1302-1320 (SS.)	0.19 (117)	0.10	[0.29]	[0.09]	[0.19]

L.SS. - Poorly consolidated sandstone
SS. - Sandstone
LIME. - Limestone (massive)/shaley limestone

* E = "Dynamic" Young Modulus. $6 \leq E \leq 11$GPa for poorly consolidated sandstone
** for "soft" case, with E = 15GPa
*** for "stiff" case, with E = 25GPa
( ) number of values averaged
[ ] values estimated (no geophysical logs available)

Table 11.
Estimation of overburden stress at selected injection sites.

Operator Name/ Injection Aquifer	Location	Estimated[1] Pore Pressure (MPa)	Depths to Mid-Points of Injection Intervals (m)	Overburden[2] Stress from empirical correlation with depth (MPa)	Overburden[3] Stress from integration of density logs (MPa)
Westmin/Mannville (A)	11-1-55-5-W4	3.75	518.3	12.84	10.91
Westmin/Mannville (B)	11-1-55-5-W4	4.28	562.5	13.92	11.89
Westmin/Beaverhill Lake	3-13-55-6-W4	5.30	682.0	16.95	14.68
Murphy/Mannville	5-13-58-5-W4	3.30	510.5	12.65	10.49
Murphy/Beaverhill Lake	5-13-58-5-W4	4.11	596.5	14.81	12.38
Suncor/Clearwater	5-28-61-4-W4	3.35	435.0	10.75	9.21
Suncor/McMurray (A)	5A-28-61-4-W4	3.36	448.0	11.08	9.49
Suncor/McMurray (B)	5A-28-61-4-W4	3.88	501.0	12.41	10.68
BP/Mannville	8-7-66-5-W4	2.83	440.7	10.90	9.02(3)
BP/Lower Paleozoic	10-8-66-5-W4	11.66	1325.0	33.08	29.40(4)
Dome/McMurray	10-5-67-4-W4	2.78	540.0	13.39	11.26
Dome/Lower Paleozoic	10-5-67-4-W4	11.06	1311.0	32.73	29.24

[1] using regular grid values of freshwater hydraulic heads

[2] S_v (MPa) = 2.509×10^{-2} D(m) - 0.16065 (inferred from Bell and Babcock, 1986), where S_v is the overburden stress and D is the depth

[3] using best estimates for bulk density when logged intervals are missing (Appendix A)

( ) number of values averaged from neighbouring locations

Constants α and K

As suggested by Anderson et al. (1973), who derived equation 26, α is evaluated as ϕ_D, the density log porosity, which is calculated with:

$$\alpha = \phi_D = \frac{\rho_b - \rho_{ma}}{\rho_w - \rho_{ma}} \qquad (36)$$

where ρ_{ma} is the dry matrix density, ρ_w is the pore fluid density and ρ_b is the bulk density derived as an average for the injection interval. For ρ_{ma}, we use the mean values of hundreds of laboratory measurements given in Lama and Vutukuri (1978), i.e. 2434 kg/m^3 for sandstone and 2500kg/m^3 for limestone. For ρ_w, we use the regional average values of in situ formation water densities evaluated in the previous phase of the study (Basin Analysis Group, 1987). The results of the calculations for the coefficient α are presented in table 12 for selected sites in the Cold Lake area.

The determination of the tectonic stress constant K for use in equation 33 is based on the single value of fracture pressure resulting from a "Mini-Frac" test and publicly available in the Cold Lake study area (Bell and Babcock, 1986, table 2). Using values for P_f and μ inferred from the neighbour BP/Mannville site (see tables 8 and 9, respectively) and using the reported values for S_v (11.25 MPa) and P_b (9MPa), it is found K=0.27 as a back-calculation of equation 32. This value has been used for all the calculations of breakdown pressures, calculations based on equation 33 derived in this study. Table 11 presents, for comparison purposes, the values of the breakdown pressure P_b calculated using equations 24 (Eaton's), 26 (Anderson's) and 33.

CRITICAL HYDRAULIC HEAD BUILDUPS

An interpretative "blend" of the results for breakdown pressures of table 12 is given in terms of "recommended hydraulic head buildups ΔH to preclude fracturing" in table 13. Three values are presented as a range

Table 12.
Estimation of breakdown pressures (P_b in MPa) for rocks at selected injection sites

Operator Name/ Injection Aquifer	Location	Results from Eaton's Equation 24		Results from Anderson et al. Equation 26			Results from Equation 33	
		$\bar{P}_b$	Range of P_b	α	$\bar{P}_b$	Range of P_b	$\bar{P}_b$	Range of P_b
Westmin/Mannville (A)	11-1-55-5-W4	8.05	7.21- 9.02	0.21	12.93	10.58-15.69	10.27	9.02-11.74
Westmin/Mannville (B)	11-1-55-5-W4	8.87	7.98- 9.90	0.18	14.17	11.58-17.20	11.10	9.76-12.65
Westmin/Beaverhill Lake	3-13-55-6-W4	9.75	8.46-11.32	0.14	13.98	10.13-18.65	11.89	9.95-14.24
Murphy/Mannville	5-13-58-5-W4	6.81	5.71- 8.17	0.25	10.26	7.30-13.93	8.88	7.23-10.92
Murphy/Beaverhill Lake	5-13-58-5-W4	8.04	6.90- 9.42	0.15	11.79	8.55-15.72	10.20	8.49-12.28
Suncor/Clearwater	5-28-61-4-W4	5.85	4.86- 7.16	0.26	7.98	5.16-11.72	7.02	5.54- 8.99
Suncor/McMurray (A)	5A-28-61-4-W4	6.09	5.08- 7.40	0.26	8.54	5.70-12.22	7.45	5.93- 9.41
Suncor/McMurray (B)	5A-28-61-4-W4	7.11	6.05- 8.47	0.20	10.18	7.09-14.16	8.64	7.05-10.68
BP/Mannville	8-7-66-5-W4	5.68	4.82- 7.00	0.15	8.33	5.95-11.98	7.35	5.88- 9.29
BP/Lower Paleozoic	10-8-66-5-W4	15.82	13.42-18.91	0.04*	14.06	6.21-24.11	16.91	13.30-21.64
Dome/McMurray	10-5-67-4-W4	6.83	5.50- 8.48	0.22	10.77	7.44-14.93	9.77	7.79-12.26
Dome/Lower Paleozoic	10-5-67-4-W4	15.32	12.86-18.48	0.04*	13.97	6.16-23.97	16.89	13.19-21.63

$\bar{P}_b$: mean value obtained for the breakdown pressure
* estimated

Table 13.
Evaluation of fracturing thresholds using equation 33: maximum hydraulic head buildups to preclude fracturing (in equivalent freshwater head, m)

Operator Name/ Injection Aquifer	Location	Midpoint Elevation of Injection Intervals (m)	Initial Freshwater Hydraulic Head (m)	Recommended Maximum Buildups (m)		
				$(\Delta H)_{min}$	$(\Delta H)_{best}$	$(\Delta H)_{max}$
Westmin/Mannville (A)	11-1-55-5-W4	+95.7	478.5	438	537	664
Westmin/Mannville (B)	11-1-55-5-W4	+42.4	478.5	468	559	696
Westmin/Beaverhill Lake	3-13-55-6-W4	-38.7	502.0	322	474	672
Murphy/Mannville	5-13-58-5-W4	+140.5	476.5	358	570	710
Murphy/Beaverhill Lake	5-13-58-5-W4	+54.7	474.0	400	541	620
Suncor/Clearwater	5-28-61-4-W4	+123.1	465.0	255	374	472
Suncor/McMurray (A)	5-28-61-4-W4	+108.5	451.0	278	417	528
Suncor/McMurray (B)	5-28-61-4-W4	+55.5	451.0	329	486	642
BP/Mannville	8-7-66-5-W4	+208.3	497.0	291	460	560
BP/Lower Paleozoic	10-8-66-5-W4	-681.0	508.0	424	535	739
Dome/McMurray	10-5-67-4-W4	+145.6	429.0	413	511	713
Dome/Lower Paleozoic	10-5-67-4-W4	-624.4	504.0	296	594	756

of ΔH and are essentially based on ranges of Poisson's ratio. The use of a low estimate for ΔH refers to the most conservative and secure prediction for fracture initiation, given all the uncertainties previously discussed.

In order to illustrate the use of table 13, the Theis analytical solution has been applied to calculate the buildups at a well fully penetrating the Lower Paleozoic aquifer system at the BP injection site. The calculations are performed for a constant period of injection, 10 a, at the actual constant injection rate of Q=3335 m^3/d and at two hypothetical values of 1000 and 1500 m^3/d. The test is run for a hydraulic conductivity of 0.11 m/d, a specific storage of 2.8×10^{-4} m^{-1} and an aquifer thickness of 34.5 m; the calculations are made at 1 m from the wellbore axis. Table 14 illustrates that for Q=1000 m^3/d, the low estimate $(\Delta H)_{min}$ of the critical fracturing buildup is not reached during the entire period of injection (10 a). At 1500 m^3/d, the same low estimate would be reached after about 2.5 a (912.5 d) but the best estimate recommended by this study is not yet reached for the entire simulation period. At the operating rate of Q=3335 m^3/d, the best estimate $(\Delta H)_{best}$ is reached after less than 5 d and the maximum estimate $(\Delta H)_{max}$ after one month. It is concluded that for 10 a of injection, the safest rate is slightly above 1500 m^3/d in order to avoid fracturing.

A trial and error method can be used in order to determine maximum values of injection rates that would preclude fracturing. Preliminary results with analytical solutions (accounting for partial penetration of the well in the aquifer) can be used to "approach" these values of injection rates. Then, the more sophisticated use of a numerical model could account for potential interferences between injection zones and leaky boundary conditions. This refinement is necessary to conclude the trial and error process that evaluates the maximum injection rate in order to avoid fracturing. Such fracturing would be vertical in all cases considered, given the in situ stress regime in the Cold Lake area (Bell and Babcock, 1986). To remain on the conservative side, $(\Delta H)_{min}$ could be used in estimating the critical injection rates.

In the case when fracturing cannot be avoided and is *de facto*

Table 14.
An example of the use of breakdown pressure estimations
BP/Lower Paleozoic aquifer system: Theis analytical model

Time (d)	Hydraulic Head Buildup (m) using Theis equation Q=1000 m^3/d	Q=1500 m^3/d	Q=3335 m^3/d (actual rate)	
1.0	141.143	211.714	470.711	
5.0	174.577	261.865	582.213	$(\Delta H)_{best}$=535
10.0	188.979	283.469	630.245	
30.0	211.807	317.711	706.378	
60.0	226.211	339.316	754.413	$(\Delta H)_{max}$=739 m
180.0	249.040	373.560	830.549	
270.0	257.466	386.199	858.648	
365.0	263.730	395.596	879.541	
547.5	272.156	408.234	907.640	
730.0	278.134	417.201	927.577	
912.5	282.771	424.156	943.041	
1095.0	286.560	429.839 $(\Delta H)_{min}$=424 m	955.676	
1277.5	289.763	434.644	966.359	
1460.0	292.538	438.807	975.613	
1642.5	294.985	442.478	983.776	
1825.0	297.175	445.762	991.077	
2190.0	300.963	451.445	1003.710	
2555.0	304.167	456.250	1014.400	
2920.0	306.941	460.412	1023.650	
3285.0	309.389	464.083	1031.810	
3650.0	311.578	467.367	1039.110	

$(\Delta H)_{min, best, max}$ are taken from table 17

initiated, additional modelling should be conducted to predict the propagation of the fracture, especially at the level of lithological interfaces where the geomechanical properties change and where farther upward propagation might be stopped. Azimuths of fracture propagation may be inferred from Bell and Babcock (1986). Preliminary modelling of fracture propagation can be done using, for example, the analytical but approximate solutions of Nordgren (1972). More accurate modelling requires the use of three-dimensional simulators (Chouet, 1986; Settari and Cleary, 1984). Appreciation of fracture penetration through an interface can be made from Biot et al. (1983) and Labudovic (1984).

CONCLUSIONS

Because of their importance in the evaluation of safe subsurface injection of liquid wastes in the Cold Lake area, a detailed analysis of possible breakdown pressures has been conducted. New methods of evaluating the breakdown pressure and the required Poisson's ratio are proposed and applied for twelve selected injection sites. Anisotropic horizontal stress field, superposed tectonic stress, as well as accurate calculations of overburden stresses are incorporated; evaluation of Poisson's ratio does not require the intermediate knowledge of the shear wave transit time. Optimal use of density and acoustic digitized curves from existing geophysical logs supports this new analysis.

In spite of substantial improvements with regard to the commonly used techniques of evaluation of breakdown pressures, the lack of calibrating data from "Mini-Frac" tests explains why the final results of table 13 are expressed in terms of a range of possible values rather than a single value.

NUMERICAL SIMULATION OF LOCAL EFFECTS OF INJECTION

Stefan Bachu

INTRODUCTION

Regional effects of deep waste injection in the Cold Lake area were simulated and reported in the first part of this study (Basin Analysis Group, 1987). The numerical simulations were done on a regional scale for clustered injection sites which were grouped into four model areas: Lower Paleozoic, and northern, central and southern Post-Prairie successions. The main conclusions of the simulations were that there will not be interference between the different injection sites for the projected period of 30 a, and that, for most of the sites, the pressure buildups will probably be below the respective fracturing threshold. However, the above conclusions are subject to the following caveats: (1) there is an uncertainty associated with the determination of aquifer characteristics; (2) the hydraulic conductivity and specific storage values used in simulations are regional and characteristic to the entire Cold Lake area and not to any particular site; (3) no evaluation of fracturing thresholds was specifically performed; and (4) the resolution of finite element modelling at the regional scale is such that the hydraulic head values obtained at FEM nodes represent in reality an area with a radius of 500 to 1000 m. As such, the results of previously reported numerical simulations apply on a regional scale, starting at a distance between 500 and 1000 m from the individual injection wells. The purpose of the present work is to simulate the effects of injection in terms of hydraulic head buildup at selected individual sites, using local values of hydraulic parameters and an FEM grid with a higher resolution. The results of local-scale modelling can then be compared with the respective fracturing thresholds calculated in the previous section.

LOCAL HYDRAULIC PARAMETERS

The theoretical basis of modelling of effects of deep waste disposal in the Cold Lake area in terms of fluid flow and pressure buildups was presented and discussed in the previous part of the study (Basin Analysis

Group, 1987). It was shown through dimensional analysis of the Driving Force Ratio (Davies, 1987) that the buoyancy effects due to variations of formation water density can be neglected. In this case, the flow of formation waters and hydraulic head buildups at injection sites can be modelled using the following partial differential equation:

$$\mathrm{div}[\bar{\bar{K}}\,\mathrm{grad}(H)] - Q = S_s(\partial H/\partial t) \qquad (37)$$

where $\bar{\bar{K}}$ is the hydraulic conductivity tensor, H is freshwater hydraulic head, Q represents the rate of injection, S_s is volumetric specific storage (Bear, 1972), and t is time.

The initial and boundary conditions needed for solving equation 37 are given by the baseline freshwater potentiometric surfaces determined in the hydrogeological section of the study (Basin Analysis Group, 1987). The depths and rates of injection at all 27 sites in the Cold Lake area were presented previously (Basin Analysis Group, 1987, Table 8). Therefore, for the solution of equation 37 it is necessary to know the local values of hydraulic conductivity and specific storage for all hydrostratigraphic units at each individual injection site.

The first task was to find values of hydraulic parameters at the injection wells themselves, to be used in the simulations. However, the latest version (July 1987) of the ERCB data base, installed at the Alberta Research Council and used at the time the work was done, does not contain any information of this type at the particular injection sites and for the formations under consideration. Therefore, the local values of hydraulic parameters had to be estimated based on data within a given distance from the respective sites. This distance had to vary from site to site and/or from formation to formation, depending on data availability.

In most instances, the radius of the data search was of the order of 20 to 30 km, but in a few cases, the lack of data imposed the use of regional values. Also, the number of data found within this radius was on average less than 5 values for aquifers in Paleozoic strata, and between 10 and 20 for aquifers in the Cretaceous. This point is very important in the sense that the values used in the numerical simulations may be more representative for each individual model area around an injection site than the regional values used in the simulations of regional effects of

injection. However, these values may still not be representative close to the injection sites themselves. Overall, there is a question of the representativeness of such a small data sample. Therefore, the results of numerical modelling of local effects of injection have to be considered bearing in mind the uncertainty associated with the determination of aquifer characteristics, particularly the hydraulic head buildup at the nodes representing injection sites.

The values of hydraulic conductivity and specific storage used in the numerical simulations of local effects of injection are presented in table 15 for the respective host aquifer at the selected injection sites. Local values were used for all the hydrostratigraphic units in the succession, but they are not shown because, basically, the effects of injection are limited mainly to the host aquifer, as it will be seen later. The regional values used in previous simulations are also given for comparison purposes. It can be seen that the local values of hydraulic conductivity are greater than the regional ones by a factor varying between 1.4 for the Grand Rapids Formation and 6.7 for the Cooking Lake Formation, except for the Clearwater Formation for which the ratio is 21.6. This means that, according to equation 37, the hydraulic head buildup at the injection sites will be proportionally smaller in the case of local simulations than in the case of regional simulation, if all other elements and parameters are the same (geometry, specific storage and FEM grid). For the specific storage, the ratio between the local values and the regional ones varies between 0.1 at an injection site in the Grand Rapids Formation, and 3.6 for the Basal Cambrian sandstone. No local values were found for the sites in the McMurray Formation and Lloydminster sandstone, and therefore the regional values of specific storage were used in the numerical simulations of local effects of injection at these sites. The variations in specific storage values have a similar effect on the results of numerical simulations as the variations in hydraulic conductivity. Namely, higher specific storage means lower hydraulic head buildup, and vice versa.

It should be mentioned here that the hydraulic conductivity values presented in table 15 are actually values of the horizontal component of the hydraulic conductivity tensor. There were not enough data available to determine local values of the vertical hydraulic conductivity for any

Table 15.

Local versus regional values of hydraulic parameters used in simulation of effects of injection in the Cold Lake area

Site		Local values		Regional values	
Location	Formation	K_h (m/d)	S_s (1/m)	K_h (m/d)	S_s (1/m)
11-1-55-5-W4	Lloydminster	0.10	5.0×10^{-3}	0.035	5.0×10^{-3}
3-13-55-6-W4	Cooking Lake	0.02	5.5×10^{-4}	0.003	4.0×10^{-4}
5-13-58-5-W4	Lower Grand Rapids	0.10	5.0×10^{-4}	0.035	5.0×10^{-3}
5-13-58-5-W4	Cooking Lake	0.02	5.0×10^{-4}	0.003	4.0×10^{-4}
5-28-61-4-W4	Clearwater	0.80	4.0×10^{-4}	0.037	8.0×10^{-4}
6-28-61-4-W4	Cummings	0.10	8.0×10^{-3}	0.027	8.0×10^{-3}
10-8-66-5-W4	Cambrian	0.10	1.0×10^{-3}	0.043	2.8×10^{-4}
8-7-66-5-W4	Grand Rapids	0.05	7.5×10^{-3}	0.035	5.0×10^{-3}
10-5-67-4-W4	Cambrian	0.10	1.0×10^{-3}	0.043	2.8×10^{-4}
10-5-67-4-W4	McMurray	0.10	8.0×10^{-3}	0.027	8.0×10^{-3}

site considered for local simulations. Consequently, the regional values of hydraulic conductivity anisotropy (Basin Analysis Group, 1987, Table 6) were used in the simulations. This aspect has to be considered as well in the context of the degree of confidence in the data used in numerical simulations and in the corresponding results.

It was initially intended to consider the effects of geochemical reactions between injected water, formation water and rocks, on hydraulic parameters such as porosity and permeability (therefore, on specific storage and hydraulic conductivity). Geochemical modelling of water rock interactions (see earlier section) has shown that the effects of silica precipitation and aluminum-bearing silica minerals are negligible over the predicted period of 30 a of deep waste injection. The average saturation index of calcite is negative, indicating that dissolution of calcite in the formation mineralogy would be expected, increasing the local porosity and permeability. With the exception of the Cooking Lake/Beaverhill Formation, the amount of change is expected to be small because calcite is present in trace amounts only. The rapid kinetic properties of calcite indicate that this will occur primarily in the 'near well region'. Besides, even if some geochemical effects would have been considered, the uncertainty and the associated error in the determination of local values of hydraulic parameters are much larger than these possible effects, particularly over relatively large areas (more than 100 km^2) such as the ones considered in the local simulations. Any geochemical reactions have to be considered possibly in the close vicinity of the injection sites, which is at a scale 2 to 3 orders of magnitude smaller than the scale of the simulations considered in this study.

NUMERICAL MODELLING

The ten injection sites selected for local simulations of hydraulic head buildup are distributed over the entire Cold Lake area in Alberta, and cover all the host aquifers. However, some of them are at the same location but different injection depths, and others are relatively close to each other. This distribution made it possible to delineate only five model areas for local simulations, covered by appropriate finite element grids. One area in the north (figure 22A) includes the two Basal Cambrian

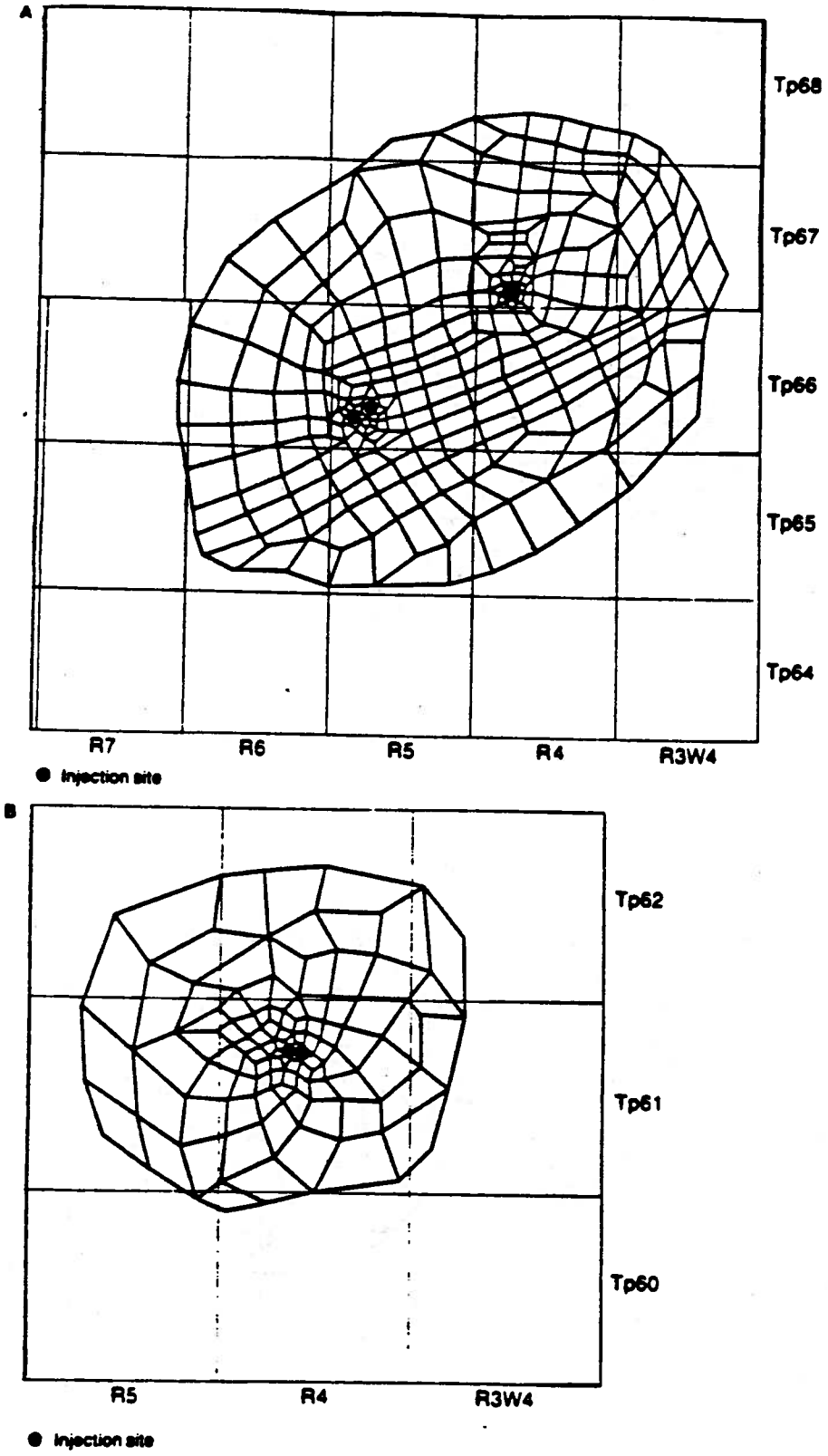

Figure 22 Plan view of the finite element grids used for local simulation of effects of injection in the Cold Lake area: A. Lower Paleozoic, northern area; B. Post-Prairie, north-central area; C. Post-Prairie, south-central area; and D. Post-Prairie, southern area

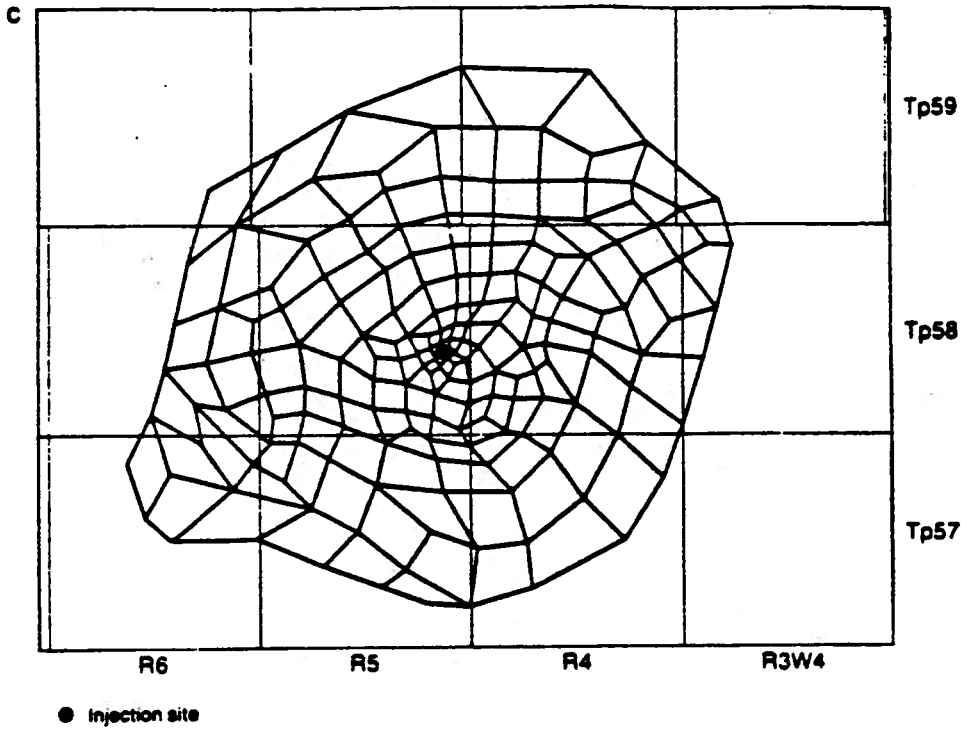

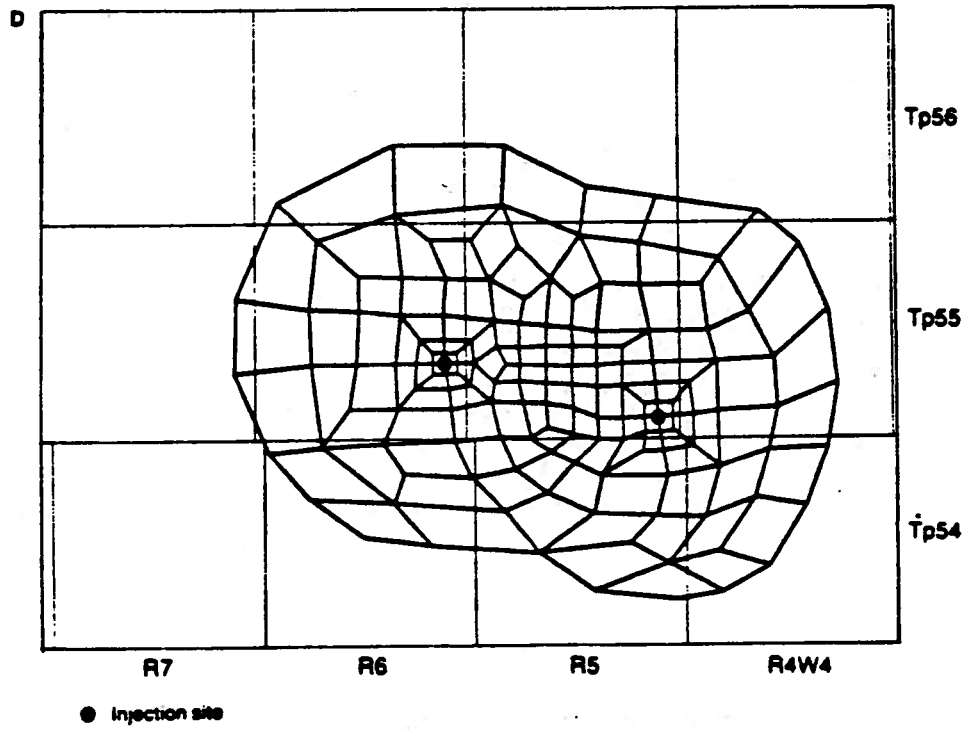

Figure 22 Continued

sandstone injection sites (10-8-66-5-W4 and 10-5-67-4-W4). For the Post-Prairie succession, a northern model area, almost identical to the Cambrian one, but with fewer surface elements, includes the sites injecting in the Grand Rapids (8-7-66-5-W4) and McMurray (10-5-67-4-W4) Formations. A north-central area (figure 22B) includes two sites which are very close: in the Clearwater Formation at 5-28-61-4-W4, and in the Cummings sandstone at 6-28-61-4-W4. A south-central area (figure 22C) is centred around a site at 5-13-58-5-W4 where injection takes place in both the Lower Grand Rapids Formation at 510 m depth, and in the Cooking Lake Formation at 600 m depth. Finally, a southern model area (figure 22D) covers two sites: 11-1-55-5-W4 injecting into the Lloydminster sandstone, and 3-13-55-6-W4 injecting into the Cooking Lake Formation. Table 16 presents the characteristics of the finite element grids, and the computer resources (CPU time) needed to simulate the deep injection of liquid wastes over a period of 30 a with a time step of 60 d.

The finite element grids covering these model areas have a higher resolution than the grids used in the regional simulations of effects of injection (Basin Analysis Group, 1987). As a result, each injection node represents an equivalent distance (radius) of 80 to 160 m from the actual well, which is 5 to 10 times smaller than the equivalent radius of the injection sites in the regional simulations. The theoretical solution of equation 37 depends only on the initial and boundary conditions, and on the values of the hydraulic parameters and injection rates. The numerical solution depends on the grid resolution in such a way that the value of the hydraulic head buildup at the injection site is bigger for smaller finite elements around it (smaller equivalent radius), therefore, the hydraulic head buildups at the injection sites will be larger in the case of local simulations than in the case of regional simulations, if all other parameters and conditions are the same. However, the values of the hydraulic parameters used in the local simulations are different than those used in the regional simulations (table 15), so the final result will depend on the interplay between higher hydraulic conductivity values, smaller or larger specific storage values, and higher resolution of the areal finite element grids. The magnitude of the vertical dimension of the three-dimensional finite elements is unchanged in the local simulations with respect to the regional simulations, because this

Table 16.
Characteristics of the finite element grids and CPU time used for local simulation of deep waste disposal at selected sites in the Cold Lake area

Model area	Surface nodes	Surface elements	Total nodes	Total elements	B.C. nodes	Unknowns	CPU time for 183 timesteps
Lower Paleozoic	269	250	1016	716	35	981	40.5 min
Northern Post-Prairie	210	194	2099	1800	330	1769	2 h 20 min
North-central Post-Prairie	103	93	1338	1122	175	1163	1 h 3 min
South-central Post-Prairie	174	160	2216	1964	252	1964	2 h 50 min
Southern Post-Prairie	148	136	1652	1458	192	1460	1 h 53 min

dimension is given by the actual thicknesses of the hydrostratigraphic units in the succession.

The actual location of the vertical nodes, and the boundary and initial values of hydraulic heads, were obtained through automatic interpolation in the grids of top surfaces and freshwater hydraulic heads, respectively, determined in the first part of the study (Basin Analysis Group, 1987). The same three-dimensional finite element model for groundwater flow, FE3DGW (Gupta et al., 1984a, 1984b) was used for local simulations. The results and conclusions of sensitivity analysis and calibration of modelling at the regional scale were considered as being valid for the simulations at the local scale (Basin Analysis Group, 1987).

LOCAL SIMULATIONS OF INJECTION

In the hydrogeological part of the study, a range and an average value were given for hydraulic conductivity and specific storage (Basin Analysis Group, 1987). Subsequently, regional simulations of injection were performed assuming worst, normal and best combinations of these parameters. No range of variation is given for the local values of hydraulic parameters (table 15), considering that the data samples are too small and too scattered to be truly representative. Consequently, a single simulation was performed for each model area. Table 17 presents the projected rates of injection at the 10 injection sites in the Cold Lake area selected for local simulations.

Simulation of injection in the Basal Cambrian aquifer at the BP and Dome sites confirmed the previous result that there is no interference between the two sites (figure 23). The variation of hydraulic head at the nodes representing the injection sites are presented in figure 23. The hydraulic head increase is higher in the case of local simulations than in the case of regional simulations, as expected for a smaller equivalent radius. However, the difference is not proportionally larger, due to the attenuating effect of larger values for hydraulic conductivity and specific storage used in local simulations (see table 15). The changes in the pattern of hydraulic head increase are due to changes in injection rates. Although the injection rates are higher at the BP site than at the Dome site by a factor of 3 to 4, the hydraulic head increase is larger at the Dome site due to a smaller thickness of the host aquifer. It must be

Table 17.
Projected injection rates for the period 1985-2015 at selected deep well disposal sites in the Cold Lake area, Alberta

Operator	Field/Area	Location	Stratigraphic Unit	Depth (m below KB)	Injection Rate Realistic 1985-1995	High 1995-2005	High 2005-2015
Dome	Primrose	10-5-67-4-W4	Cambrian	1310	3587	7173	7173
Dome	Primrose	10-5-67-4-W4	McMurray	540	2934	5868	5868
BP	Wolf Lake	8-7-66-5-W4	Grand Rapids	430	12887	20530	31530
BP	Wolf Lake	10-8-66-5-W4	Cambrian	1325	3335	5132	7883
Suncor	Fort Kent	5-28-61-4-W4	Clearwater	450	923	2211	786
Suncor	Fort Kent	6-28-61-4-W4	Cummings	450	755	1809	643
Murphy	Lindberg	5-13-58-5-W4	Lower Grand Rapids	510	1431	2324	1772
Murphy	Lindberg	5-13-58-5-W4	Cooking Lake	600	477	775	591
Westmin	Lindberg	11-1-55-5-W4	Lloydminster	530	1809	7602	7617
Westmin	Lindberg	3-13-55-6-W4	Cooking Lake	680	609	2534	2539

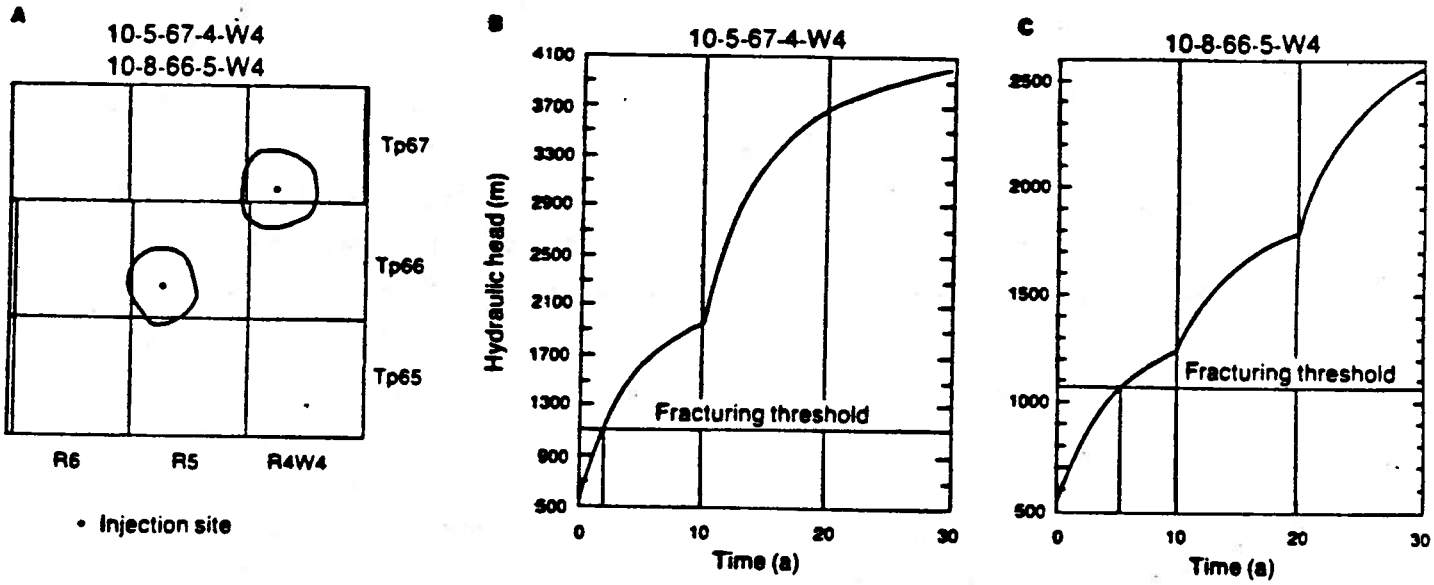

Figure 23 Effects of injection in Lower Paleozoic (Cambrian) aquifers at Dome (10-5-67-4-W4) and BP (10-8-66-5-W4) sites: A. spread of hydraulic head buildup (the contour represents the 10 m isoline of hydraulic head increase after 30 a); B. hydraulic head increase at Dome site and C. hydraulic head increase at BP site

stressed here that the aquifer geometry used in these simulations was determined on a regional scale, and may not correspond to the actual thickness at a particular site.

With respect to fracturing, comparison of the hydraulic head increases at these two sites with the respective values of acceptable buildups (table 13) shows that the fracturing threshold will be reached after a few years of operation. After initiation of vertical fractures, the flow regime will change due to corresponding changes in hydraulic parameters, such that the results of the present modelling are no longer valid. The study of effects of injection in terms of fracturing must be done at the scale of the well, using a different mathematical and numerical model which takes into account the stress regime and the fracturing process (initiation, propagation, etc.). It is believed that the fractures will not propagate all the way up to the Post-Prairie succession, due to the thickness of the intervening strata, particularly of the salt beds (Lotsberg, Cold Lake, Prairie) which exhibit elastic properties.

Local simulations of injection at the Dome and BP sites in the Post-Prairie succession (northern model area) again show a greater increase in hydraulic heads (figure 24) than in the case of regional simulations, due mainly to a higher resolution finite element grid, but no interference between the sites (figure 24). The local values of hydraulic conductivity and specific storage are of the same magnitude as the regional ones at the BP site, so the numerical increase is clearly a result of a smaller equivalent radius. Comparison with the fracturing threshold (table 13) at the BP site in the Grand Rapids (Mannville) aquifer shows that the fracturing threshold will be reached after 15 to 20 a of injection. The fractures will be vertical, but probably will be deflected at the top of the Mannville Group, and change from vertical to horizontal before reaching the top of the bedrock (Dusseault and Simmons, 1982). At the Dome site the increase in hydraulic head is still below the fracturing threshold for the McMurray Formation (the effect of higher resolution of the finite element grid is attenuated by a fourfold increase in the value of hydraulic conductivity).

The injection at the Suncor sites in the north-central model area were simulated previously at the regional scale, at a single injection node, due to the limits imposed by the finite element grid. The higher

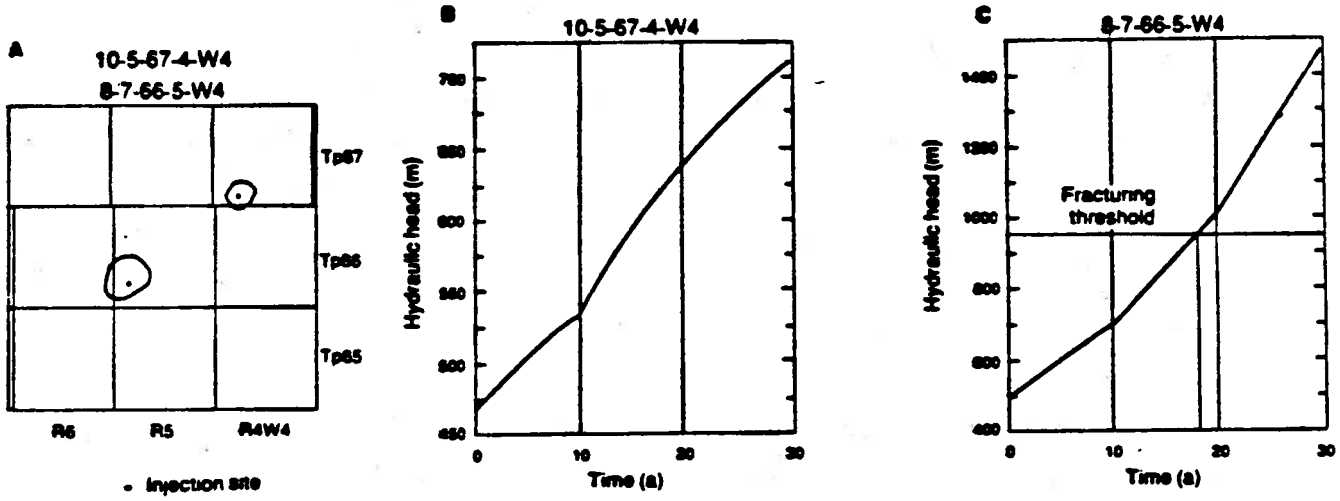

Figure 24 Effects of injection in Post-Prairie aquifers at Dome (10-5-67-4-W4) and BP (8-7-66-5-W4) sites: A. spread of hydraulic head buildup (the contour represents the 10 m isoline of hydraulic head increase after 30 a); B. hydraulic head increase at Dome site and C. hydraulic head increase at BP site

resolution of the grid used for local simulations allowed them to be modelled individually. The variations of hydraulic head at the respective sites are shown in figure 25, while the radii of influence are shown in figure 26. The decrease in hydraulic head after 20 a is due to decreases in the injection rates. The combined effect of higher hydraulic conductivity values (table 15) and higher grid resolution is such that, while higher than in the case of regional simulations, the hydraulic head increase at these two sites is still significantly lower than the fracturing threshold (table 13). This fact allows extrapolation from the radius of equivalence to the well and the assumption that fracturing will not occur. This assumption should still be verified with modelling of fracture initiation at the injection wells themselves.

In the south-central model area, injection was simulated at the same location in the Lower Grand Rapids and Cooking Lake Formations. For the Cooking Lake site (Beaverhill Lake aquifer system), the hydraulic conductivity has a local value seven times greater than the regional one, with a slightly larger specific storage (table 15). This explains why the hydraulic head increase (figure 27A), although higher than in the case of regional simulations, is still significantly below the fracturing threshold (table 13). Again, it can be assumed that at this site fracturing will not occur. At the Lower Grand Rapids site (figure 27B), the hydraulic head increase is below the fracturing threshold (table 13), but not by much. In this case, the effects from a threefold increase in the value of the hydraulic conductivity used in local simulations are cancelled by the effects of a tenfold decrease in the value of specific storage (table 15). It can be assumed that at the injection well itself fracturing will occur toward the end of the injection period, depending on the real values of hydraulic and stress characteristics at the site. But again, a vertical fracture will probably be deflected at the top of the Mannville Group and change to a horizontal fracture (Dusseault and Simmons, 1982). The shape of the curves of hydraulic head increase is due to variations in the injection rates (table 17), and to different geometry of the two injection aquifers. The radius of influence around these injection sites is shown in figure 28.

In the southern model area, local simulations were carried out for both Westmin sites in the Lloydminster sandstone and Cooking Lake

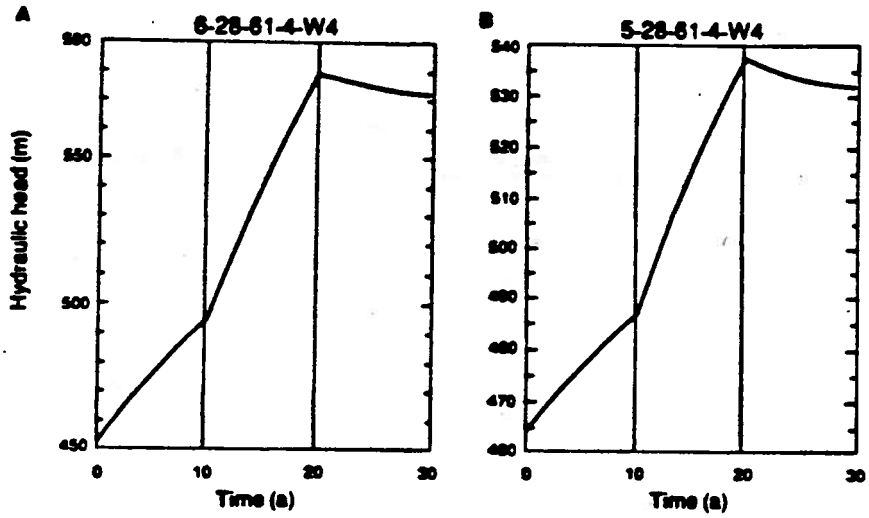

Figure 25 Hydraulic head increase at Suncor sites as a result of injection: A. in Cummings Member at 6-28-61-4-W4; and B. in Clearwater Formation at 5-28-61-4-W4

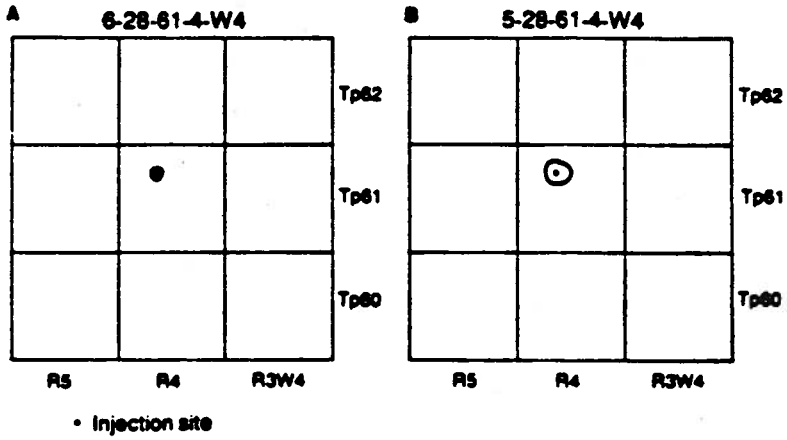

Figure 26 Spread of hydraulic head buildup at Suncor sites as a result of injection: A. in Cummings Member at 6-28-61-4-W4; and B. in Clearwater Formation at 5-28-61-4-W4 (the contour represents the 10 m isoline of hydraulic head increase after 30 a)

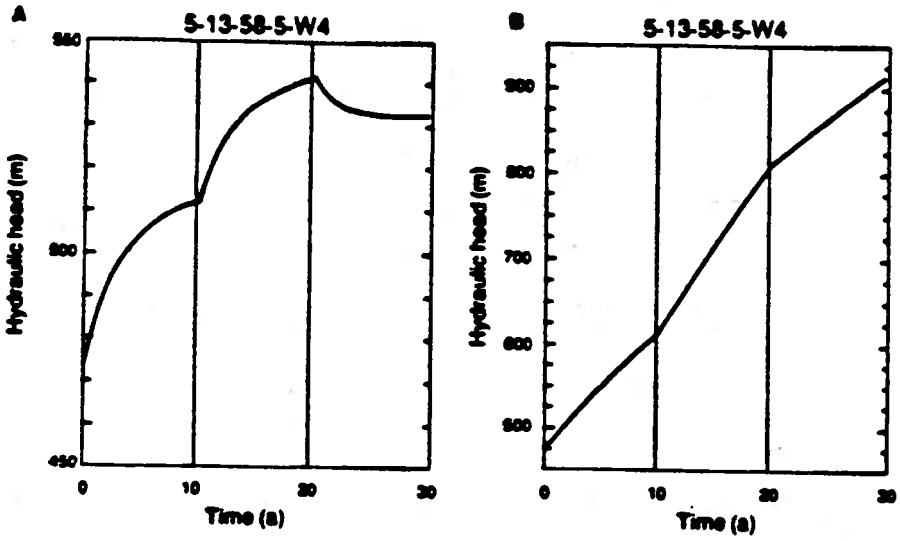

Figure 27 Hydraulic head increases at Murphy site (5-13-58-5-W4) as a result of injection in: A. Cooking Lake Formation; and B. Lower Grand Rapids Formation

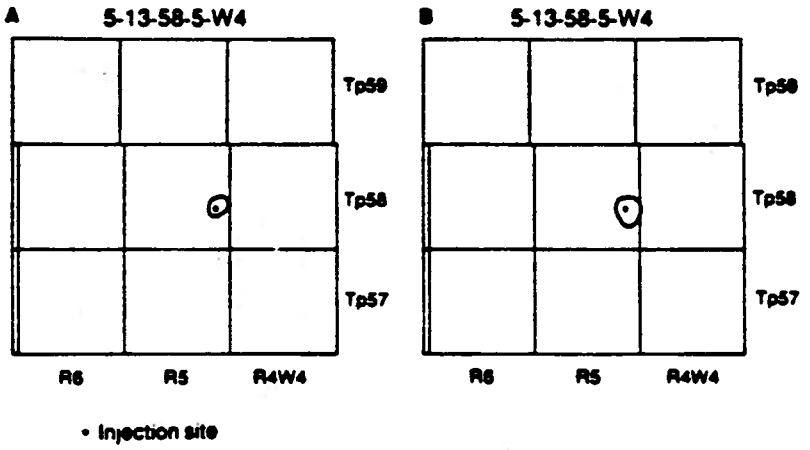

Figure 28 Spread of hydraulic head buildup at Murphy site (5-13-58-5-W4) as a result of injection in: A. Cooking Lake Formation; and B. Lower Grand Rapids Formation (the contour represents the 10 m isoline of hydraulic head increase after 30 a)

Formation. The hydraulic head increase for injection in the Cooking Lake Formation is very small, with the effect of a higher resolution grid being cancelled by significant increases in the values of hydraulic parameters used in modelling (table 15). For injection in the Lloydminster sandstone, the hydraulic head increase (figure 29) is larger than in the case of regional simulations, due to a fivefold increase in the grid resolution versus only a threefold increase in the hydraulic conductivity value used in local simulations. However, the increase in hydraulic head is still significantly below the fracturing threshold (table 13), such that, by extrapolation, it can be assumed that at both sites fracturing will not occur during the projected period of injection. The radius of influence of injection around the Lloydminster site is shown in figure 29.

CONCLUSIONS

Local simulations of effects of deep waste injection were performed for 10 selected sites in the Cold Lake area, to determine the hydraulic head buildups and compare them with corresponding fracturing thresholds. No values of hydraulic conductivity and specific storage were found at the injection wells themselves. Consequently, the respective values needed in numerical simulations were determined based on small data samples within a 20-30 km distance around each site. From this point of view, there is a high degree of uncertainty and associated error in the results. Finite element grids with higher resolution were used in the local simulations, allowing for a radius of equivalence of approximately 100 m at the injection nodes, as opposed to a radius of at least 500 m in the regional simulations reported previously. The local simulations confirmed the conclusion that there is no interference between the sites. According to these simulations, the fracturing threshold will be reached at sites injecting into the Basal Cambrian aquifer and at some sites injecting into the Post-Prairie succession. Vertical fractures initiated in Cambrian rocks will probably be stopped by the overlying thick salt formations, while the vertical fractures initiated at some sites injecting into the Mannville Group will probably be deflected and transform into horizontal fractures before reaching the top of the bedrock. The above conclusions should be confirmed by future studies of fracturing at the scale of the injection wells using locally measured values of the parameters involved.

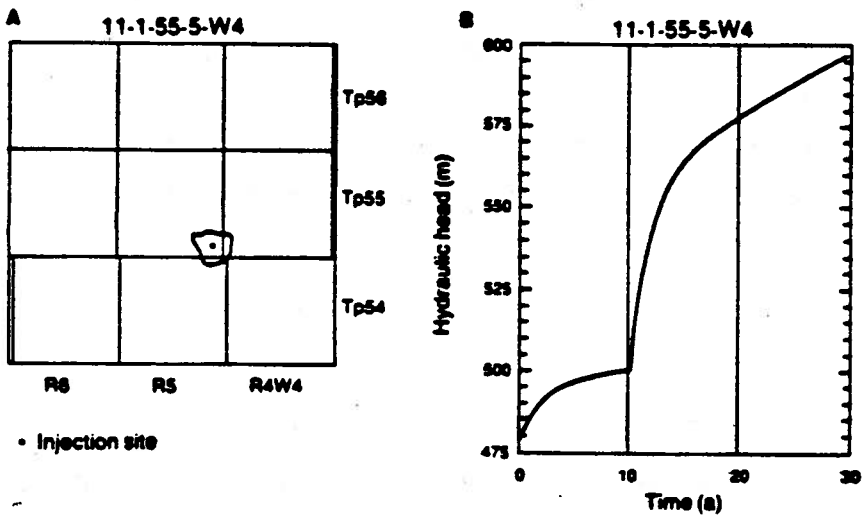

Figure 29 Effects of injection at Westmin site (11-1-55-5-W4) in Lloydminster sandstone: A. spread of hydraulic head buildup (the contour represents the 10 m isoline of hydraulic head increase after 30 a); and B. hydraulic head increase

TRANSPORT PROCESSES AS A RESULT OF DEEP WASTE DISPOSAL

Stefan Bachu

The study of effects of deep waste disposal in the Cold Lake area addressed so far hydraulic, geomechanical and geochemical aspects. However, there are also transport processes associated with the flow of formation and injected waters, mainly the transport of heat and of dissolved substances. The main concern related to deep waste disposal practices is the movement of contaminants, particularly upward migration to shallow aquifers used for human use. Heat and mass transport at the injection sites occur when the temperature and composition of the injected waters is different from the temperature and composition of formation waters. It has been shown in a previous section that there are geochemical reactions associated with the injection of residual waters in the Cold Lake area. As a result of these reactions, the composition of waters around the injection wells will be different than the composition of formation waters, and therefore mass transport processes are expected. The injected residual waters are the result of in situ recovery operations and as such have temperatures varying between 20°C and 90°C (Gunter et al., 1986), while the highest subsurface temperature recorded in the area is 70°C at 2000 m depth. Therefore, some heat transport processes are associated with the injection of residual waters in the Cold Lake area.

The heat and mass transport in the subsurface environment is described respectively by the following equations (Bear, 1972):

$$(\rho c)_m \frac{\partial T}{\partial t} + n\,\rho_f c_f\,\bar{v}\cdot \mathrm{grad}(T) = \mathrm{div}\,[\bar{\bar{\lambda}}_m\,\mathrm{grad}(T)] + R \qquad (38)$$

$$\frac{\partial C}{\partial t} + \bar{v}\cdot \mathrm{grad}(C) = \mathrm{div}[\bar{\bar{D}}_h\,\mathrm{grad}(C)] + S \qquad (39)$$

where T is temperature, t is time, n is porosity, $\bar{v}$ is the velocity vector, R represents heat sources, C is the concentration of any solute, S represents mass sources, and $\bar{\bar{D}}_h$ is the tensor of hydrodynamic dispersion, defined by:

$$\bar{\bar{D}}_h = \bar{\bar{D}}_m + D_d \qquad (40)$$

The term $\bar{D}_m$ represents the tensor of mechanical dispersion in a porous medium and is velocity dependent, while the term D_d is the effective coefficient of molecular diffusion in a porous medium. The heat capacity $(\rho c)_m$ and thermal conductivity λ_m of the fluid-saturated porous medium were defined previously (equations 2 and 3, respectively).

The heat sources R in the case of deep waste injection are given by the enthalpy of injected waters. Namely, it is the product between the injection rates, temperature, density and heat capacity of respective waters. However, the information about the temperature of injected waters at specific sites is confidential, therefore the term R could not be computed.

The mass sources S are given by the product between the rate of injection and the concentration of a dissolved substance at each site. Equation 39 has to be solved for each chemical component under consideration. Or, inversely, all the chemical components present in the fluid have to be lumped together. However, there is no methodology available to do this lumping for all the components considered previously in the study of geochemical effects.

It was shown in a previous section that the convection of heat in the natural hydrogeological regime can be neglected. The mass transport processes are basically dispersive/convective, the molecular diffusion being negligible (Bachu et al., 1986). Therefore, substances moving with the formation waters in the natural system will have a characteristic velocity of 1 cm/a. Taking into account the depths of injection and the isolating effects of the overlying halite aquicludes and shaly aquitards, the transport of injected substances by the natural flow of formation waters in the Cold Lake area should not be an environmental issue. It follows that the transport processes can be significant only within the radius of influence of each injection well, particularly close to it where the velocities are higher due to high hydraulic gradients created by hydraulic head increases, or where abandoned wells and/or fractures can create vertical conduits for fluid flow (Chia and Chiu, 1988).

On the other hand, equation 37 is no longer valid for the modelling of fluid flow in such cases because the density variations caused by changes in temperature and concentration produce buoyancy effects which are no longer negligible. Therefore, in the study of transport processes, equation 37 should be replaced by:

$$\mathrm{div}(\rho\bar{q}) + S_s^*(\partial p/\partial t) = 0 \qquad (41)$$

where ρ is the fluid density, p is pressure, $\bar{q}$ is the specific discharge vector and S_s^* is specific storativity related to pressure changes. The specific discharge $\bar{q}$ is given by Darcy's law (momentum equation):

$$\bar{q} = -(\bar{\bar{k}}/\mu)[\mathrm{grad}(p) + \rho\bar{g}] \qquad (42)$$

where $\bar{\bar{k}}$ is the permeability tensor, μ is dynamic viscosity, and $\bar{g}$ is the gravity vector.

The fluid flow equations 41 and 42 are forward linked with the transport equations 38 and 39 through the velocity vector:

$$\bar{v} = \bar{q}/n \qquad (43)$$

and backward linked through the equation of state for fluid density:

$$\rho = \rho_o[1 - \alpha(T-T_o) + \beta(C-C_o)] \qquad (44)$$

In the above relation, ρ_o is a reference density at the reference temperature T_o and concentration C_o, α is the coefficient of thermal expansion, and β is a coefficient of density dependence on concentration, a dependence assumed to be linear in the range considered here. A proper dimensional analysis of the importance of buoyancy effects could be done if the composition and density of injected and formation waters were known for each injection site. Unfortunately, this information was not available at the time of the study.

In order to study the transport processes on a local scale around the injection sites, equations 38 to 44 have to be solved simultaneously. At the present moment, the Alberta Research Council does not have such modelling capabilities, data are not available for all the parameters and variables appearing in these equations. On the other hand, the above system of equations is valid only for flow in porous media. If fracturing occurs, the flow characteristics change and a different model has to be used.

Chia and Chiu (1988) used both a single and dual porosity model (three-dimensional, finite-difference) for mass transport in fractured porous media, to assess the upward migration of underground injected wastes. The results of their analysis show that, over a period of 20 a, the contaminants move laterally up to a few hundred metres in a typical injection aquifer, and that regional upward migration through an extensive confining formation is a very slow process. Nevertheless, injected wastes can move upward rapidly through microannuli and channels in the cement sheath of the injection well, through improperly abandoned wells in the immediate vicinity, and through fractures in the disturbed zone.

In conclusion, heat and mass transport processes associated with deep waste disposal in the Cold Lake area should be negligible outside the radius of influence of the respective wells. Even close to the well, these processes should be of no concern as long natural fractures are not present or fracturing does not occur, due to the low temperatures involved and to the isolating effects of aquitards and aquicludes in the hydrostratigraphic succession. If natural fractures are present, or if fracturing occurs, the transport of contaminants through the fracture systems should be examined.

CONCLUSIONS

In the first part of the study, reported previously (Basin Analysis Group, 1987), the baseline natural hydrogeological regime was determined for the entire Phanerozoic succession in a region defined as Tp 50-70, R 15 W3 Mer to R 17 W4 Mer (60 000 km^2) in the Cold Lake area. The regional effects of deep waste injection at 27 sites were numerically simulated, using projected rates up to the year 2015. Under the assumption of average values characterizing the hydraulic parameters, the simulations revealed no interference between the different injection sites. In this part, the study was advanced further both in terms of natural regimes and evaluation of effects of injection.

The geothermal regime in the area was described based on 19 218 bottomhole temperature (BHT) values at 10 715 different locations. The BHT values were corrected using Horner and regression type analyses. Dimensional analysis shows that the convective heat transfer in the sedimentary rocks is negligible throughout the area and that the main mechanism for heat transport from the basement to the ground surface is thermal conduction through the sedimentary column.

Local effects of deep waste injection were studied at 10 individual sites in terms of geochemical processes, fracturing thresholds and pressure buildups. The sites were chosen based on data availability and representativeness, such that all the present injection aquifers (Basal Cambrian, Cooking Lake, McMurray, Clearwater and Grand Rapids) are examined.

Water-rock interaction effects were evaluated for the Basal Cambrian, Beaverhill Lake, McMurray, Clearwater and Mannville aquifers using the computer code SOLMNEQF. Reservoir mineralogy was determined on selected cores and representative formation water analyses reevaluated for incomplete determinations and saturation with minerals in the aquifers. Twenty waste waters from the Cold Lake area were used in the modelling. The most important minerals which may precipitate from or dissolve into the fluid are quartz and calcite. Calculations indicate that 20% of the available silica will precipitate from solution in 30 a if the solution is supersaturated with respect to quartz. For a solution supersaturated with respect to calcite, 50% of the amount of calcite that can form will do so

in 3 to 4 d. This suggests that the most important change that can be made to waste water is softening or removal of CO_2. Because of the rapid dissolution and precipitation rates of calcite, if detailed water analyses over a complete production cycle are available (and they currently are not), it is recommended that a study of the near well, local effects of mineral dissolution/precipitation should be considered. These effects could then be included with a study on potential fracturing in the near well region. To the best of the author's knowledge, there currently is insufficient information, theoretical models, and numerical models to perform such a study.

Fracturing thresholds were evaluated using accurate calculations of overburden stresses, anisotropic horizontal stress field and superposed tectonic stress, as well as density and acoustic digitized curves from existing geophysical logs. The pressure buildups were simulated individually at the 10 sites, using local values for hydraulic conductivity and specific storage. A higher resolution finite element grid allowed the results to be considered as representative for distances of up to 160 to 200 m from the injection wells. The results of the simulations show that, depending on the rates of injection and aquifer characteristics, vertical fracturing will occur close to the injection well at some sites. Vertical fractures initiated in Cambrian rocks will probably be stopped by the overlying thick salt formations, while the vertical fractures initiated at some sites injecting into the Mannville Group will probably be deflected and transform into horizontal fractures before reaching the top of the bedrock.

Given the low temperature of the injected waters, the thermal effects of deep waste injection are negligible except close to the well, where they can influence geochemical reactions. As for the transport of any contaminant contained in the injected waters, it can be neglected once outside the radius of influence of each injection well. Regional migration, particularly upwards, of wastes injected deep in sedimentary aquifers below extensive confining aquitards is a slow process. Contamination of shallow groundwater aquifers can take place through vertical hydrologic conduits in the close vicinity of the wellbore.

Generally, the injection of residual waste waters in the Cold Lake area has only local effects limited to the near field close to the injection

wells. However, there is a degree of uncertainty associated with the results presented so far, due to lack of site specific values of hydraulic, geochemical and geomechanical parameters. The near field effects should be studied and predicted on a case by case basis, using site measured values of the parameters involved, any natural or artificial vertical conduits for fluid migration, and actual injection data for history matching and model calibration. If site specific modelling will predict pressure buildups over the respective fracturing thresholds, the initiation, orientation, propagation and extent of fractures should be studied furether using geomechanical modelling in conjunction with fluid flow models (hydrofracturing models) in order to assess the possibility of inducing hydraulic connectivity with the shallow groundwater aquifers used for water supply.

REFERENCES

Aggarwal, P.K., R.W. Hull, W.D. Gunter and Y.K. Kharaka (1986): SOLMNEQF: A computer code for geochemical modeling of water-rock interactions in sedimentary basins. In Hydrogeology of Sedimentary Basins: Application to Exploration and Exploitation (B. Hitchon, S. Bachu and C.M. Sauveplane, editors), Proceedings, Third Canadian/American Conference on Hydrogeology, pp. 196-203.

Anderson, R.A., D.S. Ingram and A.M. Zanier (1973): Determining fracture pressure gradients from well logs, Journal of Petroleum Technology, v. 25, pp. 1259-1268.

Bachu, S. (1985): Influence of lithology and fluid flow on the temperature distribution in a sedimentary basin: a case study from the Cold Lake area, Alberta, Canada. Tectonophysics, v. 120, pp. 257-284.

Bachu, S. (1988): Analysis of heat transfer processes and geothermal pattern in the Alberta Basin, Canada. Journal of Geophysical Research, v. 93, B7, pp. 7767-7781.

Bachu, S., B. Hitchon and P. Mortensen (1986): Preliminary analysis of transport processes in the Basal Cambrian aquifer of south-central Alberta. In Hydrogeology of Sedimentary Basins: Application to Exploration and Exploitation (B. Hitchon, S. Bachu and C.M. Sauveplane, editors), Proceedings, Third Canadian/American Conference on Hydrogeology, pp. 233-249.

Bachu, S., C.M. Sauveplane, A.T. Lytviak and B. Hitchon (1987): Analysis of fluid and heat regimes in sedimentary basins: techniques for use with large data bases. American Association of Petroleum Geologists Bulletin v. 71, pp. 822-843.

Balmer, G.G. (1953): Physical properties of some typical foundation rocks. Denver, Colorado, Design and Construction Division. U.S. Bureau of Reclamation, Engineering Laboratories Branch. Concrete Laboratory Report No. SP-39.

Basin Analysis Group (1985): Hydrogeology of the Cold Lake study area, Alberta, Canada. Consultant report prepared for Alberta Environment.

Basin Analysis Group (1987): Evaluation of deep waste disposal, Cold Lake area, Alberta and Saskatchewan: regional effects. Consultant report prepared for Alberta Environment.

Beach, R. (1985): Sedimentary heat flow in the $\Delta Q=0$ region of Alberta. M.Sc. thesis, University of Alberta.

Bear, J. (1972): Dynamics of fluids in porous media. Elsevier, 764 p.

Bear, J. and Y. Bachmat (1986): Macroscopic modelling of transport phenomena in porous media 2: Applications to mass, momentum and energy transport. Transport in Porous Media, v. 1, pp. 241-270.

Bell, J.S. and E.A. Babcock (1986): The stress regime of the Western Canadian Sedimentary Basin and implications for hydrocarbon production, Bulletin of Canadian Petroleum Geology; v. 34, pp. 364-378.

Biot, M.A. (1941): General theory of three-dimensional consolidation, Journal of Applied Physics; v. 12, pp. 155-164.

Biot, M.A., W.L. Medlin and L. Masse (1983): Fracture penetration through an interface, Society of Petroleum Engineers Journal, v. 23, pp. 857-869.

Bredehoeft, J.D., R.G. Wolff, W.S. Keys and E. Shuler (1976): Hydraulic fracturing to determine the regional in situ stress field, Piceance Basin, Colorado, Geological Society of America Bulletin; v. 87, pp. 250-258.

Chapman, D.S., T.H. Keho, M.S. Bauer and M.D Picard (1984): Heat flow in the Uinta Basin determined from bottom hole temperature (BHT) data. Geophysics, v. 49, pp. 453-466.

Cheng, P. (1978): Heat transfer in geothermal systems. Advances in Heat Transfer, v. 14, pp. 1-105.

Chia, Y. and J. Chiu (1988): Upward migration of underground injected wastes through hydrologic conduits around the wellbore. In Proceedings of Fourth Canadian/American Conference on Hydrogeology: Fluid Flow, Heat Transfer and Mass Transport in Fractured Rocks (edited by Stefan Bachu), National Water Well Association, Dublin, Ohio (in press).

Chouet, B. (1986): Dynamics of fluid-driven crack in three dimensions by the finite difference method, Journal of Geophysical Research; v. 91, no. B 14, pp. 13967-13992.

Davies, P.B. (1987): Modeling areal, variable density, ground-water flow using equivalent head-analysis of potentially significant errors; In Proceedings of the NWWA/IGWMC Conference "Solving Ground-water Problems with Models", February 10-12, 1987, Denver, Colorado, pp. 888-903.

Dusseault, M.B. and J.V. Simmons (1982): Injection-induced stress and fracture orientation changes; Canadian Geotechnical Journal, v. 9, pp. 483-493.

Eaton, A.B. (1969): Fracture gradient prediction and its application in oil field operations, Journal of Petroleum Technology, v. 21, pp. 1353-1360.

Environment Canada (1982): Canadian climate normals, temperature and precipitation 1951-1980, Prairie Provinces. Canadian Climate Program.

Gunter, W.D., B.J. Fuhr and B. Young (1986): Composition of water in waste well disposal from oil sands and heavy oil field pilots of Alberta. In Hydrogeology of Sedimentary Basins: Application to Exploration and Exploitation (B. Hitchon, S. Bachu and C.M. Sauveplane, editors), Proceedings, Third Canadian/American Conference on Hydrogeology, pp. 233-249.

Gupta, S.K., C.R. Cole, F.W. Bond and A.M. Monti (1984a): Finite-element three-dimensional groundwater (FE3DGW) flow model formulation, program listings and users' manual; Pacific Northwest Laboratory, Richland, Washington.

Gupta, S.K., C.R. Cole and G.F. Pinder (1984b): A finite-element three-dimensional groundwater (FE3DGW) model for a multiaquifer system; Water Resources Research, v. 20, pp. 553-563.

Haar, L., J.S. Gallagher and G.S. Kell (1984): NBS/NRC steam tables. Hemisphere Publishing Corp., McGraw-Hill, 320 pp.

Haimson, B. (1968): Hydraulic fracturing in porous and non-porous rock and its potential for determining in situ stresses at great depth, Ph.D thesis, University of Minnesota, Minneapolis.

Haimson, B. and C. Fairhurst (1969): Hydraulic fracturing in porous permeable materials. Journal of Petroleum Technology, v. 21, pp. 811-817.

Harrison, D.B., R.P. Glaister and H.W. Nelson (1982): Reservoir description of the Clearwater oil sand, Cold Lake, Alberta. In Proceedings of The Future of Heavy Crude and Tar Sands (edited by R.F. Meyer, J.C. Wynn and J.C. Olson). McGraw-Hill, New York. pp. 264-280.

Hitchon, B., G.K. Billings and J.E. Klovan (1971): Geochemistry and origin of formation waters in the western Canada sedimentary basin - III. Factors controlling chemical composition. Geochimica et Cosmochimica Acta, v. 35, pp. 567-598.

Hitchon, B., S. Bachu, C.M. Sauveplane and A.T. Lytviak (1987): Dynamic basin analysis: an integrated approach with large data bases. In Fluid Flow in Sedimentary Basins and Aquifers (J.C. Goff and B.P.J. Williams, editors), pp. 31-44, Geological Society Special Publication No. 34.

Howard, G.C. and C.R. Fast (1970): Hydraulic Fracturing, Society of Petroleum Engineers Monograph Series, v. 2, no. 34, Richardson, Texas, 203 pp.

Hubbert, M.K. (1945): Strength of the earth, American Association of Petroleum Geologists Bulletin, v. 29, pp. 1630-1653.

Hubbert, M.K and D.G. Willis (1957): Mechanics of hydraulic fracturing; American Institute of Mining Engineers Transactions, v. 210, pp. 153-168.

Jaeger, J.C. and N.G.W. Cook (1976): Fundamentals of rock mechanics, Chapman and Hall, 2nd ed., London.

James, D.P. and T.A. Oliver (1977): The sedimentology of the McMurray Formation, East Athabasca. In Proceedings of The Oil Sands of Canada-Venezuela (edited by David A. Redford and Alvin G. Winestock). The Canadian Institute of Mining and Metallurgy Special Volume 17, pp. 17-26.

Labudovic, D. (1984): The effect of Poisson's ratio on fracture height, Journal of Petroleum Technology, v. 36, pp. 287-290.

Lama, R.D. and V.S. Vutukuri (1978): Handbook on Mechanical Properties of Rocks. Vol. II-IV, Trans. Tech. Publications.

MacDonald, J. (1987): The Basal Cambrian sandstone, mineralogy and diagenesis. Unpublished thesis, Department of Geological Sciences, University of Alberta, under supervision of Dr. F. Longstaffe.

McLennan, J.D., J. Elbel, E. Mattheis and L. Lindstrom (1982): A critical evaluation of the Mechanical Properties Log (MPL) on a Basal Quartz well in the Caroline area, Alberta: Paper 82-33-45, 33rd Annual Technical Meeting of the Petroleum Society of the Canadian Institute of Mining and Metallurgy, Calgary, June 6-9. 11 pp.

Mossop, G.D., J.W. Kramers, P.D. Flach and B.A. Rottenfusser (1982): Geology of Alberta's oil sands and heavy oil deposits. In Proceedings of The Future of Heavy Crude and Tar Sands (edited by R.F. Meyer, J.C. Wynn and J.C. Olson). McGraw-Hill, New York. pp. 197-207.

Nordgren, R.P. (1972): Propagation of a vertical hydraulic fracture, Transactions of Society of Petroleum Engineers of AIME, v. 253, pp. 306-314.

Nolte, K.G. (1984): A general analysis of fracturing pressure decline, SPE paper 12941, 59th Fall Meeting of Society of Petroleum Engineers.

Pickett, G.R. (1963): Acoustic character logs and their application in formation evaluation, Journal of Petroleum Technology, v. 15, pp. 659-667.

Pugh, D.C. (1973): Subsurface Lower Paleozoic stratigraphy in northern and central Alberta; Geological Survey of Canada, Paper 72-12, 29 pp.

Settari, A. and M.P. Cleary (1984): Three-dimensional simulation of hydraulic fracturing, Journal of Petroleum Technology, v. 36, pp. 1177-1190.

Visser, K., P.H.M. Dankers and D. Leckie (1985): Mineralogy and geology of the Clearwater reservoir sands in the Cold Lake aera, Cold Lake, Alberta. In Proceedings of Third International Conference on Heavy Crude and Tar Sands, Long Beach, California. pp. 17-26.

Warpinski, N.R., P. Branagan and R. Wilmer (1985): In-situ stress measurements at US's DOE's Multiwell Experiment site, Mesaverde Group, Rifle, Colorado, Journal of Petroleum Technology, v. 37, pp. 517-536.

Willett, S.D. and D.S. Chapman (1986): On the use of thermal data to resolve and delineate hydrologic flow systems in sedimentary basins: an example from the Uinta Basin, Utah. In Proceedings of Third Canadian/American Conference on Hydrogeology: Hydrogeology of Sedimentary Basins: Application to Exploration and Exploitation (B. Hitchon, S. Bachu and C.M. Sauveplane, editors). National Water Well Association, Dublin, Ohio. pp. 159-168.

EVALUATION OF DEEP WASTE DISPOSAL COLD LAKE AREA, ALBERTA AND SASKATCHEWAN: REGIONAL EFFECTS

OPEN FILE REPORT 1996 - 2B

Prepared by
Basin Analysis Group
Alberta Geological Survey
Alberta Research Council
(Project Manager: Dr. Stefan Bachu)

Project jointly funded by
Alberta Research Council
and
Alberta Environment

1988 - 08 - 31

TABLE OF CONTENTS

	Page
Executive Summary	xv
Introduction	1
Regional Geology (Anne Ing)	5
Introduction	5
Western Canada Sedimentary Basin	6
Basin Analysis	9
Development of the Passive Continental Margin Succession	10
Precambrian Basement	10
Cambrian	10
Ordovician	14
Lower Devonian	17
Middle Devonian	21
Upper Devonian	24
Evolution of the Foreland Basin	29
Lower Cretaceous (Mannville)	31
Cold Lake Oil Sands	38
Upper Cretaceous (Colorado)	40
Upper Cretaceous (Post-Colorado)	41
Analysis of the Natural Flow Regime (Claude M. Sauveplane and Brian Hitchon)	43
Introduction	43
Lateral Flow	46
Precambrian Aquiclude	46
Basal Cambrian Aquifer	46
Other Cambrian Aquifers	50
Ordovician Aquifer	52
Basal Red Beds "Aquifer"	52
Lower Paleozoic Aquifer System	53
Lower Devonian Aquiclude System	55
Winnipegosis Aquifer System	58
Prairie Aquiclude	61
Dawson Bay "Aquifer"	61

Page

Beaverhill Lake Aquifer System 65
Ireton Aquitard 73
Camrose Tongue Aquifer 73
Grosmont Aquifer 75
Winterburn Aquifer 79
McMurray Aquifer 79
Clearwater Aquifer 83
Mannville Aquifer 86
Joli Fou Aquitard 91
Viking Aquifer 91
St. Walburg Aquifer 95
Colorado Aquitard System 95
Cross-Formational Flow 98
Vertical Flow in the Paleozoic 98
Vertical Flow Between Paleozoic and Lower Cretaceous 100
Vertical Flow Within the Cretaceous 103
Conclusions 110
Numerical Simulation of Regional Effects of Injection
(Stefan Bachu) 114
Mathematical and Numerical Modelling 114
Calibration of the Numerical Model 124
Sensitivity Analysis 124
Calibration of the Model 135
Simulation of Effects of Injection 141
Conclusions 162
References 164

Appendices
Appendix A. Data Base and Data Processing
(Stefan Bachu, Andre T. Lytviak and Claude M. Sauveplane) A1

Appendix B. Regional Hydrodynamic Results
(Claude M. Sauveplane) B1

List of Tables

Page

Table 1. Generalized stratigraphic nomenclature and hydrostratigraphy, Cold Lake study area 7

Table 2. Chemical composition (mg/L), physical properties and production data for formation waters from Basal Cambrian aquifer, Cold Lake study area 49

Table 3. Chemical composition (mg/L), physical properties and production data for raw brine produced by artificial solution of the Prairie Formation halite at the Lindberg salt plant and formation water from the Dawson Bay aquifer, Cold Lake study area 64

Table 4. Chemical composition (mg/L), physical properties and production data for formation water from Leduc aquifer, Cold Lake study area 70

Table 5. Chemical composition (mg/L), physical properties and production data for selected formation waters from aquifers in the Colorado aquitard, Cold Lake study area 97

Table 6. Recommended hydraulic parameters (regional estimates) 111

Table 7. Values of the Driving Force Ratio (DFR) for selected aquifers in the Cold Lake study area around deep waste disposal sites 120

Table 8. Projected injection rates for the period 1985-2015 at deep well disposal sites in the Cold Lake study area, Alberta 126

Page

Table 9. Characteristics and results of numerical simulations of natural steady-state flow regime in three model areas in the post-Prairie injection sequence 139

Table 10. Theoretical increases in hydraulic heads at the four injection sites in the Basal Cambrian aquifer, for two cases of either minimum hydraulic conductivity or minimum specific storage, for the periods of 10, 20 and 30 a 149

List of Figures

Page

Figure 1. Cold Lake study area, Alberta and Saskatchewan 2

Figure 2. Total preserved thickness of Phanerozoic rocks east of the Cordilleran foreland thrust belt 8

Figure 3. A. Structure contour map of the Precambrian surface (contour interval 50 m); B. Isopach map of the Basal Cambrian sandstone (contour interval 50 m) 11

Figure 4. A. Structure contour map on top of the Cambrian (contour interval 50 m); B. Isopach map of the Cambrian (contour interval 50 m) 13

Figure 5. Cratonic arches and basins of western Canada (after Stelck, 1975) 15

Figure 6. A. Structure contour map on top of the Ordovician (contour interval 50 m); B. Isopach map of the Ordovician (contour interval 10 m) 16

Figure 7. A. Configuration of the Western Canada Sedimentary Basin during the Early Devonian (simplified from Grayston et al., 1964); B. Isopach of the Lower Devonian (contour interval 50 m) 18

Figure 8. Distribution of Lower Devonian Elk Point Subgroup salts in the Cold Lake region (after Hamilton, 1971) ... 19

Figure 9. A. Isopach map of the Lotsberg Formation (contour interval 50 m); B. Isopach map of the Cold Lake Formation (contour interval 10 m) 20

Page

Figure 10. A. Geometry of the basin during Middle Devonian time (simplified from Grayston et al., 1964); B. Isopach map of the Middle Devonian (contour interval 25 m) 22

Figure 11. Isopach map of the Winnipegosis Formation (contour interval 10 m) 23

Figure 12. A. Structure contour map on top of the Prairie Formation (contour interval 50 m); B. Isopach map of the Prairie Formation (contour interval 20 m) 25

Figure 13. Schematic diagram illustrating carbonate onlap and offlap during the Upper Devonian (after Wendte, 1982) .. 26

Figure 14. A. Isopach map of the Beaverhill Lake Group (contour interval 50 m); B. Isopach map of the Cooking Lake and Leduc Formations (contour interval 50 m) 27

Figure 15. A. Structure contour map on top of the Pre-Cretaceous unconformity surface (contour interval 50 m; 3608 data points used); B. Isopach map of the Upper Devonian (contour interval 50 m) 30

Figure 16. Approximate Mannville paleogeography at the Aptian-Albian boundary, showing basin outlines and topographically high areas with inferred drainage (after O'Connell, 1985) 32

Figure 17. A. Structure contour map on top of the Mannville Group (contour interval 50 m; 7345 data points); B. Isopach map of the Mannville Group (contour interval 50 m) 33

Page

Figure 18. Progradation of upper Mannville shoreline from south-central Alberta northward to the Clearwater Formation marine shale basin (simplified from Jackson, 1984) 35

Figure 19. Schematic cross-section across eastern Alberta; note the tongues of the Clearwater shale (simplified from Jackson, 1984) 36

Figure 20. Conceptual diagram illustrating the occurrence and postulated relative positions of blanket and channel sands within the Mannville sequence (after Gross, 1980) 37

Figure 21. Cold Lake Oil Sands structural cross-section, showing generalized lithologies and reservoir configurations (after Mossop et al., 1981) 39

Figure 22. A. Structure contour map on the base of the Quaternary (contour interval 50 m); B. Isopach map from the top of the Mannville Group to the base of the Quaternary (contour interval 50 m) 42

Figure 23. Cambrian hydrogeology. A. Isopachs (contour interval 50 m) of preserved Cambrian strata; B. Salinity (mg/L) of formation waters; C. Potentiometric surface of Basal Cambrian aquifer 47

Figure 24. Cross-formational flow as illustrated by pressure head/depth plots in the Lower Paleozoic aquifer system. A. at the indicated well locations; B. just south of the study area at B12-30-49-27 W3 Mer 54

Figure 25. Isopachs (contour interval 50 m) of the Lower Paleozoic aquifer system 56

Page

Figure 26. Isopachs (contour interval 50 m) of the Lower Devonian aquiclude system 57

Figure 27. Winnipegosis aquifer system hydrogeology. A. Isopachs (contour interval 50 m); B. Salinity (mg/L) of formation waters; C. Potentiometric surface; D. Relation of SO_4 and HCO_3 in formation waters 59

Figure 28. Vertical hydraulic continuity in the Winnipegosis aquifer system. A. at well location 14-29-52-02 W4 Mer; B. at well location 12-10-56-23 W3 Mer 62

Figure 29. Isopachs (contour interval 20 m) of Prairie aquiclude 63

Figure 30. Beaverhill Lake aquifer system hydrogeology. A. Isopachs (contour interval 50 m); B. Salinity (mg/L) of formation waters; C. Potentiometric surface 66

Figure 31. Cross-formational flow as illustrated by pressure head/depth plots in the Paleozoic. A. at well location 7-19-59-23 W3 Mer; B. at well location 4-5-66-16 W3 Mer; C. at well location 13-36-51-07 W4 Mer 68

Figure 32. Isopachs (contour interval 50 m) of the Ireton aquitard, including the thin Camrose Tongue aquifer 72

Figure 33. Camrose Tongue aquifer hydrogeology. A. Isopachs (contour interval 2 m); B. Salinity (mg/L) of formation waters; C. Potentiometric surface 74

Page

Figure 34. North-south cross-section showing the hydraulic separation between the Camrose Tongue aquifer and the Grosmont aquifer 76

Figure 35. Grosmont aquifer hydrogeology. A. Isopachs (contour interval 20 m); B. Salinity (mg/L) of formation waters; C. Potentiometric surface (10 m interval) 77

Figure 36. McMurray aquifer hydrogeology. A. Isopachs (contour interval 20 m); B. Salinity (mg/L) of formation waters; C. Potentiometric surface 81

Figure 37. Clearwater aquifer hydrogeology. A. Isopachs (contour interval 5 m); B. Salinity (mg/L) of formation waters; C. Potentiometric surface 84

Figure 38. Diagrammatic strike cross-section through the Lower Cretaceous Mannville Group in the Cold Lake study area showing the complex relations of aquifers, and oil sands deposit and shale aquitards 87

Figure 39. Mannville aquifer hydrogeology. A. Isopachs (contour interval 50 m); B. Salinity (mg/L) of formation waters; C. Potentiometric surface 88

Figure 40. Viking aquifer hydrogeology. A. Salinity (mg/L) of formation waters; B. Potentiometric surface 94

Figure 41 Isopachs (contour interval 50 m) of the Colorado aquitard system 96

Page

Figure 42. A. Dip hydraulic head cross-section showing potential cross-formational flow between the Paleozoic aquifers; B. Strike hydraulic head cross-section showing potential cross-formational flow between the Paleozoic aquifers 99

Figure 43. Pressure head/depth plots illustrating hydraulic continuity between the Lower Cretaceous and Paleozoic aquifers. A. at location 06-14-55-02 W4 Mer; B. at location 10-34-61-08 W4 Mer 101

Figure 44. General hydraulic head cross-sections showing potential cross-formational flow between the aquifers located above the Prairie aquiclude. A. Dip; B. Strike; C. Northeast-southwest in the western part of the study area 102

Figure 45. Hydraulic head cross-sections across the three model areas. A. Northern; B. Central; C. Southern 104

Figure 46. Pressure head/depth plots illustrating cross-formational flow between the Lower Cretaceous aquifers. A. at well location 10-20-60-07 W4 Mer; B. at well location 01-31-64-08 W4 Mer; C. at well location 10-36-56-10 W4 Mer; D. at well location 10-12-53-12 W4 Mer; E. at well location 11-10-67-14 W4 Mer 106

Figure 47. Isopachs of oil sands deposits. A. McMurray Formation, layer 1; B. McMurray Formation, layer 2; C. Clearwater Formation; D. Lower Grand Rapids Formation, layer 2; E. Lower Grand Rapids Formation, layer 1; F. Upper Grand Rapids Formation, layer 2; G. Upper Grand Rapids Formation, layer 1 107

Page

Figure 48. Pressure head/depth plots illustrating cross-formational flow in the Mannville Group within the area of the oil sands deposits (Tp 53-66, R 1-11, W4 Mer). A. Regional between the top of the Mannville and the top of the Upper Grand Rapids oil sands, layer 1; B. Regional between the top of the Upper Grand Rapids oil sands, layer 1, and the Pre-Cretaceous unconformity; C. at well location 11-36-54-04 W4 Mer; D. at well location 11-35-55-06 W4 Mer; E. at well location 11-21-60-08 W4 Mer 109

Figure 49. A. Location of injection sites ( ) in the Cold Lake study area; B. Schematic representation of the position of injection wells in the stratigraphic sequence 127

Figure 50. Plan view of the finite elements grid used for sensitivity analysis, Cold Lake study area 130

Figure 51. Computed freshwater potentiometric surface for the single-layered Basal Cambrian aquifer, Cold Lake study area 131

Figure 52. Outline of the model areas for simulation of effects of injection; A. In the Lower Paleozoic aquifer system; B. in the post-Prairie sequence: (A) Northern, (B) Central, and (C) Southern 136

Figure 53. Hydraulic head increase at the four injection sites in the Basal Cambrian aquifer, assuming average hydraulic properties in the Lower Paleozoic aquifer system 143

Page

Figure 54. Spread of the pressure build-up at the top of (A) Basal Red Beds, (B)Basal Cambrian aquifer, and (C) Precambrian, assuming average hydraulic properties in the Lower Paleozoic aquifer system 145

Figure 55. Hydraulic head increase at the four injection sites in the Basal Cambrian aquifer, assuming maximum values for hydraulic properties in the Lower Paleozoic aquifer system 147

Figure 56. Spread of pressure build-up at the top of the Basal Cambrian aquifer in the Lower Paleozoic aquifer system assuming (A) maximum values for both hydraulic conductivity and specific storage; (B) minimum hydraulic conductivity and average specific storage; and (C) average hydraulic conductivity and minimum specific storage 148

Figure 57. Predicted increase in hydraulic head at injection sites in Mannville aquifer. A. in Grand Rapids and B. in Lower Grand Rapids; assuming (a) average hydraulic parameters, and (b) minimum hydraulic parameters 154

Figure 58. Predicted increase in hydraulic head at injection sites in Mannville aquifer. A., C., and E. in the Rex Member; B., D., and F. in the Lloydminster Formation; assuming (a) average hydraulic parameters, and (b) minimum hydraulic parameters 155

Figure 59. Predicted increase in hydraulic head at injection sites in Clearwater aquifer. A. in Mannville C, and B. in Clearwater Formation; assuming (a) average hydraulic parameters, and (b) minimum hydraulic parameters 156

Page

Figure 60. Predicted increase in hydraulic head at injection sites in Clearwater and Mannville aquifers. A. in Clearwater Formation, B. in Lloydminster and Clearwater Formations, C. and D. at the top of the McMurray Formation; assuming (a) average hydraulic parameters, and (b) minimum hydraulic parameters 157

Figure 61. Predicted increase in hydraulic head at injection sites: A., C., D., and E. at the top of Cooking Lake Formation, B. and F. at the bottom of the McMurray Formation; assuming (a) average hydraulic parameters, and (b) minimum hydraulic parameters 158

Figure 62. Predicted increase in hydraulic head at injection sites in Beaverhill Lake aquifer system at the bottom of the Cooking Lake Formation; assuming (a) average hydraulic parameters, and (b) minimum hydraulic parameters 159

Figure 63. Spread of hydraulic head build-up as a result of injection in Mannville, Clearwater and McMurray aquifers: A. in the Mannville Group; B. in Clearwater sandstone; C. at the top of the McMurray Formation; and D. at the bottom of the McMurray Formation (also in some places top of the Cooking Lake Formation); assuming minimum hydraulic parameters for the injection aquifers 160

EXECUTIVE SUMMARY

This report, and the accompanying Atlas, represent the results of the first year of a two-year jointly funded study by the Alberta Research Council and Alberta Environment. The natural steady-state hydrogeology of a region defined as Tp 50-70, R 15 W3 Mer to R 17 W4 Mer (60 000 km^2) has been determined, using stratigraphic information from 15 000 wells, 2155 drillstem tests, 46 700 core analyses and 1858 analyses of formation waters.

The regional effects of deep waste injection were simulated with the numerical model FE3DGW at 27 sites, using projected rates up to the year 2015. The assessment of the regional effects of injection was done in terms of hydraulic head build-up only. Under the assumption of average values characterizing the hydraulic parameters, the numerical simulations revealed no interference between the different injection sites. For injection in the Basal Cambrian aquifer the resulting hydraulic head build-ups are significant, but even if formation damage (fracturing) takes place, the overlying thick Lower Devonian aquiclude will prevent propagation higher in the sequence. Due to the complexity of the hydrostratigraphic sequence, injection in the post-Prairie Formation rocks was simulated for three partially overlapping areas. The hydraulic head build-up in this sequence is predicted to be below fracture pressures for the next 30 years. It is concluded that the system can sustain the projected rates of injection on a regional scale, at distances from the injection wells greater than 500 to 1000 m. Further studies should evaluate the effects of injection on a local scale, near the injection wells.

INTRODUCTION

This report, together with the accompanying Atlas, represents the results of the first year of a two-year jointly funded contract between the Alberta Research Council and Alberta Environment. The present contract work is an extension of a previous jointly funded study which examined the hydrogeology of the Cold Lake region of Alberta in a more restricted area. Following that study it was decided to expand the area of investigation to the south in Alberta, and eastward to Tp 15 W3Mer in Saskatchewan, in order to include pilot and commercial operations in all major oil sands and heavy oil occurrences in the region which either practiced deep waste disposal or predicted the need for deep waste disposal in the future. The study area was made large enough to ensure both adequate representation of the natural steady-state flow regime and eliminate artificial boundary effects in the selected model area. The approach and techniques used were generally similar to those of the previous study, and only details of significant differences in technology are given in this report. It should be pointed out that since the previous study was completed there have been some changes in the accepted stratigraphic terminology which have been incorporated here, but which are not substantive with respect to the broad results of both studies.

For the purpose of this report the Cold Lake study area is defined as Tp 50-70, R 15 W3Mer to R 17 W4Mer (figure 1). The study area straddles the Alberta-Saskatchewan border and includes the entire Lower Cretaceous Cold Lake oil sands deposit and the adjacent heavy oil region to the south, from Lindberg to the northern part of the Lloydminster field.

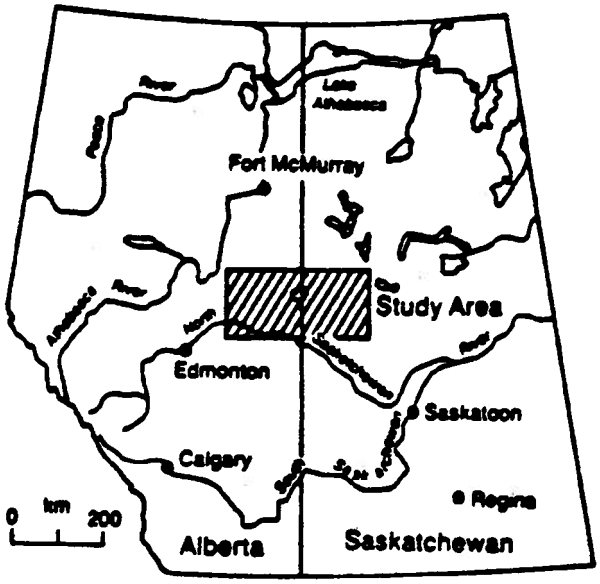

Figure 1. Cold Lake study area, Alberta and Saskatchewan

Included within this oil sands/heavy oil belt are a number of pilot plants, commercial oil sands recovery projects and heavy oil recovery schemes. Deep waste injection of residual waters from these pilot plants and commercial operations is projected to the year 2015 at 27 sites. The objective of this part of the study was to determine the present steady-state natural flow regime and to perturb the regime using the projected injection rates in order to evaluate the regional effects of deep waste injection. It must be remembered that in the previous study it was demonstrated that flow in the Quaternary could be decoupled from flow in the Phanerozoic, and hence the present investigation was concerned only with perturbed flow in the Phanerozoic.

The report is presented in three sections: regional geology (by Anne Ing), analysis of the natural flow regime (by Claude M. Sauveplane and Brian Hitchon), and numerical simulation of regional effects of injection (by Stefan Bachu). The report contains two appendices; the first (by Stefan Bachu, Andre T. Lytviak and Claude M. Sauveplane) briefly reviews the data base and data processing techniques and provides the reader with an overview of the technology and any significant changes introduced since the previous jointly funded study was completed; the second (by Claude M. Sauveplane) presents the regional hydrodynamic information in tabular and graphical form without comments. The accompanying Atlas (Hydrogeology of the Cold Lake Study Area, Alberta and Saskatchewan, Canada) is a compilation of 127 geological, hydrodynamic and hydrochemical maps and cross-sections. Two copies only have been prepared, one for each of the two funding agencies.

It is the intention of the Alberta Research Council to publish information on the regional steady-state flow regime as a Council bulletin, and hence the text and illustrations have been prepared in an appropriate format. Subject to agreement with Alberta Environment, it is planned to incorporate the numerical simulation of regional effects of injection into a second Council bulletin together with detailed studies of more local effects of injection to be carried out in the second year of this jointly funded study. Standard SI units have been used throughout this report, including those for time: s = second, min = minute, h = hour, and a = year (annum).

REGIONAL GEOLOGY

Anne Ing

INTRODUCTION

This section of the report presents an overview of the Phanerozoic history of the Cold Lake study area, in the context of the major depositional and erosional events that have taken place in this part of the Western Canada Sedimentary Basin. The stratigraphic column is broken up into discrete sedimentary packages each of which represents deposition in a distinct paleogeographic configuration with characteristic overall geometry and internal facies patterns. This provides the necessary background information fundamental to the hydrogeological portion of this study.

The two main sources of information used to generate regional geological maps for the Cold Lake study area were the well data files of the Alberta Energy Resources Conservation Board (ERCB) and Saskatchewan Energy and Mines. Variation in the amount and distribution of data throughout the stratigraphic column reflects the distribution of oil and gas reservoirs. In general, the amount of data increases dramatically for formations within the Upper Devonian and Cretaceous, where most of the major oil and gas discoveries have been made. This bias is also reflected in the literature where the sedimentological understanding is far greater in formations that have economic implications.

Reference to geophysical well logs was undertaken for formations that are geologically more complex, and which required a greater degree of refinement. For example, delineation of discontinuous, thin oil sand layers was done manually using a network of well log cross-sections.

The geological synthesis of the study area was compiled and illustrated through a series of slice maps spanning from the Precambrian to the top of the bedrock. These slice maps were used to determine the geometry of the sedimentary basin during various stages in its overall evolution. The stratigraphic nomenclature used in the study area is shown in Table 1.

WESTERN CANADA SEDIMENTARY BASIN

The Western Canada Sedimentary Basin is a westward-thickening wedge of sedimentary strata which attains a maximum thickness of more than 6 km in the axis of the Alberta Syncline (figure 2). It extends southwest from a zero edge at the Canadian Shield outcrop to a maximum thickness at the front of the Cordilleran Foreland Thrust Belt. Regional dips are 5 to 10 m/km.

Publications by McCrossan and Glaister (1964), Parsons (1973) and Porter et al. (1982) provide good overall reviews of the geological history of the Western Canada Sedimentary Basin.

The geological history of the Western Canada Sedimentary Basin is linked to two fundamentally different tectonic settings. The initial platformal phase involved transgressive onlap of the Precambrian crystalline basement of the North American craton and the development of epeirogenic arches and basins on the cratonic platform (Porter et al., 1982). It coincides with deposition of Proterozoic to Jurassic sediments and is dominated by shallow water carbonates and evaporitic sequences.

Table 1. Generalized stratigraphic nomenclature and hydrostratigraphy, Cold Lake study area

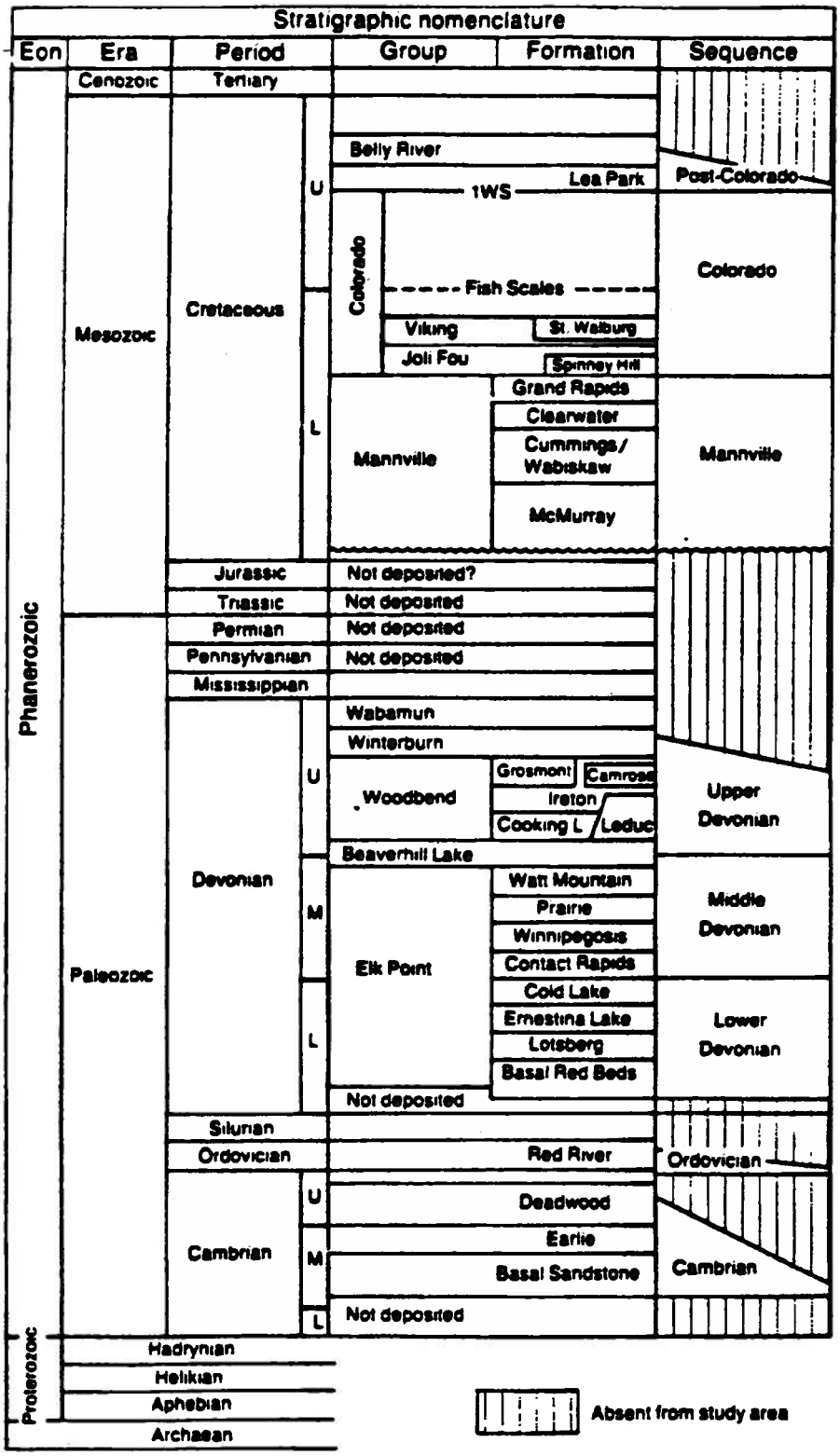

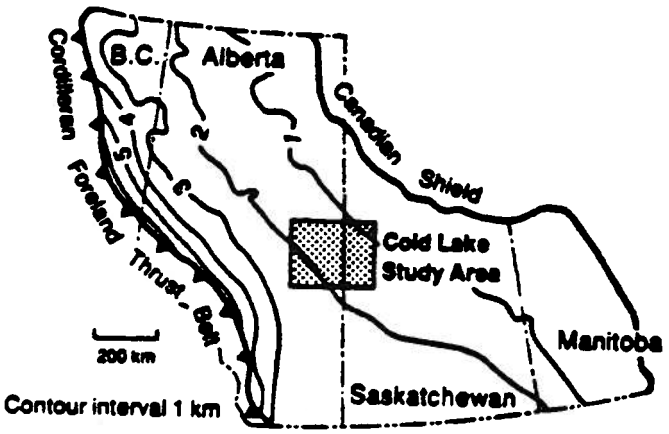

Figure 2. Total preserved thickness of Phanerozoic rocks east of the Cordilleran foreland thrust belt

During the Late Jurassic to Paleocene interval, exotic terrains were accreted to the western margin of North America. The continental terrace wedge was compressed, detached from its basement, and thrust over the flank of the craton to form the present eastern part of the Cordillera. The continental lithosphere responded to the tectonic loading by isostatic flexure, thus initiating the development of a foreland basin. The sediments that filled the foreland basin comprise clastic detritus shed by the evolving Cordillera.

BASIN ANALYSIS

In order to assess the stratigraphic evolution of the subject part of the Western Canada Sedimentary Basin, it is necessary to subdivide the strata into smaller, geologically significant sequences. Hubbard et al. (1985) defined a depositional sequence as a representation of a single basin configuration that has basin margins, a depocentre and an internal facies pattern. The distribution of a depositional sequence defines the geometry of the basin while the internal architecture reflects the nature of the infilling. Sedimentation and subsidence are factors that control the duration of a sequence. In turn, megasequences (superposed sequences) represent major phases of basin evolution which are the result of tectonic processes.

The regional geology of the Cold Lake study area is discussed in terms of sequences that represent deposition during the different configurations of the Western Canada Sedimentary Basin through time (Table 1). However, as discussed earlier, this is done in two parts, corresponding to the two major tectonic regimes that controlled deposition in the Western Canada Sedimentary Basin.

DEVELOPMENT OF THE PASSIVE CONTINENTAL MARGIN SUCCESSION

Precambrian Basement

The Precambrian continental craton, which forms the basement of the Western Canada Sedimentary Basin, consists mainly of Archaean crystalline rocks and Aphebian (2500-1750 Ma) supracrustal rocks that were modified by deformation, metamorphism and magmatism during the early Proterozoic (1750 Ma) Hudsonian orogeny, and are exposed in the Churchill Province of the Canadian Shield (Porter et al., 1982). The exposed rocks of the Churchill Province have a strong northeast-southwest structural trend. The parallel orientation of some of the cratonic arches, such as the Peace River Arch, suggests that this structural grain continues into the subsurface. In the Cold Lake study area, the Precambrian basement dips gently towards the southwest (figure 3A).

Cambrian

The first sequence, comprising Middle to Upper Cambrian strata, marks the beginning of the Phanerozoic record of deposition on the cratonic platform. Unlike much of the later Phanerozoic, the pattern of sedimentation was not influenced by vertical movement of cratonic arches. The sea trangressed eastward and deposited a basal quartz sand over the entire western flank of the craton (Pugh, 1973). This basal sandstone unit is derived from the Precambrian basement, and becomes progressively younger towards the east. An isopach map of the Basal

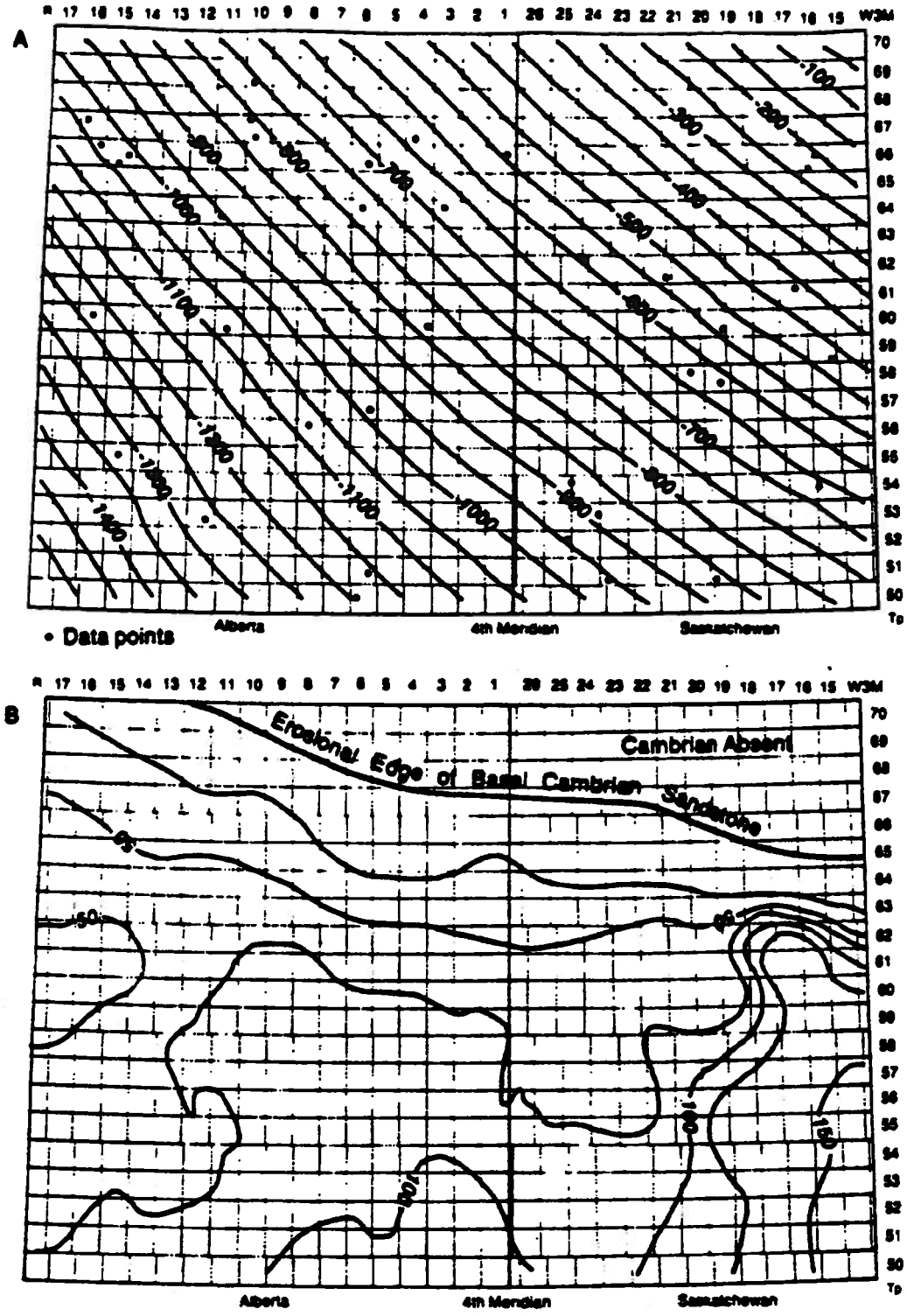

Figure 3. A. Structure contour map of the Precambrian surface (contour interval 50 m); B. Isopach map of the Basal Cambrian sandstone (contour interval 50 m)

Cambrian sandstone (figure 3B) reflects the uneven distribution of the unit. Substantial thickening occurs in the southeast part of the study area, whereas the sandstone is significantly thinner in the vicinity of Tp 60, R 16 W4. The Basal Cambrian sandstone thins northward, with the approximate zero edge between Tp 65-70.

North of this erosional edge is the Granite Wash. However, mapping the Granite Wash poses a number of problems. Although it is a reworked sand deposit, it shows a high gamma ray signature, making it indistinguishable from shaly deposits. In addition, due to the lack of well control in the northern portion of the study area, it is not possible to resolve whether the Granite Wash is actually present, whether it is porous and permeable, or whether it is in contact with the Basal Cambrian sandstone.

With continued transgressions, the basal sand gave way to a series of shallowing upward cycles. Each cycle begins with shale and grades upward into carbonate rocks. Laterally, three broad facies belts can be recognized: an inner detrital belt, a middle carbonate belt, and an outer detrital belt. The study area is situated in the inner detrital belt where there is a higher proportion of shale, siltstone and sandstone (Pugh, 1973). It represents detritus eroded from the Precambrian craton. As a result, Cambrian rocks in the Cold Lake study area are represented only by a series of glauconitic siltstones and shales of the Earlie and Deadwood formations. Figure 4A is a structure contour map on the top of the Cambrian and figure 4B shows the total thickness of the Cambrian in the study area.

Following the accumulation of the Cambrian sequence, the Western Canada Sedimentary Basin was affected by a pre-Middle Ordovician episode

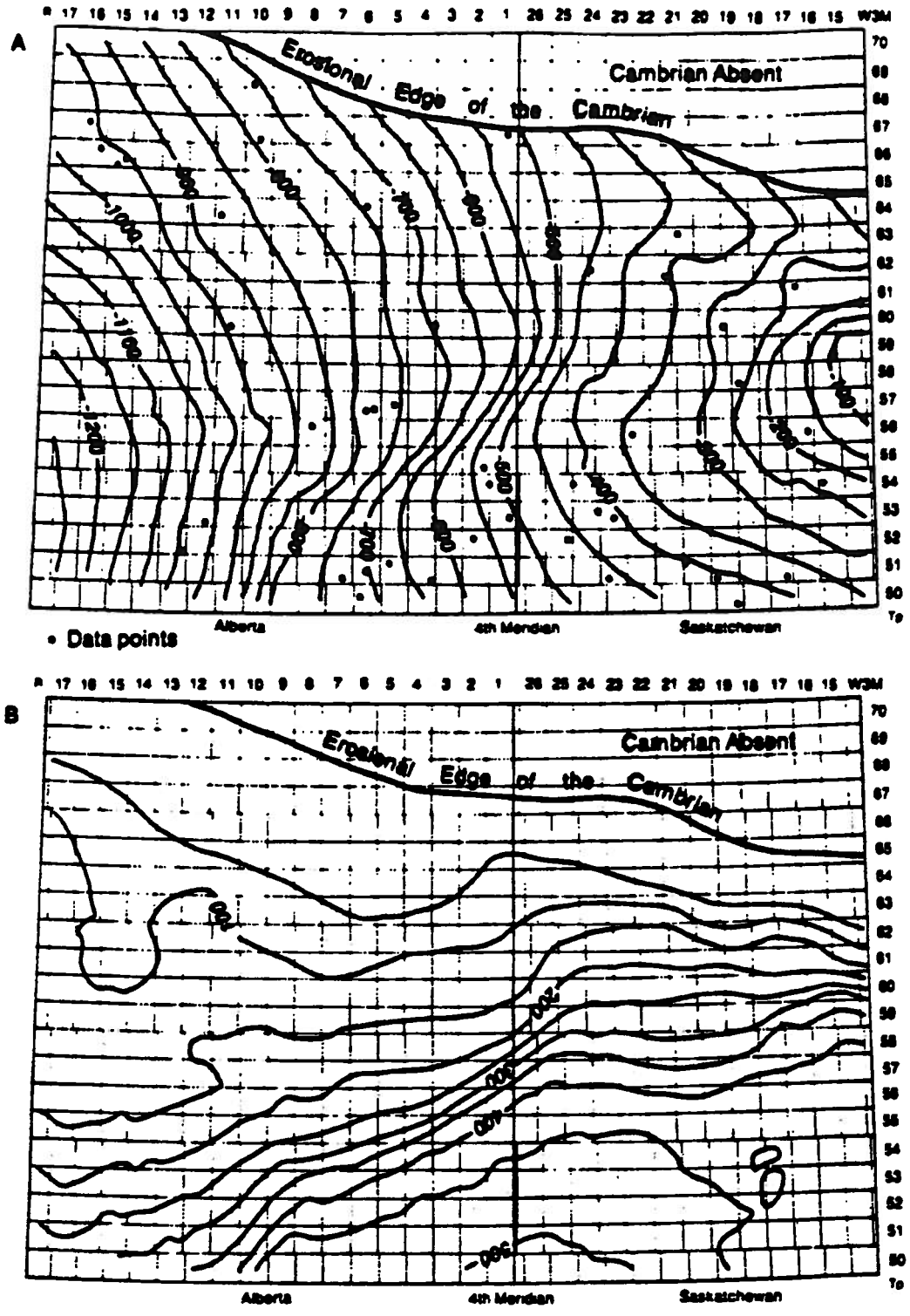

Figure 4. A. Structure contour map on top of the Cambrian (contour interval 50 m); B. Isopach map of the Cambrian (contour interval 50 m)

of uplift and erosional bevelling. The regional eastward bevelling marked a relatively uniform westward tilt of the craton. Cratonic arches and basins also developed at this time and had a profound influence on the patterns of sedimentation (figure 5).

Ordovician

The Ordovician transgression extended eastward over most of the cratonic platform, depositing basal sands followed by shallow-water carbonate sediments. The shallow-water carbonate shelf environment and associated evaporitic conditions persisted well into Silurian time. An extensive pre-Devonian episode of erosion removed most of the Ordovician and Silurian strata except in the Williston Basin, which was established during the early stages of this depositional sequence. Only a portion of the Red River Formation, a carbonate unit, is preserved in the southeastern corner of the study area (figure 6B). Silurian rocks are confined to the central part of the Williston Basin and are not present in the study area.

Pre-Devonian erosion was more pronounced than the previous erosional episode, affecting parts of the Cambrian sequence not covered by Middle Ordovician strata. It left behind a northward facing curvilinear, erosional feature known as the Meadow Lake Escarpment (figure 6A). South of the escarpment, the Cambrian was unaffected by pre-Devonian erosion, while to the north, the Cambrian thins markedly (figure 4B). The north side of the Meadow Lake Escarpment, a topographic low, became a depocentre for Devonian sedimentation.

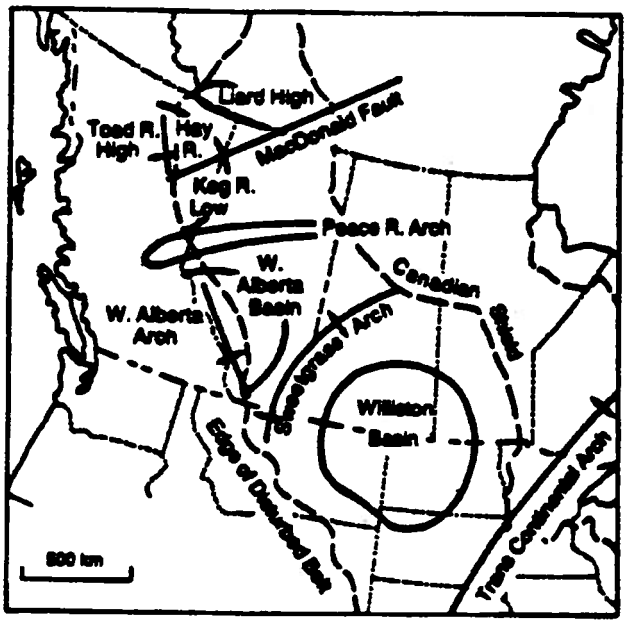

Figure 5. Cratonic arches and basins of western Canada (after Stelck, 1975)

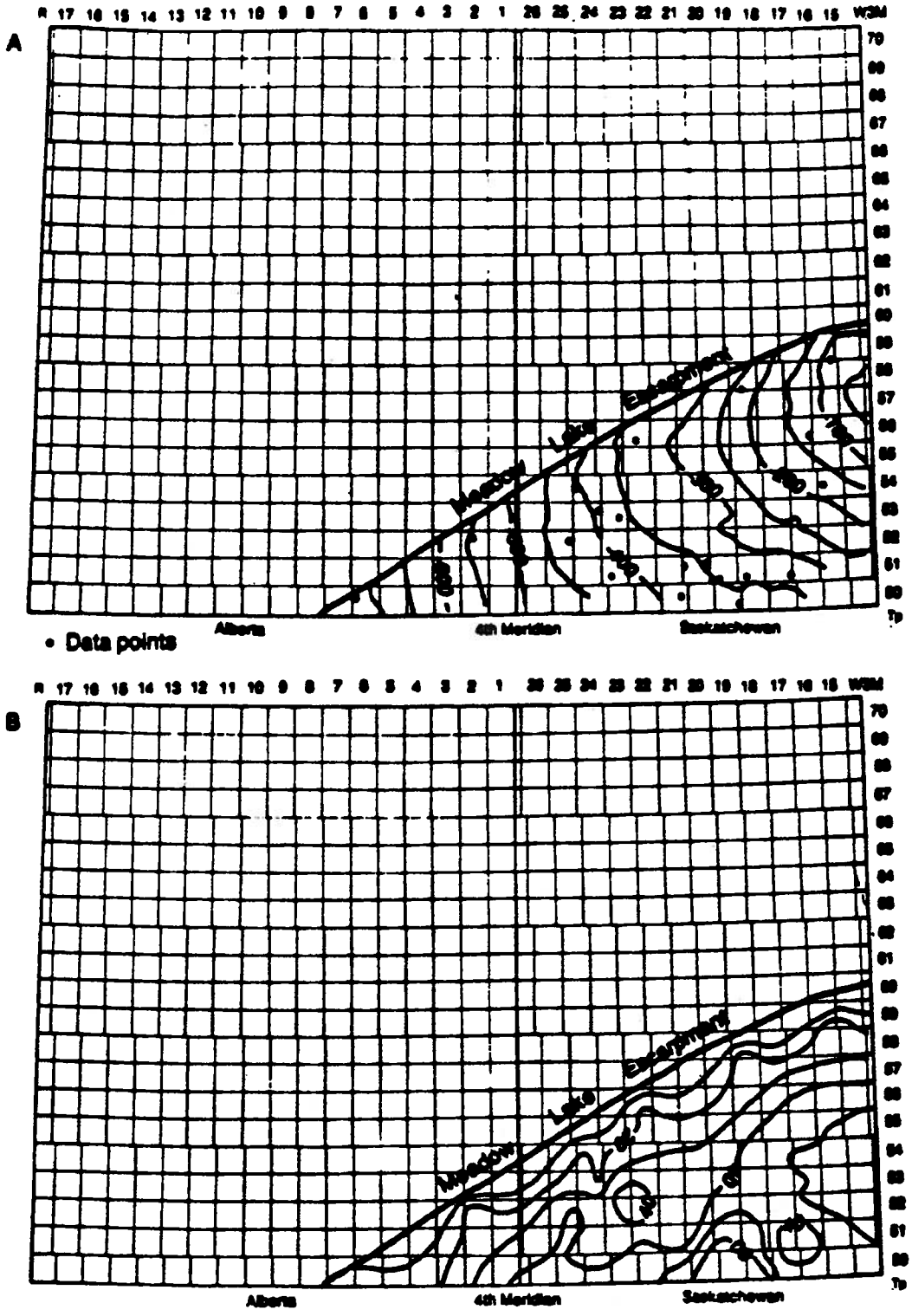

Figure 6. A. Structure contour map on top of the Ordovician (contour interval 50 m); B. Isopach map of the Ordovician (contour interval 10 m)

Lower Devonian

The Lower Devonian comprises formations within the lower Elk Point Group (Table 1). The basin configuration was controlled by the epeirogenic uplift of the cratonic arches and by the pattern of erosional relief. The lower Elk Point basin was bounded by the Tathlina Uplift, the Western Alberta and Peace River Arches, and the Meadow Lake Escarpment (figure 7A). The relief on the pre-Devonian unconformity surface forced epeiric seas to transgress from northwest to southeast instead of from the previous westerly direction. Up to 400 m of Lower Devonian rocks are present in the study area (figure 7B).

Initial Lower Devonian deposits consisted of clastics of the Basal Red Beds, sourced from the surrounding cratonic arches. A series of massive halite beds (Lower Lotsberg, Upper Lotsberg and Cold Lake salts) onlapped the edge of the lower Elk Point basin. They reflect restricted circulation due to the presence of carbonate build-ups across the northern outlet (Fuller and Porter, 1969). Between the Lotsberg and Cold Lake Formations is the thin (less than 20 m) Ernestina Lake Formation, which comprises argillaceous dolomite and dolomitic shales. Figure 8 shows the distribution of the three main salt bodies deposited during this period in the Cold Lake region. Note that their western and southeastern margins are depositional, whereas their eastern boundaries are the result of subsequent salt dissolution by meteoric water. The maximum total thickness of salt beds is about 270 m in the study area (figure 9).

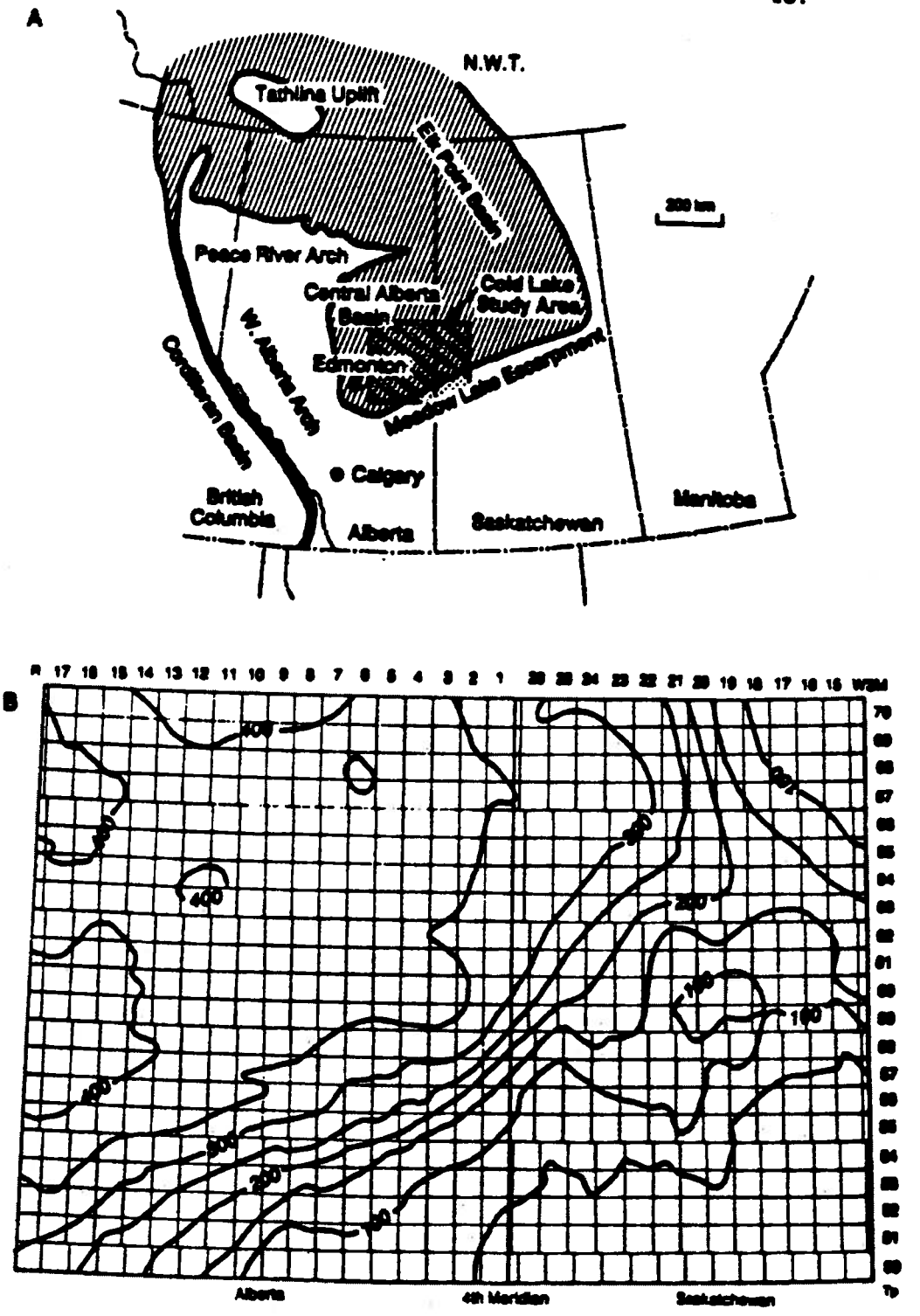

Figure 7. A. Configuration of the Western Canada Sedimentary Basin during the Early Devonian (simplified from Grayston et al., 1964); B. Isopach of the Lower Devonian (contour interval 50 m)

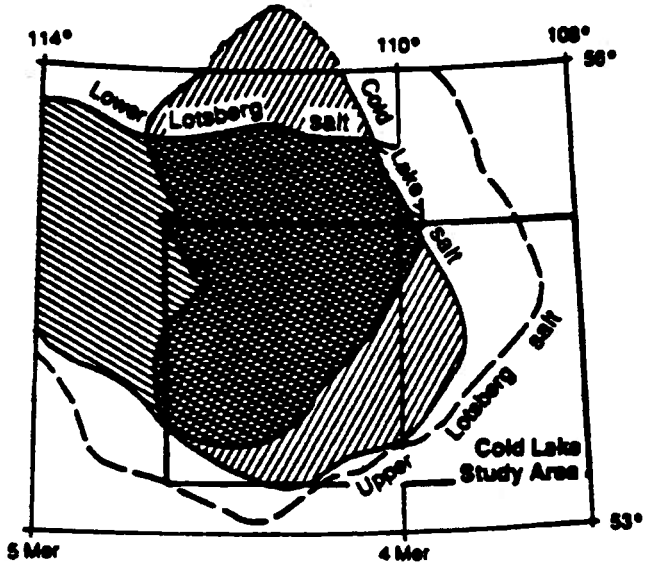

Figure 8. Distribution of Lower Devonian Elk Point Subgroup salts in the Cold Lake region (after Hamilton, 1971)

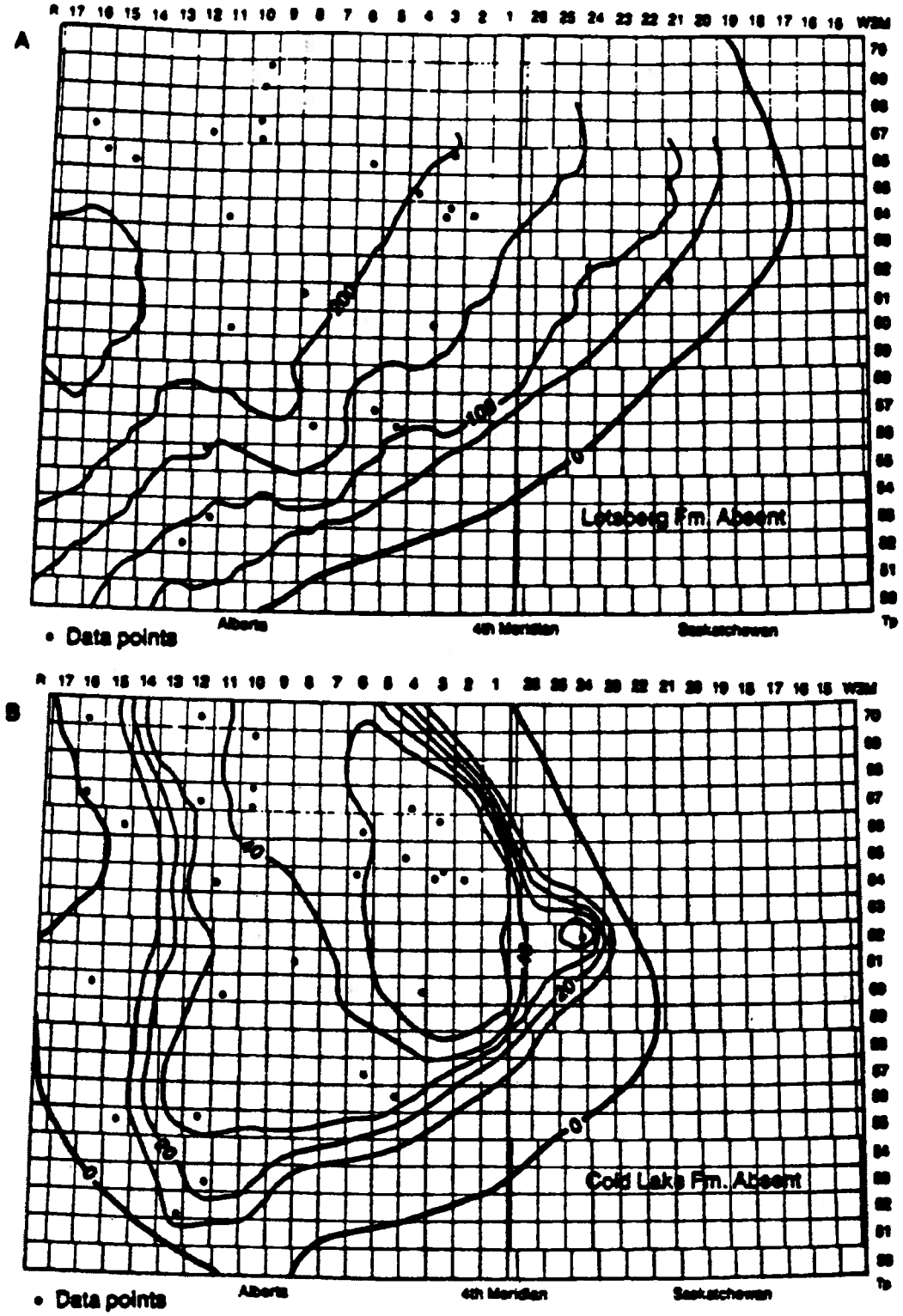

Figure 9. A. Isopach map of the Lotsberg Formation (contour interval 50 m);
B. Isopach map of the Cold Lake Formation (contour interval 10 m)

Middle Devonian

During the Middle Devonian, the sea transgressed further south into the U.S.A. and the geometry of the basin changed correspondingly (figure 10A). The Peace River and Western Alberta Arches remained emergent while the Meadow Lake Escarpment was completely submerged. In the Cold Lake study area Middle Devonian rocks range in thickness to more than 250 m (figure 10B).

The oldest unit of the Middle Devonian comprises the argillaceous dolomite and dolomitic shales of the Contact Rapids Formation, indicating a transition from restricted to more open water conditions.

This was followed by deposition of the widespread basal carbonate unit of the upper Elk Point Group, which is known as the Winnipegosis Formation in the Cold Lake study area and ranges from 30 m to 80 m in thickness. It is commonly highly dolomitized although varying thicknesses of original limestone are preserved in some areas. An isopach map of the Winnipegosis Formation shows thickening in isolated parts of the eastern portion of the study area (figure 11). These represent reefal build-ups close to the eastern edge of the upper Elk Point basin.

The remaining history of the Elk Point basin was dominated by deposition of evaporites. The Prairie Formation, the most extensive evaporitic unit, developed southeast of the Presqu'ile carbonate barrier. The Peace River and Western Alberta Arches remained emergent and supplied clastic sediments to the western margin of the evaporitic basin. In the Cold Lake study area, the Prairie Formation is dominantly salt, and ranges from 10 m to 160 m in thickness, except along the

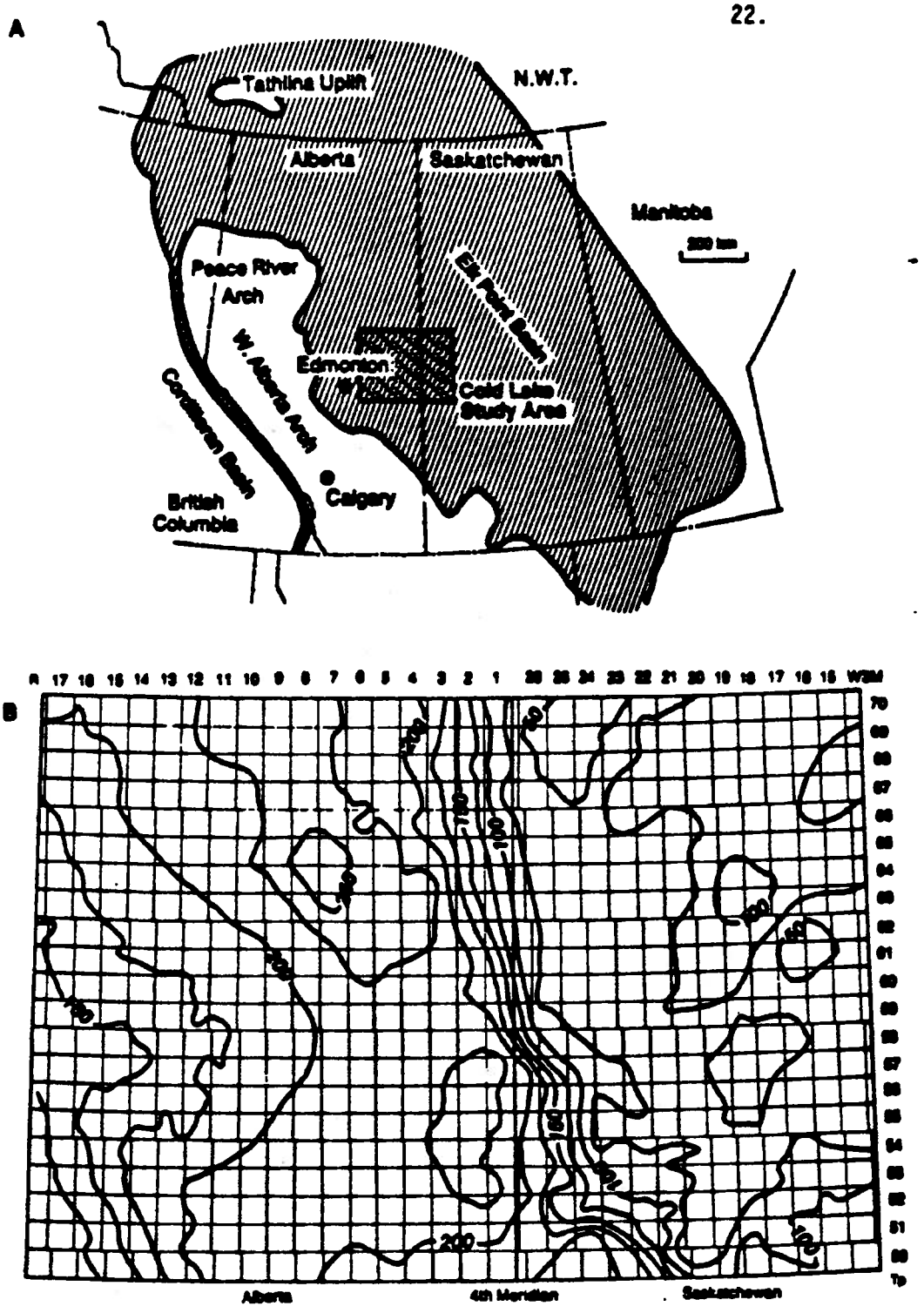

Figure 10. A. Geometry of the basin during Middle Devonian time (simplified from Grayston et al., 1964); B. Isopach map of the Middle Devonian (contour interval 25 m)

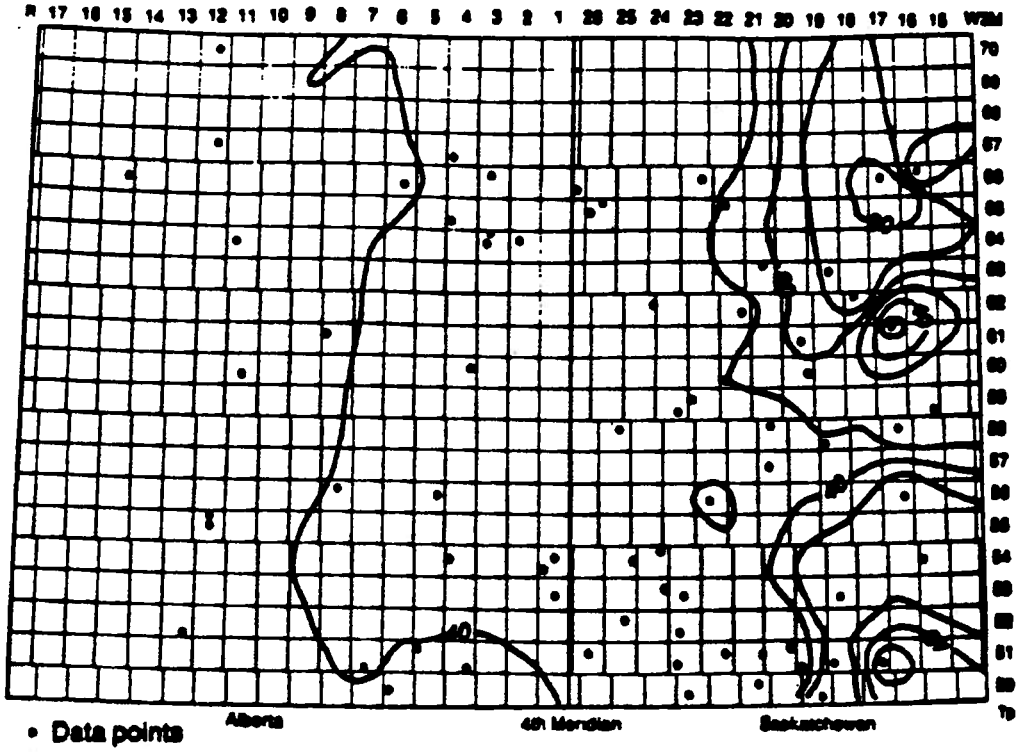

Figure 11. Isopach map of the Winnipegosis Formation (contour interval 10 m)

eastern margin where extensive salt solution has taken place (figure 12B). The effects of salt solution and the subsequent collapse of overlying strata is well illustrated by a structure contour map on top of the Prairie Formation (figure 12A). Upper Elk Point sedimentation ended with the deposition of the First Red Bed - Watt Mountain clastic interval, and a return to the more widespread, normal marine conditions (Grayston et al., 1964).

Upper Devonian

The Upper Devonian depositional sequence records major back-stepping and onlap of shallow marine carbonate platforms towards the interior of the continent (Wendte, 1982). There was a progressive southeastward shift of platform margins and their associated reef complexes from the Slave Point edge in northwestern Alberta to the Leduc shelf-margin complex in southern Alberta (figure 13). Widespread carbonate platforms and isolated reef complexes constitute the major components of the sequence, while basin-filling limestones and shales are minor components.

In the Cold Lake study area, the Beaverhill Lake Group represents the first of these carbonate platforms and is of Middle Devonian/Upper Devonian age. Thicknesses are uniform, around 250 m, except in the subcrop region where as little as 36 m remain along the eastern margin (figure 14A). A structure contour map of the Beaverhill Lake Group shows a uniform regional dip towards the southwest except in the subcrop region where collapse due to salt-solution in the underlying Prairie Formation has disturbed the structure. Collapse due to salt removal continued to influence the structure of formations up to Cretaceous time.

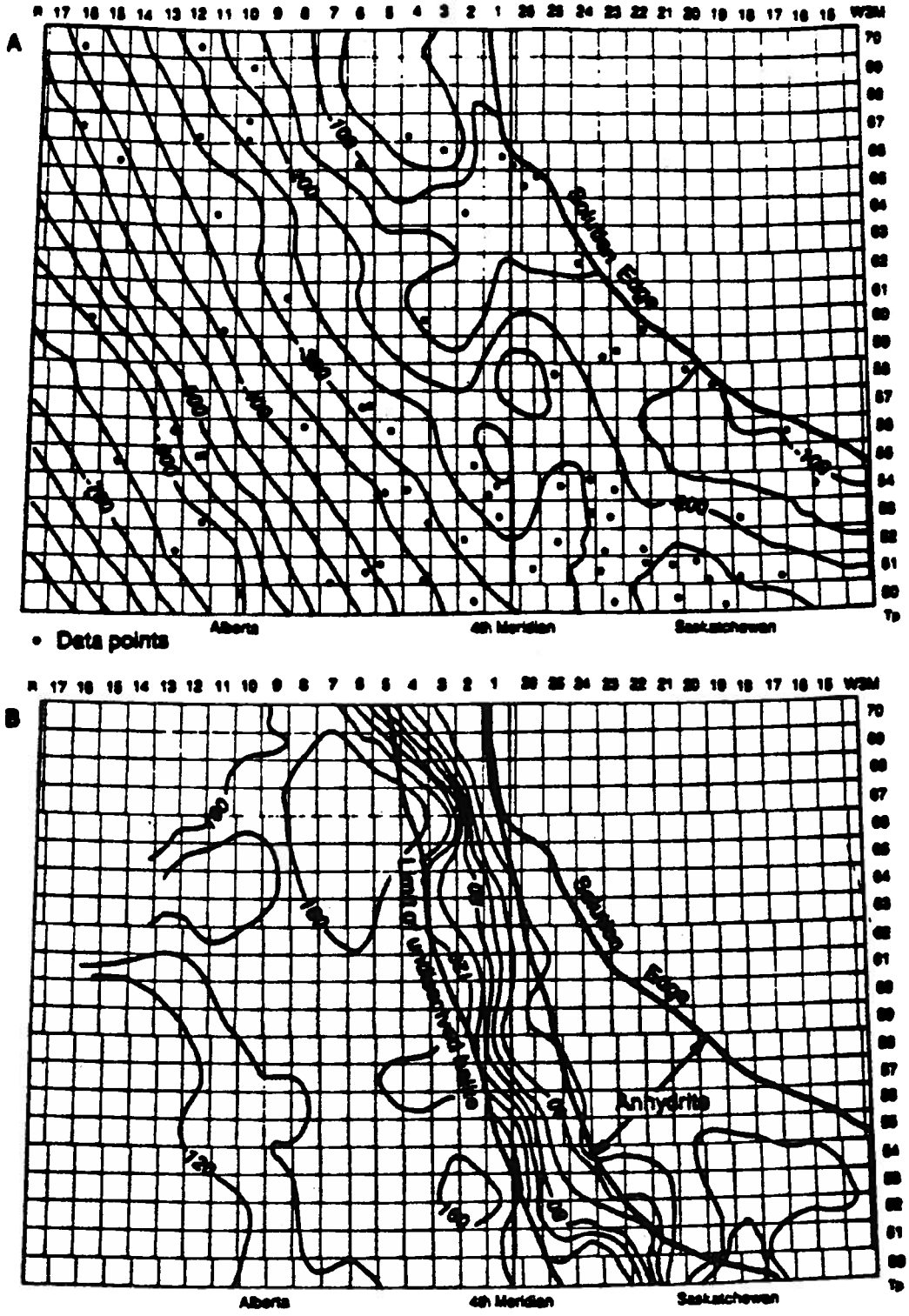

Figure 12. A. Structure contour map on top of the Prairie Formation (contour interval 50 m); B. Isopach map of the Prairie Formation (contour interval 20 m)

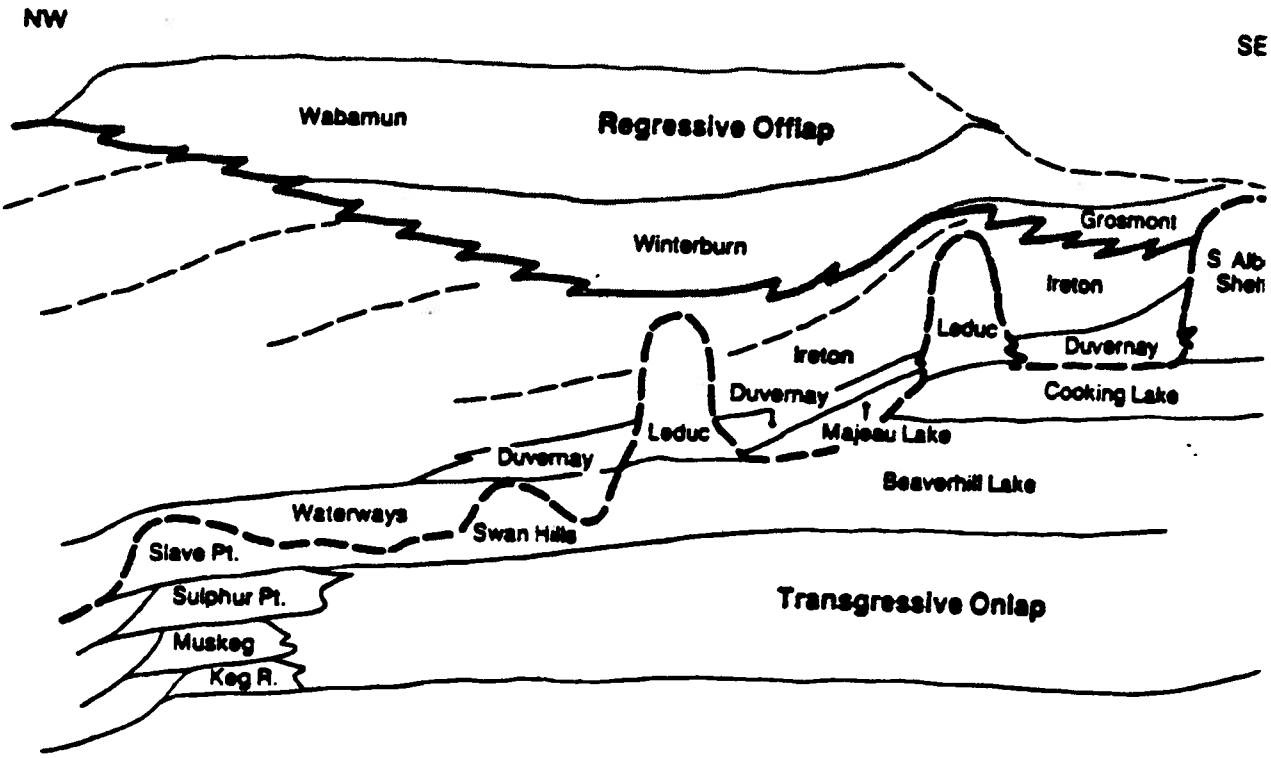

Figure 13. Schematic diagram illustrating carbonate onlap and offlap during the Upper Devonian (after Wendte, 1982)

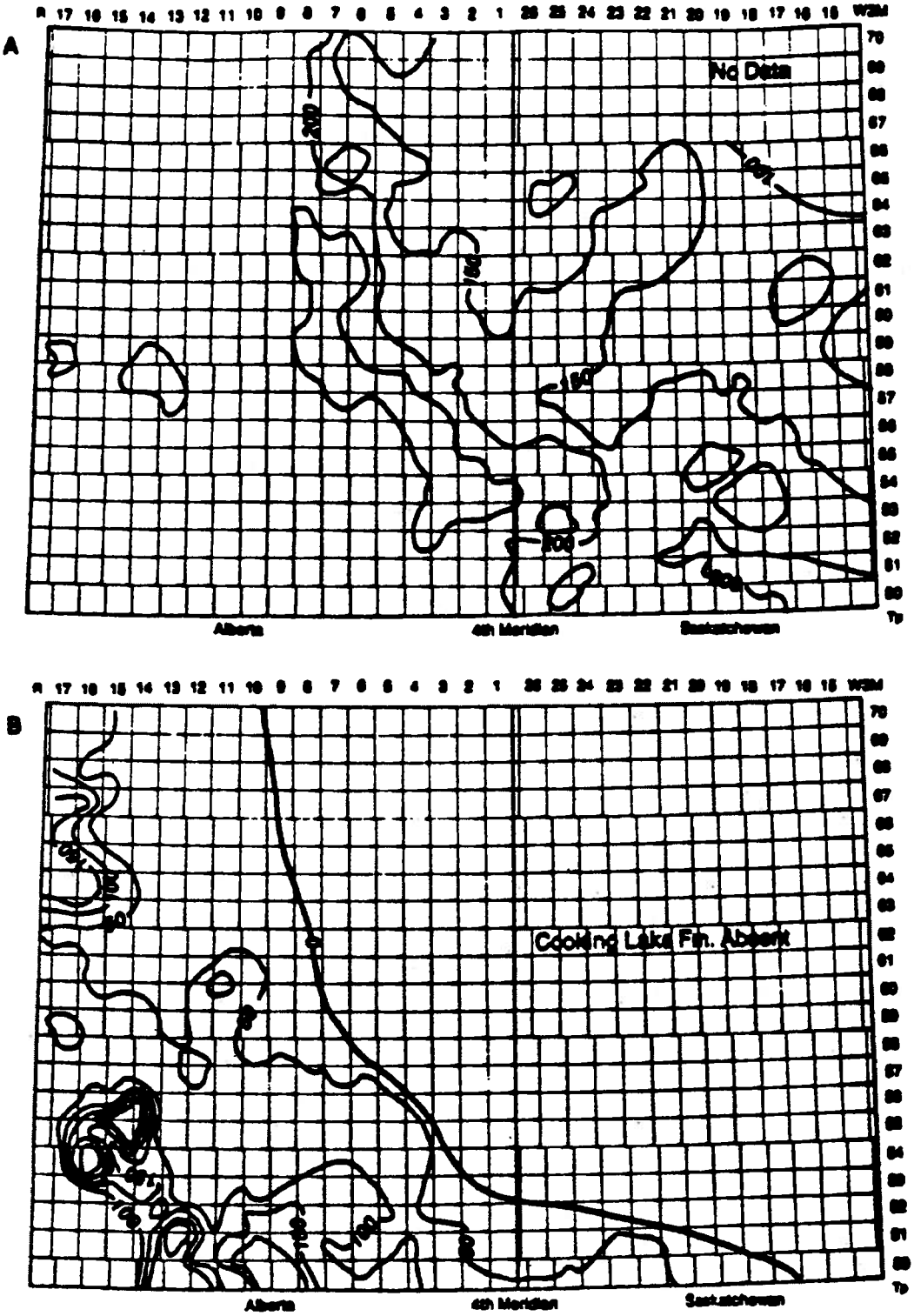

Figure 14. A. Isopach map of the Beaverhill Lake Group (contour interval 50 m); B. Isopach map of the Cooking Lake and Leduc Formations (contour interval 50 m)

With continued transgression, the platform margin backstepped from the Swan Hills (Beaverhill Lake Group) edge in west-central Alberta to the Cooking Lake edge in central Alberta (figure 13). The platformal limestones of the Cooking Lake Formation conformably overlie the Beaverhill Lake Group and range in thickness up to 75 m in the study area. Localized reefal carbonates of the Leduc Formation occur on the edge of the platform margin. The combined Leduc and Cooking Lake isopach map (figure 14B) shows the position of the reefs at the southwest corner of the study area.

Shales (more correctly argillaceous lime mudstones) of the Ireton Formation infilled the basin where reef complexes did not develop. With each southward transgression of the platform margin, reef complexes drowned, to re-establish themselves on the next successive platform margin.

The succeeding Upper Devonian strata record major basin-filling and offlap of shallow-marine, carbonate platforms away from the interior of the continent (figure 13). This regressive sequence is characterized by argillaceous lime mudstones (generally referred to as basinal shales) capped by a widespread diachronous blanket of thinly developed carbonate platforms (Stoakes, 1982).

During the initial regression, growth of Leduc Formation reefs was terminated by the progradation of the Grosmont carbonate platform and by shales of the Ireton Formation. The Grosmont Formation is a widespread dolomitized platform carbonate, which crops out along the Peace River in northern Alberta and extends 500 km south to its limit in the Cold Lake study area. Correlative surfaces can be traced from the platform into the basin and reflect the depositional topography at various stages during basin-filling (Stoakes, 1982).

In ascending order, the overlying Upper Devonian Camrose Member, Winterburn and Wabamun Groups, and Mississippian strata, formed in the same manner as the Grosmont Formation. However, due to severe Cretaceous erosion, only remnants of the Grosmont, Camrose and Winterburn complexes are preserved along the western margin of the Cold Lake study area. Figure 15B is an isopach map showing the total thickness of Upper Devonian strata.

A structure map of the Pre-Cretaceous unconformity (figure 15A) shows the severity of the erosion that took place. The period from Late Fammenian (Late Devonian) to Early Neocomian (Early Cretaceous) was one of net erosion in the study area.

EVOLUTION OF THE FORELAND BASIN

A major tectonic event (Columbian Orogeny) took place between the Middle Jurassic and Early Cretaceous, transforming the Western Canada Sedimentary Basin from a passive cratonic platform to an active foreland basin. Exotic oceanic terrains and island arc complexes collided with, and accreted to, the western margin of the continent. The stable continental lithosphere responded by isostatic flexure to form a foreland basin migrating ahead of the advancing mountain front (Beaumont, 1981).

The shallow-water carbonates and associated evaporites that dominated the Paleozoic were replaced by stacked wedges of synorogenic clastics shed from the Cordilleran foreland thrust belt. Cretaceous strata are divided into three depositional sequences corresponding to the Mannville, Colorado and Post-Colorado Groups. The Mannville

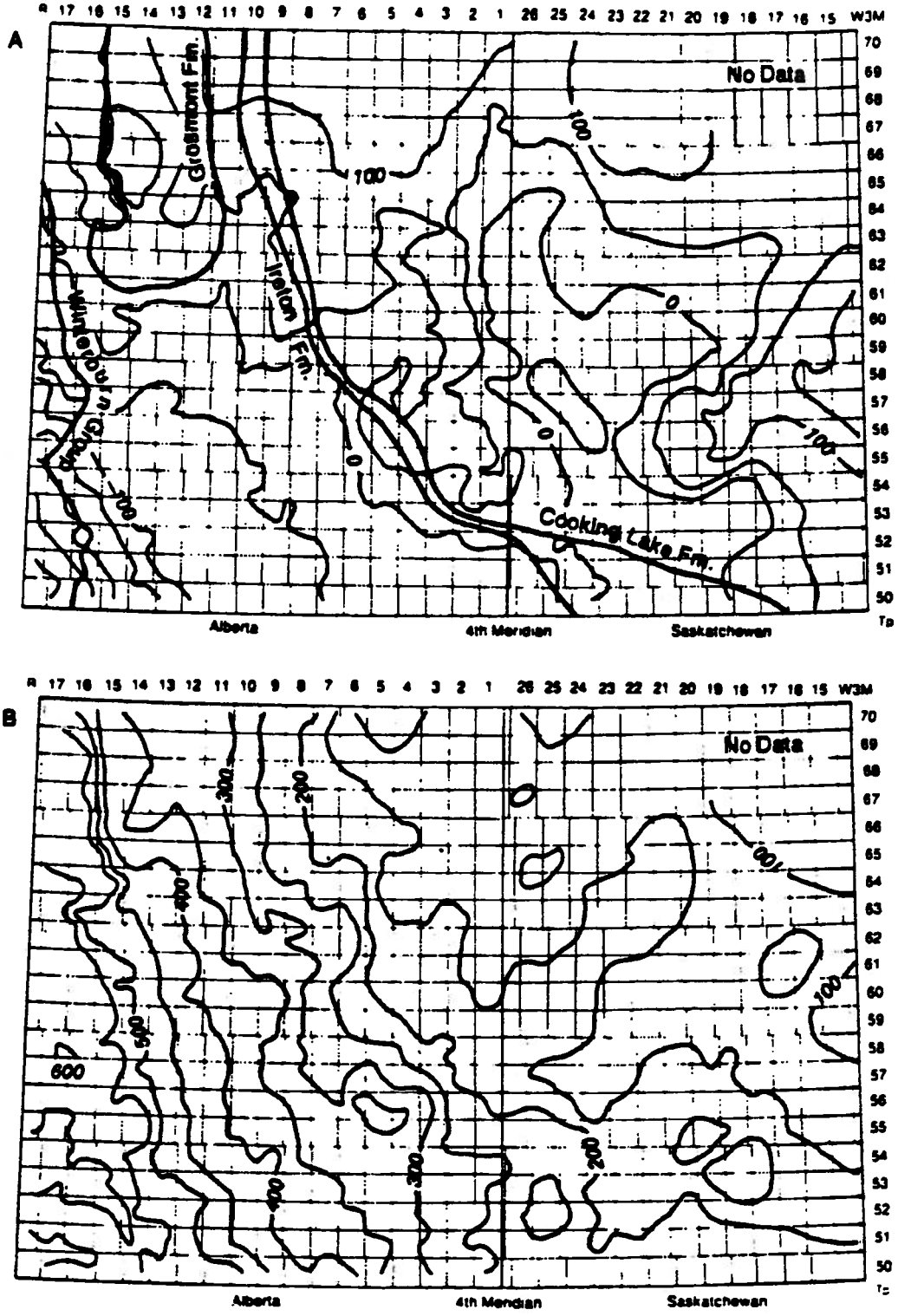

Figure 15. A. Stracture contour map on top of the Pre-Cretaceous unconformity surface (contour interval 50 m; 3608 data points used); B. Isopach map of the Upper Devonian (contour interval 50 m)

represents the Columbian phase of Cordilleran deformation, the Colorado belies a lull in plate convergence, and the Post-Colorado strata represent response to the Laramide phase of Cordilleran deformation (Beaumont, 1981).

Lower Cretaceous (Mannville)

The earliest synorogenic clastic wedge shed from the emerging Cordillera consists of formations within the Mannville Group. The Mannville Group was deposited within a shallow-water basin that opened towards the northwest. The pre-Mannville unconformity surface, the basin floor, comprised westward dipping strata ranging in age from Jurassic in the west to Devonian in the east. Differential erosion and incised drainage led to the development of a series of northwest-southeast trending ridges and valleys (figure 16). The topographic relief created by these ridges and valleys influenced sedimentation and the subsequent entrapment of heavy oil. Figure 17A shows the structure on the top of the Mannville Group and figure 17B the overall thickness.

The Mannville Group has been divided into three subunits: (Putnam, 1982; Jackson, 1984).

The lower Mannville was deposited as fluvial, valley-fill sediments in the incised valleys of the Pre-Cretaceous unconformity surface. Lower Mannville sedimentation was activated by a marine transgression that originated from the northwest (Williams, 1963). In the Cold Lake study area, these sands are known as the McMurray Formation.

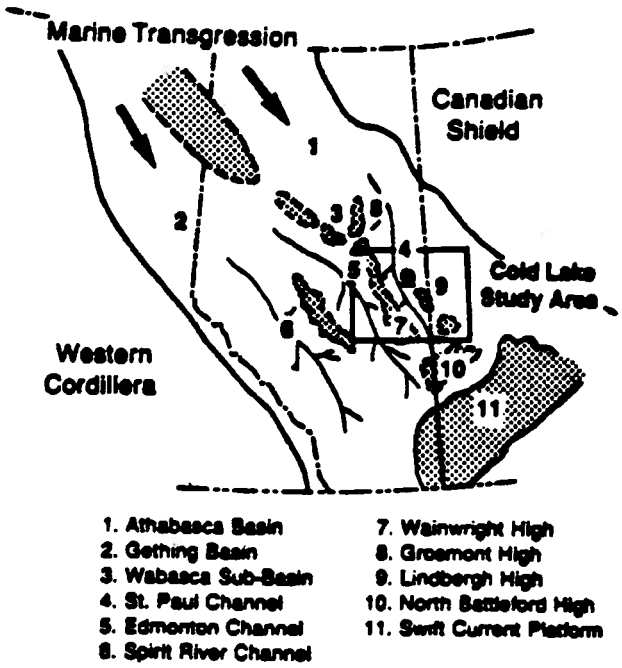

Figure 16. Approximate Mannville paleogeography at the Aptian-Albian boundary, showing basin outlines and topographically high areas with inferred drainage (after O'Connell, 1985)

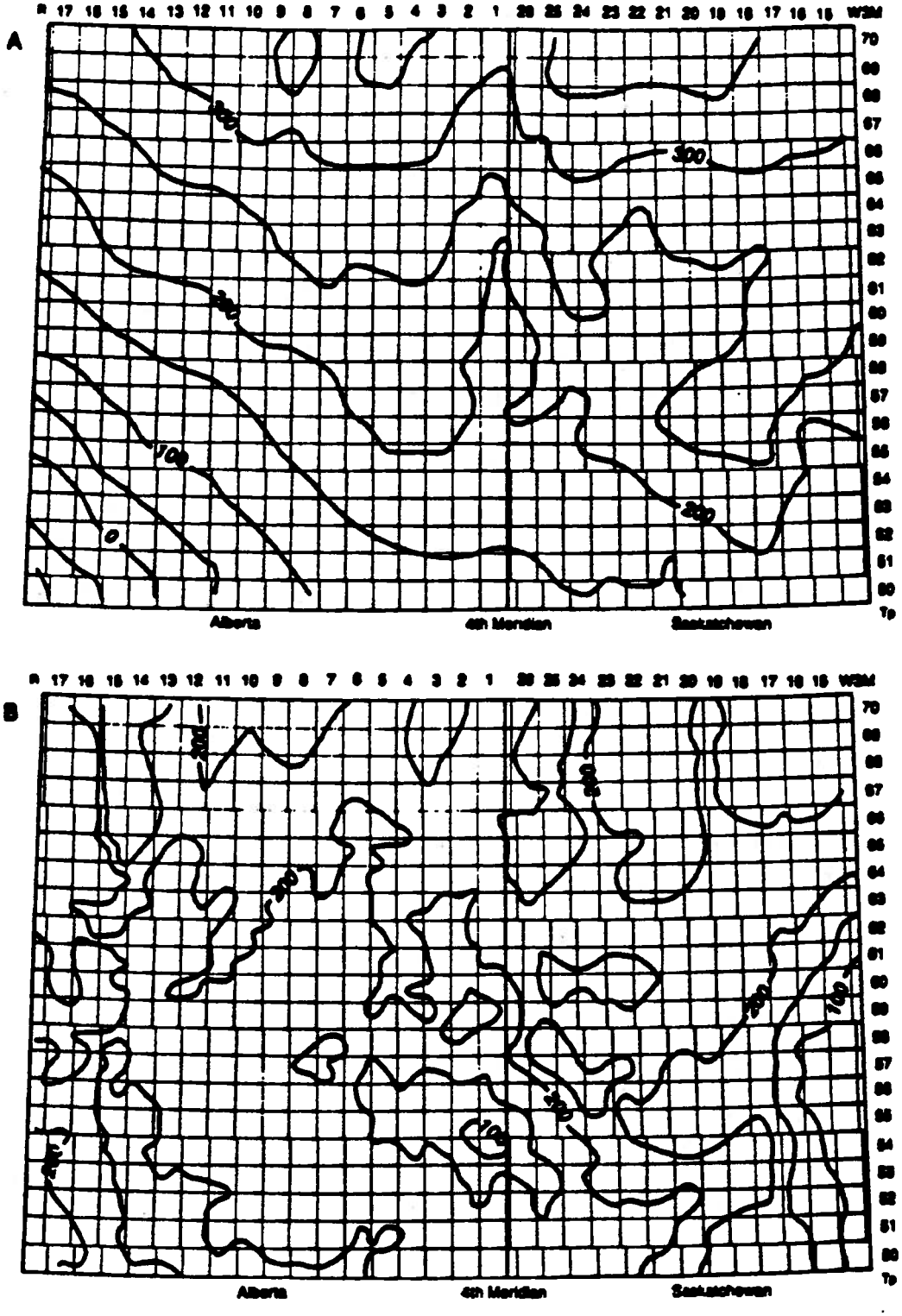

Figure 17. A. Structure contour map on top of the Mannville Group (contour interval 50 m; 7345 data points); B. Isopach map of the Mannville Group (contour interval 50 m)

The middle Mannville consists of sheet sands and shales deposited by repeated marine transgressive-regressive events (O'Connell, 1985). According to Jackson (1984), middle Mannville deposition resulted from the stalling of the southward transgression of the Boreal Sea and the initiation of a major regression. The Cummings Formation represents the middle Mannville in the Cold Lake study area.

By upper Mannville time, a large influx of clastic sediments overcame basin subsidence, causing a relative lowering of sea level and the return of regressive conditions (Jackson, 1984). Figure 18 shows the progradation of the shoreline from the Hoadley Barrier in central Alberta, to the Clearwater shale basin in the northwest. The upper Mannville consists of non-marine sediments in southern Alberta, nearshore marine sediments capped by non-marine sediments in central Alberta (Cold Lake study area) and marine sediments in northern Alberta. In the Cold Lake study area, the Clearwater and Grand Rapids Formations make up the upper Mannville. The Clearwater Formation consists of a thick sandstone unit between thin shale layers. The shale layers represent transgressive marine pulses (figure 19). Although the shales are generally less than 10 m thick, they are the two most continuous aquitards within the Mannville Group.

In general, the Mannville Group consists of repeated alternations of marine and non-marine deposits. Deep channels occur at all levels and are filled with either sand, or shale and silt. The complexity of Mannville sedimentation is illustrated in figure 20.

Deposition of the Mannville Group was terminated by major transgressions from the north (the Harmon shale) and from the south (the

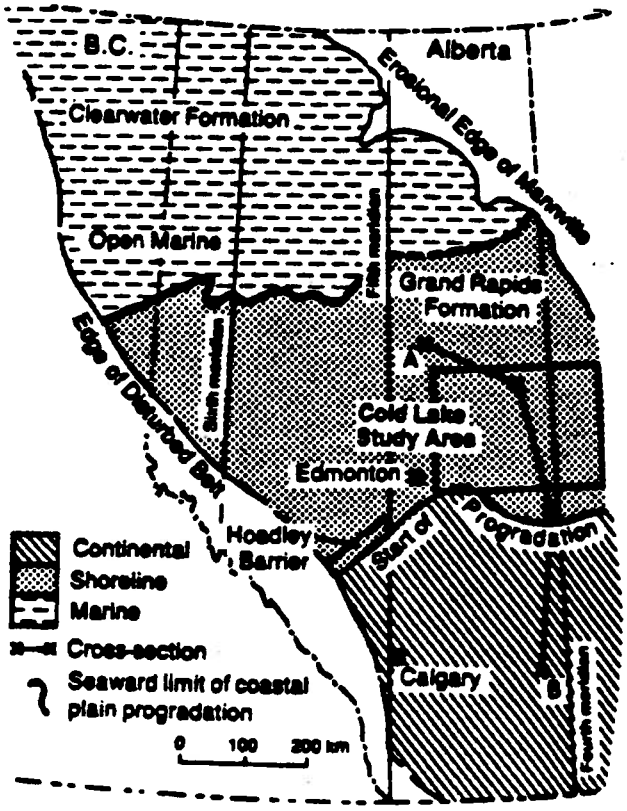

Figure 18. Progradation of upper Mannville shoreline from south-central Alberta northward to the Clearwater Formation marine shale basin (simplified from Jackson, 1984)

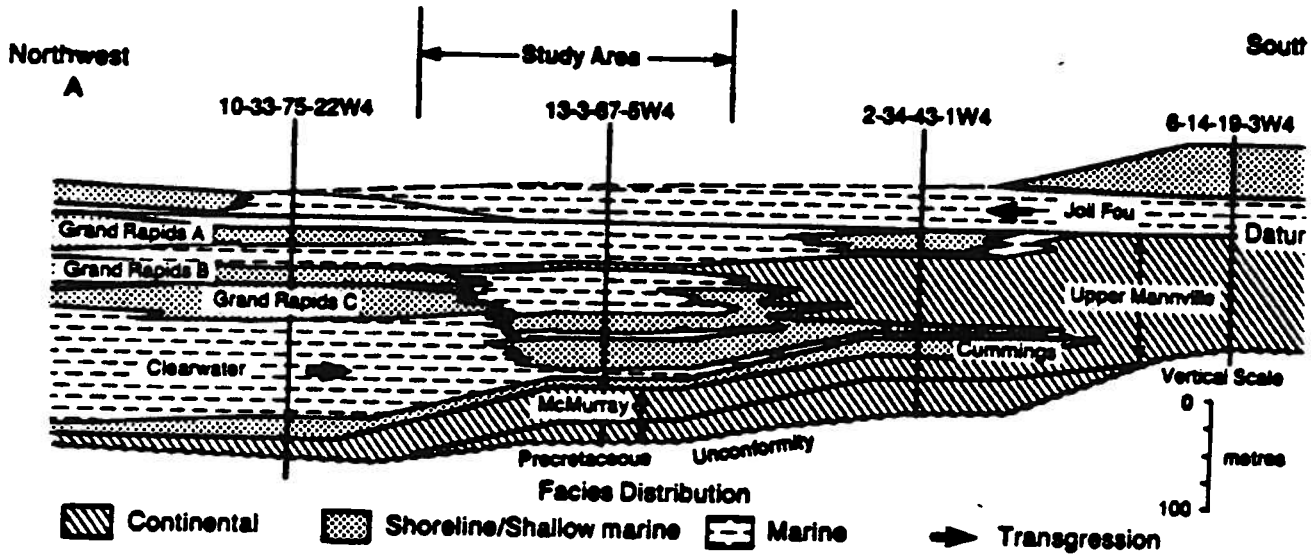

Figure 19. Schematic cross-section across eastern Alberta; note the tongues of the Clearwater shale (simplified from Jackson, 1984)

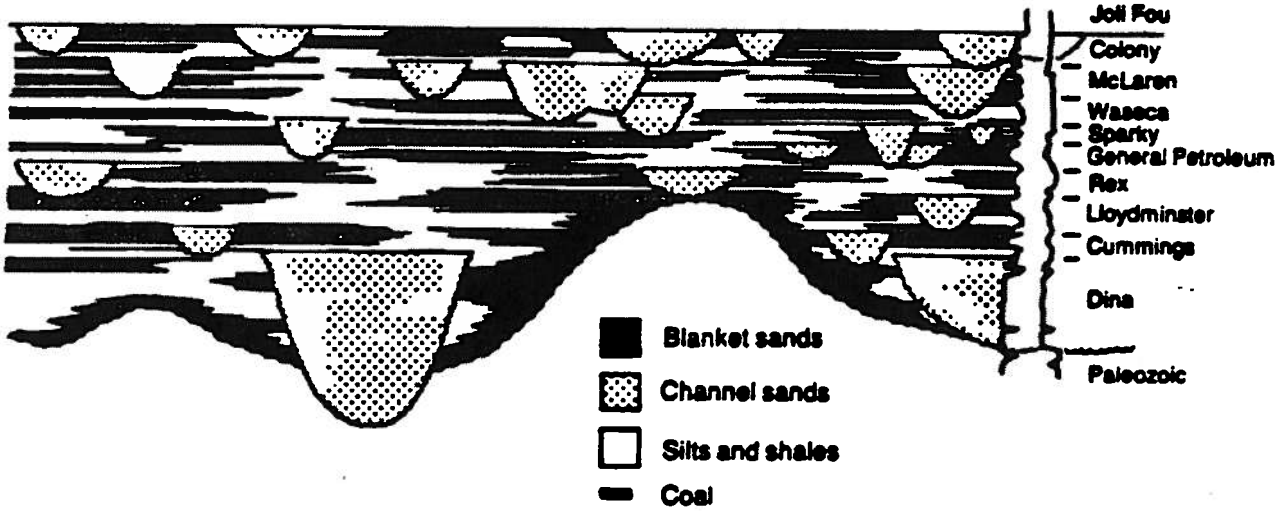

Figure 20. Conceptual diagram illustrating the occurrence and postulated relative positions of blanket and channel sands within the Mannville sequence (after Gross, 1980)

Joli Fou shale). This led to complete inundation of the western interior, marking the beginning of the Colorado depositional sequence.

Cold Lake Oil Sands

The Cold Lake Oil Sands Deposit contains reserves in the McMurray, Clearwater and Grand Rapids Formations. A cross-section through the northern part of the deposit is shown in figure 21. Delineation of the lateral extent and thicknesses of the individual reservoirs was obtained through several sources. Resource mapping of the Clearwater reservoir was provided by Wightman and Berezniuk (1985). The other six oil sand layers were mapped using a network of geophysical well log cross-sections (unpublished) constructed by Wightman and Berezniuk (1985) and Tilley (1984). Due to the broad scale of the present study, precise mapping of the oil sand layers was not necessary. The presence of bitumen is based on above-average porosity and resistivity geophysical log readings corresponding to lower gamma ray log readings. Most of the reservoirs in the Cold Lake Oil Sands Deposit are not homogeneous or continuous (with the exception of the Clearwater reservoir), and were lumped together. Bitumen-saturated sands act as aquitards and, therefore, it is important to locate these and to incorporate them into the flow model. Seven main oil sand layers have been identified as a result: McMurray 1 and 2, Clearwater, Lower Grand Rapids 1 and 2, and Upper Grand Rapids 1 and 2.

The McMurray Formation is characterized by a continuous basal sand unit and an upper interbedded sand and shale unit. Minor amounts of bitumen are present in the upper thin sands, trapped against topographic

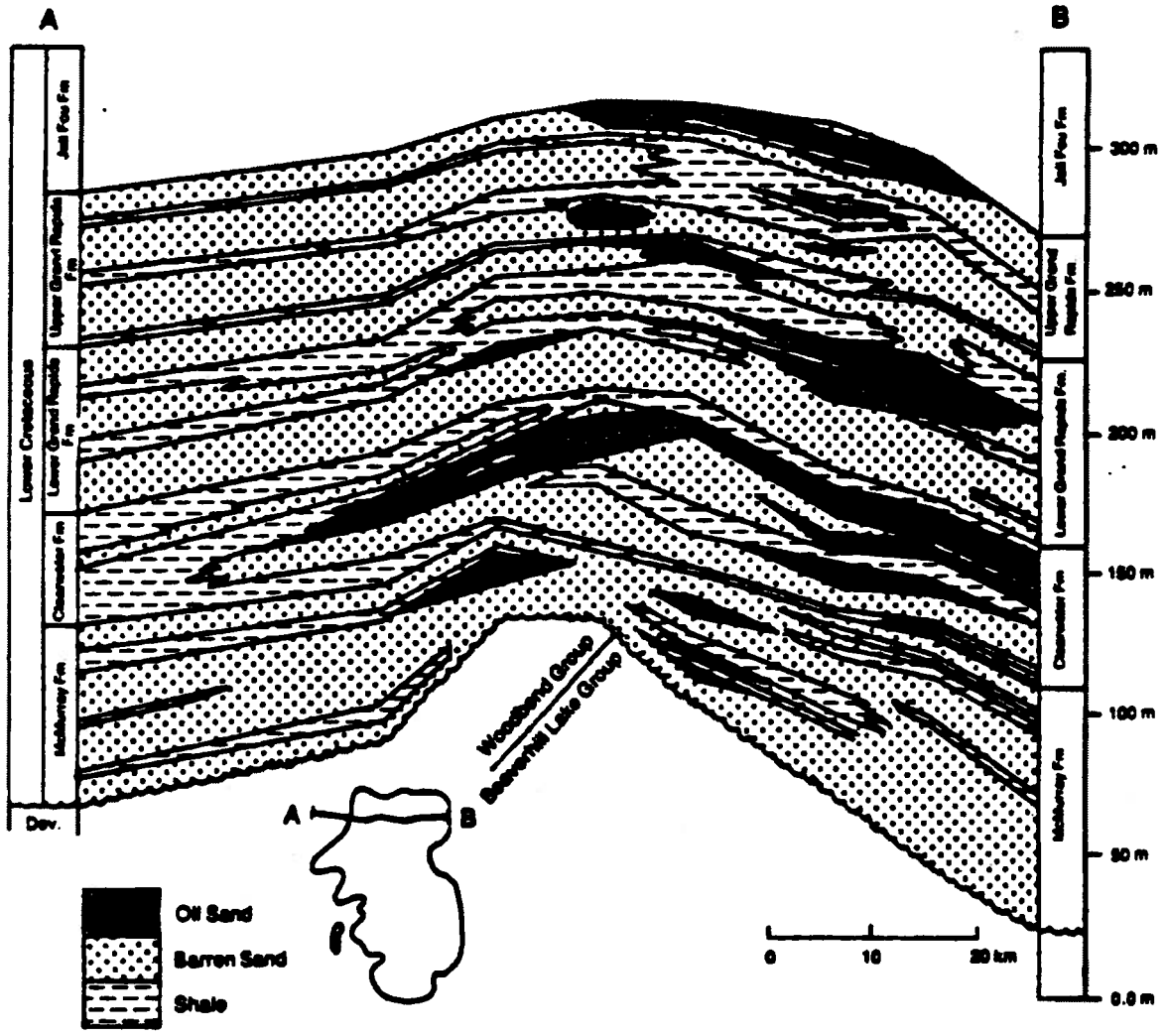

Figure 21. Cold Lake Oil Sands structural cross-section, showing generalized lithologies and reservoir configurations (after Mossop et al., 1981)

highs of the Pre-Cretaceous unconformity surface. The basal McMurray sands are mainly water bearing (Harrison et al., 1981).

The Clearwater, which contains highly saturated sands, is the most prolific reservoir and accounts for a significant portion of the total bitumen in place at Cold Lake (Harrison et al., 1981). The Clearwater reservoir has been the target of most pilot operations at Cold Lake because of the homogeneity and continuity of the sands.

Oil accumulation is highly variable in the Upper and Lower Grand Rapids Formation because the strata consist primarily of thin sands interbedded with shales. The trapping mechanisms in the Cold Lake region are mainly stratigraphic in nature, with some structural control over Paleozoic highs.

Upper Cretaceous (Colorado)

Deposition of the Colorado sequence was initiated by a major marine transgression which united the Boreal and Gulfian seas. By early lower Colorado time, the whole of the plains, as well as the northern foothills regions, were covered by marine waters. The dominantly argillaceous Colorado sequence was deposited during two transgressions and an intervening regression (Simpson, 1975). Mud, with subordinate sand derived from the Canadian Shield, was deposited during the transgressions, and northeast-thinning sands, derived from the Cordillera, during the regression (Simpson, 1975).

In the Cold Lake study area, the early transgression is represented by the dark grey shales of the Joli Fou Formation. The Spinney Hill and Viking sandstones, clastic equivalents of the first transgression and

regression, are very thin (less than 4 m) in Alberta and absent in Saskatchewan because of the offshore setting of the study area. The St. Walburg sandstone, however, reaches a maximum thickness of 40 m and is the product of the last transgression, being found only in Saskatchewan. In general, the Colorado Group consists of 300 m of marine shales with very minor influxes of sand.

Upper Cretaceous (Post-Colorado)

Laramide deformation and Cordilleran erosion triggered deposition of a series of eastward-thinning non-marine clastic wedges, intercalated with muds. The cyclicity of Post-Colorado Group strata is best developed in the southern Alberta plains because of frequent marine incursions by the seaway entering the region from the south. The eastern interior plains, in which the Cold Lake study area is situated, was still a depocentre for deep water muds (Williams and Stelck, 1975). These deep water muds are represented by the Lea Park and Belly River Formations. Figure 22B is an isopach map showing the thickness of the dominantly shaley sequence of strata that overlies the Mannville Group.

The remainder of Phanerozoic history in the Cold Lake study area is speculative due to subsequent Tertiary and Recent erosion. It is probable that at least 1 km of strata have been removed due to this erosion (Hitchon, 1984), but how much of this thickness comprised Tertiary strata is unknown. A structure contour map on the base of the Quaternary shows the paleotopography on the bedrock surface (figure 22A). Overlying the bedrock is a variety of glacial and post-glacial surficial deposits of Quaternary age.

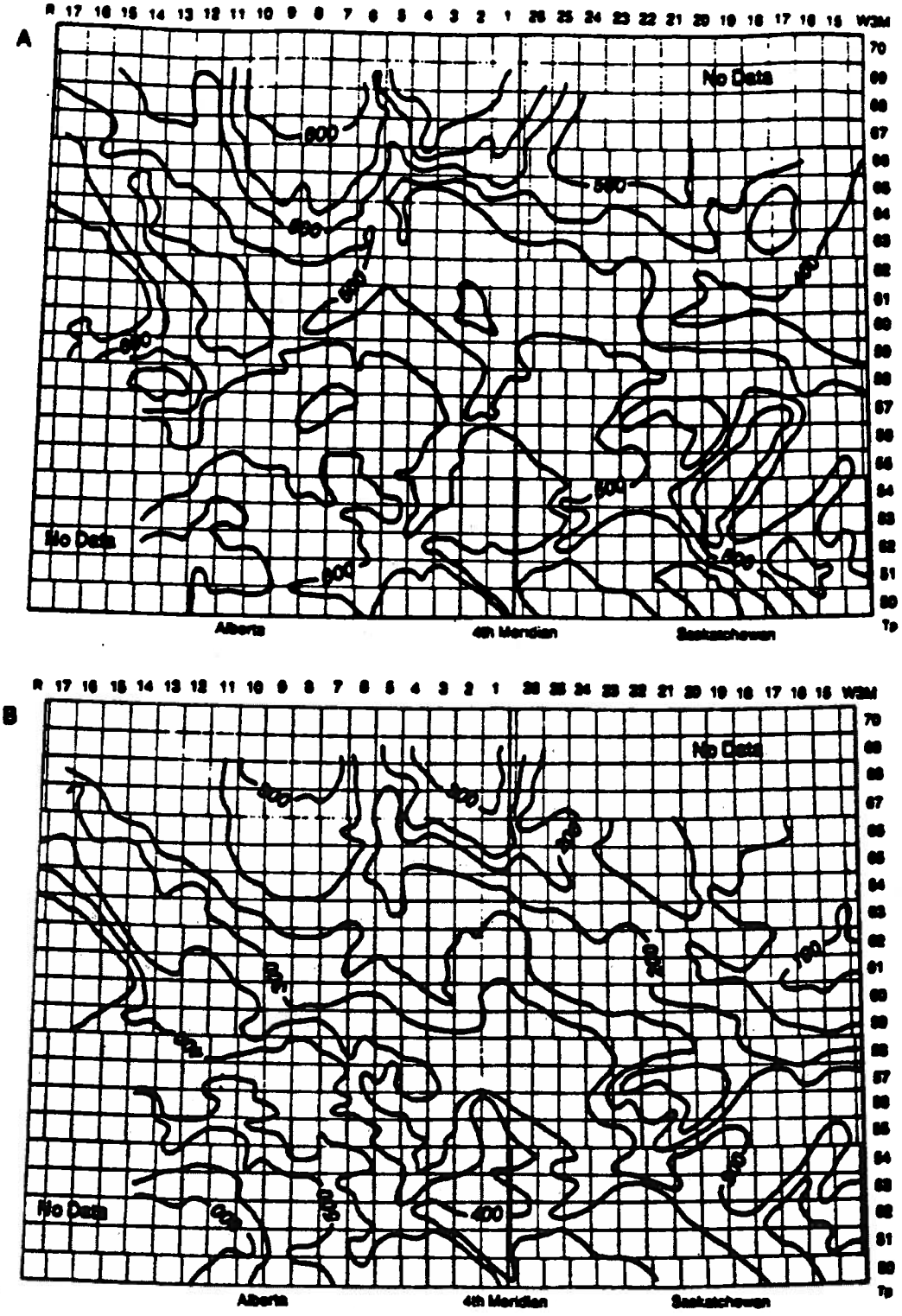

Figure 22. A. Structure contour map on the base of the Quaternary (contour interval 50 m); B. Isopach map from the top of the Mannville Group to the base of the Quaternary (contour interval 50 m)

ANALYSIS OF THE NATURAL FLOW REGIME

Claude M. Sauveplane and Brian Hitchon

INTRODUCTION

The word "natural" refers to the undisturbed (essentially steady-state) regime that has been established in the subject block of sediments throughout geologic time. Local perturbations may have been introduced into the system, especially in the study area, through the exploitation of hydrocarbon resources, but these are neglected in this regional analysis.

It is also assumed that the sedimentary rocks are fully saturated with water and that the movement of this liquid is gravity-driven only, although it is recognized that other driving mechanisms may exist (e.g. osmosis). The lateral component of flow of formation waters can be described by the magnitude and direction at each point of the specific discharge, which is a function of the hydraulic conductivity and of the fresh water hydraulic head gradient (Lusczynky, 1961; De Wiest, 1965; Bear, 1972; and Frind, 1980). The vertical component of flow within and between aquifer units can be described at a local scale by pressure head versus depth plots and at a regional scale by point water hydraulic head profiles along cross-sections. Along the same vertical, aquifers of different hydraulic properties are in continuity if they exhibit a hydrostatic slope of 1 on a pressure head versus depth plot; on a more regional scale, the point water hydraulic head profiles should be coincident. These conditions of hydraulic continuity may be present even when aquifers are separated by thin (or weak) aquitards.

The aquifers can then be grouped into a single aquifer system for the purpose of this analysis. Marked deflections on pressure head versus depth plots reflect weak vertical leakage between aquifer units through the intervening (strong) aquitards that cannot be neglected. The same can be said of well separated point water hydraulic head profiles along cross-sections. It must be specified here that the potentiometric surfaces presented subsequently are computed using a reference density of 1000 kg/m^3 (freshwater), while the hydraulic head profiles are computed using the real point values of formation water density. Therefore, the hydraulic head values in potentiometric surfaces and in corresponding vertical profiles do not match due to different scaling of the pressure term (Bachu et al., 1987).

An aquifer system, as previously defined, can be regionally characterized by composite values of the aquifer parameters, depending on whether the continuity is vertical (most frequent case) or lateral (in the case of depositional boundaries). The harmonic average is used in the first instance and the arithmetic average in the second case (Matheron, 1967). Based on these principles, an objective of the analysis of the natural flow regime is to simplify the flow system into groups of units. Consequently, for a given block of sediments, one may consider two levels of definition for the hydrostratigraphy: an initial level based on the geometry and lithology of the stratigraphic units, and a second (synthesis) level based on the regional analysis of the flow. Besides its intrinsic interest, this "simplification" has obvious applications for any further modelling effort. At the same time, it explains why recommended values of the hydraulic parameters cannot be defined prior to the regional analysis of the flow regime itself.

In this section, the flow regime is analysed from the base upward and consequently the two above-defined components of flow are integrated as much as possible; because of the commonly observed relations between the flow and the hydrochemical regimes (parallel trends of hydraulic gradient and salinity gradient), the hydrochemistry is integrated in this analysis; this also reflects a fundamental feature of the data processing of the hydrodynamic information (Appendix A). Regional hydrochemical variations are illustrated, wherever possible, by maps of salinity (calculated total dissolved solids). Additional data on the regional values of hydraulic parameters and variables are presented for each hydrostratigraphic unit in Appendix B. This analysis of the natural flow regime is based on selected information for 1858 analyses of formation waters, 2155 drillstem tests and 46 700 core analyses. Because of the uneven distribution of these data in three dimensions, all of the information related to the Paleozoic strata has been examined and used whenever possible; preselections have been made for drillstem test results for the Cretaceous aquifers. Given the paucity of hydrochemical and hydrodynamic data, the hydrogeology of the Lower Paleozoic rocks is not clearly understood in the study area. Typically, for each identified hydrostratigraphic unit, the following items will be examined successively: (1) the geometry of the unit; (2) the hydrochemistry; and (3) the hydrogeology (flow conditions and hydraulic parameters).

LATERAL FLOW

Precambrian Aquiclude

For the purpose of this study, and as a general observation, the Precambrian basement is assumed to be an aquiclude and, therefore, its top is a no-flow boundary. Although recent studies (e.g. Fritz and Frape, 1982) have demonstrated the presence of saline formation waters (some exceeding 200 000 mg/L at depths greater than 1 km in the exposed Canadian Shield), no work has been done in western Canada which would indicate similar saline formation waters, even at shallower depths, in the covered Precambrian.

Basal Cambrian Aquifer

The subcrop edge of the Basal Cambrian sandstone is close to the northern boundary of the study area throughout most of the region (figure 23A). The aquifer ranges in thickness to more than 150 m in the southeast corner and to generally 75-100 m along the southern boundary.

Only six reliable analyses of formation waters are available from this aquifer (table 2). The dominant ions are Na and Cl, and the formation waters are characteristically very saline (calculated total dissolved solids 238 000 to 310 000 mg/L) with relatively low contents of Ca (1250 to 3400 mg/L) and Mg (390 to 870 mg/L), and high contents of SO_4 (1570 to 6500 mg/L). In one sample, Br and I are reported at 44 mg/L and 6 mg/L, respectively. These features suggest a source of the solutes from evaporites, dominantly halite, and all six analyses are

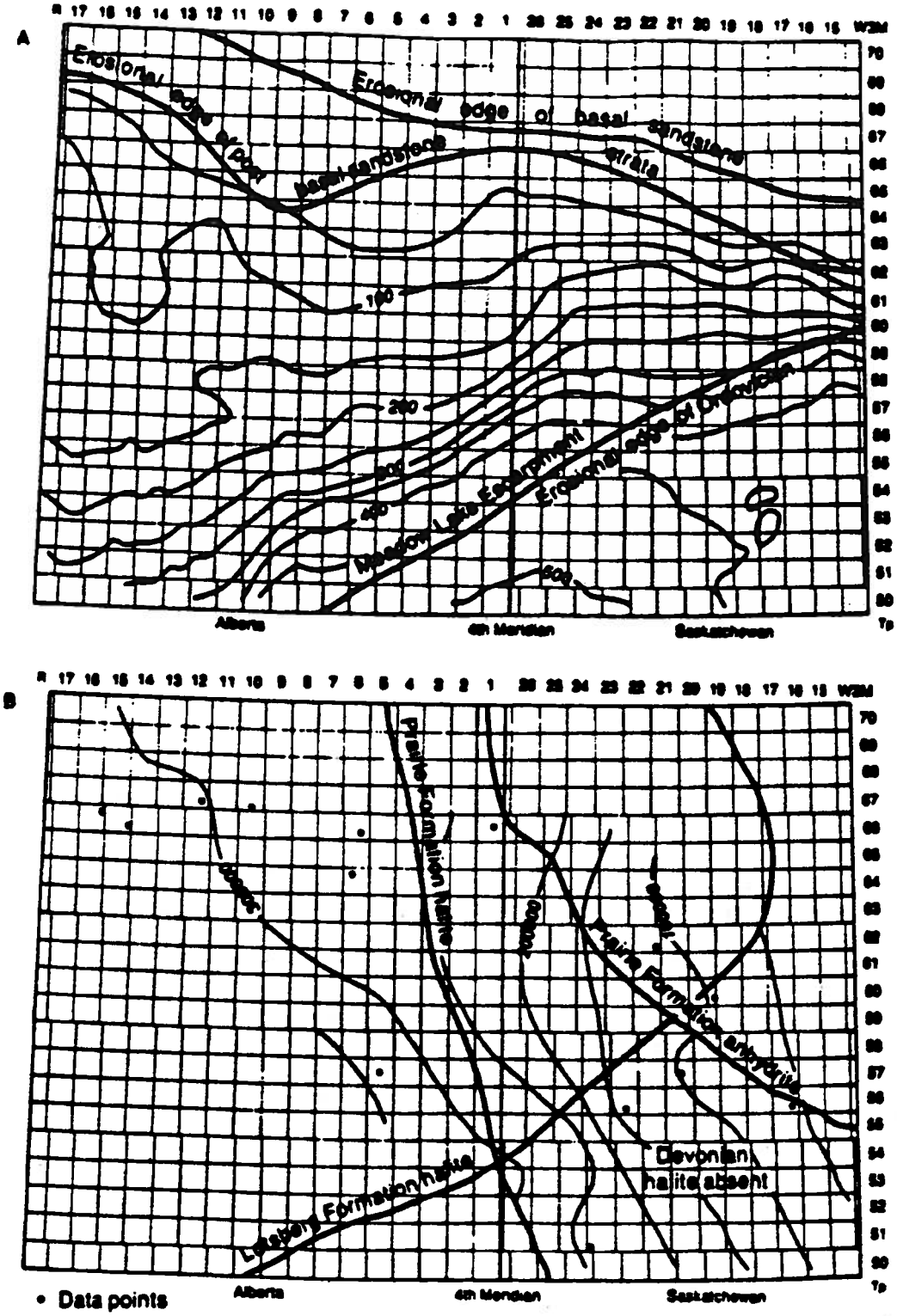

Figure 23. Cambrian hydrogeology. A. Isopachs (contour interval 50 m) of preserved Cambrian strata; B. Salinity (mg/L) of formation waters; C. Potentiometric surface of Basal Cambrian aquifer

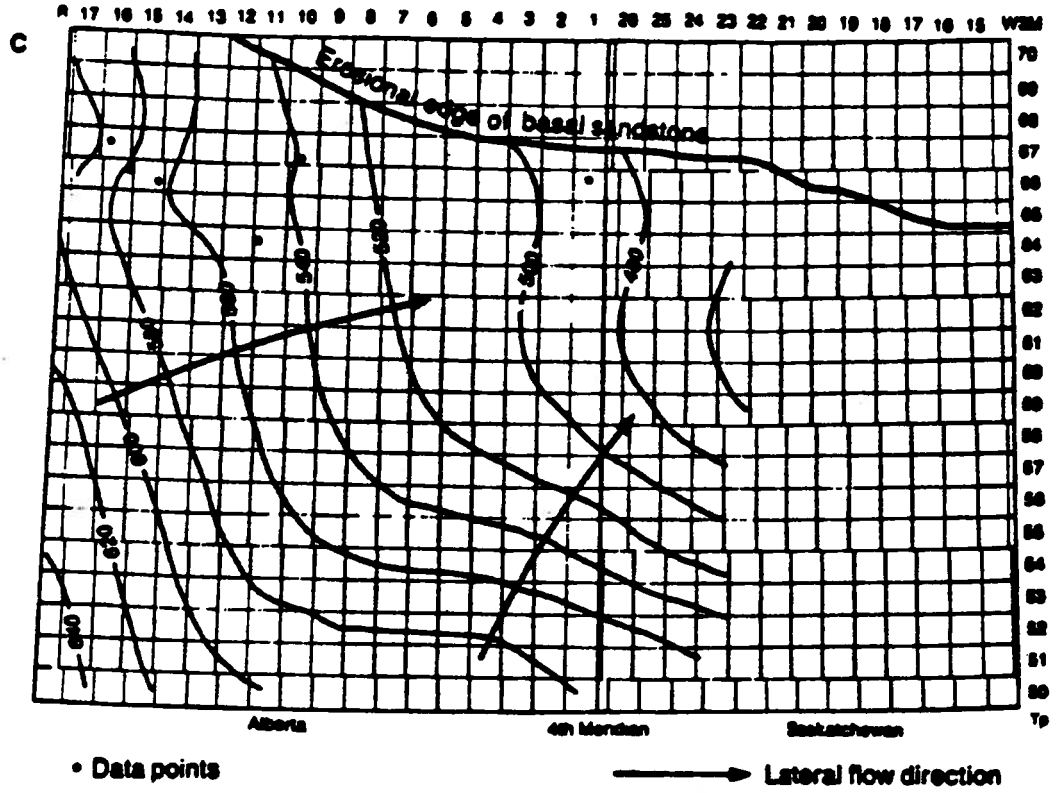

Figure 23. Continued

Table 2. Chemical composition (mg/L), physical properties and production data for formation waters from Basal Cambrian aquifer, Cold Lake region

Location	10-7-51-24-W3	7-22-66-1-W4	10-12-66-15-W4	6-25-66-16-W4	11-3-67-10-W4	10-11-67-12-W4*
Depth (m)	1506.6-1537.1	1133.6-1164.0	1531.6-1562.1	1563.6-1606.9	1449.3-1480.7	1446.0-1482.2
Source	DST 1	DST 5	DST 6	DST 5	DST 3	DST 3
Recovery	1274.1 m sw	868.7 m sw	1090 m sw 213.4 m mud	1310.6 m sw	652.3 m sw	1073.5 m sw 54.9 m mud
Na (diff.)	90 670	89 939	116 695	117 309	107 184	116 663
Ca	2 127	2 158	1 247	3 416	1 696	1 759
Mg	867	508	630	389	566	751
Cl	143 704	139 000	180 800	186 843	167 125	182 965
HCO_3	220	290	320	120	102	30
SO_4	3 080	6 526	4 066	1 565	3 718	3 000
TDS (110°C)	-	240 001	306 920	322 920	-	316 060
TDS (ignition)	-	232 730	301 020	302 160	-	307 150
TDS (calc.)	240 557	238 274	303 595	309 581	280 338	305 153
pH (laboratory)	6.4	7.6	7.1	7.8	6.4	5.91
Density (15.56°C)	1.1642	1.154	1.195	1.199	1.1622	1.2032
Refractive Index	-	-	1.3818 (25°C)	-	1.377 (22.8°C)	-
Resistivity (ohm m)	0.045 (22.8°C)	0.053 (20°C)	0.055 (20°C)	0.047 (20°C)	0.044 (22.8°C)	0.0312 (25°C)

- = Not determined

* Br = 44 mg/L; I = 6 mg/L

found in the region of preserved Middle Devonian Prairie Formation halite.

Lateral flow is in two main directions (figure 23C): from the southwest to northeast in the southern part of the study area, and from west to east in the western part. Because only six reliable drillstem tests are available, the potentiometric surface of figure 23C was produced from a more regional trend that includes a well in the Lloydminster area (B12-30-49-27 W3 Mer) and other information south and west of the Cold Lake study area. This was automatically produced by "cutting" the electronic (computer based) potentiometric surface for the Basal Cambrian aquifer in south-central Alberta (Bachu et al., 1986) and transferring it to the Cold Lake study area with the proper coordinate transform and change of scale. The absence of the aquifer in the north-northeastern part of the area explains why the majority of the lateral flow in this aquifer is to the east after the merging of the two previously described components. This is in agreement with the decrease of the salinity gradients (figure 23B).

Based on the values determined from the six drillstem tests and from the core data (available at five different locations in the north-central part of the study area), the hydraulic conductivity is typically between 0.002 and 0.2 m/d and the specific storage between $1x10^{-5}$ m^{-1} and $5x10^{-4}$ m^{-1}.

Other Cambrian Aquifers

The subcrop margin of Middle and Upper Cambrian strata younger than the basal sandstone is a sinuous boundary lying about five townships

south of the northern edge of the study area (figure 23A). These strata are less than 100 m thick to the northwest of the Meadow Lake Escarpment, but the preserved thickness increases to 100 to 250 m along the escarpment edge. Beneath overlying Ordovician rocks the thickness of post-basal sandstone Cambrian sequence is in the range 350 to more than 400 m.

Nine reliable formation water analyses are available from these aquifers. Although salinities are lower (60 000 to 130 000 mg/L) in the eastern part of the study area, where depths are generally less than 1 km, all nine analyses are dominantly NaCl solutions with similar ranges to those in the Basal Cambrian aquifer for Ca (1190 to 4760 mg/L), Mg (315 to 2400 mg/L) and SO_4 (1300 to 6260 mg/L). The lower salinities in the eastern part of the study area are related more to the absence of halite beds in the overlying Lower and Middle Devonian than to the shallower depths (figure 23B). These facts suggest that all 15 formation water analyses from Cambrian aquifers should be treated as a single population and the salinity map (figure 23B), therefore, includes all data from these rocks. Regional trends of Na, Cl and density, and to a lesser degree Ca and Mg, are generally parallel to those for salinity, but the isoconcentration contours for SO_4 and HCO_3 tend to have a more east-west component and the concentration gradient of these ions is opposite to that of salinity; the cause of this difference is explained in the section dealing with the Winnipegosis aquifer system.

Middle and Upper Cambrian strata are generally composed of thin intercalations of sandstone and shale. A value of 0.01 m/d, similar to the values obtained for the Basal Cambrian aquifer, was found for the

only reliable drillstem test available; at two locations in the north-central part of the study area (Tp 64 and 65, R 3 W4Mer), the average maximum horizontal conductivity is five times greater than that determined at the same location in the Basal Cambrian aquifer. Thus, in spite of the presence of thin beds of shale and siltstone in the Middle and Upper Cambrian, the Cambrian rocks dominantly play the role of a single aquifer system, albeit with contrasting permeabilities within it.

Ordovician Aquifer

A thin (less than 60 m) sequence of Ordovician rocks caps the Meadow Lake Escarpment, preserved beneath Devonian strata. No reliable formation waters have been recovered from this aquifer in the study area, mainly due to poor recovery or sampling position. However, what data are available suggests that formation waters from Ordovician rocks will be similar to those in the underlying Cambrian.

No information from drillstem test or core is available for the Ordovician aquifer within the study area and, wherever present, this aquifer is amalgamated with the Cambrian aquifer system described above.

Basal Red Beds "Aquifer"

These Lower Devonian rocks of evaporitic clastic origin have the typical hydraulic conductivity (7.5×10^{-8} m/d) of an aquitard at 7-22-66-1 W4Mer, but at 4-5-66-16 W4Mer, the drillstem test hydraulic conductivity is 0.62 m/d. This observation is confirmed by the core data; at two locations in 64-3 W4Mer the horizontal component of

hydraulic conductivity has values between $5x10^{-5}$ and $8x10^{-2}$ m/d in cores which were recovered from about 80 percent of the total formation thickness. Although the range is large, the representative average is 0.01 m/d. Cores from the lower half of this unit at 57-6 W4Mer and 66-6 W4Mer have an overall range of $2.1x10^{-4}$ to 0.41 m/d for the horizontal conductivity. Although these values are confined to a narrow north-south band in the centre of the study area, this information shows that the Basal Red Beds are more typical of an aquifer than of an aquitard.

Lower Paleozoic Aquifer System

The plot of figure 24A illustrates the similarity of hydraulic behaviour at a variety of locations for the three above-described units: all point data fall within a narrow (50 m) range of pressure head, which is an acceptable variation considering the wide areal distribution of the data. The plot in figure 24B, although corresponding to a well located just outside the study area, shows that there is an overall differential in hydraulic head between the Winnipegosis and Basal Cambrian aquifers in the area where Lower and Middle Devonian halite beds are absent. It is a matter of interpretation whether the head differential occurs gradually over the Cambrian or occurs as a sharp break at some level within it. Because data simply are not available to support interpretation, and for the purpose of the study, the entire Cambrian, Ordovician and Lower Devonian Basal Red Beds are combined into the Lower Paleozoic aquifer system with hydraulic continuity and contrasting hydraulic conductivities between the four subunits.

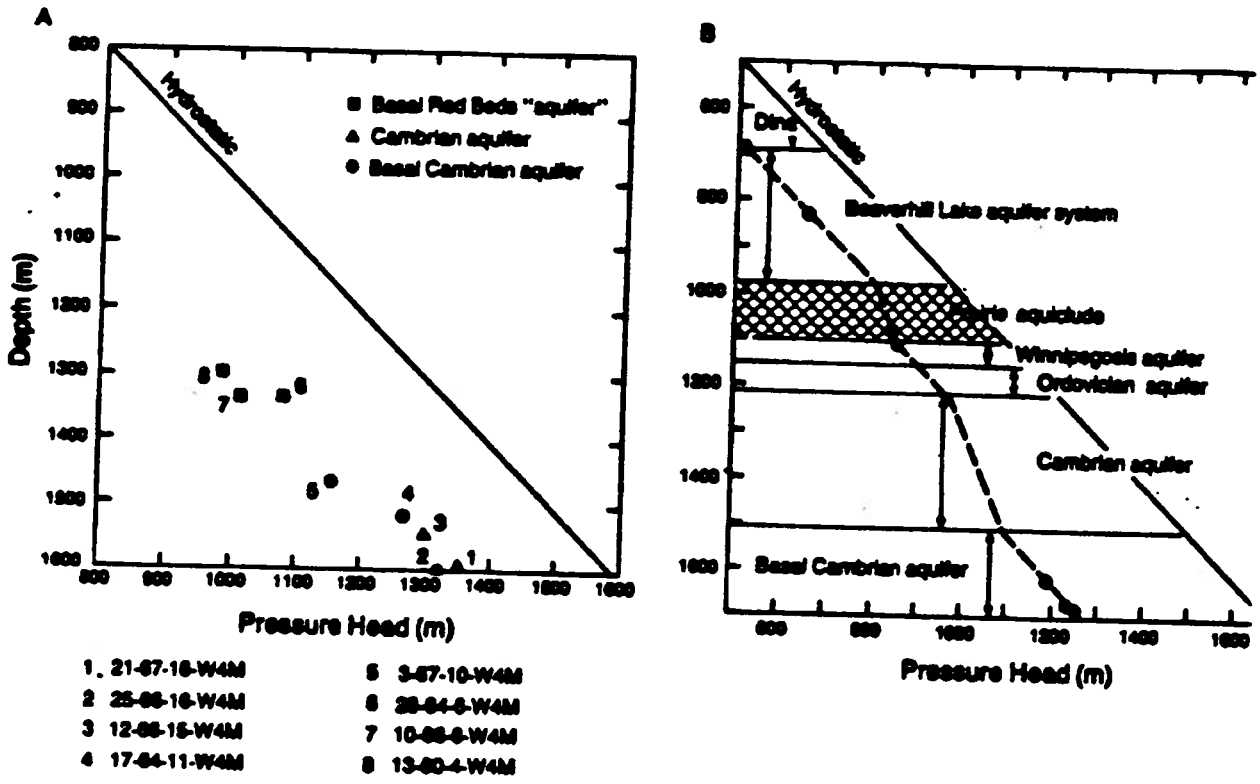

Figure 24. Cross-formational flow as illustrated by pressure head/depth plots in the Lower Paleozoic aquifer system. A. at the indicated well locations; B. just south of the study area at B12-30-49-27 W3 Mer

The Lower Paleozoic aquifer system ranges in thickness up to 562 m (figure 25). Over most of the study area it is confined between the underlying Precambrian aquiclude and the overlying Lower Devonian aquiclude; along parts of the eastern and southeastern margins of the study area, however, this unit is in direct contact with the Winnipegosis aquifer system (see figure 27B).

Lower Devonian Aquiclude System

Lower Devonian rocks of the Lower Elk Point Group (Grayston et al., 1964) overlie Lower Paleozoic strata north of the Meadow Lake Escarpment. They comprise, in ascending order, evaporitic clastics (Basal Red Beds, included within the Lower Paleozoic aquifer system) and massive halite beds (Lotsberg and Cold Lake Formations) and argillaceous dolomite and dolomitic shales (Ernestina Lake Formation). Although formation waters have been recovered from a few thin, more porous beds none of the analyses are reliable, for a variety of reasons. Because halite beds dominate, and porous units are effectively insignificant, the lower Elk Point Group above the Basal Red Beds has been termed the Lower Devonian aquiclude system. It ranges in thickness up to 375 m (figure 26); the western and southeastern margins are depositional, whereas the eastern boundary is the result of salt solution.

Hydrodynamic information is not available from the thin and confined Ernestina Lake aquifer, lying between the Lotsberg and Cold Lake halite beds. The thinness, lithology and position of this aquifer suggests that it is not likely to have any significant impact on the overall flow

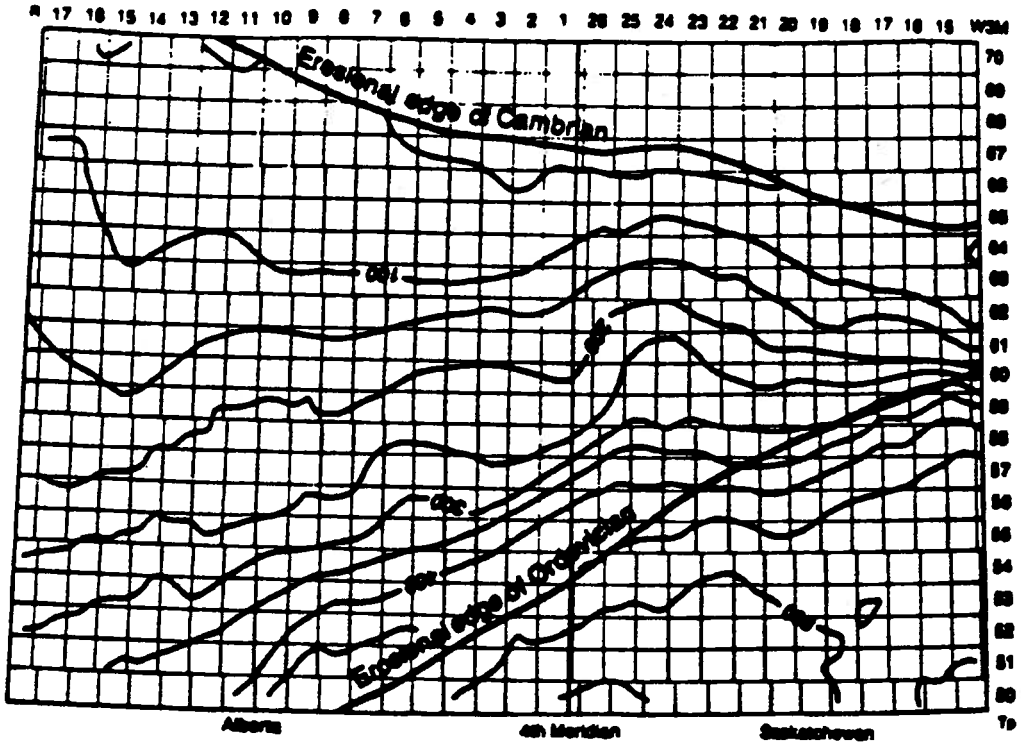

Figure 25. Isopachs (contour interval 50 m) of the Lower Paleozoic aquifer system

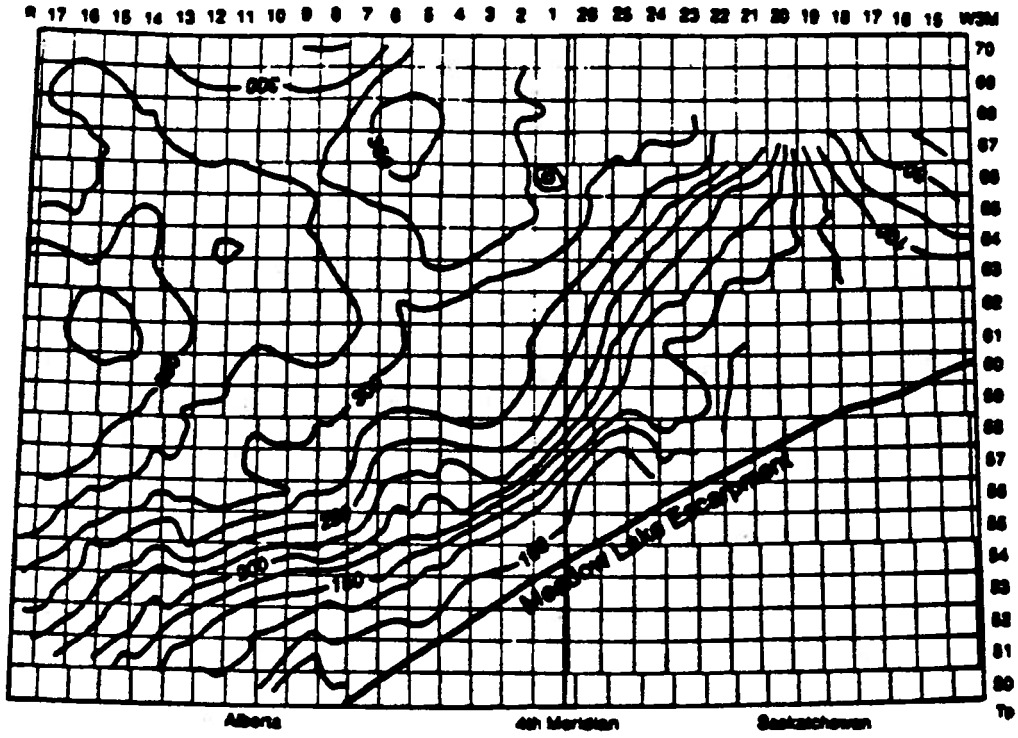

Figure 26. Isopachs (contour interval 50 m) of the Lower Devonian aquiclude system

system. Hydraulic parameters for the halite beds have been derived from laboratory measurements reported in the literature (Gloyna and Reynolds, 1961).

Winnipegosis Aquifer System

The Contact Rapids Formation at the base of the Middle Devonian Upper Elk Point Group is the oldest aquifer which extends throughout the study area. It consists of argillaceous dolomite and dolomitic shales, ranging in thickness from 12 to 100 m. Overlying this aquifer is the Winnipegosis Formation which ranges in thickness from 30 to 80 m but in the region in which reliable formation waters have been recovered, it is between 40 and 60 m thick. Figure 27A shows the combined thickness of these two aquifers. Salinity decreases northeastward from about 295 000 mg/L to 55 000 mg/L (figure 27B) with corresponding decreases in Cl (175 000 to 30 000 mg/L), Ca (4500 to 1250 mg/L) and Mg (1150 to 290 mg/L). Sulfate shows an opposite trend; values are in the range 2000 to 2500 mg/L where the aquifer is overlain by the Prairie Formation halite and anhydrite but increase sharply updip from the solution edge to more than 5000 mg/L (figure 27D). Bicarbonate isoconcentration contours have an approximately east-west trend with values less than 200 mg/L in the south, and increasing to nearly 400 mg/L beyond the solution edge of the Prairie Formation (figure 27D). All these trends are consistent with an origin of the dissolved components from dissolution of halite and anhydrite.

Based on the results of some 20 well-distributed drillstem tests, fresh water hydraulic heads range from 432 to 562 m in the study area.

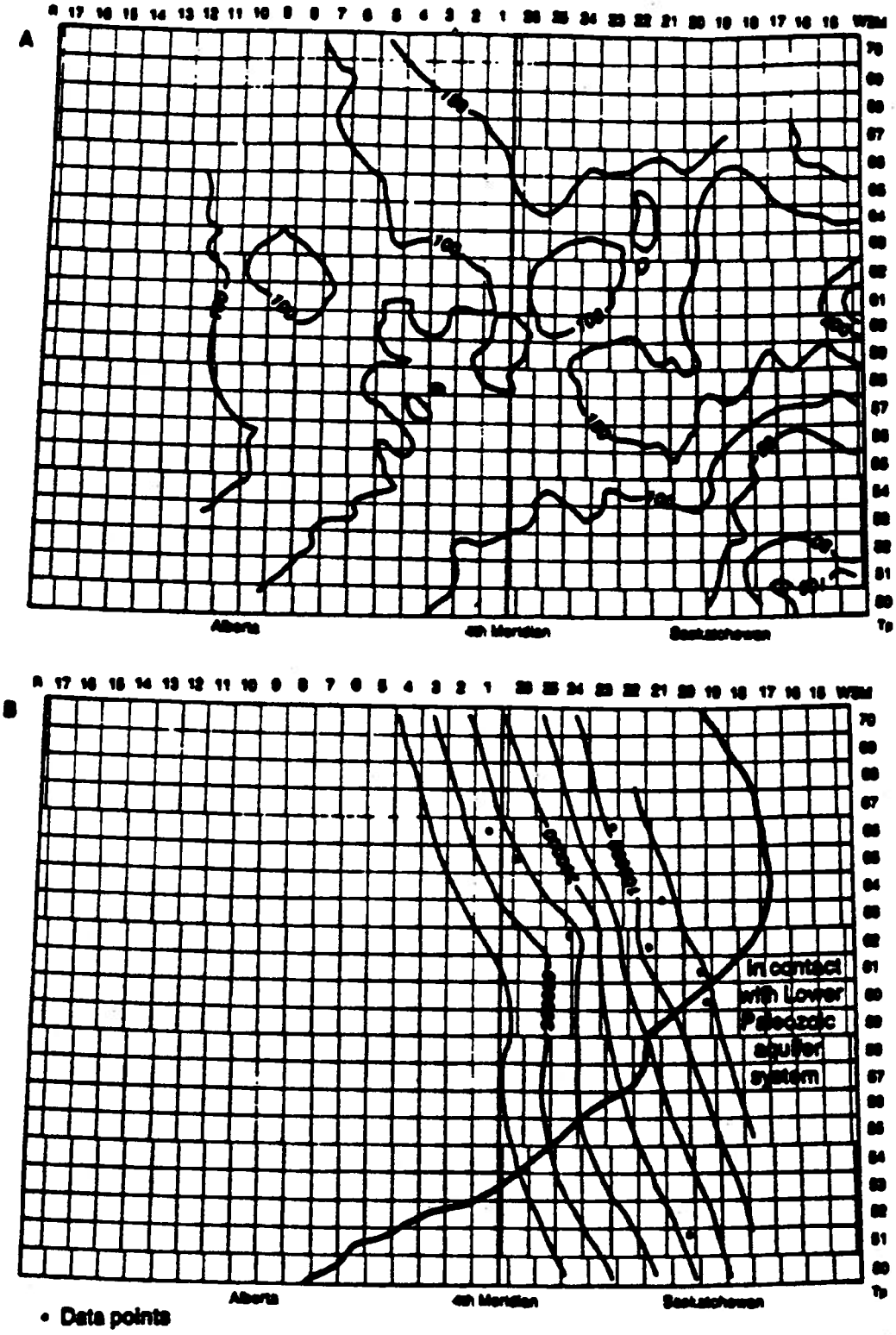

Figure 27. Winnipegosis aquifer system hydrogeology. A. Isopachs (contour interval 50 m); B. Salinity (mg/L) of formation waters; C. Potentiometric surface; D. Relation of SO_4 and HCO_3 in formation waters

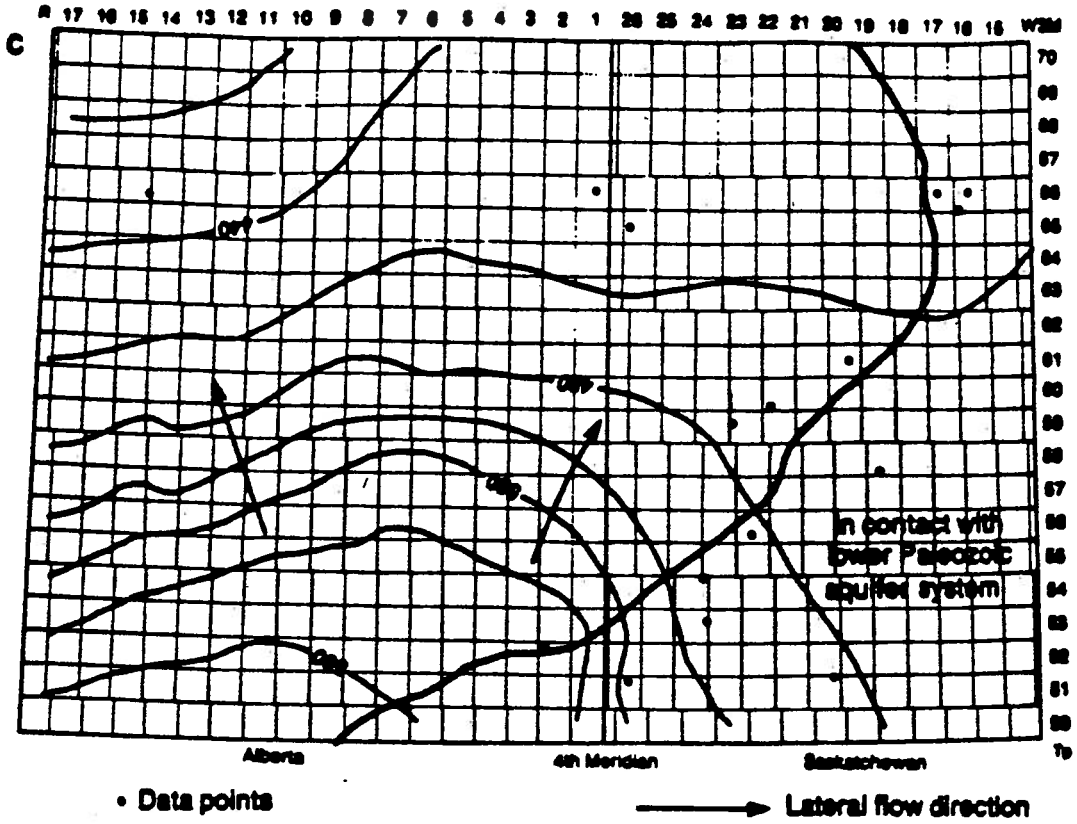

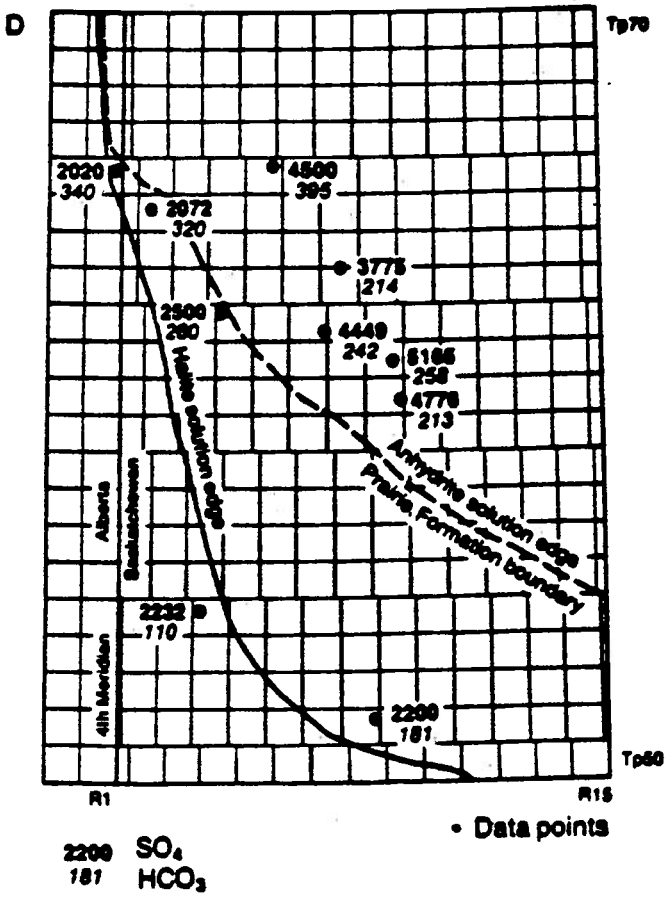

Figure 27. Continued

The flow is northwestward in the western part and changes progressively to the northeast in the central and eastern parts (figure 27C).

In the eastern half of the study area, some drillstem tests allocated to the Contact Rapids Formation yield similar hydraulic parameters as the Winnipegosis aquifer itself. Evidence of hydraulic continuity between these two units is illustrated in figure 28; hence, the Contact Rapids Formation and the Winnipegosis Formation are combined into the Winnipegosis aquifer system, which ranges in thickness between 40 and 270 m (average 120 m).

Prairie Aquiclude

The Prairie Formation halite and anhydrite overlie the Winnipegosis aquifer in the western two-thirds of the study area and comprise one of the major aquicludes (sensu stricto). Where not subject to solution by meteoric water this aquiclude is 120 to 160 m thick (figure 29). Table 3 shows the composition of the raw brine produced by artificial solution of the Prairie Formation halite and anhydrite at the Lindberg salt plant.

Dawson Bay "Aquifer"

The sediments overlying the Prairie Formation comprise the First Red Beds-Watt Mountain clastic interval and are generally less than 25 m thick throughout the Cold Lake study area, although there are isolated regions up to 150 m. Included in this interval is the Dawson Bay "aquifer", which is commonly a dolomitized argillaceous limestone with

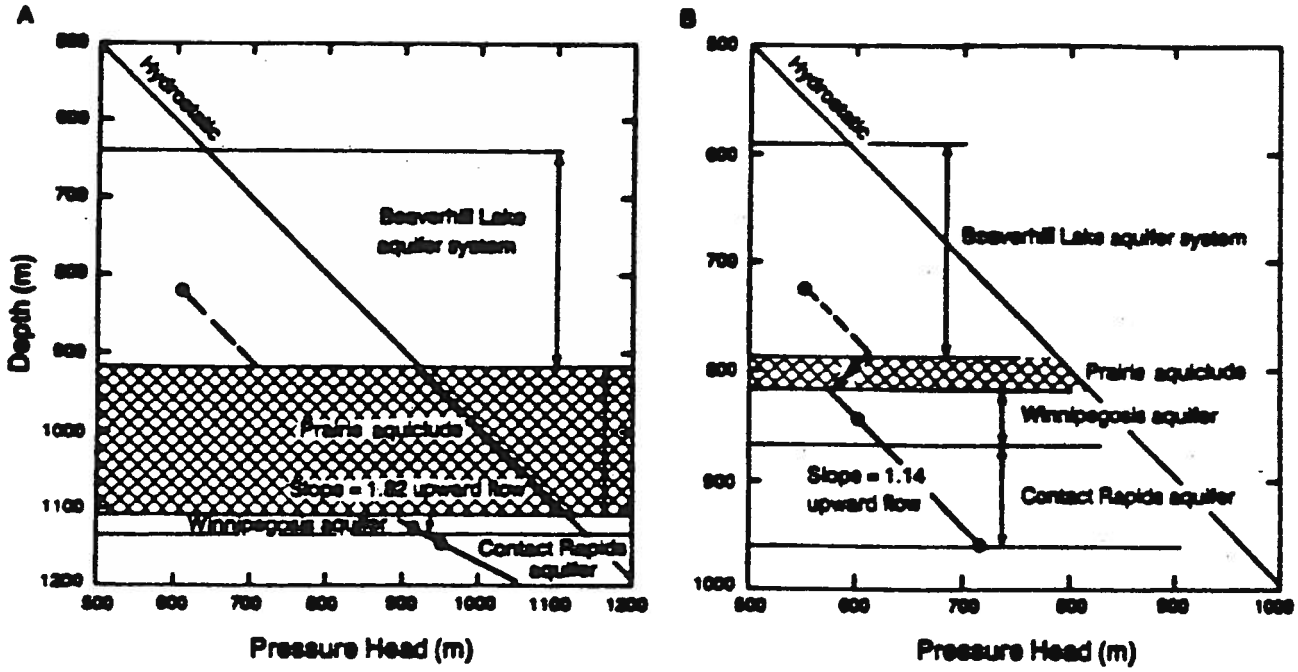

Figure 28. Vertical hydraulic continuity in the Winnipegosis aquifer system. A. at well location 14-29-52-02 W4 Mer; B. at well location 12-10-56-23 W3 Mer

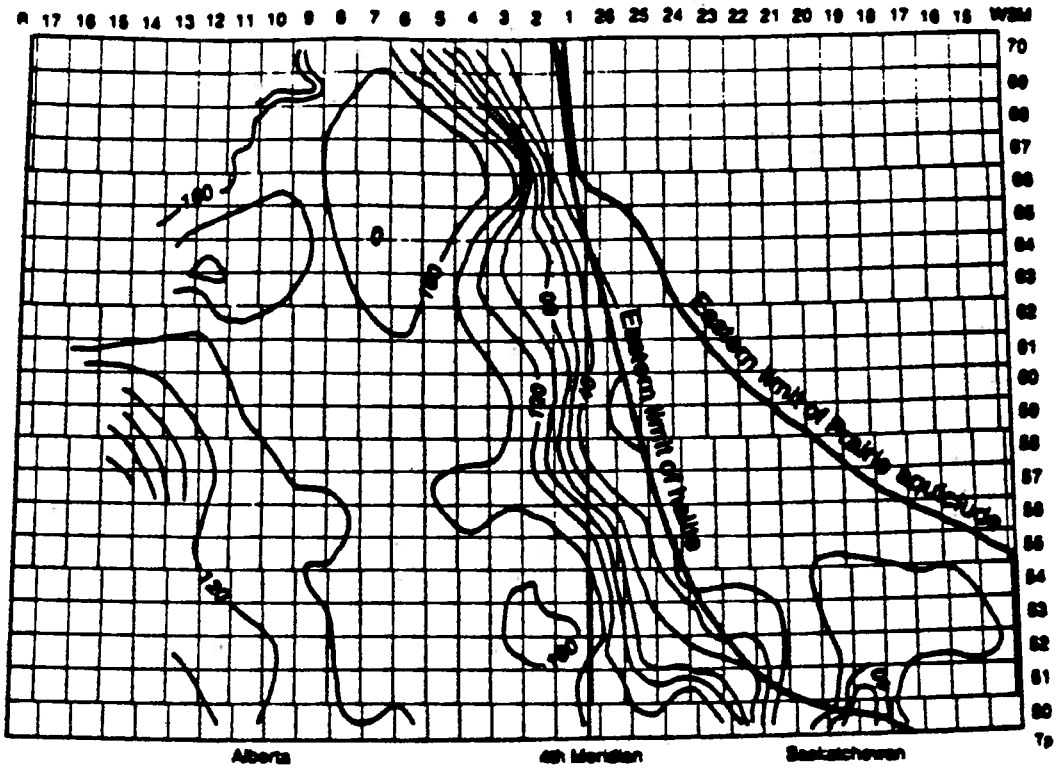

Figure 29. Isopachs (contour interval 20 m) of Prairie aquiclude

Table 3

Chemical composition (mg/L), physical properties and production data for raw brine produced by artificial solution of the Prairie Formation halite at the Lindberg salt plant and formation water from the Dawson Bay aquifer, Cold Lake study area

Stratigraphic unit	Prairie aquiclude*	Dawson Bay aquifer
Location	3-26-56-5-W4	2-11-50-20-W3
Depth (m)	901.6-933.6	816.6-828.8
Source	Plant inlet line	DST 1
Recovery	-	292.6 m sw
Na (diff.)	136 642	58 069
Ca	1 838	4 290
Mg	666	1 555
Cl	213 366	97 500
HCO_3	177	56
SO_4	3 221	5 600
TDS (calc.)	355 975	167 041
pH (laboratory)	7.2	6.8
Density (15.56°C)	1.209	1.113
Resistivity (23.33°C)	0.026	0.052

*Br = 66 mg/L; I = 0 mg/L

much of the upper part of the carbonate now filled with halite (Grayston et al., 1964, fig. 5-7). As a result, only one reliable formation water has been recovered from this aquifer (table 3); this sample came from an area still underlain by the Prairie Formation halite in the zone subject to solution effects and its composition reflects this situation and is similar to formation waters in the underlying Cambrian, although somewhat less saline. No drillstem test or core data are available for this unit.

Beaverhill Lake Aquifer System

The Middle Devonian First Red Beds-Watt Mountain clastic interval is overlain by carbonates of the Middle/Upper Devonian Beaverhill Lake Group and the Upper Devonian Cooking Lake and Leduc Formations. Although there is little information on the hydrogeology of the latest Middle Devonian rocks (see Dawson Bay "aquifer"), the stratigraphic position of all these aquifers between the underlying Prairie aquiclude and the overlying Ireton aquitard means that they can be grouped into the Beaverhill Lake aquifer system. Where this aquifer system has been preserved from erosion beneath the Ireton aquitard, thicknesses range from about 300 m to more than 500 m (figure 30A). East of the limit of the Ireton aquitard as little as 100 m remains in the Cold Lake study area, and here this aquifer system is in hydraulic continuity with the overlying McMurray and Mannville aquifers. This hydraulic continuity is demonstrated at two locations by the plots in figures 31A and 31B for the Mannville aquifer; in addition, the vertical flow is downward (see also figure 31C).

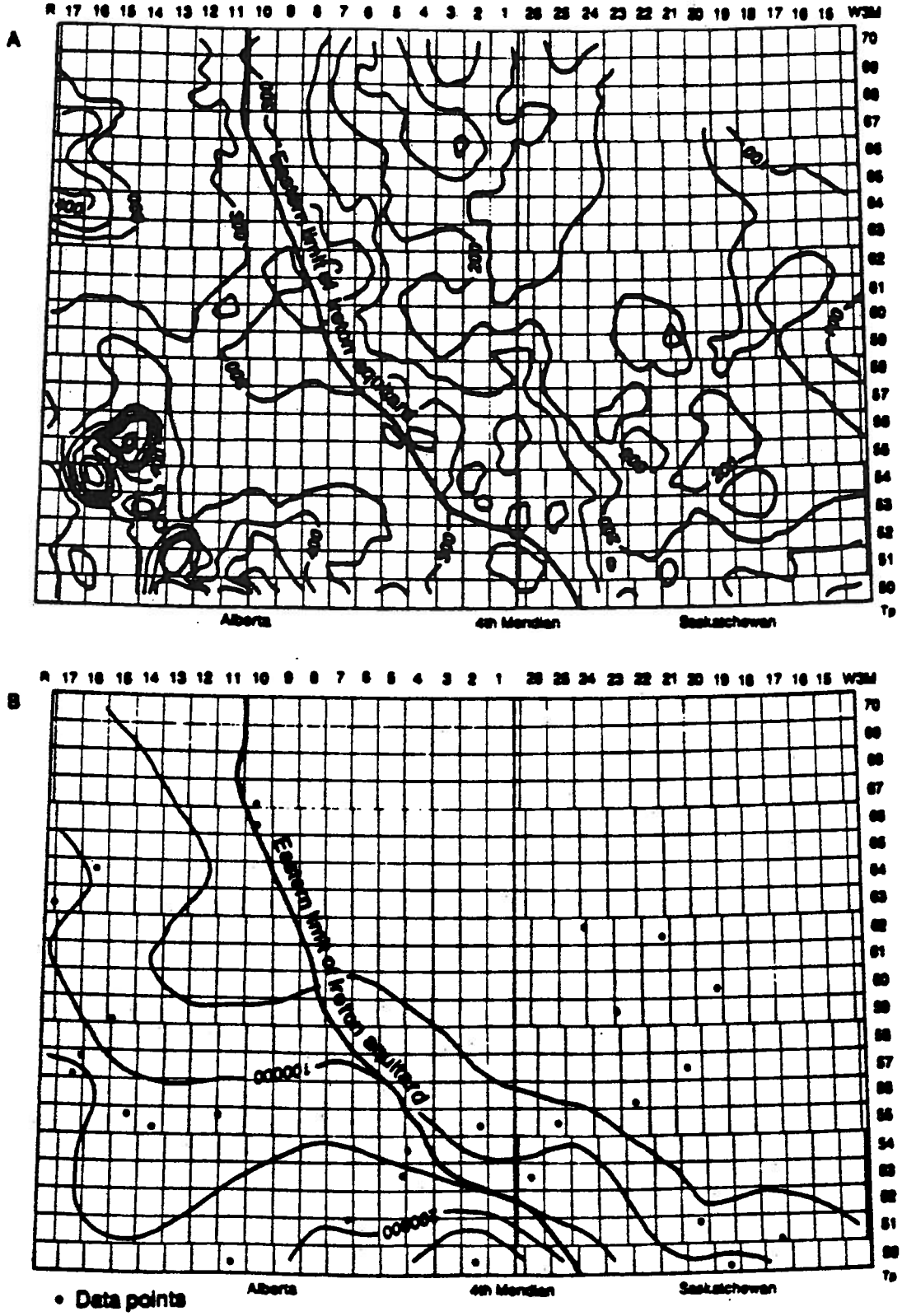

Figure 30. Beaverhill Lake aquifer system hydrogeology. A. Isopachs (contour interval 50 m); B. Salinity (mg/L) of formation waters; C. Potentiometric surface

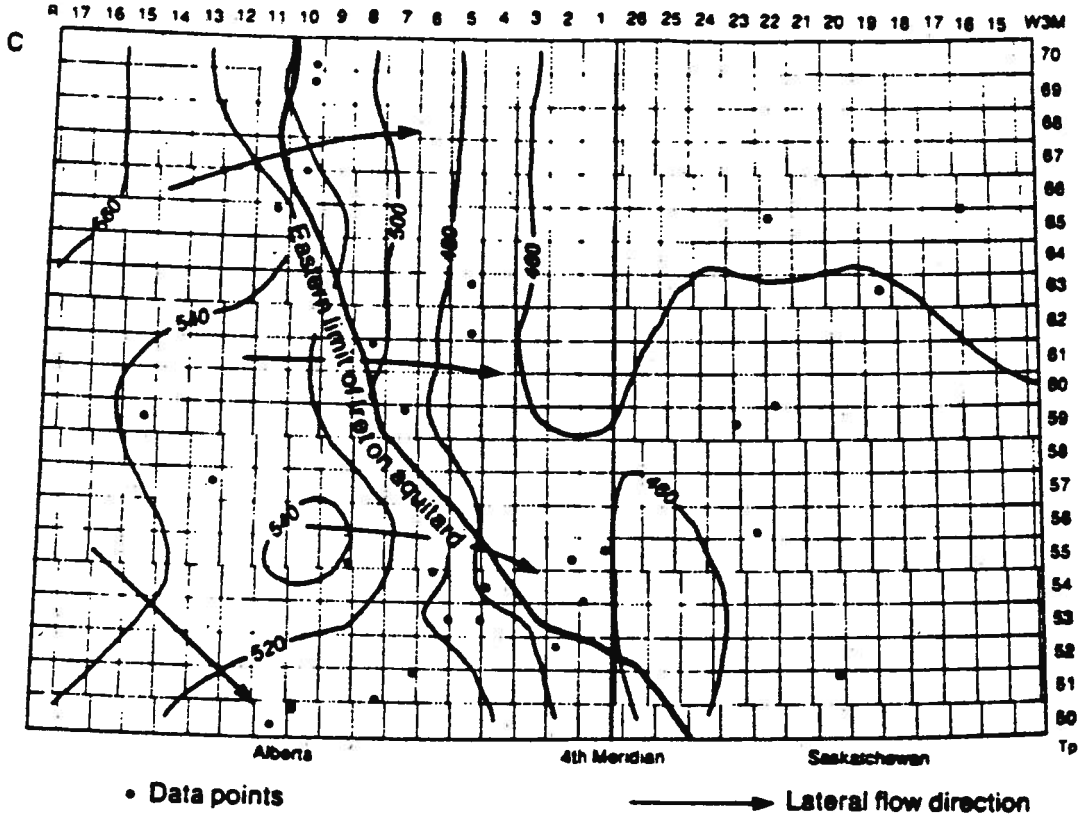

Figure 30. Continued

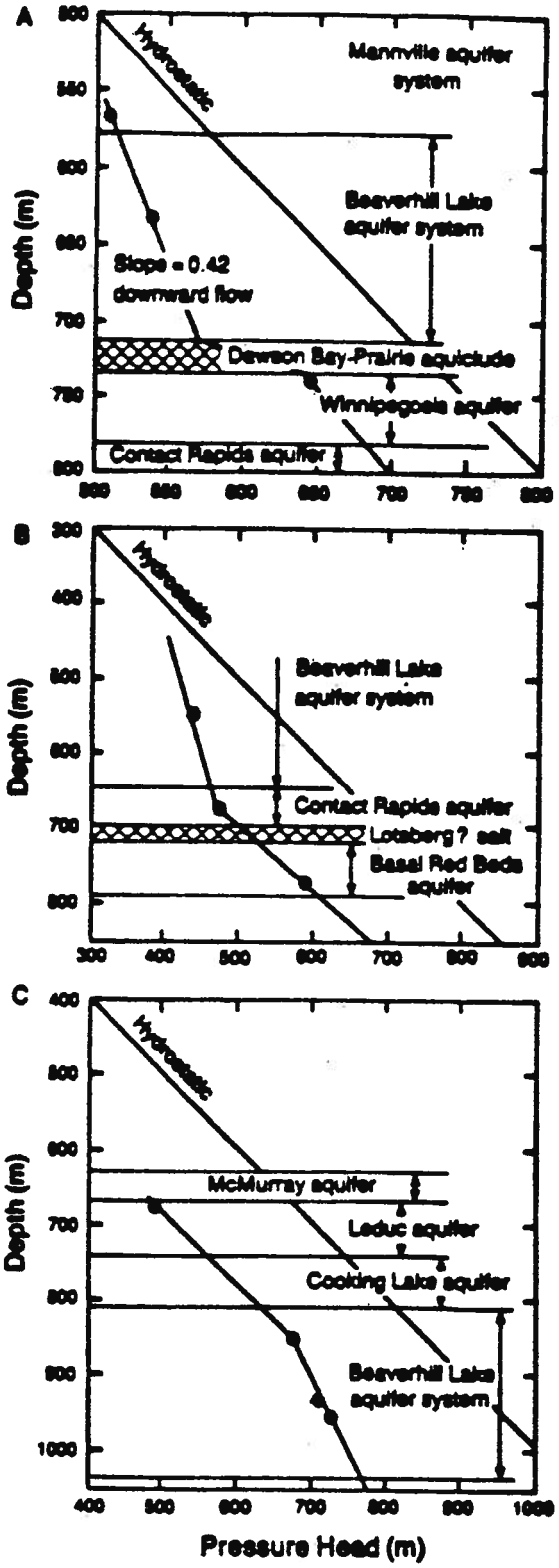

Figure 31. Cross-formational flow as illustrated by pressure head/depth plots in the Paleozoic. A. at well locat 7-19-59-23 W3 Mer. B. at we location 4-5-66-16 W3 Mer; (at well location 13-36-51-0 W4 Mer

Previous studies of basin-wide flow in the Western Canada Sedimentary Basin (Hitchon, 1969a), including a potentiometric surface of the Beaverhill Lake aquifer (Hitchon, 1969b, fig. 1) have shown that this aquifer is in the regional flow regime. The distribution of Cl (Hitchon, 1964, fig. 15-15) and Ca and Mg (Hitchon and Holter, 1971, figs. 14 and 15) are consistent with the regional trends and gradients on the potentiometric surface. Superimposed on the regional trends is an area of formation waters with Cl generally greater than 200 000 mg/L, Ca greater than 60 000 mg/L and Mg greater than 9000 mg/L, all of which are associated with an evaporite-carbonate sequence in south-central Alberta. As expected from the association with evaporites, these very saline formation waters have high contents of Br and very low contents of I (Hitchon et al., 1977, fig. 3 and table 4).

The Cold Lake study area lies immediately north and adjacent to the region with the very saline formation waters; that is, it is structurally updip and hydraulically downflow. Accordingly, highest salinities in the Beaverhill Lake aquifer system (about 200 000 mg/L) are found in the extreme south-central part of the study area, and the salinity decreases rather uniformally and gradually towards the northeast where values of about 20 000 to 50 000 mg/L are found in the region where the Beaverhill Lake Group subcrops beneath the Lower Cretaceous Mannville Group (figure 30B). There are corresponding decreases in the contents of Cl (150 000 to 10 000 mg/L), Ca (20 000 to 1000 mg/L) and Mg (4000 to 250 mg/L). Isoconcentration contours for HCO_3 and SO_4 are more irregular and difficult to interpret; there is a tendency for low HCO_3 ($\approx$200 mg/L) and high SO_4 (1000 to 2000 mg/L) in formation waters from the part of this aquifer system that is overlain

Table 4

Chemical composition (mg/L), physical properties and production data for formation water from the Leduc aquifer, Cold Lake study area

Location	2-26-55-15-W4
Depth (m)	662.0-663.5
Source	DST 18
Recovery	91 m gassy sw
Na (diff.)	44 102
Ca	560
Mg	261
Cl	69 500
HCO_3	133
SO_4	244
TDS (calc.)	114 800
pH (laboratory)	8.4
Density (15.56°C)	1.020

by the Ireton aquitard, with higher values for HCO_3 (up to 800 mg/L) and lower values for SO_4 (≈300 mg/L) in the eastern two-thirds of the study area. These trends for HCO_3 and SO_4 (as well as Na and Cl) are probably related to solution of evaporites (either from within the Beaverhill Lake Group or from the underlying Middle Devonian Prairie Formation), with dilution of the formation waters as they move updip from below the protective cover of the Ireton aquitard into regions with direct hydraulic connection with the Lower Cretaceous McMurray and Mannville aquifers (see figure 32).

Included within the Beaverhill Lake aquifer system is the Leduc Formation reef at Willingdon (Tp 55 R 15 W4 Mer). Formation waters were recovered from only one well penetrating the top of this reef complex, the best of which is shown in table 4. Salinity and Cl are similar to those of formation waters in the underlying Beaverhill Lake Group and Cooking Lake Formation, but the contents of Ca, Mg, HCO_3 and SO_4 are all lower.

The Beaverhill Lake aquifer system is the first Paleozoic unit for which hydrodynamic information of good quality (31 values of hydraulic head) is distributed well enough to enable an unequivocal flow regime analysis. As already mentioned, the lateral flow is regional with two components in the western half of the study area: in the southwest, the flow is southeastward and in the centre and northwest areas, the flow is eastward. In the eastern half of the study area, flow is mostly vertically downward from the Cretaceous aquifers, and the fresh water potentiometric surface becomes practically flat indicating a very slow lateral motion. The overall range of fresh water hydraulic head is between about 450 m in the northeast and 550 m along the western

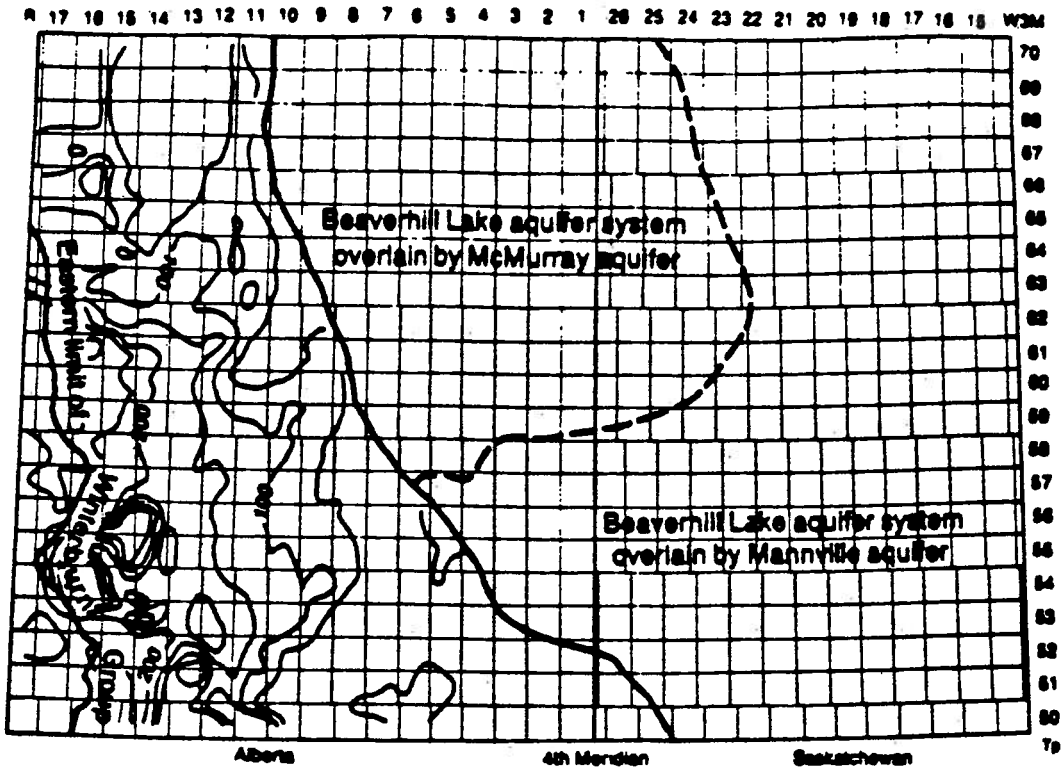

Figure 32. Isopachs (contour interval 50 m) of the Ireton aquitard, including the thin Camrose Tongue aquifer

boundary of the study area. The salinity gradients are in general agreement with the trend of the hydraulic gradients (compare figures 30B and 30C).

Ireton Aquitard

The argillaceous lime mudstones of the Ireton Formation occur only in the western third of the Cold Lake study area, and along part of the southern boundary. Except for a narrow band on the western margin of the study area, where it is conformably overlain by carbonates of the Winterburn Group, it is overlain unconformably by Lower Cretaceous Mannville Group rocks. Maximum thickness of this aquitard is about 250 m (figure 32) including the thin Camrose Tongue. A previous study (Basin Analysis Group, 1985) estimated the vertical hydraulic conductivity of the Ireton aquitard to be 2×10^{-9} m/d with good to high leaky properties.

Camrose Tongue Aquifer

The southwest corner of the Cold Lake study area includes the northeastern margin of the Camrose Tongue dolomite, a thin (less than 10 m) aquifer within the Ireton Formation (figure 33A). This aquifer lies about 10 to 20 m below the top of the Ireton aquitard and about 150 m above its base. As a result, formation waters in the Camrose Tongue aquifer tend to resemble those in the overlying aquifers rather than those in the Beaverhill Lake aquifer system. Salinities are in the range 80 000 mg/L in the south to less than 40 000 mg/L in the north

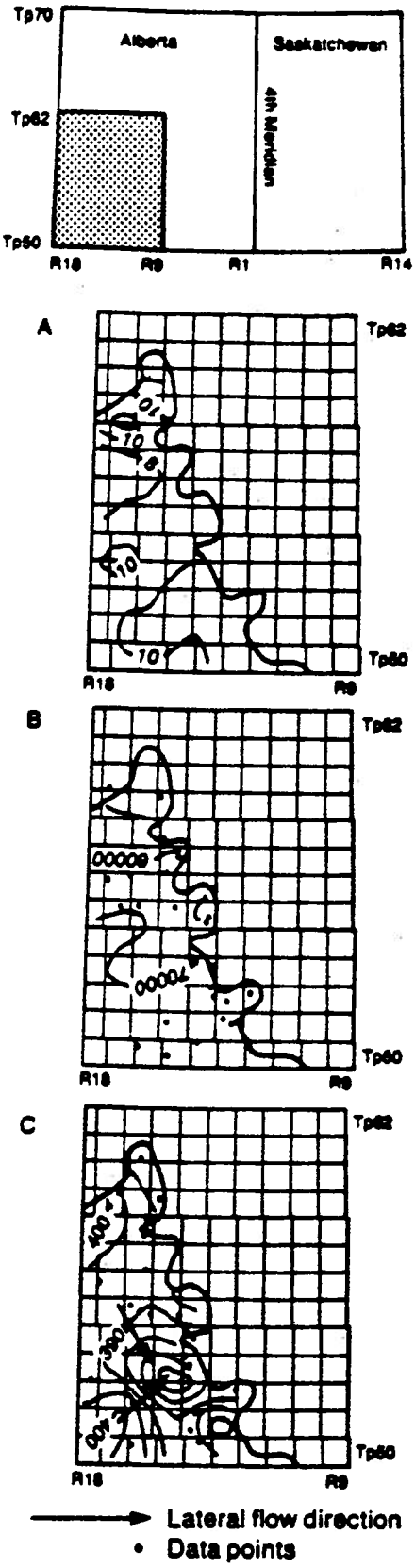

Figure 33. Camrose Tongue aquifer hydrogeology. A. Isopachs (2 m interval); B. Salinity (mg/L) of formation waters C. Potentiometric surface

(figure 33B), with east-west oriented isoconcentration contours. Corresponding ranges for other components are Cl (45 000 to 25 000 mg/L), Ca (3000 to 1250 mg/L) and Mg (1000 to 500 mg/L). Sulfate is generally about 50 mg/L without any obvious regional trend. The content of HCO_3 decreases from about 600 mg/L along the western margin of the study area to just over 200 mg/L along the formation boundary, that is, the isoconcentration contours trend north-south, at right angles to those for salinity, Cl, Ca and Mg.

The lateral flow, although dominantly updip, northward, and in agreement with the major hydrochemical gradients, also has an eastward component (see figure 33C) that could be responsible for the anomalous direction of the HCO_3 gradient. The eastward flow could also be related to downward flow from the Winterburn aquifer. There is insufficient hydrodynamic information for this unit in the study area to be more precise about flow directions. As shown on figure 34, there is a decrease in hydraulic head of 30 m over a distance of about 12 km at the northern margin of the Camrose Tongue aquifer between this aquifer and the Grosmont aquifer.

Grosmont Aquifer

The Grosmont Formation is a dolomitized platform carbonate which is approximately coeval with the Ireton Formation. It extends 500 km south from outcrops along the Peace River to the northwest corner of the Cold Lake study area, where it ranges in thickness from 50 to 100 m (figure 35A).

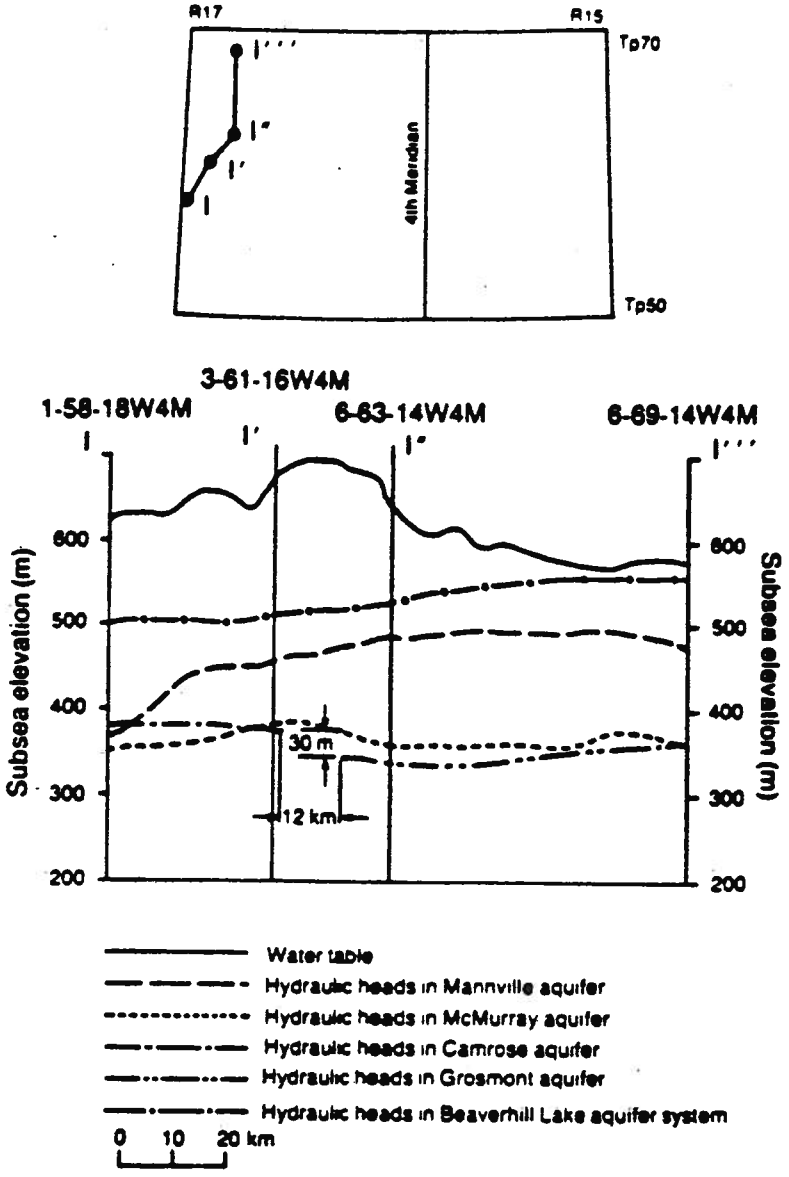

Figure 34. North-south cross-section showing the hydraulic separation between the Camrose Tongue aquifer and the Grosmont aquifer

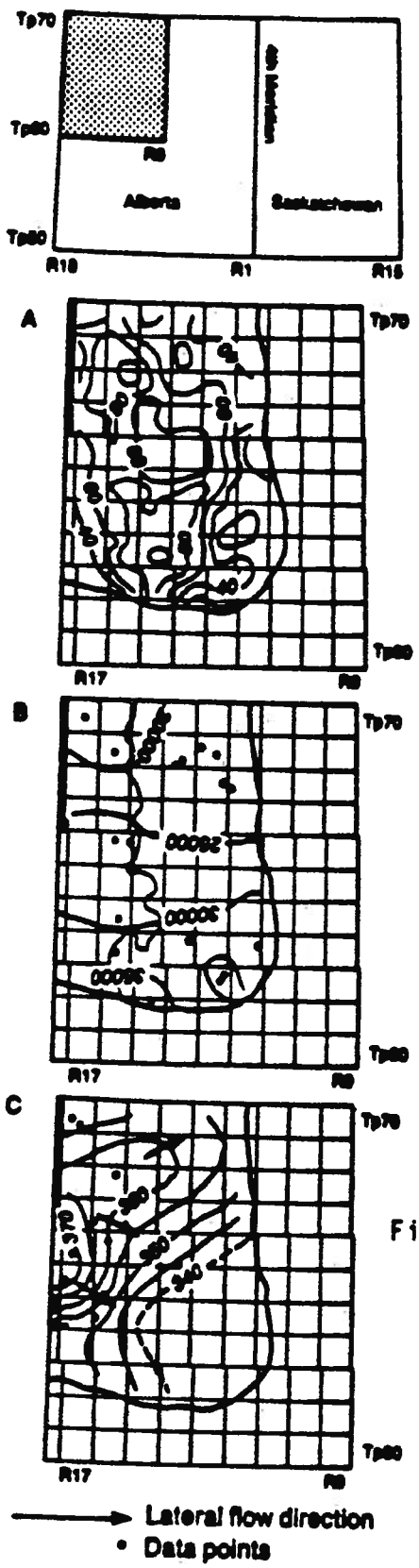

Figure 35. Grosmont aquifer hydrogeology. A. Isopachs (contour interval 20 m); B. Salinity (mg/L) of formation waters; C. Potentiometric surface (10 m interval)

Early studies of the potentiometric surfaces of the individual Woodbend Group carbonates in the Western Canada Sedimentary Basin demonstrate the dominant regional flow within the carbonate complexes, with the lowest hydraulic heads being found in the Grosmont Formation (Hitchon, 1969b, fig. 2). Pressure-elevation, temperature-depth, and temperature-elevation profiles confirm the continuous flow system between the Rimbey-Meadowbrook reef chain and the updip Grosmont Formation carbonate complex (Hitchon, 1984, figs. 15 to 17). These trends are reflected in the distribution of Cl in the formation waters (Hitchon, 1964, fig. 15-17), and also Ca and Mg (Hitchon and Holter, 1971, figs. 8 and 9) and to a lesser extent Br (Hitchon et al., 1977, fig. 2).

Like the formation waters in the Camrose Tongue aquifer to the south, the salinity decreases northward from about 35 000 mg/L to just under 15 000 mg/L (figure 35B). There are corresponding decreases in Cl (25 000 to 10 000 mg/L) and, less clearly, Ca (500 to 200 mg/L) and Mg (350 to 150 mg/L). Sulfate increases towards the northwest in the direction of the Hondo Formation anhydrites (Belyea, 1964, fig. 6-16) which are interlayered within the Grosmont Formation. Bicarbonate is generally less than 1000 mg/L on the southern and eastern margins of the formation, and increases to about 1250 mg/L in the northwest corner of the study area. Areally, the southern margin of the Grosmont aquifer and the northern extent of the Camrose Tongue aquifer are only 5 km apart. In general, formation water composition is similar in the extremities of these separate aquifers, which strongly suggests excellent hydraulic continuity through the thin intervening Ireton aquitard.

In the Grosmont aquifer, the lateral flow diverges in two directions (southeast and northeast) from a potentiometric high located at Tp 66, R 17 (figure 35C). Some of the lowest values of fresh water hydraulic head for the study area are found in this aquifer (between 300 m and 350 m) suggesting that it plays the role of a hydraulic (regional) drain. The hydraulic conductivity (0.017 m/d on average) is similar to that of the Camrose Tongue aquifer (0.022 m/d on average).

Winterburn Aquifer

In the Cold Lake study area the Upper Devonian Winterburn Group consists of an eroded remnant along the western boundary, with a maximum thickness of about 50 m. Only eight reliable formation waters are available, with salinities decreasing northward from about 55 000 mg/L at Tp 57 to 25 000 mg/L at Tp 61. There are corresponding decreases in all other components except HCO_3, which exhibits an increase from 50 to nearly 800 mg/L over the same five townships.

Insufficient hydrodynamic data and the marginal position of this aquifer in the study area preclude an analysis of the flow.

McMurray Aquifer

In the Cold Lake study area the basal stratigraphic unit of the Cretaceous is the McMurray Formation, which is overlain everywhere by the Clearwater Formation. In the northwestern half of the study area the basal unit of the Clearwater Formation is argillaceous; this serves to distinguish two hydrostratigraphic regions within the McMurray

Formation: (1) the McMurray aquifer where the basal unit of the Clearwater Formation is argillaceous; and (2) the remainder designated as part of the Mannville aquifer. From west to east the McMurray aquifer rests on successively older Upper Devonian rocks which comprise the Winterburn and Grosmont aquifers, the Ireton aquitard, and the Beaverhill Lake aquifer system. The extreme eastern margin of the McMurray aquifer is east of the solution edge of the Prairie Formation halite and hence there is hydraulic continuity in this area between the McMurray aquifer, the Beaverhill Lake aquifer system and the Winnipegosis aquifer; unfortunately, reliable formation water analyses were not recovered from drillstem tests in this critical area. The McMurray aquifer ranges up to 120 m thick (figure 36A).

Isoconcentration contours for components in the formation waters have a general east-west orientation, with salinity decreasing northward from 60 000 mg/L to 10 000 mg/L (figure 36B), and corresponding decreases for Cl (35 000 to 5000 mg/L), Ca (1000 to less than 250 mg/L) and Mg (700 to less than 100 mg/L). Bicarbonate increases northward from about 400 to more than 1200 mg/L. Sulfate is generally less than 100 mg/L with no clearly defined trends.

Where the McMurray aquifer and Beaverhill Lake aquifer systems are in contact, both the directions and gradients of the respective isoconcentration contours are similar, with generally lower values in the McMurray aquifer by 10 000 mg/L for salinity, and corresponding decreases for Cl (5000 mg/L), Ca (500 mg/L), Mg (50 mg/L), HCO_3 (100 mg/L) and SO_4 (≈50 mg/L). These facts strongly suggest excellent hydraulic continuity between these aquifers in the region of contact. Similar relations are found where the McMurray aquifer overlies the

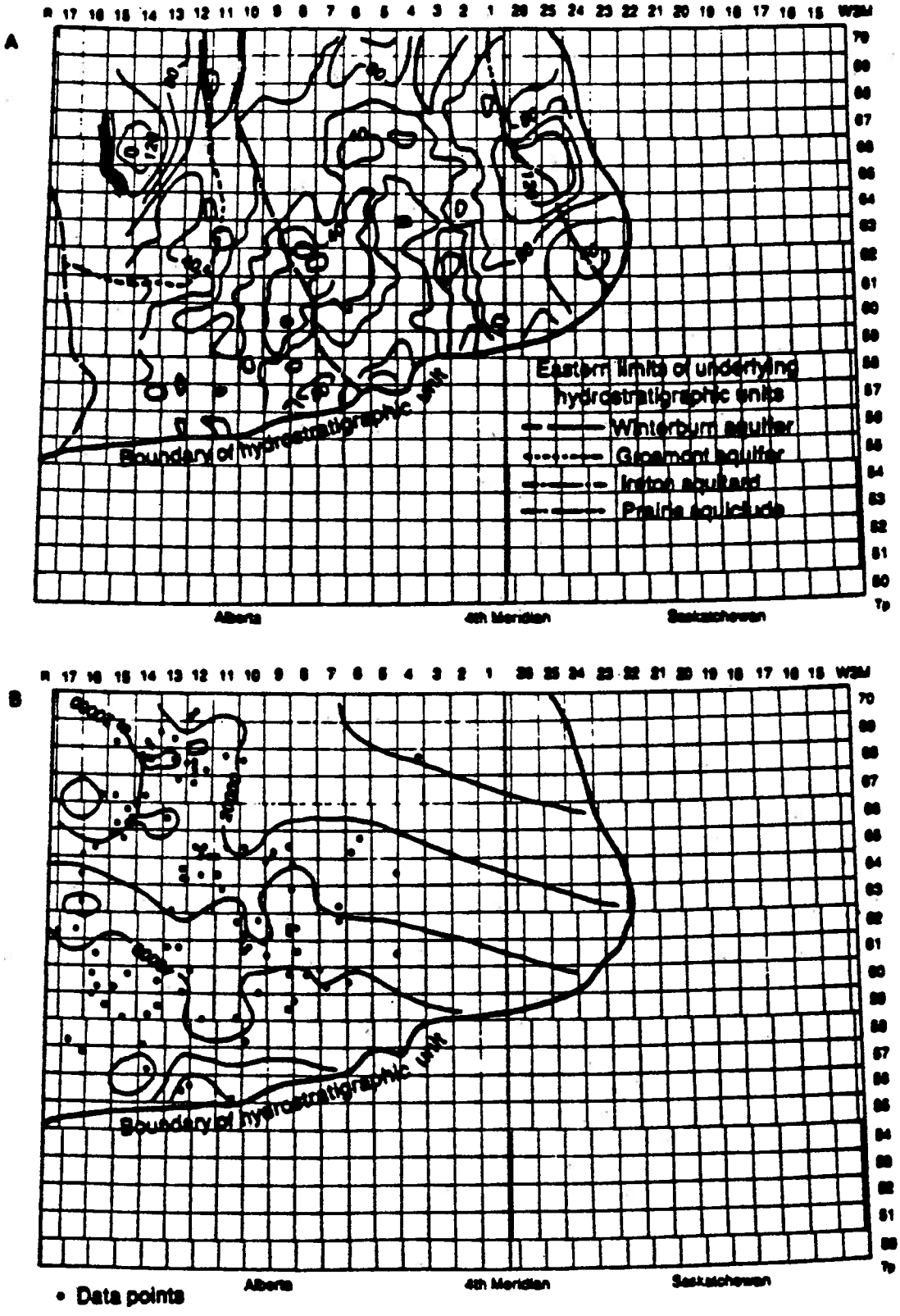

Figure 36. McMurray aquifer hydrogeology. A. Isopachs (contour interval 20 m); B. Salinity (mg/L) of formation waters; C. Potentiometric surface

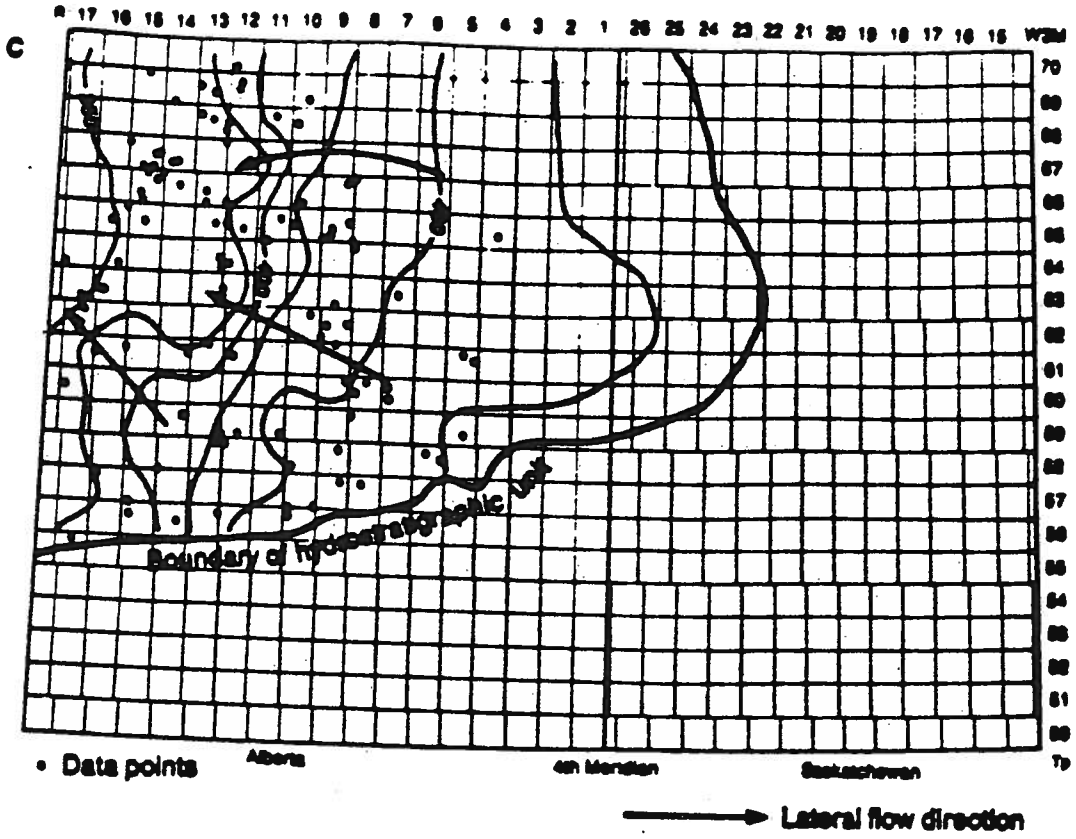

Figure 36. Continued

Grosmont and Winterburn aquifers. In the region where the McMurray aquifer and Beaverhill Lake aquifer system are separated by the Ireton aquitard (which is about 100 m thick), salinities vary by as much as 40 000 mg/L, with corresponding differences for the other components. Although data are sparser in the Beaverhill Lake aquifer system, the broad trends and isoconcentration gradients for the two aquifers are similar; for example, the southwest-trending re-entrant on many formation water composition maps associated with the Leduc Formation reef complex at Willingdon can be seen on both sets of maps. This suggests that the Ireton aquitard is not tight and that the effects of flow in the underlying Beaverhill Lake aquifer system are reflected in the overlying McMurray aquifer.

Based on 152 good quality drillstem tests, the fresh water hydraulic heads in the McMurray aquifer range between 320 m (in the northwest part of the study area) to 490 m close to the southeastern boundary of the aquifer.

The potentiometric surface of the McMurray aquifer (figure 36C) shows that the influence of the underlying Grosmont aquifer dominates the lateral flow in this unit: the 375 and 400 m isocontours are effectively coincident with the eastern boundary of the Grosmont carbonate platform and all of the lateral flow is focused towards the area of overlap between the two aquifers.

Clearwater Aquifer

The arenaceous unit within the Clearwater Formation is defined as the Clearwater aquifer. It is thin (average 35 m) and is underlain and overlain by shales of the Clearwater Formation (figure 37A). The

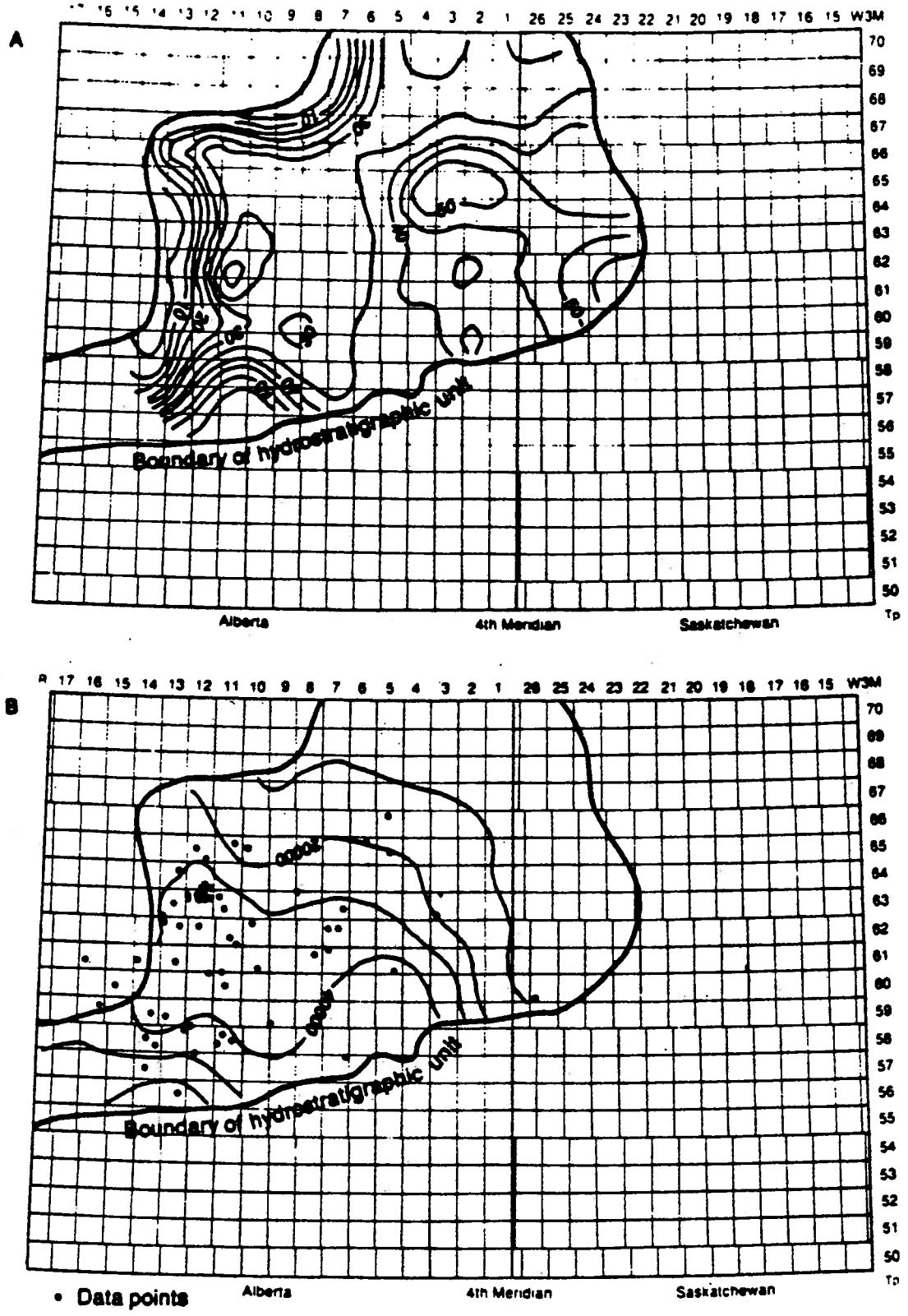

Figure 37. Clearwater aquifer hydrogeology. A. Isopachs (contour interval 5 m); B. Salinity (mg/L) of formation waters; C. Potentiometric surface

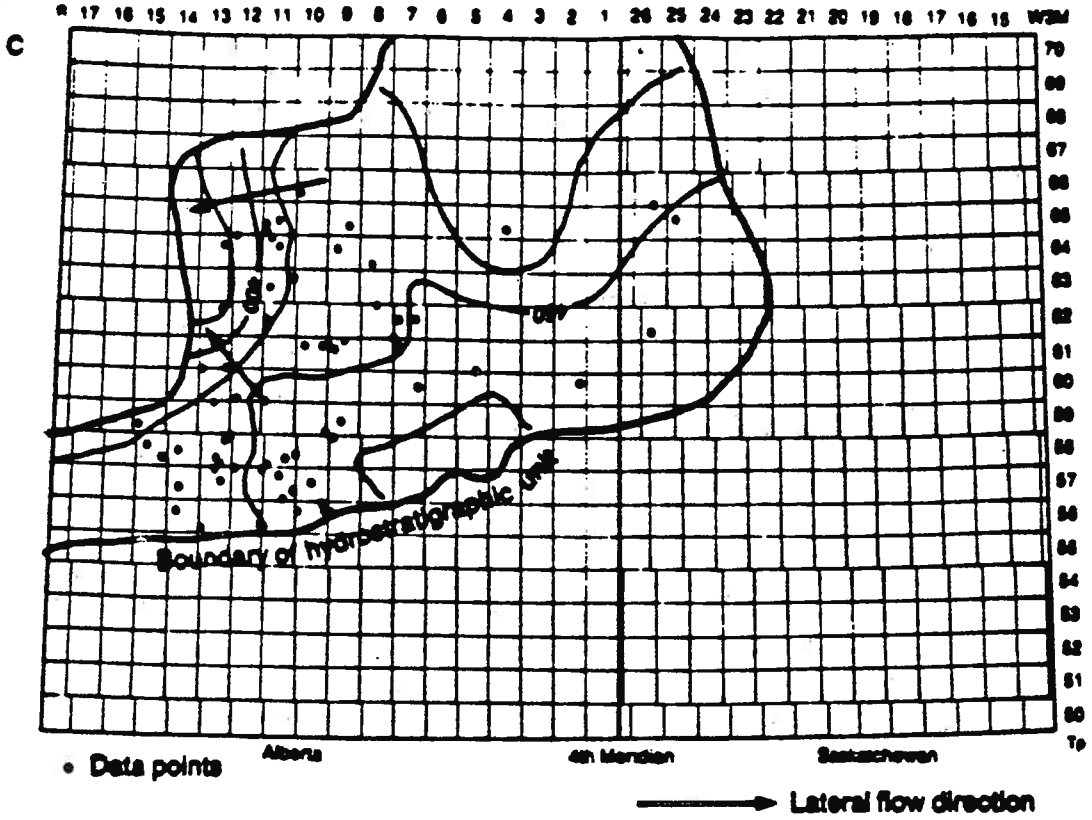

Figure 37. Continued

southern and eastern boundaries are depositional, marking the shoreline at this time in Cretaceous history. The northwestern margin is also depositional and represents the seaward extent of this sand body, to the north of which only Clearwater Formation shales are present. The composition of formation waters (represented by the salinity map, figure 37B) and the directions and gradients on the isoconcentration contours, are effectively the same as those in the underlying McMurray aquifer, indicating that the intervening lower Clearwater Formation shale is a weak (leaky) aquitard.

Based on 85 good quality drillstem tests, the lateral flow in the Clearwater aquifer is similar to that in the McMurray aquifer (figure 37C) as confirmed by the hydrochemistry; the fresh water hydraulic heads vary between 350 and 480 m; the regional average hydraulic conductivity is 3.7×10^{-2} m/d.

Mannville Aquifer

Hydrostratigraphic units within the Lower Cretaceous Mannville Group have a complex geometric relation. Where the Clearwater Formation is present, it is possible to distinguish both the McMurray aquifer and the overlying Clearwater Formation with its interbedded Clearwater aquifer. Mannville Group strata elsewhere in the Cold Lake study area have been designated as the Mannville aquifer and include within them oil sands aquitards. The strike cross-section in figure 38 illustrates this complex geometric relation.

The Mannville aquifer extends throughout the study area with an average thickness of 200 m (figure 39A). Formation water analyses were

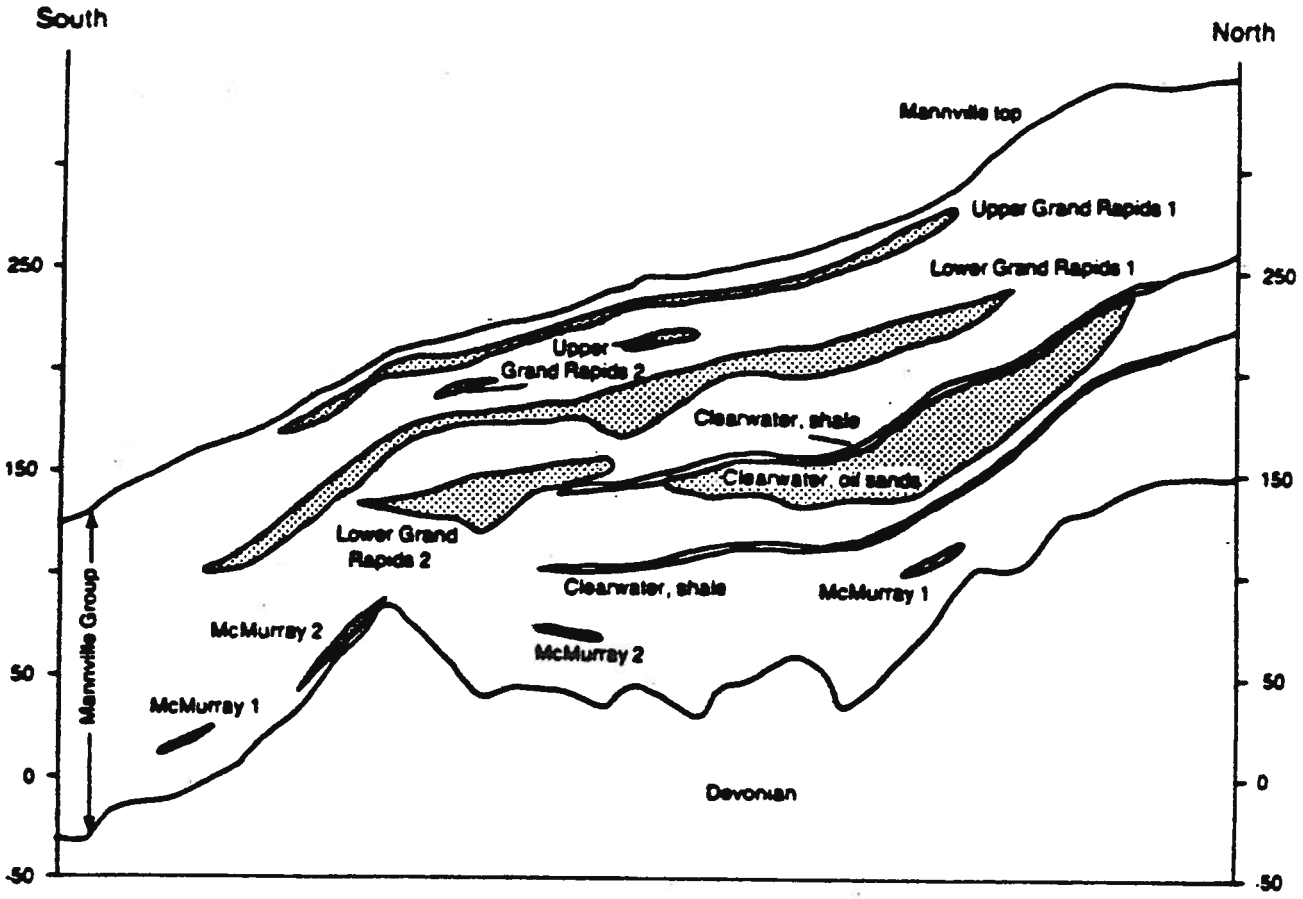

Figure 38. Diagrammatic strike cross-section through the Lower Cretaceous Mannville Group in the Cold Lake study area showing the complex relations of aquifers, and oil sands deposit and shale aquitards

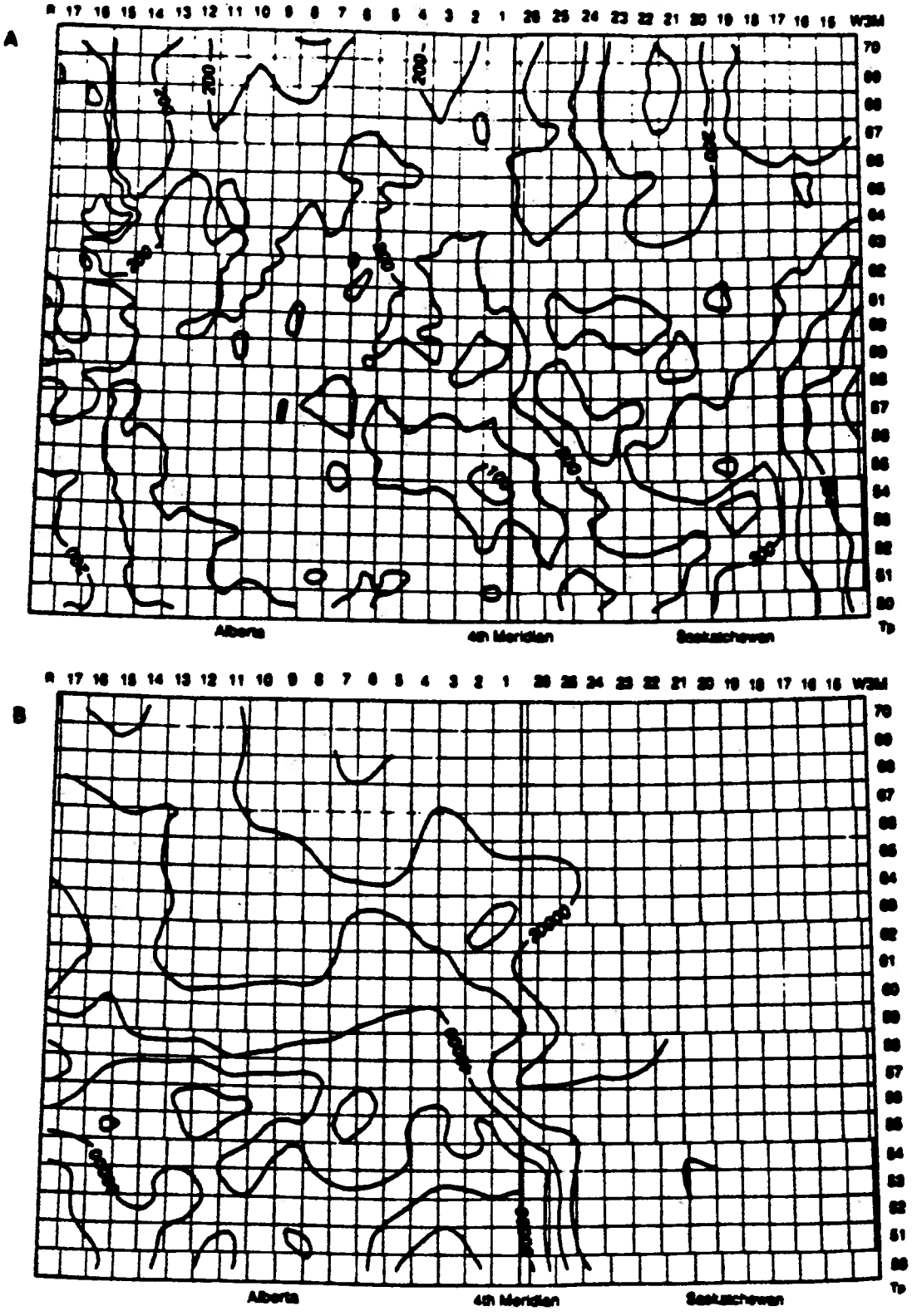

Figure 39. Mannville aquifer hydrogeology. A. Isopachs (contour interval 50 m); B. Salinity (mg/L) of formation waters; C. Potentiometric surface

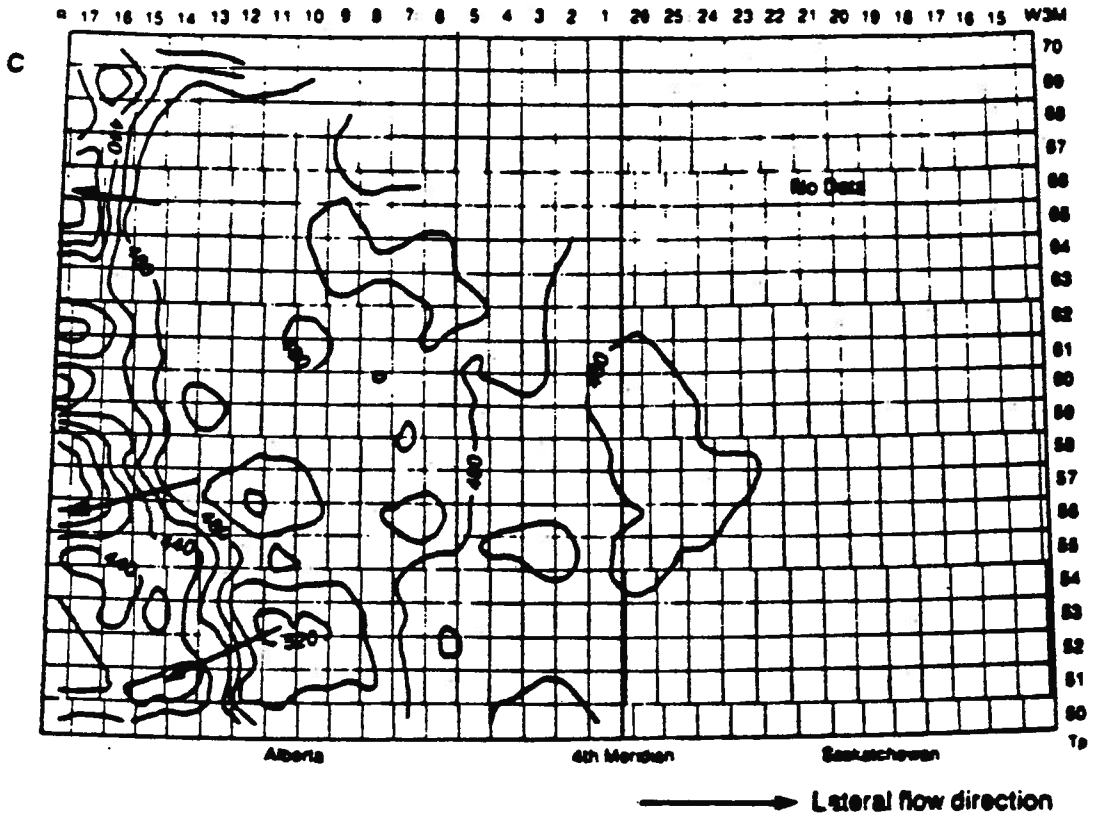

Figure 39. Continued

essentially available only for Alberta and parts of the western border region of Saskatchewan. Salinity decreases from more than 60 000 mg/L in the south to less than 10 000 mg/L in the north (figure 39B), with corresponding decreases for Cl (40 000 to 5000 mg/L), Ca (2000 to less than 250 mg/L) and Mg (800 to less than 100 mg/L), and generally corresponding increases for HCO_3 (200 to 900 mg/L). Sulfate is usually less than 100 mg/L, without obvious regional trends; however, most of the isolated regions with SO_4 greater than 100 mg/L are confined to the region with salinities greater than 50 000 mg/L. Both isoconcentration trends and gradients are effectively identical with those in the underlying Clearwater and McMurray aquifers, and it seems clear that formation waters in the entire Mannville Group are part of one complex hydrostratigraphic unit with intervening leaky aquitards. In the region south of the southern limit of the Clearwater aquifer, and which also has up to 200 m of Ireton aquitard beneath the Mannville aquifer, comparison of formation waters with those in the Beaverhill Lake aquifer system shows salinity differences about 40 000 mg/L with corresponding differences for other components. This observation is consistent with that for the McMurray aquifer and, again, confirms that the Ireton aquitard is leaky. Although there is a paucity of data from the Beaverhill Lake aquifer system, comparison of the chemistry of formation waters from this aquifer with those in the overlying Mannville aquifer where the Ireton aquitard is absent indicates very similar compositions (with the exception of SO_4), indicative of good hydraulic connection between the two aquifers.

Over most of the study area the fresh water potentiometric surface for the Mannville aquifer is "flat" indicating general vertical flow

conditions. Outward lateral flow is observed on the western and southern edges of the study area (figure 39C); this trend is only noticeable on the salinity map for the flow to the south. The overall range of hydraulic heads is large, between 320 m and 600 m, indicating possible influence of the present-day topography.

One cannot see clearly the nature of the flow regime in the Mannville aquifer (figure 39C). In the western and southwestern margins of the Cold Lake study area, where lateral flow is noticeable in this aquifer, it is not topographically-controlled, even in a subdued way. It is, in fact, of the intermediate type, like the dominantly westward flow in the Clearwater and McMurray aquifers.

Joli Fou Aquitard

The thickness of this shaley aquitard ranges from 2 to 160 m with an average of 26 m, especially W4Mer. It covers the entire study area but as the Viking sandstone becomes progressively thinner to the east and northeast the Joli Fou aquitard becomes hydraulically merged with the Colorado aquitard system. Based on published results for the Western Canada Sedimentary Basin, the vertical hydraulic conductivity of the Joli Fou aquitard is estimated at 4×10^{-9} m/d (Basin Analysis Group, 1985) with low leaky properties.

Viking Aquifer

For the purposes of this study the Viking aquifer comprises the aggregate of several thin sandstones which are present in the Viking Formation in the Cold Lake study area. It has an average thickness of

less than 10 m in the study area and thins considerably in the vicinity of St. Paul (Tp 58, R 9, W4Mer). Studies of the potentiometric surface of the Viking aquifer in the Western Canada Sedimentary Basin (Hill et al., 1961; Hitchon, 1969b, fig. 4) indicate the presence, in central Alberta, of a large closed potentiometric surface low, elongated in a general northwest direction, roughly parallel to the axis of the Alberta Basin and centred at Gilby over the southern end of the Rimbey-Meadowbrook carbonate reef chain. It has been speculated (Hitchon, 1969b) that this closed potentiometric surface low is due to osmotic effects across shale membranes, which are imposed on the gravity flow regime. In the Cold Lake study area, flow directions might, therefore, represent a complex combination of downdip flow towards the closed potentiometric surface low and regional updip flow and topographical influence as observed on local flow regimes.

In the Western Canada Sedimentary Basin the patterns of regional variations in formation water composition appear to relate more to the total thickness of sandstones in the Viking Formation (see Rudkin, 1964) than they do to the basin-wide variations in the potentiometric surface. This can be seen in maps of the regional distribution of Cl (Hitchon, 1964, fig. 15-36) and iodide (Hitchon et al., 1977, fig. 5). In the Cold Lake study area, in addition to these factors: (1) the Viking aquifer is absent in the northeast part of the region as well as parts of the eastern and southern boundaries; (2) the individual sandstones are very thin; and (3) the aquifer is as shallow as 100 m in places. Because a detailed investigation of the lithological variations within the Viking Formation was beyond the limits of the present study, the hydrochemical patterns of formation waters in the Viking aquifer can be interpreted only in general terms.

Salinities in the range 40 000 to 60 000 mg/L generally characterize the southern half of the region; values less than 40 000 mg/L occur along parts of the southern border (figure 40A). In this southern area salinity gradients are steep, compared to the northern half of the study area, which has lower salinities, generally in the range 40 000 to 10 000 mg/L. Throughout the area, however, isolated regions of higher or lower salinity occur within these broad regional trends. Corresponding ranges for other components in the southern half of the study area are Cl (40 000 to 25 000 mg/L), Ca (2000 to 1000 mg/L) and Mg (800 to 500 mg/L). In the northern half of the region the corresponding ranges are Cl (25 000 to 10 000 mg/L), Ca (1000 to less than 250 mg/L) and Mg (500 to less than 100 mg/L). Isoconcentration patterns for HCO_3 and SO_4 are difficult to interpret. Based on the previous basin-wide studies of potentiometric surface and hydrochemistry of the Viking aquifer cited above, one might speculate that the observed "patchy" isoconcentration patterns are related to the location of the Cold Lake study area at a hydraulic divide.

The potentiometric surface of the Viking aquifer (figure 40B) is based on 1171 reliable drillstem tests. The range of hydraulic heads is 440 to 640 m. Although there is some subdued similitude between topography and the potentiometric surface (figures 40B, 44 and 45), the flow in the Viking aquifer is best characterized as being of intermediate to local type.

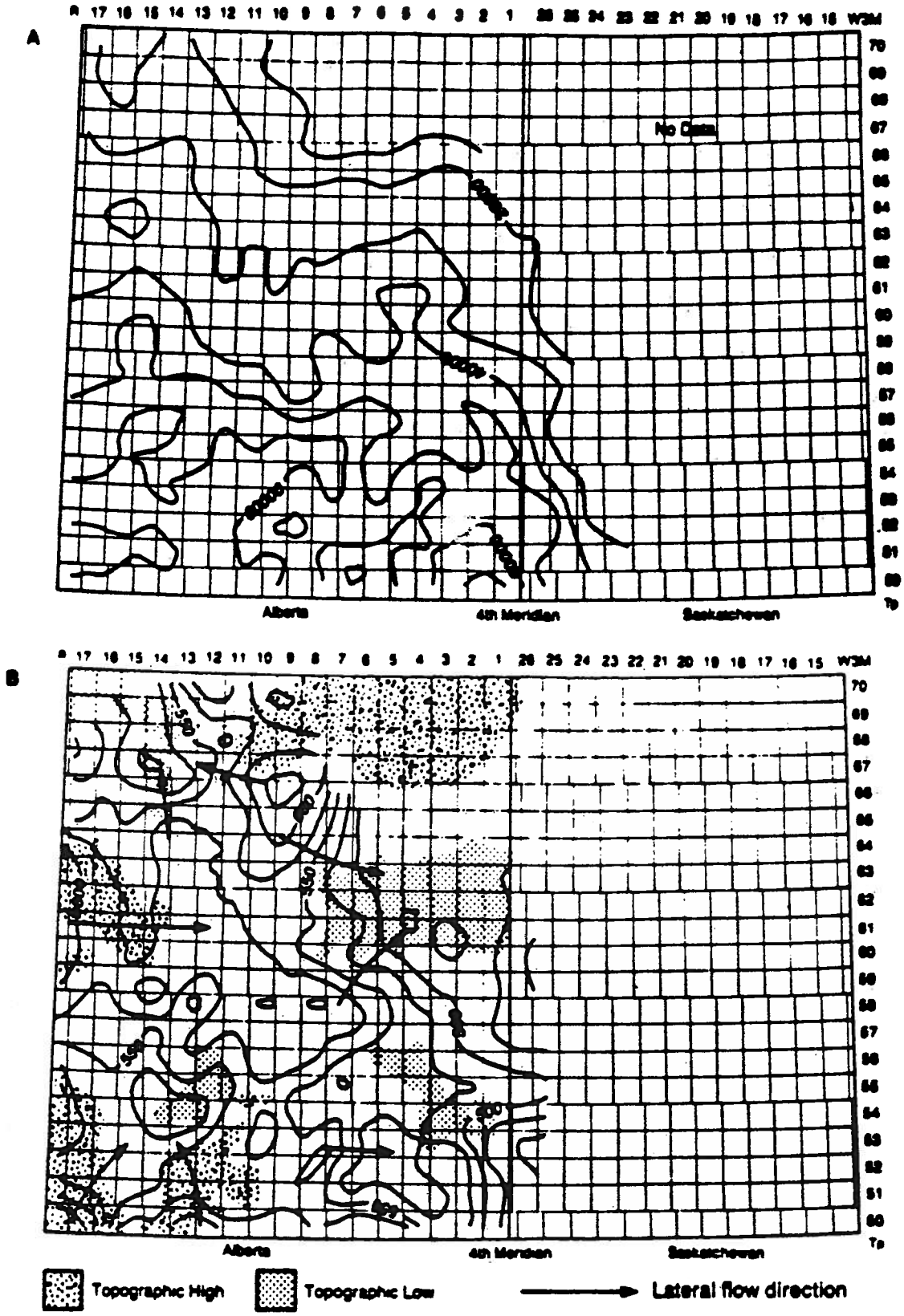

Figure 40. Viking aquifer hydrogeology. A. Salinity (mg/L) of the Viking aquifer formation waters; B. Potentiometric surface of the Viking aquifer

St. Walburg Aquifer

This sandstone aquifer is only present south of Tp 65 and east of R 1, W4Mer. Its thickness is 10 m or more east of R 22, W3Mer. It ranges in thickness from 3 to 50 m with an average of 15 m. Only two reliable drillstem tests indicate hydraulic heads in the same range as those of the Viking aquifer and, for the purpose of this study, it is sufficient to assume that the flow has the same local regime as the Viking aquifer.

Colorado Aquitard System

In the Cold Lake study area strata younger than the Viking and St. Walburg sandstones are dominantly argillaceous, and for the purpose of this study have been grouped together as the Colorado aquitard system. This aquitard system ranges in thickness from 60 to 680 m (figure 41) and forms the bedrock beneath Quaternary strata. Formation waters have been recovered from minor porous zones at the base of the Fish Scales Zone, within the Second White Speckled Zone, and from the Lea Park Formation. The Belly River Formation contains shallow sandstone aquifers that are used locally by rural residents as a source of domestic (potable) water supply in the area delineated by figure 41. These shallow groundwaters have not been evaluated in this study. Basal Belly River Formation sandstones are good aquifers and are a target for oil and gas drilling at depth in the southwest part of the study area. All the deeper formation waters range in salinity between those in the underlying Viking and St. Walburg sandstones and those in the Quaternary (table 5).

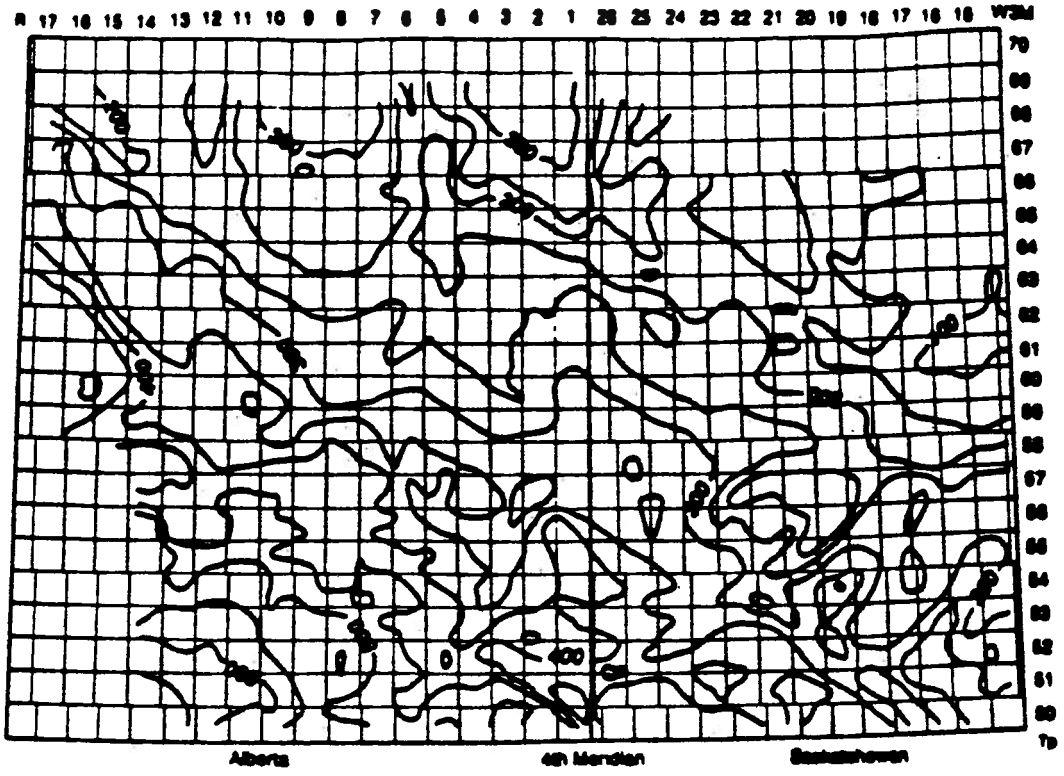

Figure 41 Isopachs (contour interval 50 m) of the Colorado aquitard system

Table 5. Chemical composition (mg/L), physical properties and production data for selected formation waters from aquifers in the Colorado aquitard, Cold Lake study area

Stratigraphic Unit	Base of Fish Scales	Base of Fish Scales	Lea Park Formation	Belly River Formation	Belly River Formation
Location	6-15-53-9-W4	10-9-55-1-W4	7-4-50-17-W4	10-28-52-17-W4	10-22-51-11-W4
Depth (m)	548.6-551.6	304-8-309.4	301.8-320.0	215.0-241.0	179.8-207.3
Source	Perforations	DST 6	DST 1	DST 2	DST 1
Recovery	-	137 m sw	219.5 m sw	37 m sw	82.3 m sw
Na (diff.)	22 280*	12 004	3 713	5 395**	1 789
Ca	1 800	586	160	374	10
Mg	790	307	32	155	5
Cl	40 000	20 240	5 920	9 170	2313
HCO_3	303	327	288	183	588
SO_4	2	25	23	189	185
TDS (110°C)	67 605	35 180	10 440	15 360	4 930
TDS (ignition)	58 990	32 150	9 400	14 570	4 220
TDS (calc.)	65 176	33 489	10 136	15 466	4 889
pH (laboratory)	7.3 (21°C)	7.8 (23.9°C)	8.4 (24.4°C)	7.7 (22°C)	6.4 (20.6°C)
Density (15.56°C)	1.049 (21°C)	1.026	1.008	1.011	1.005
Refractive Index (25°C)	1.343	1.3386	1.3347	1.3357	1.3337
Resistivity (ohm m; 25°C)	0.107	0.218	0.676	0.384	1.46

- = not determined

* Na 22 000 mg/L; K 280 mg/L

** Na 5 365 mg/L; K 30 mg/L

Because shallow drillstem test information is sparse, and certainly not sufficient to produce a potentiometric surface for any aquifer in this dominantly shaley and thick aquitard, it is postulated that whenever sandstone bodies are sufficiently continuous the lateral flow will be topographically-controlled and similar to that of the Viking aquifer. Otherwise, the dominant flow is vertically driven by the always positive difference of heads between the Quaternary system and the Mannville aquifer.

CROSS-FORMATIONAL FLOW

This section deals with the regional features of vertical flow between hydrostratigraphic units as they can be derived from point-water hydraulic head cross-sections; whenever possible, this flow is substantiated by pressure head versus depth plots.

Vertical Flow in the Paleozoic

On the dip cross-section in figure 42A, flow is potentially downward from the Beaverhill Lake aquifer system through the Winnipegosis aquifer system, to the Cambrian aquifer system, except to the northeast of Tp 66 R 2, W4Mer where there is effective hydraulic continuity between the two lower systems. As illustrated in figure 26, the intervening Lower Devonian aquiclude system becomes thinner in this northeast portion of the study area. Before continuity is completely achieved, flow is potentially upward from the Cambrian aquifer system to the Winnipegosis aquifer system through the rapidly decreasing thickness of the

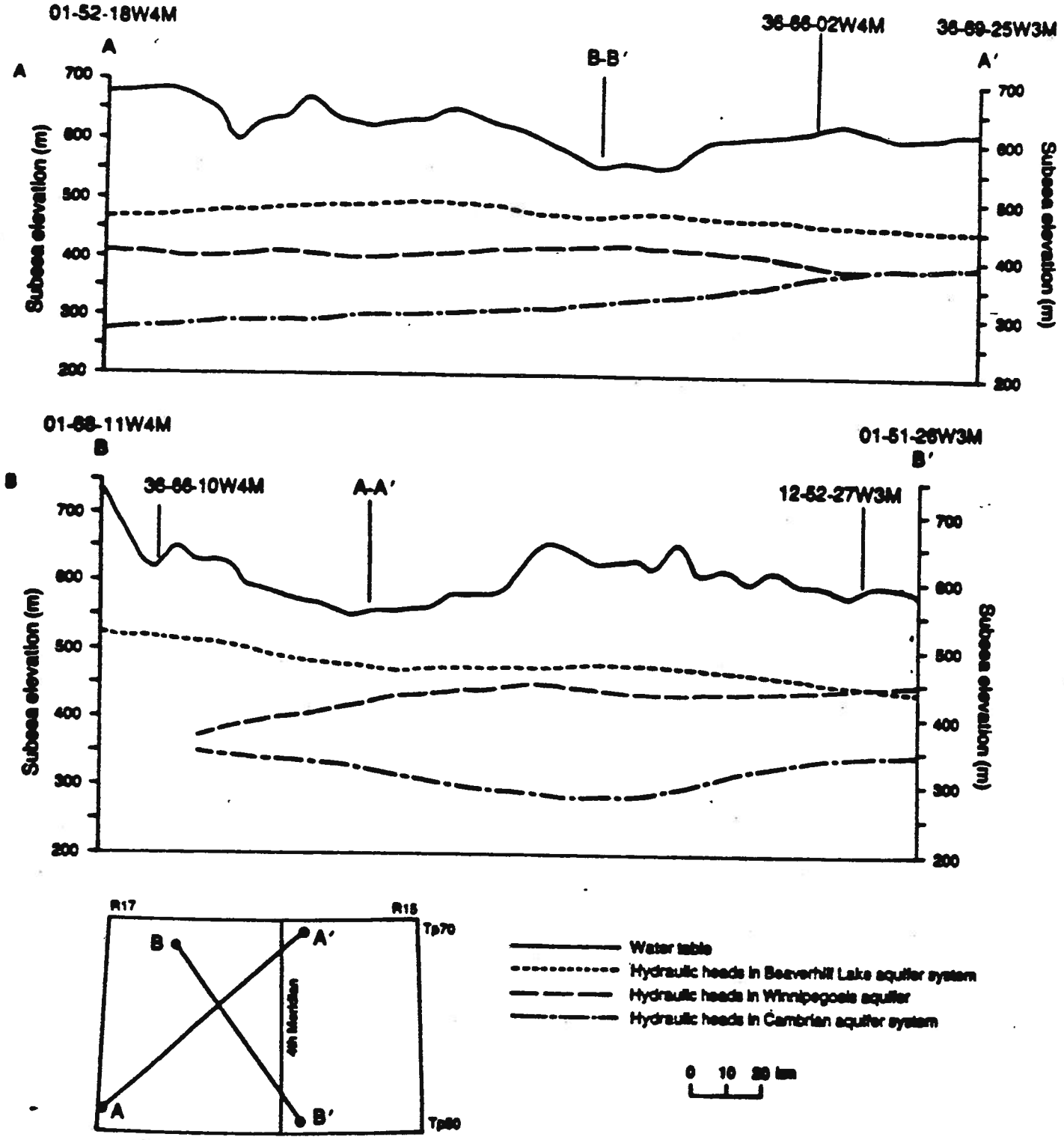

Figure 42. A. Dip hydraulic head cross-section showing potential cross-formational flow between the Paleozoic aquifers; B. Strike hydraulic head cross-section showing potential cross-formational flow between the Paleozoic aquifers

intervening aquiclude system. On the strike cross-section of figure 42B, a similar merging of the point-water hydraulic head profiles occurs northwest of Tp 66 R 10 W4Mer between the Winnipegosis aquifer system and the Cambrian aquifer system, but here the two aquifer systems are separated by about 250 m of the Lower Devonian aquiclude system and the vertical exchange is likely to be minimal. Figure 43 illustrates general downward flow conditions within the Beaverhill Lake aquifer system.

Vertical Flow Between Paleozoic and Lower Cretaceous

In the southwest part of the Cold Lake study area, figure 44A suggests a potential upward flow between the Beaverhill Lake aquifer system and the Camrose aquifer through the Ireton aquitard. Beyond the eastern limit of this aquitard, the hydraulic heads of the McMurray aquifer and the Beaverhill Lake aquifer system are effectively the same, indicating vertical continuity.

Figure 44B shows the same feature of vertical hydraulic continuity for the southeast (south of Tp 60 R 5 W4 Mer) where the Ireton aquitard is very thin or absent. In the northwest part of the study area the flow changes from McMurray to Grosmont, to Grosmont to McMurray at Tp 68 R 16 W4 Mer.

Figure 44C is a NNE-SSW cross-section in the western part of the Cold Lake study area; it shows good potential continuity between the Camrose and McMurray aquifers in the southwest. The flow is potentially upward from the Beaverhill Lake aquifer system to the Grosmont, McMurray and Clearwater aquifers. In the northwest, flow is potentially downward

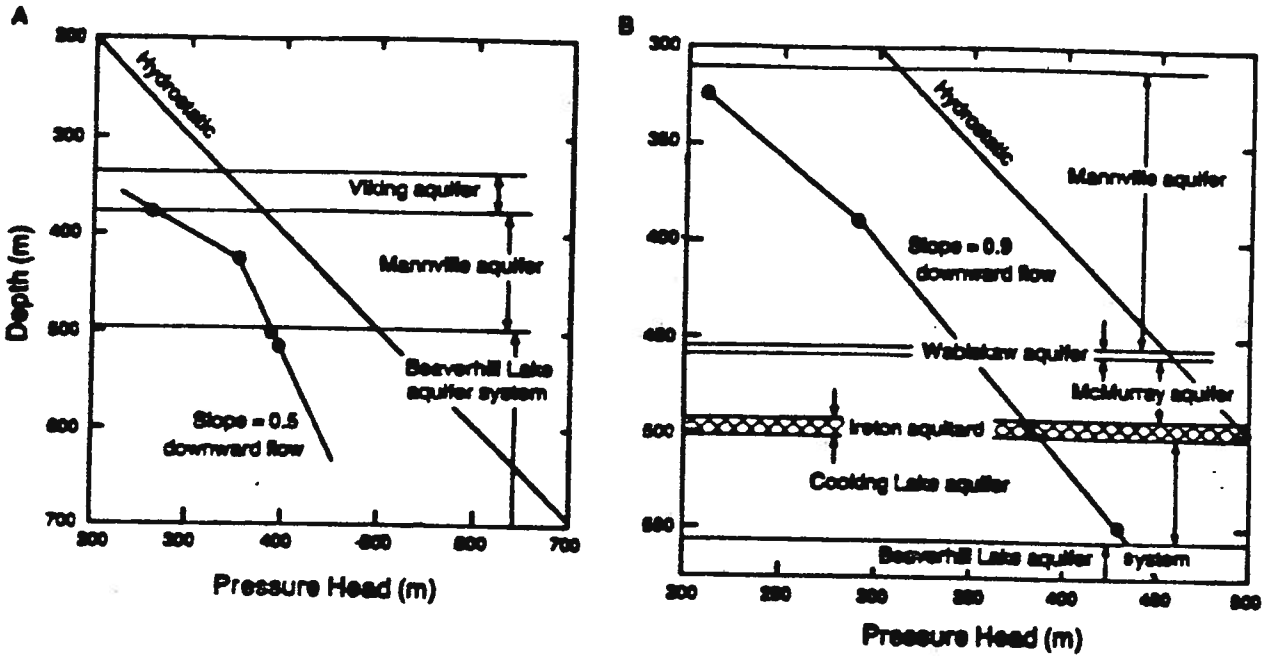

Figure 43. Pressure head/depth plots illustrating hydraulic continuity between the Lower Cretaceous and Paleozoic aquifers. A. at location 06-14-55-02 W4 Mer; B. at location 10-34-61-08 W4 Mer

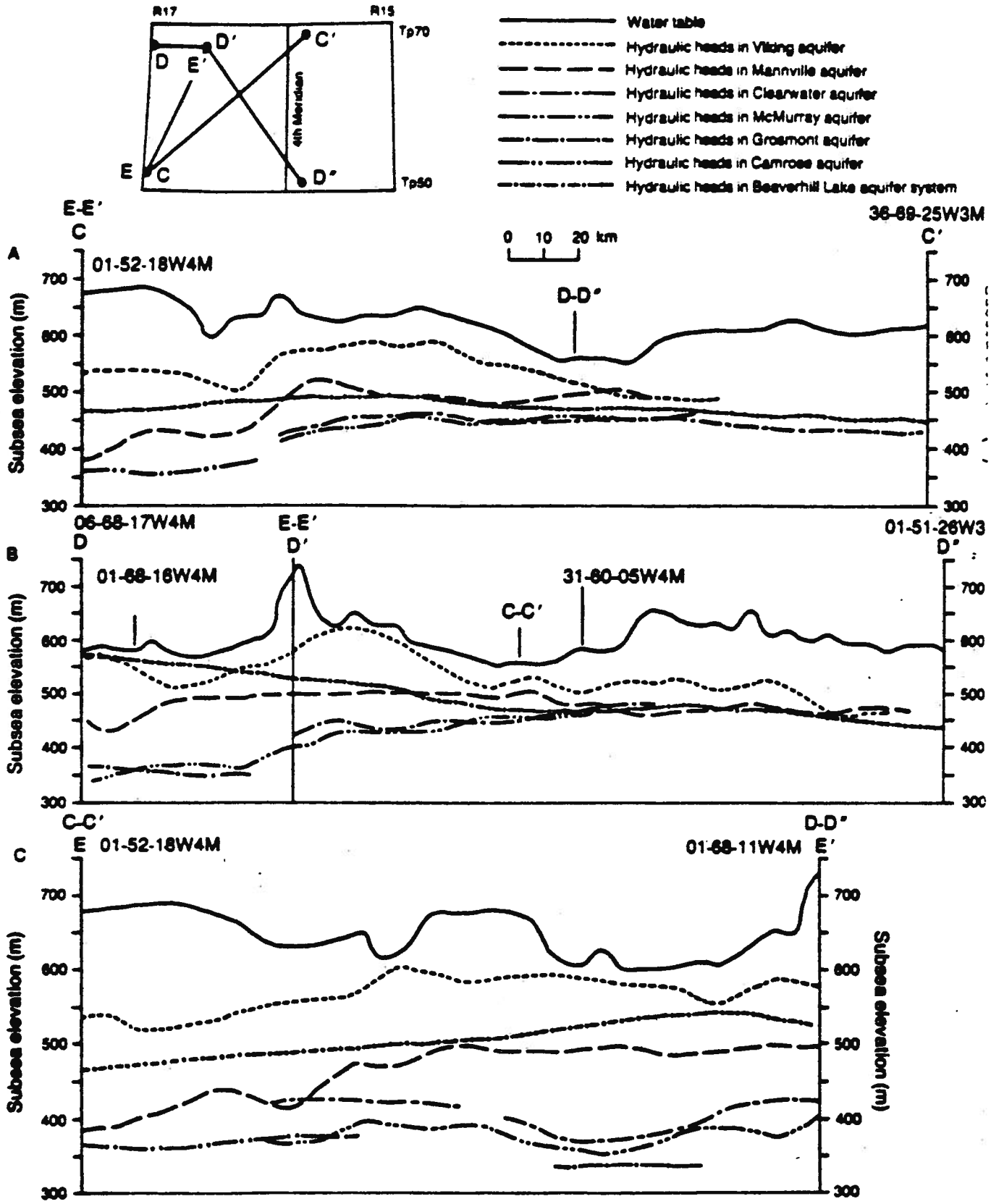

Figure 44. General hydraulic head cross-sections showing potential cross-formational flow between the aquifers located above the Prairie aquiclude. A. Dip; B. Strike; C. Northeast-southwest in the western part of the study area

from the McMurray aquifer to the Grosmont aquifer.

These basic features of the vertical flow conditions between the Paleozoic and the Lower Cretaceous are also present on the east-west cross-sections of figure 45. Figure 45A shows that the potentially upward flow from the Beaverhill Lake aquifer system to the McMurray and Mannville aquifers becomes virtual hydraulic continuity east of Tp 64 R 6 W4 Mer. Complete continuity, however, is only observed about 70 km further to the east (east of Tp 63 R 23 W3 Mer). Figure 45A also shows that the reversal of vertical flow direction between the Grosmont and the McMurray aquifers occurs at Tp 66 R 16 W4 Mer in the western part of the study area.

On figure 45B, virtual hydraulic continuity of the Beaverhill Lake aquifer system with the McMurray aquifer is already present at Tp 60 R 7 W4 Mer but complete continuity is only established about 50 km to the east (Tp 60 R 3 W4 Mer). Also, in the west-central part of the study area, the vertical flow is potentially upward from the Camrose Tongue aquifer to the McMurray aquifer. Further south (figure 45C) there is virtually no positive hydraulic head difference between the Camrose Tongue aquifer and the McMurray aquifer. The head profile of the Beaverhill Lake aquifer system and that of the Mannville aquifer are very close over most of the cross-section.

Vertical Flow Within the Cretaceous

As illustrated on figures 44 and 45, vertical flow is essentially downward from the Viking aquifer to the Mannville aquifer (with a good separation suggesting a "strong" Joli Fou aquitard) and downward again

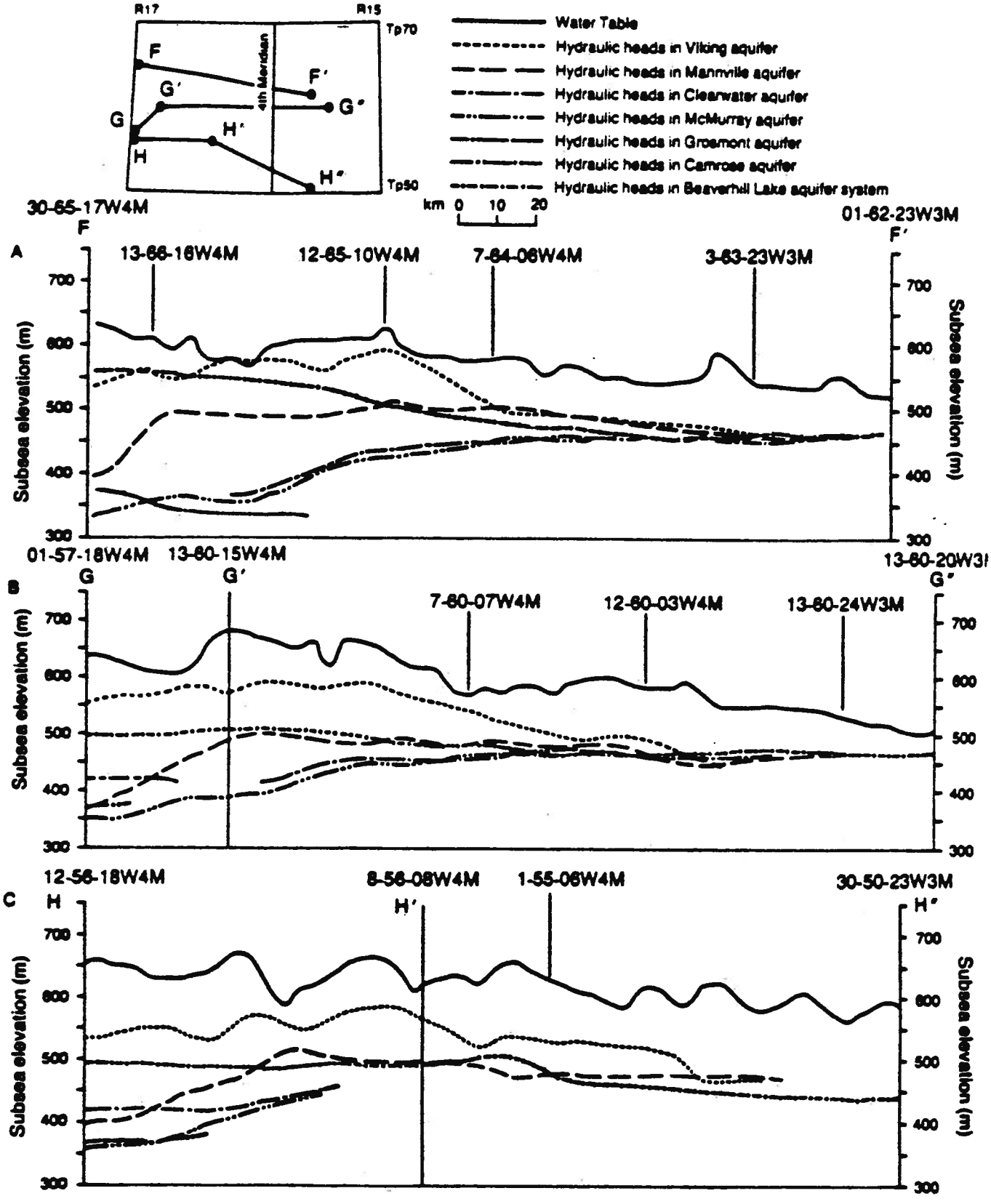

Figure 45. Hydraulic head cross-sections across the three model areas.
A. Northern; B. Central; C. Southern

from the Mannville aquifer to the Clearwater and McMurray aquifers which are hardly separated.

The topographically-controlled flow in the Viking aquifer is clear on most of the cross-sections as long as a horizontal deflection varying between 10-20 km is accepted in the analysis. Features that were not apparent in the potentiometric surface map of the Mannville aquifer show that the flow in this aquifer would be best defined as "transitional" between the intermediate flow regime of the Clearwater and McMurray aquifers and the local flow regime of the Viking aquifer.

The vertical flow within the Cretaceous aquifers is illustrated by the plots on figure 46; the conditions are hydrostatic on figure 46A between the Mannville and the McMurray aquifers. Flow is downward at the location of figure 46B and 46C and on both figures, the deflections between the Viking and Mannville aquifers are marked. Figures 46D and 46E suggest, on the contrary, that the conditions are quasi-hydrostatic between these two aquifers and that the break occurs further down at the level of the Clearwater Formation; note that these two plots are both located in the western part of the study area.

Figure 47 shows the distribution of the seven oil sands layers in the Cold Lake oil sands deposit, numbered sequentially downhole. McMurray Formation layer 1 (figure 47A) is also known as the Dina Member and has a rather spotty distribution. McMurray Formation layer 2 (figure 47B) occurs as sands trapped against topographic highs on the pre-Cretaceous erosion surface; it is also known as the Cummings Member and has an average thickness of less than 15 m. The oil sands in the Clearwater Formation (figure 47C) are confined to the northern half of the Cold Lake oil sands deposit and contain most of the bitumen; they

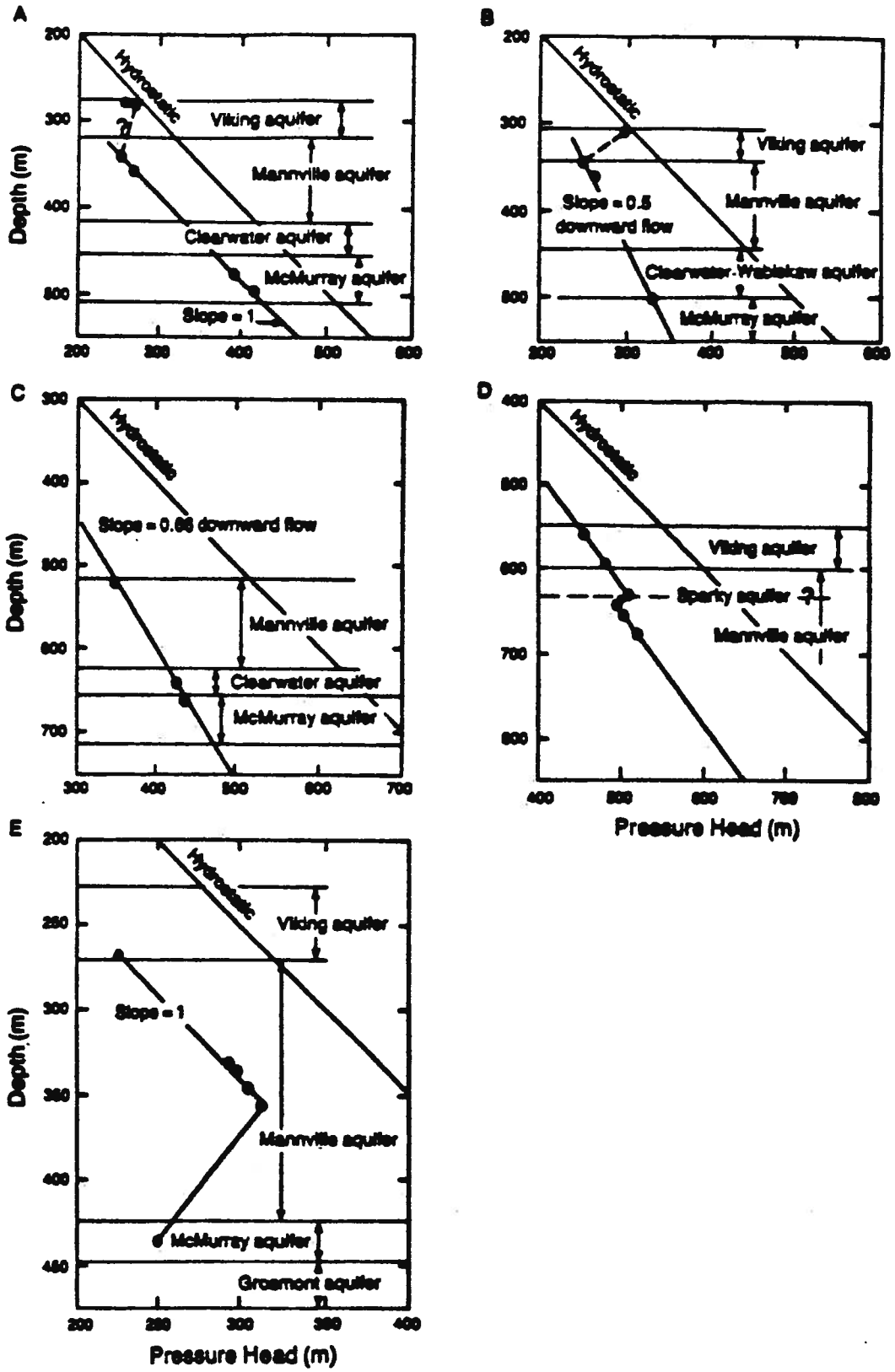

Figure 46. Pressure head/depth plots illustrating cross-formational flow between the Lower Cretaceous aquifers. A. at well location 10-20-60-07 W4 Mer; B. at well location 01-31-64-08 W4 Mer; C. at well location 10-36-56-10 W4 Mer; D. at well location 10-12-53-12 W4 Mer; E. at well location 11-10-67-14 W4 Mer

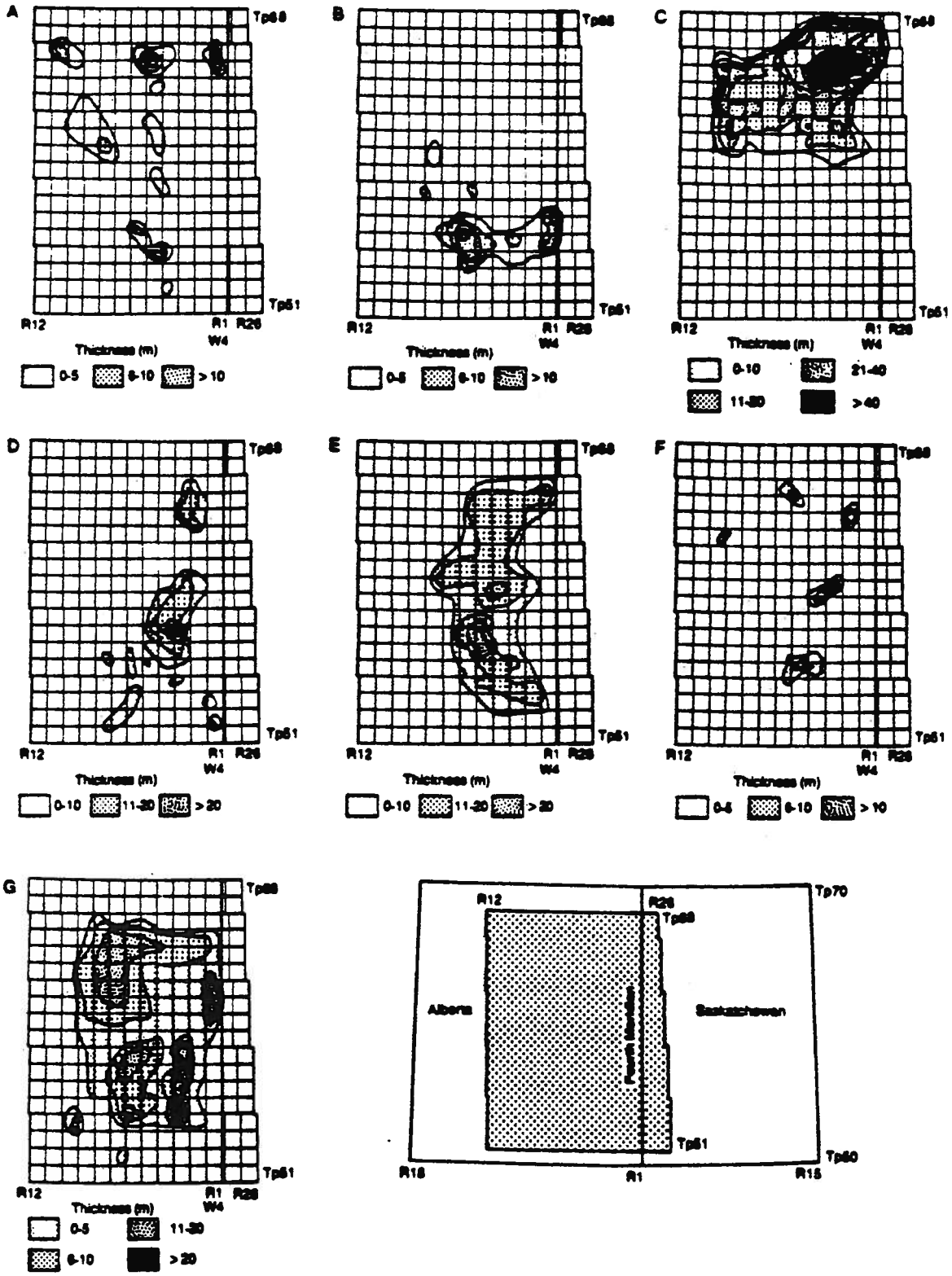

Figure 47. Isopachs of oil sands deposits. A. McMurray Formation, layer 1; B. McMurray Formation, layer 2; C. Clearwater Formation; D. Lower Grand Rapids Formation, layer 2; E. Lower Grand Rapids Formation, layer 1; F. Upper Grand Rapids Formation, layer 2; G. Upper Grand Rapids Formation, layer 1

are continuous, homogeneous, and attain a thickness greater than 40 m. Oil sands in the lower Grand Rapids Formation comprise two distinct layers; layer 1 averages 15 m thick (figure 47E) and layer 2 less than 10 m thick with a rather spotty distribution (figure 47D). The upper Grand Rapids Formation also contains two oil sands layers, the lower being thin and discontinuous (figure 47F), and the upper layer widespread, generally thin, but ranging in thickness up to more than 20 m in places (figure 47G).

In an attempt to elucidate the vertical flow conditions in the aquifers of the Mannville Group, the data of pressure heads have been allocated to the 20 possible layers that exist in the oil sands area (Tp 53-66, R 1-11, W4 Mer) between the top of the Mannville and Pre-Cretaceous unconformity. No data were found to belong to the Clearwater oil sands and intermediate aquifers and only very few in the McMurray oil sands and intermediate aquifers. Thus, most of the data considered are within the upper portion of the sequence (upper and lower Grand Rapids oil sands and intermediate aquifers). The general plots of figures 48A and 48B illustrate how the majority of these data belong to a single population with no major aquitard break caused by the oil sand layers. A general downward flow trend is evidenced by a mean regression line of slope 0.75; the data points fall within a 50 m confidence interval on each side of this line. This is interpreted as flow in a single aquifer system and implies at least lateral bypasses of the oil sand layers which act as aquitards. The hydraulic conductivity of the oil sand layers is about 9×10^{-6} m/d (Agar, 1985). The "strength" of these aquitards are illustrated by the local pressure head-depth plots of figure 48C (no deflections), and 48D and 48E (positive deflections).

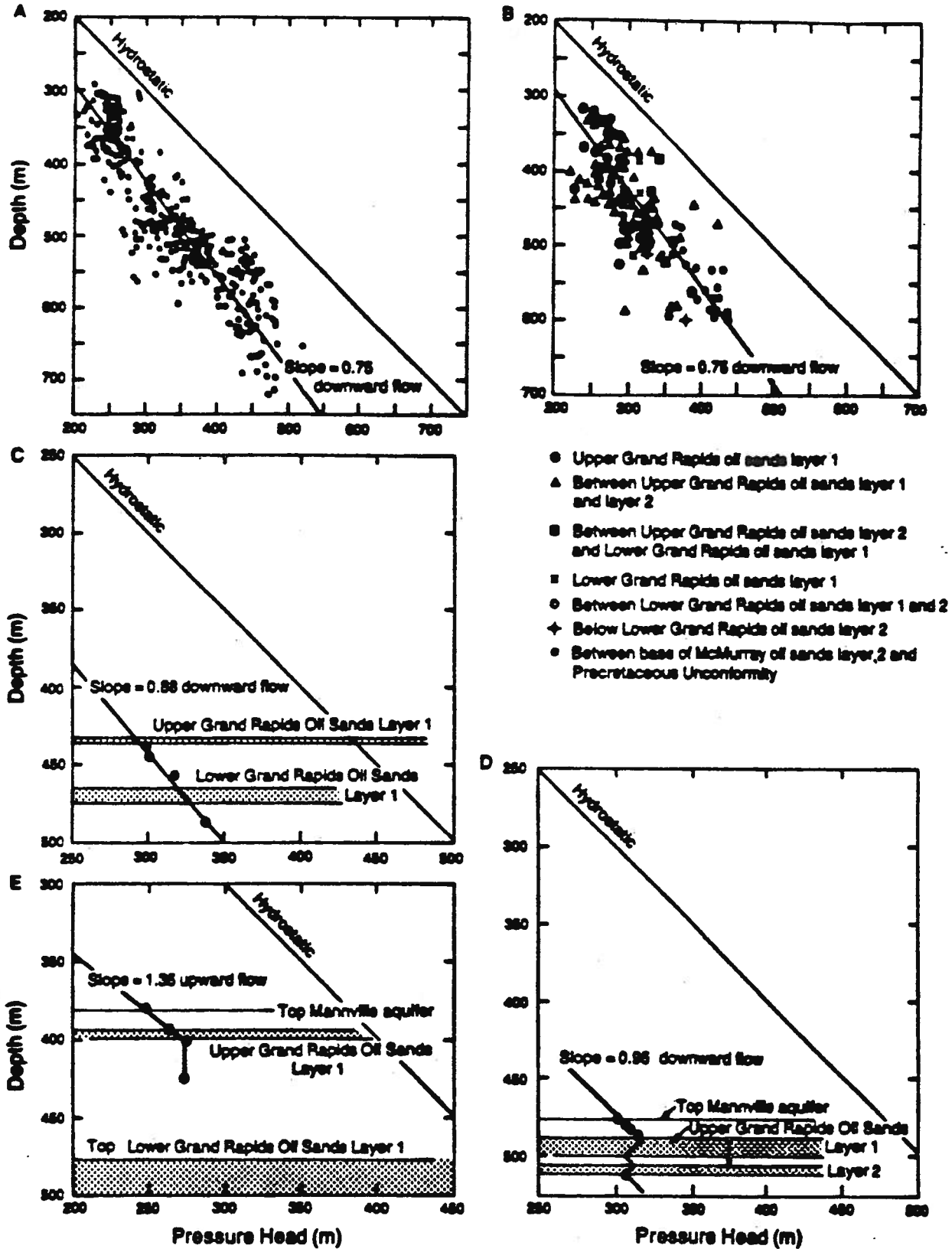

Figure 48. Pressure head/depth plots illustrating cross-formational flow in the Mannville Group within the area of the oil sands deposits (Tp 53-66, R 1-11, W4 Mer). A. Regional between the top of the Mannville and the top of the Upper Grand Rapids oil sands, layer 1; B. Regional between the top of the Upper Grand Rapids oil sands, layer 1, and the Pre-Cretaceous unconformity; C. at well location 11-36-54-04 W4 Mer; D. at well location 11-35-55-06 W4 Mer; E. at well location 11-21-60-08 W4 Mer

From this preliminary analysis of the Mannville aquifer, two partial conclusions can be drawn: (1) the oil sand layers may act as intermediate to weak aquitards; (2) the flow in the overall Mannville Group probably laterally bypasses these aquitards and thus they cannot be regarded as sufficiently strong confining layers for deep well injection.

The vertical flow in the Colorado aquitard system is mostly downward as attested by a few values of hydraulic head determined for various aquifers within it.

CONCLUSIONS

The regional analysis of the natural flow regime in the sedimentary rocks of the Cold Lake study area has used all the possible information for the Paleozoic units and selected information only for Cretaceous strata. The hydrostratigraphic units have been grouped into aquifer (and aquitard) systems based on prevailing flow and hydrochemical conditions; these systems are expected to respond to injection stress in a homogeneous fashion. For this refined definition of the hydrostratigraphy, recommended hydraulic parameters are presented in table 6. The values in this table have been selected using a qualitative judgement about the regional representativeness of the core plug and drillstem test results based on the tables of Appendix B; also, preference has been given to drillstem test results whenever possible (see Appendix A). For the hydraulic conductivities, "low side" and "high side" values are based on harmonic and arithmetic regional averages of the point values, while the best estimate (or optimal)

Table 6. Recommended hydraulic parameters (regional estimates)

Aquifer (System)	Hydraulic Conductivity K(m/d)			Anisotropy	Specific Storage Ss(m^{-1})		
	Low K	Opt. K	High K	Kh/Kv	Low Ss	Opt. Ss	High Ss
Post-Viking	-	-	-	-	0.003000	0.00470	0.00690
Viking	0.000200	0.035	1.300	-	0.000300	0.00400	0.00680
Mannville	0.000130	0.035	2.400	90.0	0.001100	0.00500	0.00850
Clearwater	0.000380	0.037	4.200	200.0	0.000140	0.00080	0.00110
McMurray	0.000920	0.027	9.900	120.0	0.000360	0.00800	0.01200
Grosmont	0.001200	0.017	8.300	10.0	0.000095	0.00055	0.00140
Camrose Tongue	0.003400	0.022	2.100	40.0	0.000100	0.00044	0.00089
Beaverhill Lake	0.000060	0.003	0.077	0.5	0.000012	0.00040	0.00150
Winnipegosis	0.000063	0.011	0.210	0.8	0.000019	0.00065	0.00600
Basal Red Beds	0.000500	0.011	0.038	110.0	0.000012	0.00020	0.00044
Cambrian	0.002000	0.043	0.170	80.0	0.000017	0.00028	0.00053

(*) from consideration of the drillstem test and core plut results in Appendix B

Opt. represents the best (or optimal) regional estimate for K or Ss
Kh is the horizontal hydraulic conductivity (essentially the recommended K of this table)
Kv is the vertical hydraulic conductivity from core plug data

values are from the geometric (or "median") regional averages. For the specific storages, "low-side" and "high-side" values are from the minimum and maximum values of porosity obtained from the core plug determinations; the best estimate is based on the arithmetic average of the point values. Regional values of vertical anisotropy presented in table 6 indicate quasi-isotropic conditions in the carbonate aquifers and a range between 80 to 200 for the sandstone aquifers.

Lateral flow is dominantly regional to the northeast in the Paleozoic aquifer systems with minor eastward and northwestward components caused by specific boundary conditions. In the Upper Devonian aquifer system, however, the major component of lateral flow is to the north, with a minor eastward component. Lateral flow in the McMurray and Clearwater aquifers is of intermediate type to the west and northwest following a drain effect by the underlying Upper Devonian system. Flow in the Mannville aquifer is indeterminate, being between intermediate and local. Lateral flow in the Viking aquifer is topographically-controlled, that is, it is of local type.

The trend of vertical flow is normally downward between the Beaverhill Lake and Lower Paleozoic aquifer systems. Hydraulic continuity may exist between the three Paleozoic aquifer systems (Beaverhill Lake, Winnipegosis and Lower Paleozoic) for a critical area to the east of the Cold Lake study area where intervening aquicludes are absent; in fact, upward hydraulic connection is possible up to the top of the Mannville aquifer in this critical area. In the west of the study area, hydraulic continuity is practically established between the McMurray and Clearwater aquifers and the Upper Devonian aquifer system. In the east of the study area, where the Ireton aquitard is either thin

or missing, hydraulic continuity of the Beaverhill Lake aquifer system exists with the overlying Mannville aquifer. Elsewhere, flow is potentially upward from the Beaverhill Lake aquifer system through the Ireton aquitard. The Joli Fou aquitard that separates the Viking aquifer from the Mannville aquifer represents a strong separation for the flow between these units, potentially downward. The oil sands deposits and the Clearwater shales are weak aquitards; the oil sands deposits are bypassed by flow within the Mannville aquifer. Vertical flow in the Colorado aquitard system is essentially downward.

NUMERICAL SIMULATION OF REGIONAL EFFECTS OF INJECTION

Stefan Bachu

MATHEMATICAL AND NUMERICAL MODELLING

The use of aquifers is increasing as both a source of water supply and a medium for storing various aqueous wastes. Due to the complexity of stratigraphic geometry and the variability of properties of the fluid and solid matrix in the subsurface environment, there are few analytical solutions to problems of flow in porous media. Numerical modelling of fluid flow in aquifers is a technique that can aid in studying and understanding subsurface flow systems.

The objective of mathematical modelling and numerical simulation of formation water flow and fluid injection in the Cold Lake study area is to provide a predictive tool for determining the effects in terms of pressure build-up of deep waste injection on the natural hydrogeological regime in the region. The modelling process was carried out in two stages. The natural conditions that existed prior to any injection were modelled in the first stage. In the second stage it was determined how the hydrogeological system reacted to, and was modified by, the volumes of waste injected. Therefore, the first step of the present investigation was to calibrate a numerical model for simulation of steady-state natural flow of formation waters within the complex hydrogeological system in the Cold Lake study area. After the calibration of the model, the system was perturbed by injecting fluids at specified rates. For a given hydrostratigraphic configuration, the sensitivity analysis of the system response for different values of

hydraulic properties indicated the effects of injection in the various aquifers in the succession.

The mathematical model for fluid flow in porous media consists of a set of partial differential equations together with appropriate boundary and initial conditions that express conservation of fluid mass and momentum over the region of interest.

The unsteady saturated flow in nonhomogeneous porous media of a slightly compressible fluid is described by the following partial differential continuity equation (Bear, 1972, p. 204-206):

$$\mathrm{div}(\rho\bar{q}) + S_s^*(\partial p/\partial t) = 0 \qquad (1)$$

where ρ is fluid density, p is pressure, $\bar{q}$ is the specific discharge vector, S_s^* is specific storativity related to pressure changes, and t is time. The specific discharge $\bar{q}$ is given by Darcy's law (momentum equation):

$$\bar{q} = -(\bar{\bar{k}}/\mu)[\mathrm{grad}(p) + \rho\bar{g}] \qquad (2)$$

where $\bar{\bar{k}}$ is the permeability tensor, μ is dynamic viscosity, and $\bar{g}$ is the gravity vector.

For a homogeneous fluid of constant density, ρ_o, a flow potential can be defined, and equations 1 and 2 can be written in terms of the hydraulic head H:

$$H = p/(\rho_o g) + z \qquad (3)$$

where z is the elevation above a reference datum. By combining

equations 1 and 2 and relation 3, and taking into account fluid sources/sinks (injection/pumping) in the area, the following single partial differential equation can be written:

$$\mathrm{div}[\bar{\bar{K}}\,\mathrm{grad}(H)] - Q = S_s(\partial H/\partial t) \qquad (4)$$

where $\bar{\bar{K}}$ is the hydraulic conductivity tensor, S_s is specific storage and Q is the strength of sources/sinks.

In the Cold Lake study area, equation 4 is not exactly applicable for the aquifers and aquitards in the Phanerozoic succession because the density of the formation waters is not constant, varying within the same hydrostratigraphic system and from one system to another. For a variable density fluid, equation 2 can be written as:

$$\bar{q} = -(\bar{\bar{k}}\rho_o g/\mu)[\mathrm{grad}(H) + (\Delta\rho/\rho_o)\mathrm{grad}(z)] \qquad (5)$$

where $\Delta\rho$ is the density variation with respect to the reference density ρ_o.

The above equation shows that the fluid flow is driven by two forces, one external and one internal. The external force is due to piezometric head differences that originate usually from the topographic relief. The internal force is the buoyancy caused by density differences within the fluid. In order to solve equations 1 and 2 for a variable density liquid, more partial differential equations have to be added to the system, equations which express the conservation of other quantities that influence the fluid density. These equations, such as conservation of energy and/or solute, are coupled with the continuity and momentum equations through the convective terms in the former equations, and through the equation of state linking the fluid density

to such variables as temperature and/or solute concentration. At this stage, the solution to the problem increases in size by the number of added variables, and in complexity due to the coupling of partial differential equations. In many cases, such problems are difficult, if not impossible, to solve. Moreover, the increase in the size and complexity of many problems is unwarranted. In such cases, the buoyancy term in equation 5 is neglected, assuming that the fluid flow is defined by the equivalent freshwater hydraulic head H.

Equivalent freshwater head at a given point within an aquifer is defined as the water-level elevation in a well filled with freshwater to a level high enough to balance the existing fluid pressure at the given point. In other words, equivalent freshwater head is a mechanism for normalizing water-level measurements and direct pressure measurements relative to a constant freshwater density so that they are related to fluid pressures in the aquifer in a consistent manner. Analysis of equation 5 shows that strictly horizontal flow in a horizontal aquifer saturated with a variable density fluid is driven by gradients of equivalent freshwater head. Density-related gravity effects are important only in the vertical direction. Use of an equivalent freshwater head rather than fluid pressure is discussed by Lusczynki (1961), De Wiest (1965), Bear (1972) and Frind (1980). This approach has the advantage that the fluid flow equation is expressed in terms of driving forces exclusive of static fluid pressure.

In practice, an aquifer is usually considered approximately horizontal if its dip does not exceed a few degrees. If the fluid density is variable, the assumption commonly made is that the fluid flow is nearly horizontal and that buoyancy effects are very small and,

therefore, negligible. As a result, equivalent freshwater heads effectively characterize the system. Davies (1987) has shown that it is not the absolute magnitude of the density-related error term, but rather the relative magnitude of this term versus the magnitude of the equivalent freshwater-head term that determines whether density-related gravity effects will be significant in a given situation. A useful measure of the relative importance of density-related gravity effects is the dimensionless ratio of the magnitude of the equivalent freshwater-head term, which is a ratio defined also by Bear (1972, p. 654). Davies (1987) calls this relative strength of the two driving forces as DFR (Driving-Force Ratio), defined by:

$$DFR = (\Delta\rho|\text{grad}(Z)|)/(\rho_o|\text{grad}(H)|) \qquad (6)$$

where $|\text{grad}(Z)|$ is the magnitude of the elevation gradient, and $|\text{grad}(H)|$ is the magnitude of the freshwater hydraulic gradient. Through numerical experiments, Davies (1987) has shown that, assuming an isotropic medium, the value DFR=0.5 is the approximate threshold at which buoyancy-related gravity effects may become significant. This threshold may vary slightly depending on the actual flow conditions, and on the scale and accuracy required for a particular study. The errors introduced by the use of equivalent freshwater hydraulic heads refer to both the magnitude and the direction of the specific discharge vector.

The aquifer systems in the Phanerozoic section in the Cold Lake study area are not horizontal. The general dip is from northeast to southwest, with Paleozoic strata having a more pronounced dip than Cretaceous strata. The density of formation waters is variable, as

shown in the previous section. Therefore, some buoyancy-related effects must be present in the flow. In order to assess the importance of these effects, the DFR was computed at a regional scale for selected aquifers in the injection area. The results are presented in table 7.

The elevation and hydraulic gradients were computed from the monoclines approximating the respective aquifer top and freshwater potentiometric surfaces. The elevation gradient for an aquifer was taken as the average between the gradients of the upper and lower bounding surfaces of that aquifer. For the Mannville, Clearwater and McMurray aquifers, the elevation gradient was considered the same as for the whole Mannville Group. Generally, the coefficients of correlation of the monoclines approximating the top and potentiometric surfaces are quite high, except for the Mannville and Viking aquifer systems. The average density was computed for each aquifer system only over an area around the injection sites (generally Tp 52-60, R 1-10, W4 Mer). The elevation gradient is not available for the Viking aquifer, but one can use the same value as for the Mannville Group as a first approximation.

It can be seen from table 7 that the DFR for the Cretaceous aquifer systems is below the threshold as defined by Davies (1987). Also for the Beaverhill Lake aquifer system, with a value of DFR=0.42, the freshwater hydraulic head approximation is acceptable. The situation becomes critical in the case of the Basal Cambrian aquifer, with a value of DFR=1.31. However, given the aquifer anisotropy (K_H/K_V=80), it is assumed that the vertical flow due to buoyancy effects is really negligible, and that the fluid flow in this aquifer is essentially horizontal. In this case, the freshwater hydraulic head approximation still applies. The above values of the DFR were computed at a regional

Table 7. Values of the Driving Force Ratio (DFR) for selected aquifers in the Cold Lake study area around deep waste disposal sites

Aquifer system	$\|grad(Z)\|$	$\|grad(H)\|$	$\rho_{(kg/m^3)}$	DFR
Viking	n.a.	1.42×10^{-4}	1002.9	-
Mannville	15.25×10^{-4}	1.29×10^{-4}	1006.8	0.08
Clearwater	15.25×10^{-4}	3.91×10^{-4}	1004.8	0.02
McMurray	15.25×10^{-4}	5.69×10^{-4}	1006.2	0.02
Beaverhill Lake	24.90×10^{-4}	1.98×10^{-4}	1003.6	0.42
Basal Cambrian	43.30×10^{-4}	5.30×10^{-4}	1160.2	1.31

scale. It could happen, in some places, that the local values of DFR exceed the threshold value, due to local variations in the elevation gradient (subsurface topography) or in the hydraulic gradient. Still, it is believed that for the purpose of this study, the equivalent freshwater head approximation is valid for the following two reasons: (1) it is valid at a regional scale; and (2) at the injection sites, on a local scale, the external driving force will increase due to injection, diminishing the influence of the internal buoyancy force. Under the assumption of the validity of using equivalent freshwater hydraulic heads, the fluid flow in the hydrostratigraphic sequence in the Cold Lake study area is described by equation 4.

In order to obtain a solution to equation 4, additional information about the boundary and initial conditions is required. Mathematically, the boundary conditions include the geometry of the boundary and values of prescribed heads and/or prescribed fluxes. For the study of transient phenomena during injection it is necessary to know the initial conditions as well, that is, the initial distribution of hydraulic heads everywhere in the domain.

In the case of the Cold Lake study area, it is not possible to obtain an analytical solution due to the complexity of the three-dimensional hydrostratigraphic structure, and the variability of the parameters and the boundary conditions. In order to solve equation 4, it is necessary to obtain a numerical solution, provided by a numerical model.

For the purpose of this study, the model FE3DGW (Finite Element 3-Dimensional GroundWater) was selected for the numerical simulation of the flow. This model was developed by Pacific Northwest Laboratory

(U.S.A.), and the complete description of the numerical formulation and of the pertinent software is given in Gupta et al. (1984a, 1984b). The latest version of the model was received in September 1986 by the Basin Analysis Group, Alberta Geological Survey, Alberta Research Council, from Battelle Memorial Institute, Ohio, and was implemented on the Research Council's computer system (VAX/VMS). The pre- and post-processors of the model, developed previously, had to be updated as well. The pre-processor automatically prepares the input data for the model FE3DGW, based on synthesized information resulting from the analysis of the natural flow regime. The post-processor transforms the distribution of hydraulic heads at all nodes in the three-dimensional finite-element grid into areal distributions in regular grids of the potentiometric surface for each hydrostratigraphic system. It also compares (numerically and graphically) the computed hydraulic heads at finite element nodes with initial values obtained by interpolation in the regular grids of potentiometric surfaces.

The purpose of the post-processing is twofold: (1) to compare observed with computed hydraulic heads during the process of model validation/calibration; and (2) to compare initial hydraulic heads with values at any time step during the prediction phase.

In assessing the results during the calibration phase, one has to take into account the approximations and assumptions made at each step in each of the data processing procedures and in the numerical simulation. A first approximation is made when values at nodes in a regular grid are obtained out of an irregular distribution of real (measured) values. The regular grid distribution depends, among many factors, on its resolution, the initial data size and sample

distribution, the gridding method, the parameters and constraints of the method itself, and the interpolation and extrapolation procedures. In the graphical representation of the regular grids as contour maps there are approximations and differences depending on the grid resolution and on the interpolation method. In the mathematical modelling there are basic assumptions about the flow (e.g., homogeneous single phase and/or single component fluid and isothermal flow), the porous matrix (e.g., isotropic) and the boundary conditions. In the numerical simulation there are assumptions (e.g., in this study, considering a constant hydraulic conductivity for each layer) and approximations inherent to the discretization process, as well as to the method (finite element or finite difference). In addition, there are approximations in the gridding and contouring of the computed values at the nodes in the finite element grid, for comparison with the initial potentiometric surface maps. As a result, one cannot expect a complete match between observed and computed data.

The grid resolution is also very important in using and interpreting the results. The hydraulic head values obtained at a node representing an injection site are <u>not</u> the actual values at the injection well. They actually represent the values to be found at an equivalent distance (radius) r_e from the well, which depends on the scale of the model, the grid resolution, and the characteristics of the hydrostratigraphic system. In two-dimensional finite differences modelling there are expressions to compute the equivalent radius r_e for a well centred in an isotropic grid block of dimensions Δx and Δy (Peaceman, 1983):

$$r_e = 0.140(\Delta x^2+\Delta y^2)^{1/2} \qquad (7)$$

There are also expressions which take into account the horizontal anisotropy of the aquifer. Beljin (1987) has shown that the well radius r_w and the blocksize Δx also have an influence on the nodal correction r_e. Very few attempts have been made to extend these results to multi-aquifer or multi-layered well systems.

In finite element modelling, there are no such expressions to compute the equivalent radius of a node. Charbeneau and Street (1979) used finite element modelling and applied a correction to the hydraulic head around a well, but their method cannot be applied here because they assign the discharge to an element instead of a node. Besides, their correction can be applied to simpler cases only (confined or leaky aquifers). The FE3DGW model used for predictive simulations of effects of injection in the Cold Lake study area is three-dimensional, finite element, multilayered in a very complex structure, and with injection at grid nodes, not at block centres. Therefore, it is impossible to compute an equivalent radius of equivalence r_e using a formula similar to equation 7.

CALIBRATION OF THE NUMERICAL MODEL

Sensitivity Analysis

For modelling purposes it is necessary to define a bounded three-dimensional region with appropriate boundary conditions for fluid flow. Because the present investigation is directed at the feasibility

and effects of deep injection of liquid wastes, the region must be centred approximately around the injection sites and include the prospective injection aquifers and the stratigraphic succession which could be affected. The actual and proposed injection aquifers are in the Mannville Group, Cooking Lake Formation and Basal Cambrian sandstone. Table 8 presents the locations, depths and projected rates of injection between the years 1985 and 2015 at sites in the Cold Lake study area. The information in this table was supplied by the Planning Division of Alberta Environment. Figure 49 shows the location of the injection sites, and schematically their position in the stratigraphic sequence.

In the central region of the Cold Lake study area, around the injection sites, there are six aquifer systems (Basal Cambrian, Winnipegosis, Beaverhill Lake, McMurray, Clearwater and Mannville) separated by two aquiclude systems (Lower Devonian and Prairie) and four aquitards (Basal Red Beds, Ireton, Clearwater and Colorado). The Mannville, Clearwater, McMurray and Beaverhill Lake aquifers are in contact, one way or another, in the area around the injection sites. Therefore, they cannot be treated individually, but must be considered as a single multilayered system. This system is separated from the Basal Cambrian aquifer by a succession comprised of, in descending order, Prairie aquiclude (140-160 m thick), Winnipegosis aquifer system, Lower Devonian aquiclude (up to 300 m thick) and Basal Red Beds aquitard. Based on the thickness and the areal extent of the Prairie and Lower Devonian aquicludes, it was decided to consider the two injection zones separately, assuming that no effects propagate from one zone to another. This assumption was confirmed later by the results of numerical simulations. Therefore, the following two hydrostratigraphic

Table 8. Projected injection rates for the period 1985-2015 at deep well disposal sites in the Cold Lake study area, Alberta

	Operator		Field/Area	Location	Stratigraphic Unit	Depth m below KB (m)	Injection Rate Realistic 1985-1995	Injection Rate High 1995-2005	Injection Rate High 2005-2015
1	Amoco		Lindberg	09-28-55-06-W4	Lloydminster	560	5081	12477	0
2	Bow Valley		Marie Lake	01-14-65-02-W4	McMurray	550	1199	1499	1499
3	BP	80%	Wolf Lake	08-07-66-05-W4	Grand Rapids	430	12887	20530	31530
4	BP	20%	Wolf Lake	10-08-66-05-W4	Cambrian	1325	3335	5132	7883
5	Can. Occidental		Manatokan	10-12-63-08-W4	Cooking Lake	495	1714	9487	8696
6	Can. Occidental		Lindberg	05-18-58-04-W4	Cooking Lake	610	2637	2293	0
7	Can. Worldwide		Muriel Lake	10-16-59-04-W4	Cummings	505	263	2847	0
8	Dome	25%	Lindberg	00-18-55-05-W4	Rex Sand	530	1287	1287	0
9	Dome	25%	Lindberg	00-30-55-05-W4	Rex	550	1287	1287	0
10	Dome	25%	Lindberg	00-10-56-06-W4	Rex Member	565	1287	1287	0
11	Dome	25%	Lindberg	00-10-56-06-W4	Cooking Lake	680	1287	1287	0
12	Dome	55%	Primrose	10-05-67-04-W4	Cambrian	1310	3587	7173	7173
13	Dome	45%	Primrose	10-05-67-04-W4	McMurray	540	2934	5868	5868
14	Drummond		Ardmore	13-20-62-03-W4	Mannville C	405	723	1449	1449
15	Esso	55%	May-Ethel	08-33-64-03-W4	Cambrian	1290	14910	12834	13328
16	Esso	45%	May-Ethel	04-17-65-03-W4	McMurray	520	12197	10501	10905
17	Husky		Tucker Lake	13-20-64-04-W4	McMurray	540	1311	1312	1482
18	Koch		Fort Kent	06-19-61-04-W4	Clearwater	570	1125	1670	1287
19	Mobil		Wolf Lake (2)	06-11-64-06-W4	Clearwater	440	252	6995	6995
20	Murphy	75%	Lindberg	05-13-58-05-W4	Low Grand Rapids	510	1431	2324	1772
21	Murphy	25%	Lindberg	05-13-58-05-W4	Cooking Lake	600	477	775	591
22	Pancanadian		Lindberg	10-09-56-06-W4	Lloydminster	560	602	602	0
23	Suncor	55%	Fort Kent	05-28-61-04-W4	Clearwater	450	923	2211	786
24	Suncor	45%	Fort Kent	00-28-61-04-W4	Cummings	450	755	1809	643
25	Suncor		Primrose	07-14-67-03-W4	Cambrian	?	3521	16354	16354
26	Westmin	75%	Lindberg	11-01-55-05-W4	Lloydminster	530	1809	7602	7617
27	Westmin	25%	Lindberg	03-13-55-06-W4	Cooking Lake	680	609	2534	2539

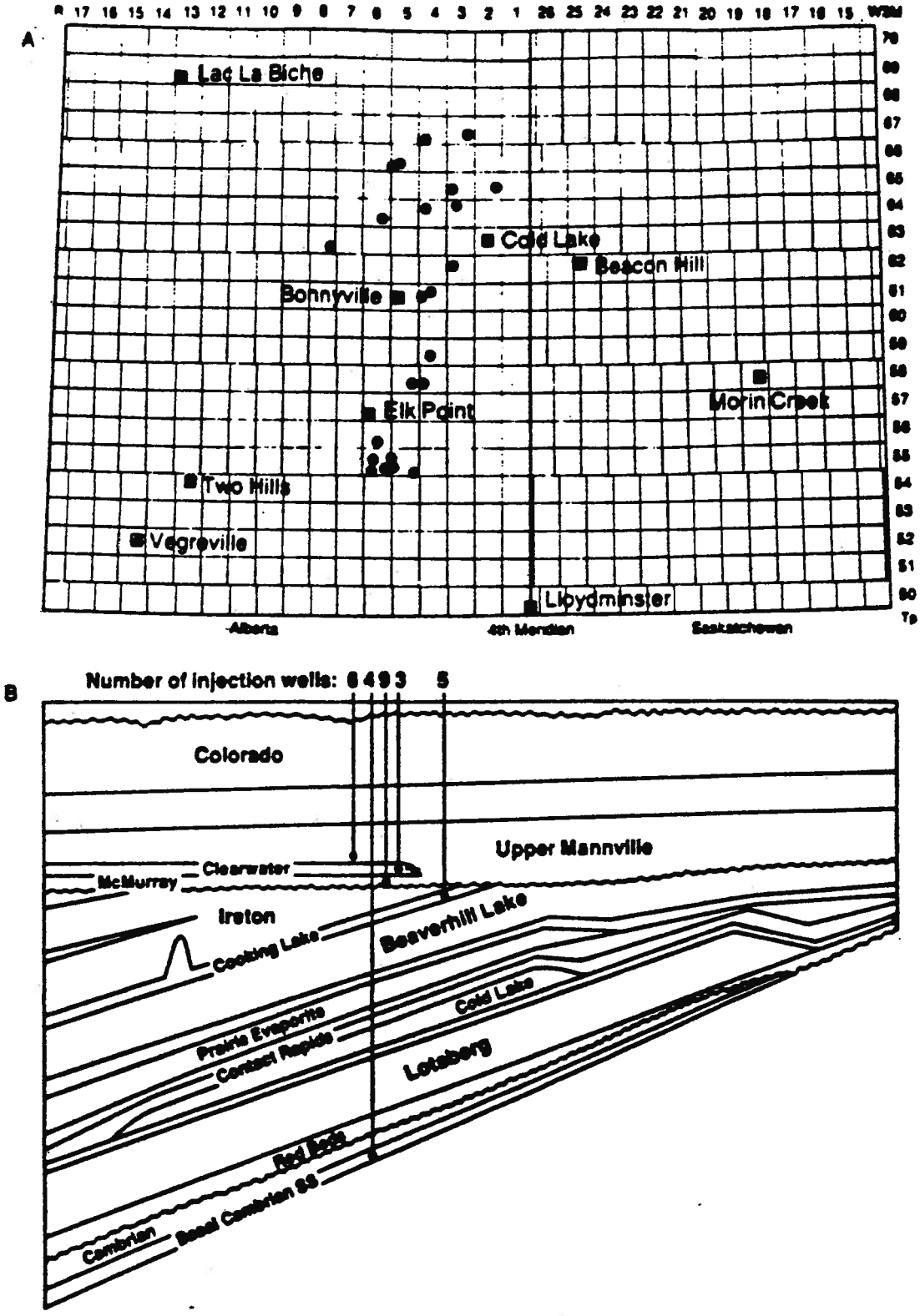

Figure 49. A. Location of injection sites (•) in the Cold Lake study area; B. Schematic representation of the position of injection wells in the stratigraphic sequence

sequences were considered for numerical simulations: (1) the Lower Paleozoic succession between the Precambrian basement (impervious bottom) and the bottom of the Lower Devonian aquiclude (impervious top); and (2) the post-Prairie succession, between the Prairie aquiclude (impervious bottom), and the top of the bedrock (top of Colorado aquitard). A previous study in the Cold Lake area (Basin Analysis Group, 1985) has shown that the Quaternary and Phanerozoic hydrostratigraphic sequences can be separated, due to a strong permeability contrast (about four orders of magnitude) and to the negligible cross-formational flow at the top of the bedrock (about $6x10^{-3}$ mm/a). The separation of the two injection successions is needed for simulation reasons, the available computer resources not being able to handle the number of nodes and elements required to model the entire Phanerozoic succession.

In the Cold Lake study area there are no lateral hydraulic boundaries for the hydrostratigraphic systems below the top of the bedrock. Only geometric boundaries separate different units, with changes in the values of hydraulic parameters. The boundary values of the hydraulic head along lateral boundaries of various model areas were obtained from the potentiometric surfaces defined in the previous section. The hydraulic heads at the top of the bedrock were considered to be those at the water table which, for the purpose of this study, was approximated by the ground surface. The values for the hydraulic parameters needed by the model (hydraulic conductivity and specific storage) used in the simulations are the ones recommended in the previous section (table 6).

Validation, calibration and sensitivity analyses of the numerical

model were done with respect to the potentiometric surfaces, radius of influence, and size of the time step for predictive simulations. A finite element grid comprising 486 surface nodes and 465 surface elements was designed to cover the central region of the Cold Lake study area (figure 50), taking into account all the injection sites and the relevant stratigraphic and hydrostratigraphic boundaries. The grid is denser around the injection sites, and coarser toward the edges. The sensitivity analysis with regard to the size of the time step and the radius of influence was performed for a single layer aquifer, in order to save on computer resources. The Basal Cambrian aquifer was chosen because it is isolated, being practically sandwiched between an aquiclude (Precambrian) and an aquitard (Basal Red Beds) covered by another aquiclude (Lower Devonian). The hydraulic heads along the external contour of the finite elements grid were obtained from the potentiometric surface (figure 23C) and imposed as boundary conditions. The computed potentiometric surface (figure 51) differs from the observed one (figure 23C) by 4.23 percent, with a maximum difference of 7 percent. Given all the assumptions and approximations, this match is considered good.

The new version of the FE3DGW model performs a mass balance for the model area, which shows that the net lateral crossflow through the area is 95 m^3/d, and that the total volume of water in this unit (porosity 0.12) is 182.8 km^3. The low value of the lateral discharge through the area is due to the very low permeability of the aquifer. The only hydraulic parameter in a steady-state fluid flow model is the hydraulic conductivity. The steady-state equation:

$$\mathrm{div}[\bar{K}\,\mathrm{grad}(H)] = 0 \qquad (8)$$

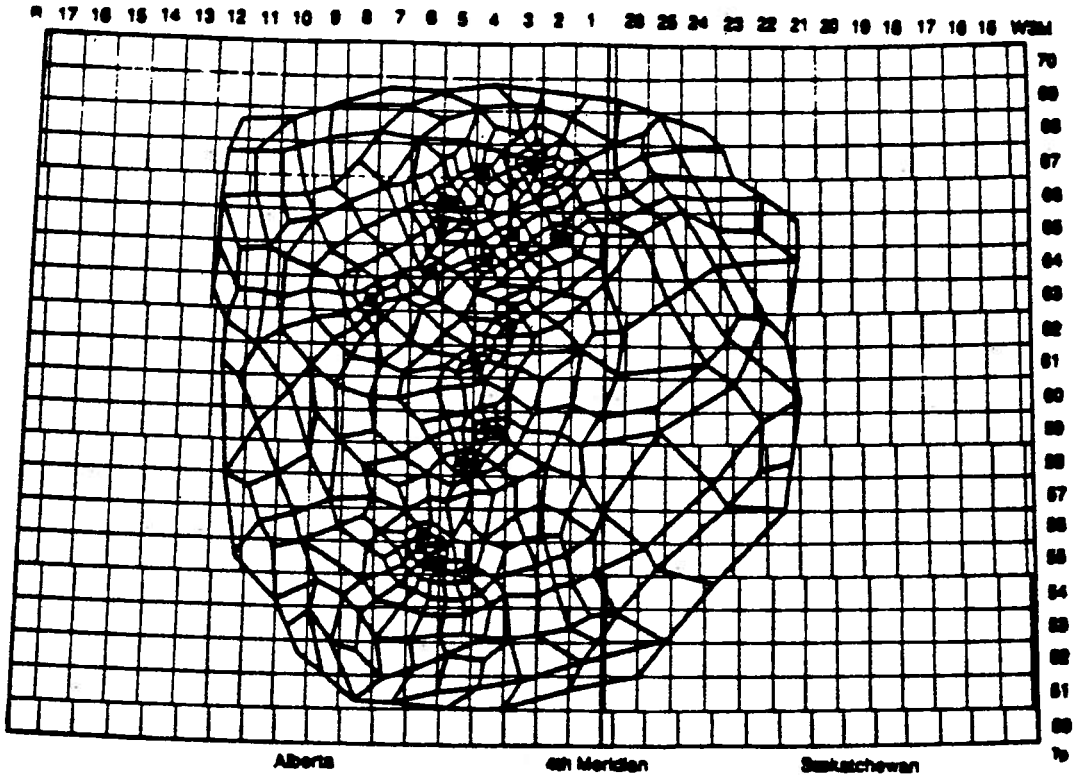

Figure 50. Plan view of the finite elements grid used for sensitivity analysis, Cold Lake study area

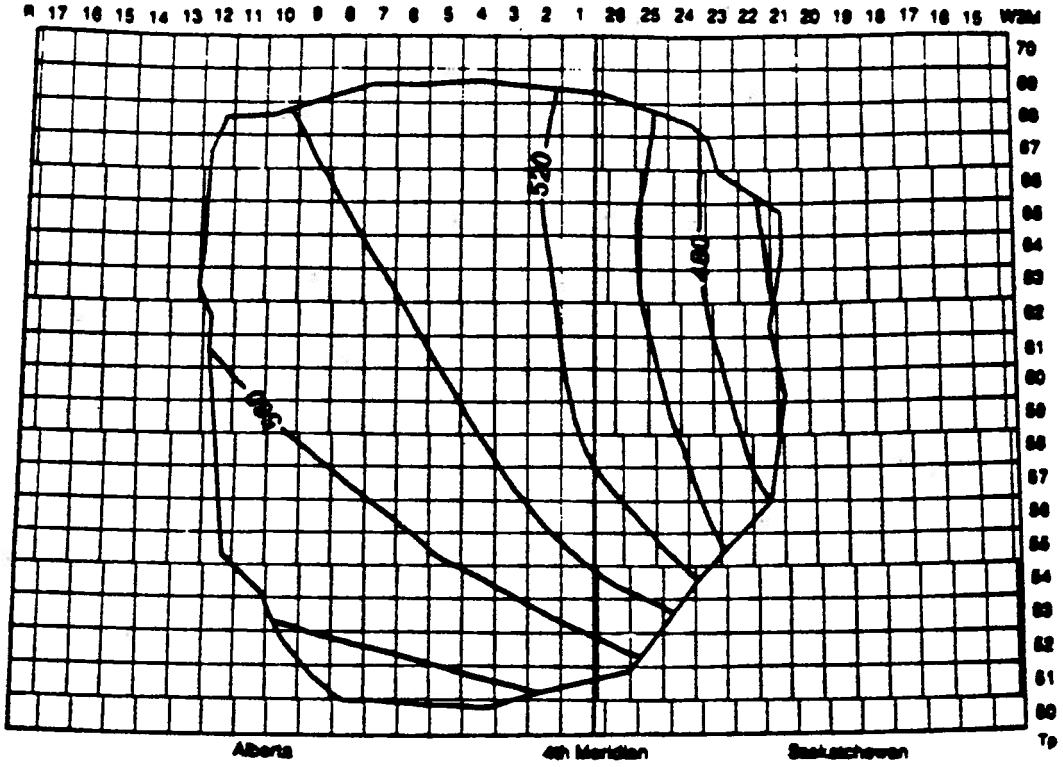

Figure 51. Computed freshwater potentiometric surface for the single-layered Basal Cambrian aquifer, Cold Lake study area

for a single aquifer with constant hydraulic conductivity depends only on the boundary conditions. For the same boundary conditions of prescribed hydraulic heads, simulations for different cases of hydraulic conductivity produce identical distributions of hydraulic heads. The only real difference between results obtained with different sets of hydraulic parameters is in fluxes, which, for given hydraulic gradients, change in direct relation with the hydraulic conductivity, according to Darcy's law. Because no fluxes were measured, and injection/pumping data are not available, it is not possible to check such results against reality in order to decide which set of data best characterizes the hydrostratigraphic sequence in the model area. Therefore, a sensitivity analysis of the influence of hydraulic conductivity on the steady-state natural flow is not relevant to the study. However, just to prove this point, simulations were carried out for the two cases of recommended and minimum values of hydraulic conductivity. No difference in results was found.

Another element which could influence the solution of equations 4 or 8 is the choice of boundary conditions. However, as discussed previously, for the aquifers in the Cold Lake study area there are no other boundary conditions than the values of hydraulic head from the natural potentiometric surfaces, or the no-flow condition at the top or bottom of the aquifer-aquitard systems bounded by aquicludes. Therefore, the influence of the boundary conditions cannot be analysed and assessed.

The sensitivity analysis with respect to the size of the time step was performed considering injection in a single well at 8-33-64-3W4, for a constant injection rate of 14 100 m^3/d. This well was chosen because

it is the site with the highest average injection rate over the 30 a period, out of the four injection wells in the Cambrian (see table 8). Runs were performed for cases of time step size of 1, 10, 30 and 60 d, for 70 time steps each. The initial hydraulic head at this injection site is 511 m. For simulations with time steps of 1, 10, 30 and 60 d, the hydraulic heads at the injection site after 60 d were 515.44, 515.41, 515.34 and 515.26 m, respectively. The difference between the computed hydraulic heads with different time steps is larger in the early stages of the simulation, and becomes smaller with time. For example, after 2100 d of injection (approximately 6 a) the hydraulic head at the injection site is 605.66 m versus 605.64 m, when computed with a time step of 30 and 60 d, respectively. This result is expected because the hydraulic head build-up per time interval is higher at the inception of injection, and becomes smaller as the total hydraulic head build-up tends asymptotically towards a steady-state value. For this reason it is desirable to have smaller time steps at least in the early stages of simulation. The difference in the values computed with different time steps depends on the aquifer characteristics (thickness, hydraulic conductivity). The case of injection analysed here is practically one of the most critical compared to the others (see table 8), due to the combination of one of the highest injection rates, lower hydraulic conductivity (Basal Cambrian versus Mannville or Beaverhill Lake aquifers), and relatively thinner aquifer when compared with the injection aquifers higher in the succession. For other projected cases of injection it is expected that there will be a smaller difference between hydraulic heads computed with different time steps, due to any combination of a lower rate of injection, greater aquifer

thickness and higher permeability (hydraulic conductivity). Based on this reasoning and on the asymptotic decrease of the difference in computed hydraulic heads for different time steps, it was decided to use a time step of 60 d in all the predictive simulations, in order to save on computer resources. The duration of 30 a (1985-2015) is equivalent to 183 time steps of 60 d each.

The radius of influence of the injection well was checked by simulating the injection of 14 100 m^3/d for the full length of the 30 a period. At the end of the projected period, the cone of hydraulic head build-up did not spread beyond about 5 km (half a township) around the injection well. A steady-state (equilibrium) solution for the case of injection will probably spread over most of the Cold Lake study area, but this will be reached after a period of time several orders of magnitude larger than the 30 a period analysed here (tens of thousands of years). The radius of influence depends on the rate of injection, hydraulic characteristics and geometry of the aquifer. Again, the simulated case is more representative of extreme conditions (see table 8 and table 6), due mainly to a high rate of injection and smaller aquifer thickness. The fact that the cone of hydraulic head build-up is about 10 km (the size of a township) or less indicates that the model area (figure 50) can be reduced, in order to save on computer resources, without imposing artificial constraints at the boundary, constraints which would distort the solution. For the Basal Cambrian aquifer, an attempt was made to find an equivalent radius r_e using a trial-and-error method. The simulation of injection of 14 100 m^3/d at a single site (see the model calibration) was performed for a single-layer isotropic aquifer having the local characteristics of the Basal Cambrian

sandstone. The hydraulic head increase after 30 a was matched with the analytical solution resulting in an equivalent radius for the injection node of about 700 m. This compares relatively well with the results of (incorrectly) using relation 7 for computing the value of the equivalent radius r_e.

Calibration of the Model

The Lower Paleozoic aquifer system is defined by four top surfaces (Basal Red Beds, Cambrian, Basal Cambrian sandstone and Precambrian). The four injection sites are situated in the northern part of the Cold Lake study area (see table 8). A smaller model area (figure 52A) was selected from the finite element grid defined previously (figure 50). The number of surface nodes for the smaller model area in the Lower Paleozoic aquifer system is 237, defining 217 surface quadrilateral elements. Because the Cambrian is not present in the northernmost part of the model area due to erosion, the total number of nodes and elements in the three layer system is 827 and 566, respectively. No potentiometric surfaces were defined previously in this succession except for the Basal Cambrian aquifer. The boundary conditions for this succession were defined as prescribed hydraulic heads along the contour of the model area at the top of the Basal Cambrian sandstone, and at three other nodes at the top of the Basal Red Beds for which hydraulic head values were available from drillstem tests, for a total of 31 nodes. Therefore, the number of unknowns in the system is 796 hydraulic head values. The difference between the computed and observed potentiometric surface at the top of the Basal Cambrian aquifer averages

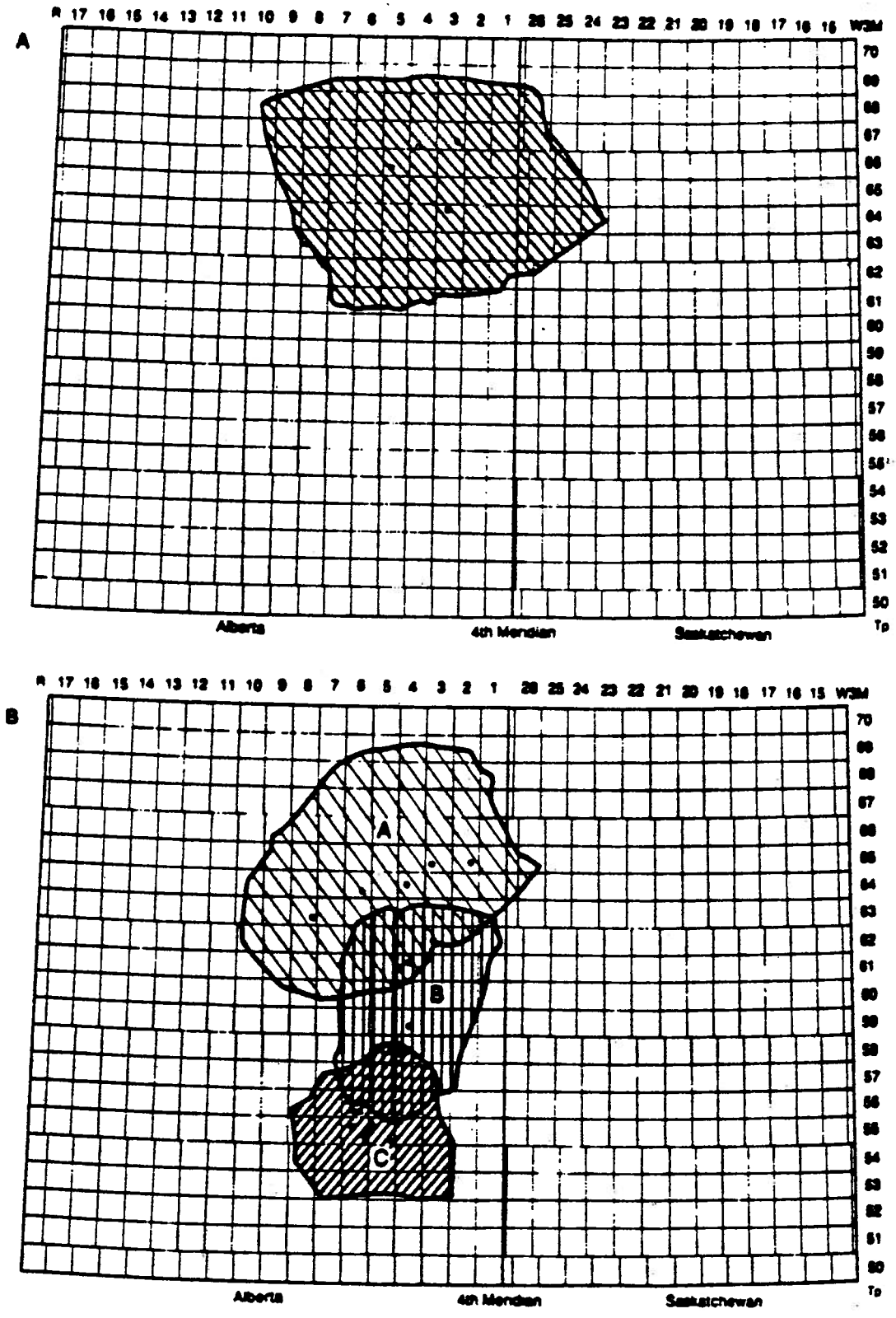

Figure 52. Outline of the model areas for simulation of effects of injection; A. In the Lower Paleozoic aquifer system; B. in the post-Prairie sequence: (A) Northern, (B) Central, and (C) Southern

1.4 percent, with a maximum value of 6 percent. This match is considered good for the natural steady-state flow regime. One of the important results of the natural steady-state simulation is that it provided the distribution of hydraulic head values everywhere in the system, including at the top of the Cambrian and Basal Red Beds. This information was missing in the previous analysis of the natural fluid flow regime due to the impossibility of performing drillstem tests in aquitards and the scarcity of data. The distribution of hydraulic heads everywhere is needed in the predictive simulations as the initial condition of the system at the start of injection. The upper injection succession between the top of the bedrock and the top of the Prairie aquiclude is much more complex. The surfaces defining the top of the Prairie aquiclude, Elk Point Group, Beaverhill Lake aquifer system, Mannville aquifer and the top of the bedrock cover the entire model area as defined in figure 50. The surfaces defining the tops and bottoms of the Ireton Formation, and the lower and upper Clearwater shales are only partially present, due to erosion or nondeposition. Besides, there are seven oil sands layers in the Mannville Group which have to be taken into account because of their different hydraulic properties. Using the finite element grid devised initially (figure 50) for such a complex structure means having to solve a system with approximately ten thousand unknown hydraulic head values at the nodes in the three-dimensional grid. This makes it prohibitive, keeping in mind that the CPU time required to solve such a system is approximately proportional to the square of the number of unknowns. Also, the memory of the computer system used for simulations would not permit such a large number of unknowns. Based on the previous sensitivity analysis regarding the

spread of the hydraulic head build-up around injection sites, and taking into account the location and the rates of injection, it was decided to divide the post-Prairie injection succession into three model areas: (A) northern; (B) central; and (C) southern (figure 52B). The finite element grids in each model area are based on the initial finite element grid (figure 50), requiring only the renumbering of the nodes and elements in each of them. The model areas were designed to overlap in order to check on the possibility of spread of pressure build-up from some injection sites beyond the near-field toward another cluster of injection sites. The validity of this separation into three model areas was confirmed later by the results of predictive simulations.

There are no potentiometric surfaces to define the initial hydraulic heads and/or the boundary conditions at all the interfaces between different hydrostratigraphic systems in the post-Prairie succession. Only the tops of the bedrock, Mannville aquifer, Clearwater, McMurray (bottom of lower Clearwater shale) and Beaverhill Lake aquifer system have a potentiometric surface to match. The potentiometric surface at the top of the Mannville Group is only partially defined in the northern area (figure 40C). This information was used to simulate the natural steady-state conditions in the three model areas above the Prairie Formation in order to calibrate the model and obtain the distribution of hydraulic heads at every point in the system to be used as initial conditions in the predictive simulations. Table 9 presents the characteristics and results of the calibration of the steady-state natural flow regime in the three model areas in the post-Prairie injection succession.

Table 9. Characteristics and results of numerical simulations of natural steady-state flow regime in three model areas in the post-Prairie injection sequence

		Northern Area (A)	Central Area (B)	Southern Area (C)
No. of surface nodes		231	110	98
No. of surface elements		213	95	84
Total No. of nodes		2550	1384	954
Total No. of elements		2251	1172	841
No. of nodes with B.C.		353	204	94
No. of unknowns		2197	1180	860
Mannville	Average	2.16%	1.16%	1.58%
	Maximum	5.77%	3.38%	4.68%
Clearwater	Average	4.3%	1.58%	0.55%
	Maximum	8.4%	2.43%	0.67%
McMurray	Average	3.91%	3.23%	0.98%
	Maximum	8.21%	8.01%	1.49%
Beaverhill Lake	Average	3.03%	1.19%	2.19%
	Maximum	10.5%	4.67%	5.7%

Difference between computed and observed potentiometric surfaces

It should be noted here that the numerical simulation of natural steady-state flow in the post-Prairie succession provided values of hydraulic heads at every node, therefore, at every top and bottom surface in the succession. This way, hydraulic head distributions were obtained at the top and bottom of every oil sands layer. The hydraulic head distribution at the top and bottom of the Upper and Lower Grand Rapids oil sands layers are basically no different from the hydraulic head distribution at the top of the Mannville aquifer. The same can be said for the top of the McMurray oil sands in the area where the Clearwater shales are absent. Where the Clearwater shales are present, the hydraulic head distribution at the top of the McMurray oil sands are no different from the hydraulic head distribution at the top of the McMurray Formation. The hydraulic head distribution at the bottom of the McMurray oil sands is closer to the hydraulic head distribution at the top of the Beaverhill Lake aquifer system than to the one at the top of the McMurray Formation. These results confirm the findings of the analysis of the natural flow regime that the oil sands layers in the Mannville Group act as intermediate to weak aquitards and that, on a regional scale, the fluid flow in the Mannville Group bypasses them.

The match between computed and observed hydraulic heads in the three post-Prairie model areas is considered good, if one takes into account the approximations in data processing, the lack of information for many of hydrostratigraphic units, and the fact that the numerical model is based on the conservation of fluid mass, which may not necessarily be the case for the entire hydrostratigraphic system described in the previous section, or parts of it. It should also be noted that the Clearwater shale and sandstone layers are rarely present in the southern area and partially present in the central area.

Once the numerical model is calibrated for each of the model areas considered previously, predictive simulations can be performed in order to study the regional effects of deep waste injection in the Cold Lake study area. The results of the simulation of steady-state natural flow are used as initial conditions for the predictive simulations and the results of simulation of injection will be compared with these initial conditions.

SIMULATION OF EFFECTS OF INJECTION

The main purpose of this study is to check, on a regional scale, the effects of deep waste injection in the Cold Lake study area in terms of pressure build-up for given rates and sites of injection over a projected 30 a period. The analysis of the natural fluid flow regime in the Cold Lake study area produced, among other things, estimations of the hydraulic parameters for the hydrostratigraphic systems considered for modelling. Table 6 contains recommended values (best estimate), as well as a low and high value for hydraulic conductivities and specific storage, values which define an accepted range of variability at the regional scale. It must be pointed out that the low and high values in table 6 are not the minimum or maximum values in point data distributions (see Appendices A and B). The FE3DGW model used for these simulations is deterministic and not able to take into account geostatistical distributions of hydraulic parameters or the uncertainty associated with their determination. The value of any parameter is constant at least in a volume element, but generally the same value is allocated to an entire hydrostratigraphic unit. While an average value

still characterizes a given distribution, and can be used as a most probable case in a simulation, the use of a low value in a deterministic model represents an unreal case, and is theoretically a worse case for fluid flow and hydraulic head build-up. However, it is important to check this scenario as well, because it represents an upper limit of the regional effects of injection. Also, it could happen that, in reality, this combination of low values is found at a particular injection site. The play of the hydraulic parameters (see equation 4) is such that, for a lower hydraulic conductivity the injected fluid is moved away more slowly with resulting higher hydraulic head build-up. For a lower specific storage, less injected fluid can be "absorbed" in the fluid-solid matrix system, again with the result of a higher hydraulic head build-up. The highly improbable combination of a low hydraulic conductivity and a low specific storage in all the hydrostratigraphic systems represents the worst case (a very pessimistic scenario). The opposite combination of high values for both parameters represents the best case, a particularly optimistic scenario. It was intended at the beginning of the project to run predictive simulations for all three cases: normal, worst and best. However, after simulating the effects of injection with an average combination of hydraulic parameters, it became apparent that it is not always necessary to run simulations for the best case. Therefore, in order to save on computer resources, generally only the most probable (average) and worst cases were simulated for the given sites and rates of injection.

The results of simulation of injection at the four sites in the Basal Cambrian aquifer are presented in figure 53 as variation of the hydraulic head during the entire period of injection, for the case of

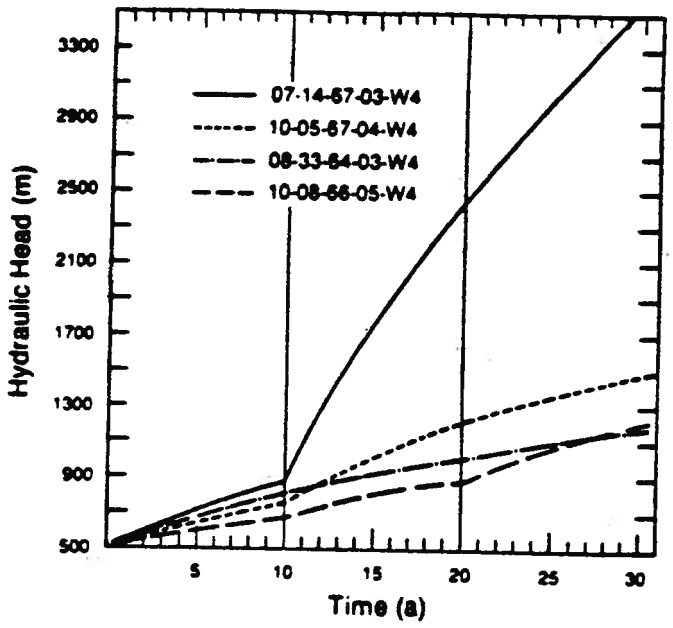

Figure 53. Hydraulic head increase at the four injection sites in the Basal Cambrian aquifer, assuming average hydraulic properties in the Lower Paleozoic aquifer system

average hydraulic parameters. The change in the shape and slope of hydraulic head increase is evident for the cases where the change in the rate of injection is significant. The different hydraulic head build-ups at the four injection sites are due to the differences in the rates of injection and in the geometry (thickness) of the Basal Cambrian aquifer at the sites (the hydraulic conductivity and specific storage being the same). At the Esso (08-33-64-3-W4) and BP (10-08-66-05-W4) sites the thickness of the Basal Cambrian aquifer is about 33-36 m. At the Dome site (10-05-67-04-W4), although the rates of injection are smaller than at Esso and comparable with the ones at BP, the hydraulic head increase is larger due to a reduced thickness of the injection aquifer. At the Suncor site (07-14-67-03-W4) the theoretical hydraulic head build-up is very high, due to very high rates of injection projected for the last 20 a (over 16 000 m^3/d) in a place where the host aquifer is very thin (18 m). The Cambrian aquifer system (post Basal Sandstone) is absent at the BP, Dome and Suncor sites. Figure 54 shows the spread of the cone of hydraulic head build-up at the top of the Basal Red Beds (top of the Lower Paleozoic succession), top of the Basal Cambrian aquifer and the top of the Precambrian (bottom of the Lower Paleozoic succession).

The spread of hydraulic head build-up is defined by the 10 m contour marking the difference between the hydraulic heads at the FEM nodes at any time step, and the initial hydraulic heads at the start of predictive simulations. The value of 10 m was chosen because it represents about 2 percent, on average, of the initial hydraulic heads in the entire hydrostratigraphic sequence, well within the error margin of all the measurements, processing and interpretation of the data.

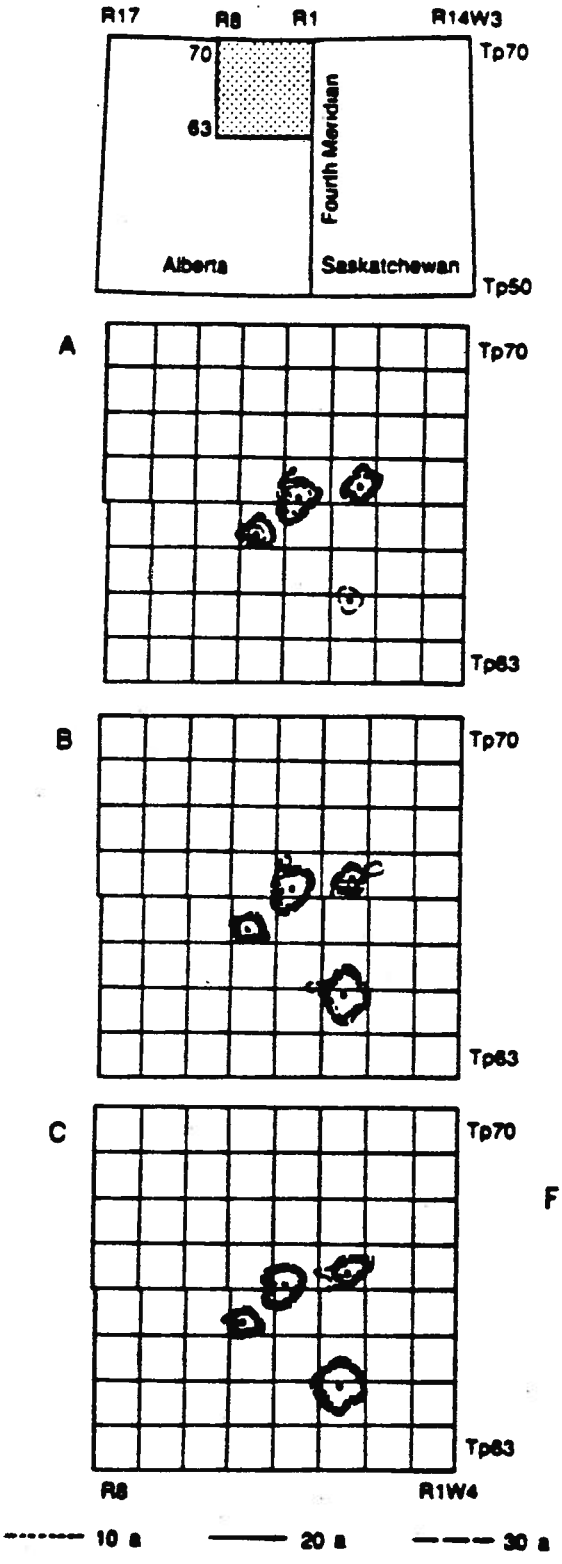

Figure 54. Spread of the pressure build-up at the top of (A) Basal Red Beds, (B) Basal Cambrian aquifer, and (C) Precambrian, assuming average hydraulic properties in the Lower Paleozoic aquifer system

Where the Cambrian aquifer system (post Basal Sandstone) is present, there is no significant propagation of hydraulic head build-up at the top of the succession (Esso site). Where the Basal Red Beds directly overlie the Basal Cambrian sandstone, the effects of injection at the top of the Basal Cambrian aquifer propagate at the top of the succession to about 50 to 70 percent of the increase at the top of the aquifer with a corresponding larger area of influence (figure 54A). There is also significant hydraulic head increase at the bottom of the injection aquifer (figure 54C). In any case, the results of simulation show that under the assumption of average hydraulic parameters, there is no interference between the injection sites during the projected period of 30 a. For the case of assumed maximum hydraulic conductivity and maximum specific storage, the increase in hydraulic head at the injection sites is about 60 to 65 percent lower than in the case of average hydraulic parameters (figure 55). Figure 56A presents the spread of the hydraulic head build-up after 10, 20 and 30 a at the four injection sites at the top of the injection aquifer, in the case of maximum values of hydraulic parameters.

The worst case of low hydraulic conductivity and low specific storage proved to be a totally unrealistic case from the point of view of the effects of injection (the rock would have been fractured long before the end of the period of injection). For this reason, two other less extreme cases are presented: (1) low hydraulic conductivity and average specific storage; and (2) average hydraulic conductivity and low specific storage. Table 10 presents the computed hydraulic heads at the four injection sites after 10, 20 and 30 a, for these two less extreme cases. Figures 56B and 56C present the spread of hydraulic head

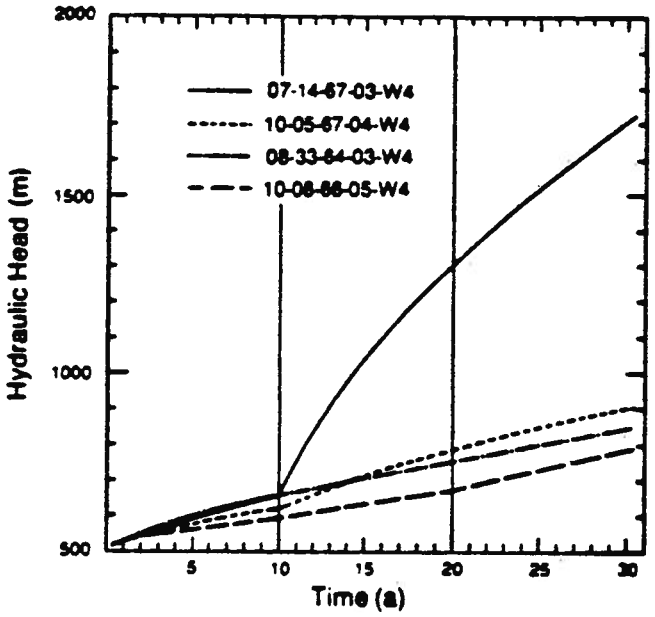

Figure 55. Hydraulic head increase at the four injection sites in the Basal Cambrian aquifer, assuming maximum values for hydraulic properties in the Lower Paleozoic aquifer system

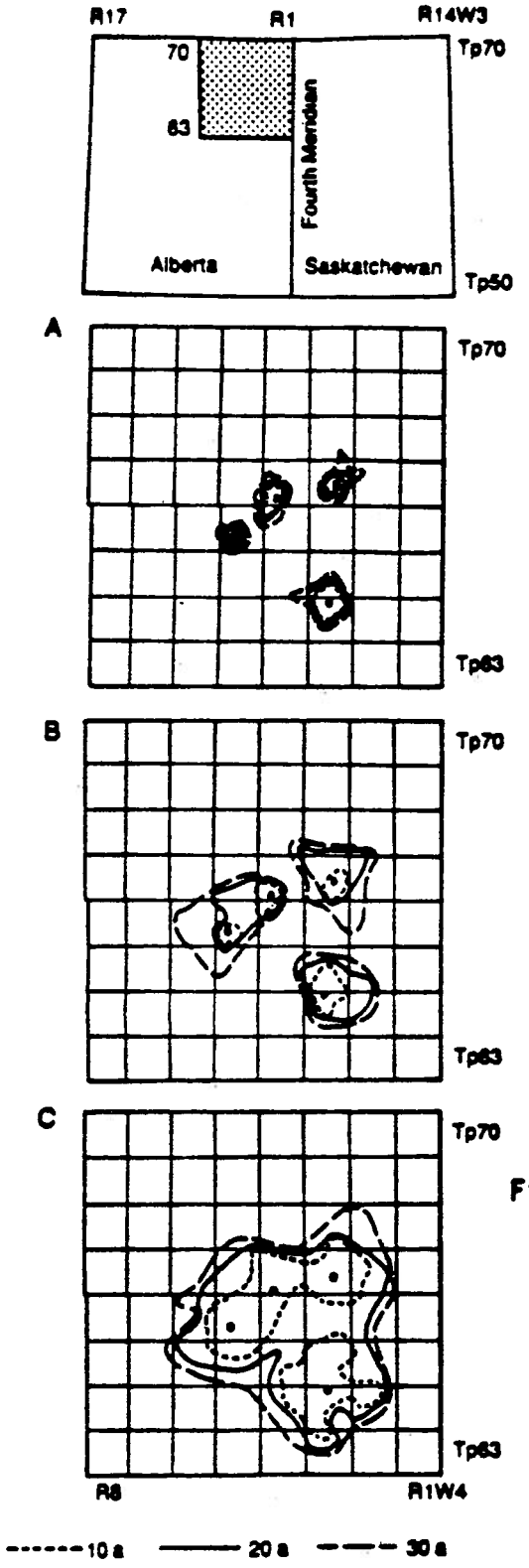

Figure 56. Spread of pressure build-up at the top of the Basal Cambrian aquifer in the Lower Paleozoic sequence, assuming (A) maximum values for both hydraulic conductivity and specific storage; (B) minimum hydraulic conductivity and average specific storage; and (C) average hydraulic conductivity and minimum specific storage

Table 10.
Computed increases in hydraulic heads at the four injection sites in the Basal Cambrian aquifer, for two cases of either minimum hydraulic conductivity or minimum specific storage, for periods of 10, 20 and 30 a

	Hydraulic Head (m)					
	Minimum Hydraulic Conductivity			Minimum Specific Storage		
Time of Injection	10 a	20 a	30 a	10 a	20 a	30 a
08-33-64-03-W4	1084	1486	1872	2766	3215	3556
10-08-66-05-W4	780	1136	1681	1470	2136	3117
07-14-67-03-W4	1090	3505	5745	2793	9532	11033
10-05-67-04-W4	867	1508	2122	2011	3645	4102

build-up at the top of the injection aquifer for these two combinations of values of hydraulic parameters. It can be seen that a lower value for specific storage has a more drastic effect on the hydraulic head build-up than does the case of a lower hydraulic conductivity. In the case of low hydraulic conductivity, after a period of 20 a there will be interference between the BP (10-08-66-05-W4) and Dome (10-05-67-04-W4) sites (figure 56B). In the case of low specific storage, there will be interference between Suncor, Dome and BP sites after 10 a, and between all four injection sites after 20 a (figure 56C).

However, these worst cases are not likely to occur for the following reason. The FE3DGW model used for simulations is a fluid flow model only. As such, the mathematical solution will allow for any value of pressure build-up. In reality, the pressure will increase until the fracturing threshold is reached. At that point, fracturing will occur, increasing the hydraulic conductivity around the injection site. The increase in the real value of hydraulic parameters around the injection sites will release pressure, with the effect of slowing down, and even temporarily reversing, the hydraulic head build-up. The fractures can be both horizontal and vertical. Horizontal fractures are not likely to occur, but in any case they are of no concern, bringing about only an increase in the transport properties of the injection zone. Vertical fracturing will possibly allow cross-formational flow between the injection aquifer and other aquifers higher in the succession. However, in this particular situation it is felt that this should not be the case. The Basal Cambrian aquifer is overlain by the Basal Red Beds aquitard and by the Lower Devonian aquiclude (about 300 m thick in the area). Fractures will probably propagate through the Basal Red Beds

aquitard. Possibly some fracturing will also occur at the bottom of the Lower Devonian aquiclude, but these fractures are unlikely to propagate all the way through it, due to the elastoplastic properties of salt, which constitute most of the aquiclude (Lotsberg and Cold Lake Formations). Even if some fractures were to propagate completely through the Lower Devonian aquiclude to the overlying Winnipegosis aquifer system, another thick (160 m) salt aquiclude (Prairie Formation) overlies this aquifer system which definitely will stop any further propagation. It should be pointed out that, in the assessment of the effects of injection for any possible situation defined within the limits of the best and worst cases, a self adjusting process will take place, by which, once the fracturing threshold is reached, fracturing will increase the value of hydraulic parameters, relieving and lowering the pressure. A more detailed study of these situations should be made at a local scale using a model which includes fracturing and flow in fractures. As for the wastes themselves, once outside the cone of hydraulic head build-up, they will be carried away by the natural flow regime, with velocities of the order of 1 cm/a. Another aspect which should be mentioned here is the fact that the above results are based on a very definite set of aquifer characteristics (thickness, geometry, hydraulic parameters). However, these are based on a very limited and sparse data sample and on extrapolation or interpolation of the known information. It is clear that the results are very sensitive to the values of any of these parameters. If local values were known, local scale simulations could be performed as long as the assumption of absence of interference between the injection sites is valid.

While the injection in the Lower Paleozoic aquifer system takes place in a single aquifer (Basal Cambrian sandstone), injection in the post-Prairie succession takes place in different individual aquifers or sections, all interconnected. As explained previously, the predictive simulations were performed on three overlapping model areas. However, the results will be presented by individual injection sites in terms of hydraulic head increase, and by planes of injection in terms of spread of hydraulic head build-up. The average values of hydraulic conductivity of the aquifers in the post-Prairie succession are of the same magnitude as the hydraulic conductivity of the Basal Cambrian aquifer, while the values of specific storage are generally one order of magnitude higher (see table 6). Also, with the exception of the Clearwater aquifer, the thicknesses of the aquifers at the injection sites are greater than that of the Basal Cambrian aquifer. The oil sands are a barrier to flow only in the case of widespread strata such as the Upper and Lower Grand Rapids Formation. On the other hand, the rates of injection in the post-Prairie succession are lower than for the Lower Paleozoic aquifer system, with the exception of the BP-Grand Rapids site (8-7-66-5-W4). As a result, it is expected that the effects of injection in the post-Prairie succession will be smaller than in the case of injection in the Basal Cambrian aquifer. Indeed, the results of simulations indicate that, for the normal case (average hydraulic properties), the increase in hydraulic head at the end of the 30 a period is minimal. With the exception of the BP site (8-7-66-5-W4), the increase in hydraulic head is less than 10 percent of the initial hydraulic head. In some cases the increase is so low that it is well within the limits of the noise in the system, that is, it is in the

range of the cumulated errors from measuring to modelling. Even for the BP site, the increase in hydraulic head is from about 525 m to about 590 m. Based on the results, it was decided not to run any simulations for the best case (maximum values of hydraulic parameters). It could be said that the average case is already a best case. The full worst case scenario (low values for both hydraulic conductivity and specific storage) was run for the post-Prairie injection succession. Figures 57 to 62 present the increase in hydraulic head at each individual injection site for both average and worst cases. For the Dome site at 10-5-67-4-W4, the depth of the point of injection falls midway between the top of the Paleozoic and the top of the McMurray Formation. For this reason, the rate of injection was split into two equal parts allocated at each node defining the top and the bottom of the interval (figures 60C and 60D). For a few injection sites in the Lindberg area an artificial (fictive) surface was introduced in order to have FEM nodes at these particular depths. Otherwise, the depths of injection were sufficiently close to an actual node defining a surface as to be allocated to that node. Due to the resolution of the FEM grid, the two Suncor injection sites at Fort Kent (5-28-61-4-W4 and 6-28-61-4-W4) could not be differentiated, and were lumped into a single site with the cumulated injection rate (figure 60B). It could be seen from figures 57 to 62 that, in the worst case scenario, the increase in hydraulic heads at the injection sites is generally within the range of natural hydraulic heads in the post-Prairie succession. At seven sites the increase in hydraulic heads is between 800 to 1100 m.

Figure 63 presents the spread of hydraulic head build-up in four different planes of injection for the worst case combination of

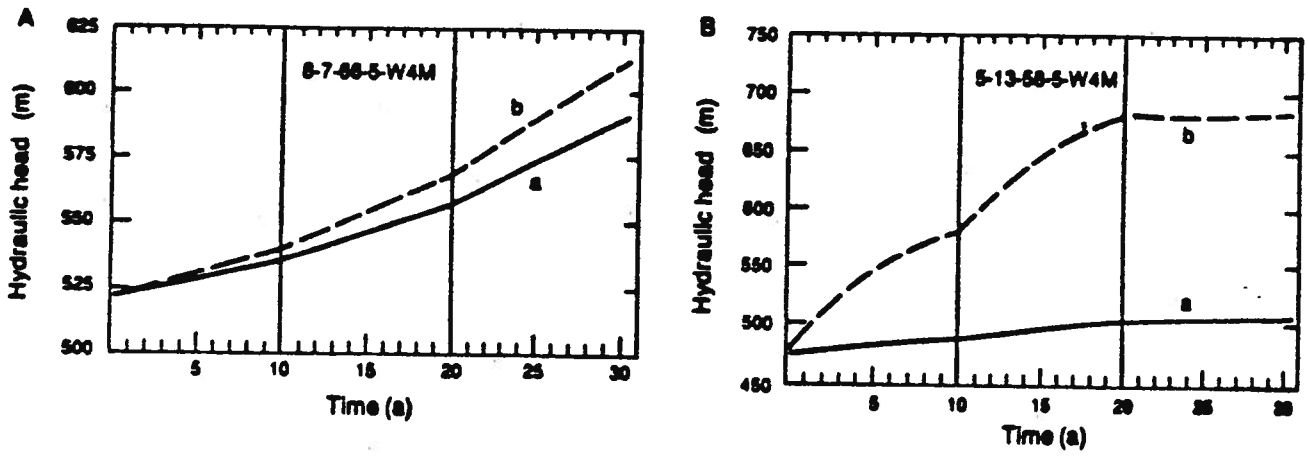

Figure 57. Predicted increase in hydraulic head at injection sites: A. in Grand Rapids and B. in Lower Grand Rapids; assuming (a) average hydraulic parameters, and (b) minimum hydraulic parameters

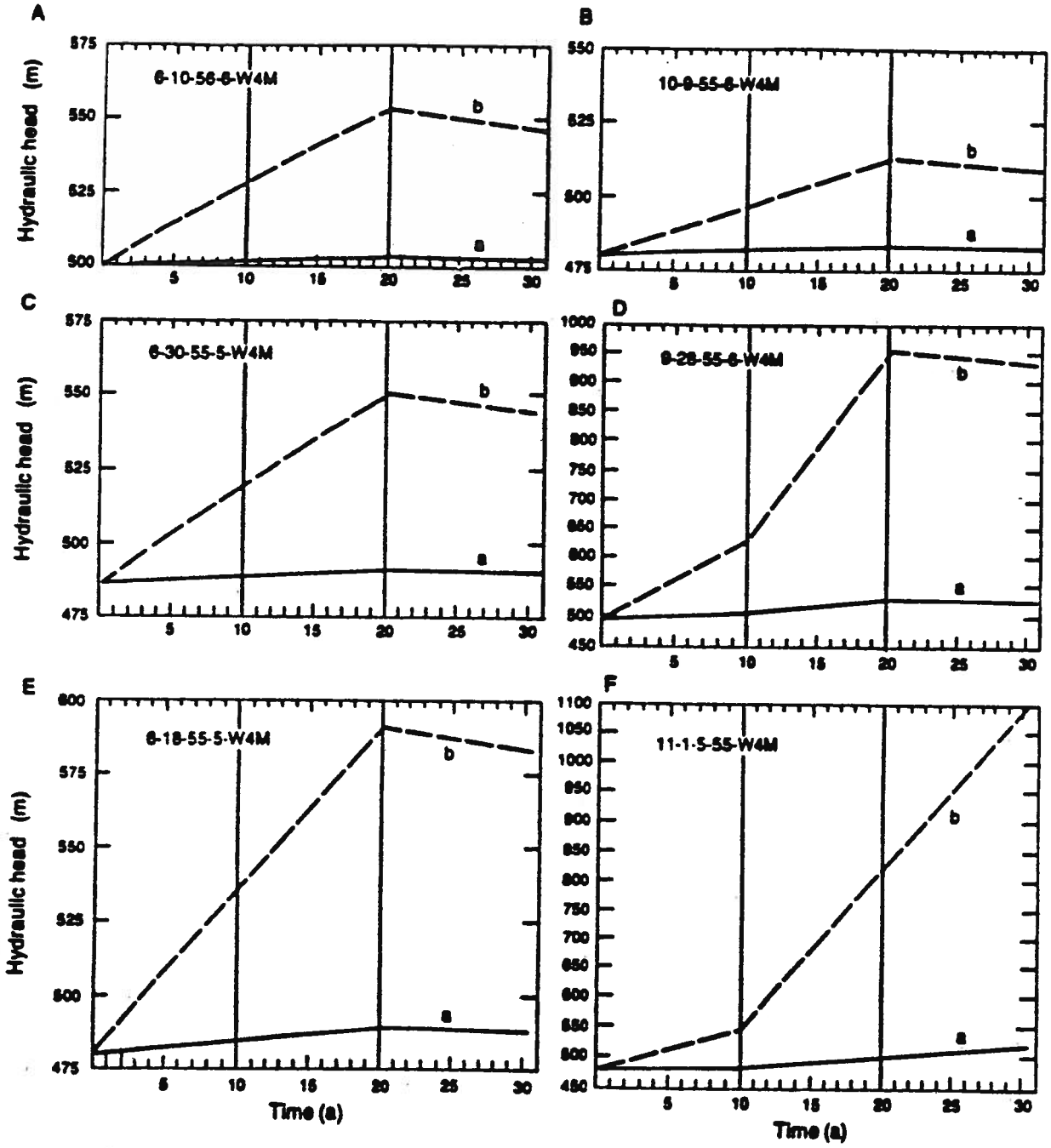

Figure 58. Predicted increase in hydraulic head at injection sites: A., C., and E. in the Rex Member; B., D., and F. in the Lloydminster Formation; assuming (a) average hydraulic parameters, and (b) minimum hydraulic parameters

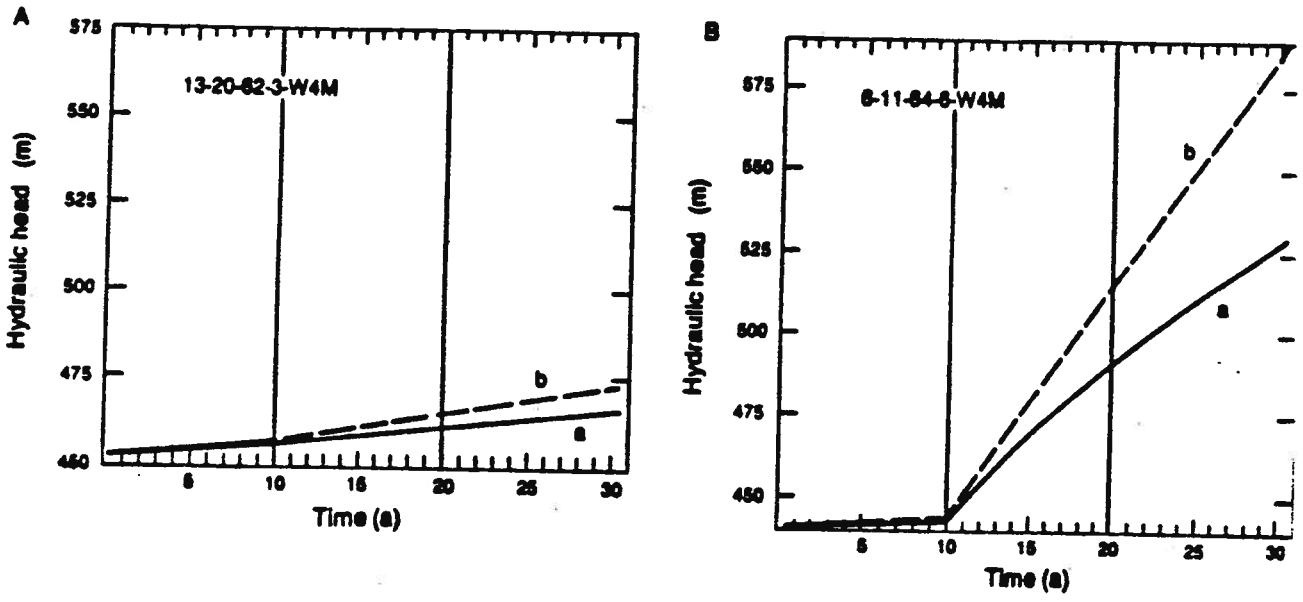

Figure 59. Predicted increase in hydraulic head at injection sites: A. in Mannville C, and B. in Clearwater Formation; assuming (a) average hydraulic parameters, and (b) minimum hydraulic parameters

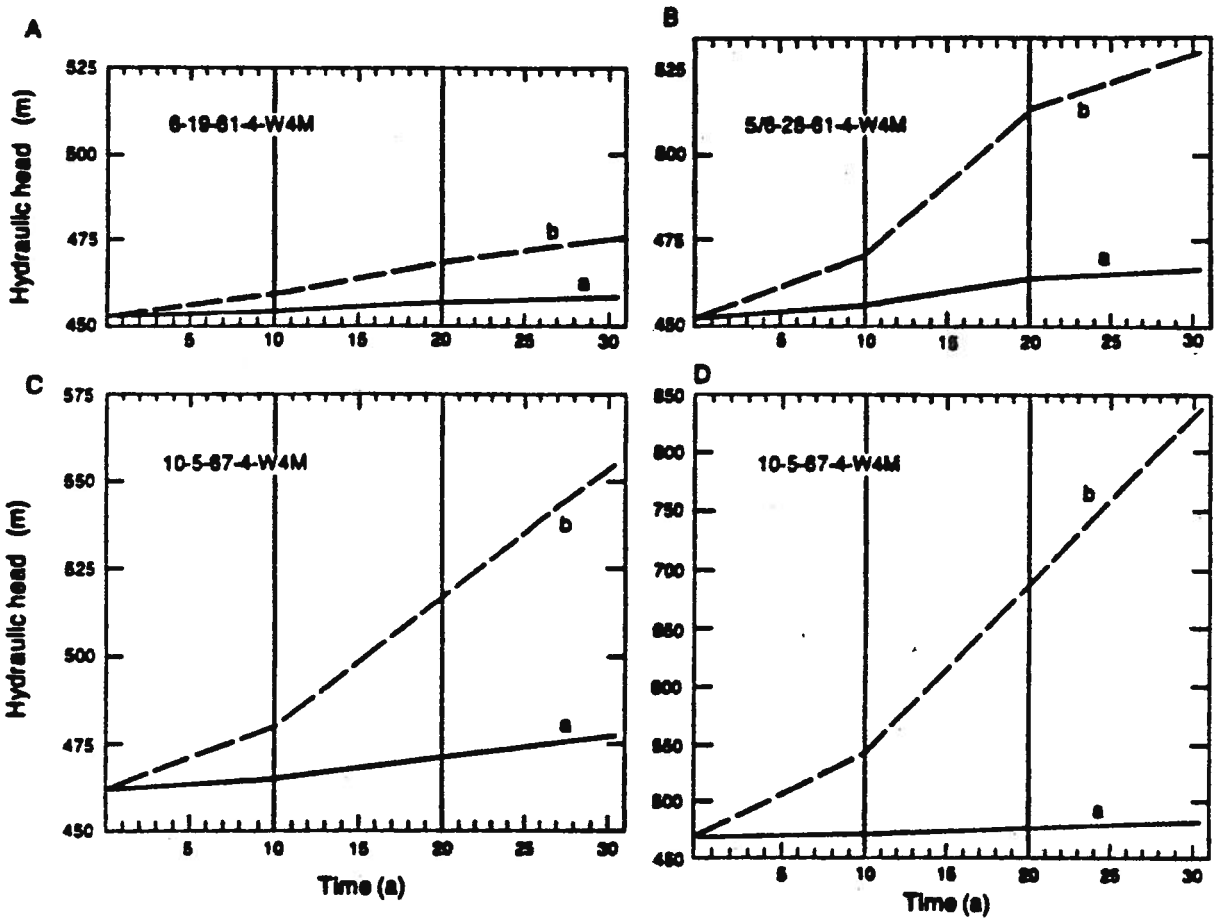

Figure 60. Predicted increase in hydraulic head at injection sites: A. in Clearwater Formation, B. in Lloydminster and Clearwater Formations, C. and D. at the top of the McMurray Formation; assuming (a) average hydraulic parameters, and (b) minimum hydraulic parameters

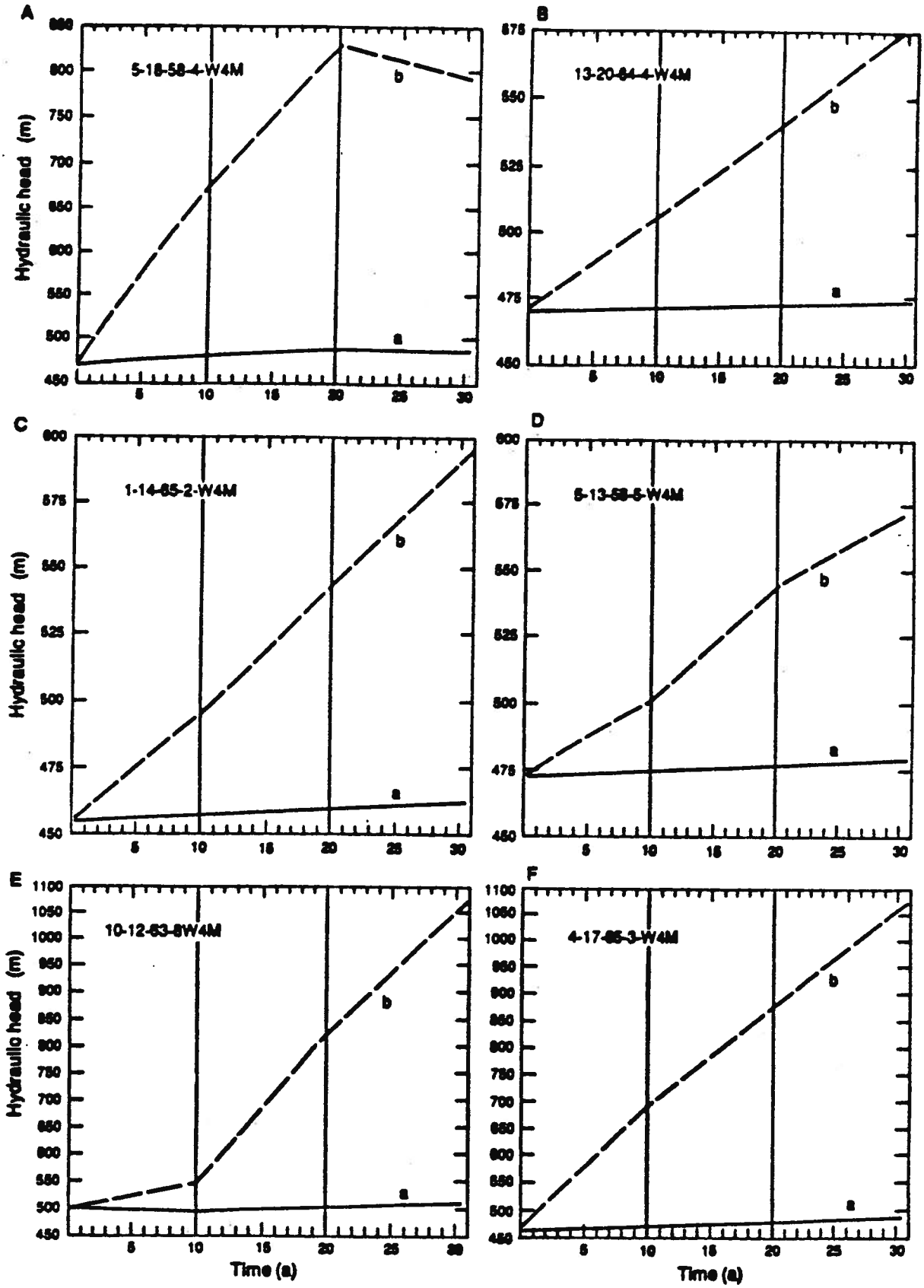

Figure 61. Predicted increase in hydraulic head at injection sites: A., C., D., and E. at the top of Cooking Lake Formation, B. and F. at the bottom of the McMurray Formation; assuming (a) average hydraulic parameters and (b) minimum hydraulic parameters

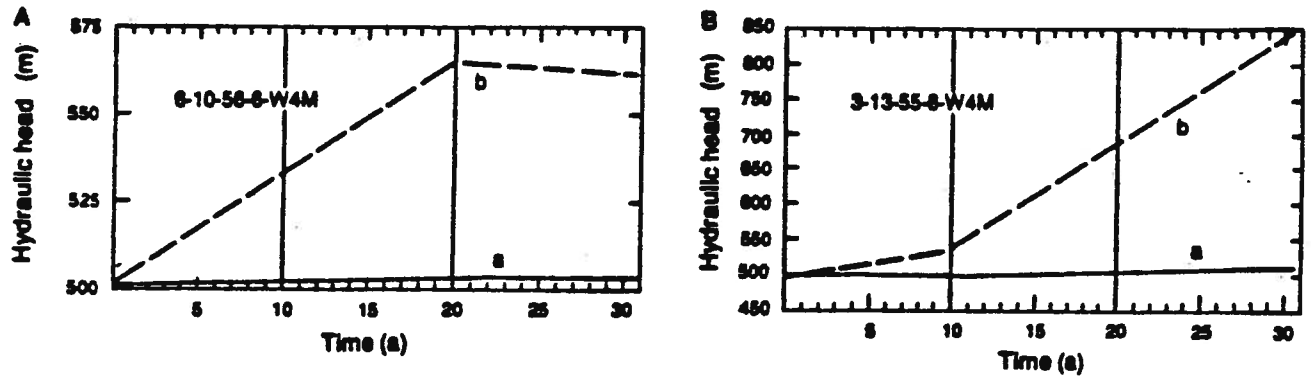

Figure 62. Predicted increase in hydraulic head at injection sites at the bottom of the Cooking Lake Formation; assuming (a) average hydraulic parameters, and (b) minimum hydraulic parameters

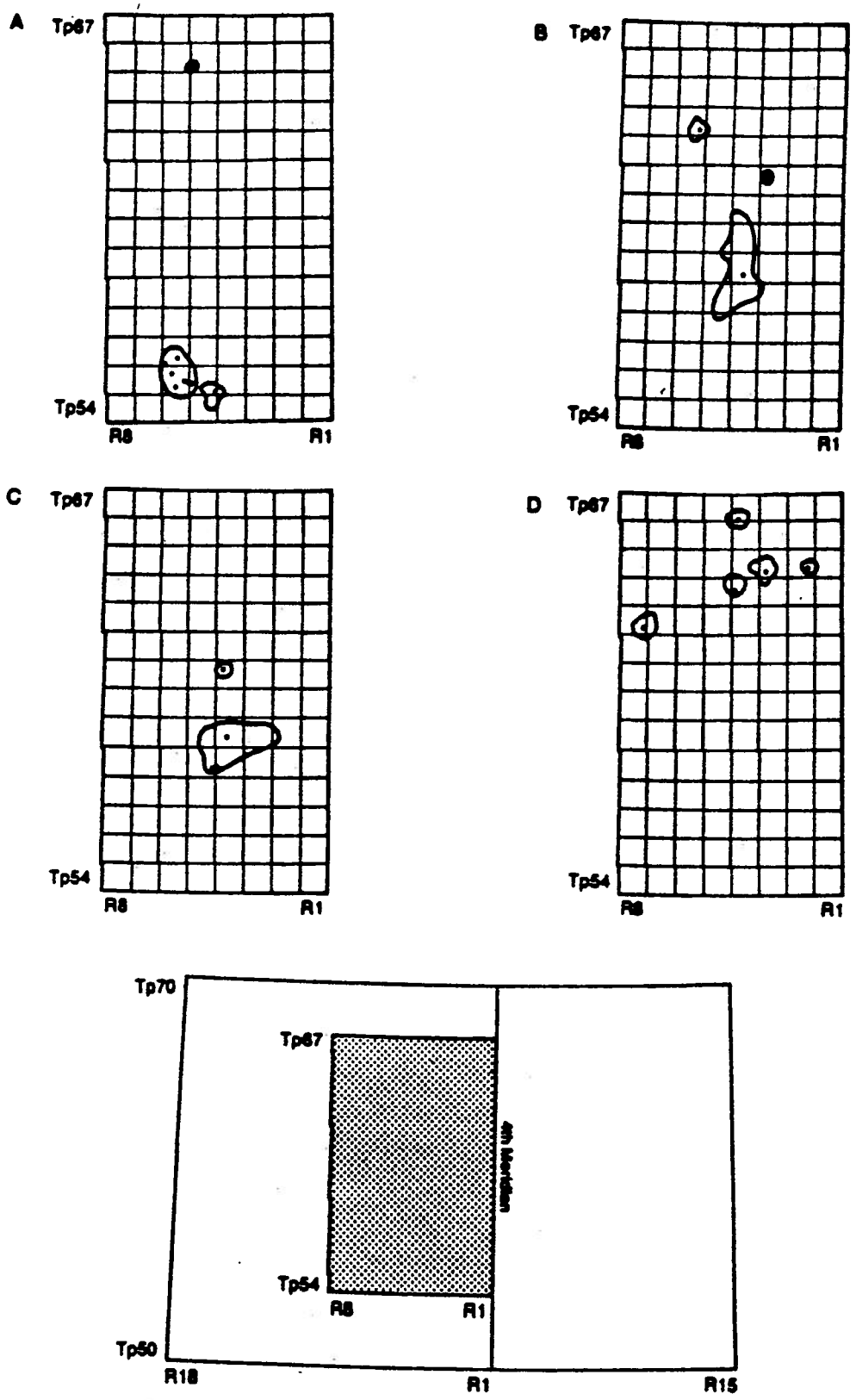

Figure 63. Spread of pressure build-up as a result of injection: A. in the Mannville Group; B. in Clearwater sandstone; C. at the top of the McMurray Formation; and D. at the bottom of the McMurray Formation (also in some places top of the Cooking Lake Formation); assuming minimum hydraulic parameters for the injection aquifers

hydraulic parameters. For the average case, the build-ups are so small that, using the same 10 m contour interval as a marker, it is not significant to represent them. There is no interference between the different injection sites in the post-Prairie succession in the case of average hydraulic parameters. In the worst case scenario, there is some interference in the cluster of injection sites in the Lindberg area (figure 63A) and at the top of the McMurray aquifer in the central area (figure 63C). Also, the spread of the hydraulic head build-up is larger for injection in the Clearwater Sandstone aquifer (figure 63B) and in the McMurray aquifer between the McMurray oil sands layer and the bottom of the Clearwater shale (figure 63C), due to a smaller thickness of the injection aquifers. The southern contour of the hydraulic head build-up spread in these two cases is practically coincident with the boundary of the Clearwater Formation. South of this boundary, the thickness of the injection aquifer increases rapidly with a corresponding drop in the hydraulic head build-up. There is no interference between the injection wells at the bottom of the McMurray aquifer (figure 63D). Very little pressure build-up takes place at the top of the Mannville Group, and it is well within the limits of natural hydraulic heads in the system. This result shows that the assumption of considering the whole post-Mannville succession as a single aquitard is basically correct in terms of regional effects of injection.

CONCLUSIONS

Numerical simulations of effects of injection at a regional scale in the Cold Lake study area have shown that basically the system can sustain the projected rates of injection over the next 30 a. The resulting hydraulic head build-ups are significant and, to a certain degree, critical for the Lower Paleozoic aquifer system, but then, even if damage to the formation takes place, the overlying thick Lower Devonian aquiclude will probably stop any further propagation higher up in the sequence. Under the assumption of average values characterizing the hydraulic parameters, the numerical simulations revealed no interference between the different injection sites. In the case of minimum values of hydraulic conductivity and/or specific storage, the numerical simulations show areas of superposition of effects of injection from different sites. Once outside the cones of hydraulic head build-up around the injection sites, the injected wastes will be carried by the natural flow regime with a velocity of the order of magnitude of 1 cm/a.

In using the results of predictive simulations of effects of injection in the Cold Lake study area, one should take into account two aspects: (1) the uncertainties associated with the determination of aquifer characteristics and of initial and boundary conditions; and (2) the resolution of finite element modelling. With respect to aquifer characteristics (geometry, thickness, hydraulic conductivity and specific storage), it should be kept in mind that all the values used in simulations were determined at a regional scale, based on different methods of data processing (interpolation, extrapolation, averaging,

etc.). The local values could actually be different from the regional values used in modelling.

In conclusion, it can be stated that the results of numerical simulations presented so far apply on a regional scale, starting at a distance between 500 to 1000 m from the individual injection wells. To find out what happens closer to the wells, a much finer grid must be used in simulations, which is not possible at the scale of the problem due to limitations of computer resources. However, if such simulations are necessary, the injection sites can be modelled individually, at a local scale, based on the present results which indicate that there probably will be no interference between the wells. Modelling at a local scale should be able also to consider the effects of possible fracturing.

Finally, it should be pointed out that the modelling of effects of injection used considerable computer resources, notwithstanding the data processing effort in describing the natural flow regime in the Cold Lake study area. For example, a complete run for the northern area in the post-Prairie succession (2197 unknowns, 183 time steps) used about 20 h and 33 min CPU time on a VAX11/780 computer. Generally, the amount of CPU time needed for simulations is directly proportional to the square of the number of unknowns. This rule was verified in the present simulations when comparing the computer resources used for different model areas. The need for computer memory during the simulations was also significant.

REFERENCES

Agar, J. (1985): Geotechnical behaviour of oil sands at elevated temperatures and pressures. Unpublished Ph.D. thesis, Department of Civil Engineering, University of Alberta, 2 volumes, 906 pp.

Bachu, S., B. Hitchon and P. Mortensen (1986): Preliminary analysis of transport processes in the Basal Cambrian aquifer of south-central Alberta; in proceedings of the Third Canadian/American Conference on Hydrogeology: Hydrogeology of Sedimentary Basins: Application to Exploration and Exploitation, June 22-26, 1986, Banff, Alberta, Canada.

Bachu, S., C.M. Sauveplane, A.T. Lytviak and B. Hitchon (1987): Analysis of fluid and heat regimes in sedimentary basins: techniques for use with large data bases; American Association of Petroleum Geologists Bulletin, v. 71, no. 7, pp. 822-843.

Basin Analysis Group (1985): Hydrogeology of the Cold Lake study area, Alberta Canada. Consultant report to Alberta Environment.

Bear, J. (1972): Dynamics of fluids in porous media. Elsevier, 764 p.

Beaumont, C. (1981): Foreland basins; Geophysical Journal of the Royal Astronomical Society, v. 65, pp. 291-329.

Beljin, M.S. (1987): Representation of individual wells in two-dimensional ground water modeling; in proceedings of the NWWA/IGWMC Conference "Solving Ground-water Problems with Models", February 10-12, 1987, Denver, Colorado. National Water Well Association, Dublin, Ohio, pp.340-351.

Belyea, H.R. (1964): Upper Devonian, Part II - Woodbend, Winterburn and Wabamun Groups; in Geological History of Western Canada (R.G. McCrossan and R.P. Glaister, editors), Alberta Society of Petroleum Geologists, Calgary, pp. 66-88.

Charbeneau, R.J. and R.L. Street (1979): Modeling groundwater flow fields containing point singularities: a technique for singularity removal. Water Resources Research, v. 15, no. 3, pp. 583-594.

Davies, P.B. (1987): Modeling areal, variable density, ground-water flow using equivalent head-analysis of potentially significant errors; in proceedings of the NWWA/IGWMC Conference "Solving Ground-water Problems with Models", February 10-12, 1987, Denver, Colorado, pp.888-903.

De Wiest, R. (1965): Geohydrology. John Wiley and Sons, 366 p.

De Wiest, R. (1969): Fundamental principles of ground-water flow; in Flow Through Porous Media (R.J.M. de Wiest, editor). Academic Press, New York and London, pp. 1-52.

Earlougher, R.C. Jr. (1977): Advances in well test analysis. Henry L. Doherty Memorial Fund of AIME, Society of Petroleum Engineers of AIME, New York.

Frind, E.O. (1980): Seawater intrusion in continous coastal aquifer-aquitard systems; paper presented at the Third International Conference on Finite Elements in Water Resources, Univ. Miss., Oxford, May 1980.

Fritz, P. and S.K. Frape (1982): Saline groundwaters in the Canadian Shield - a first overview; Chemical Geology, v. 36, pp. 179-190.

Fuller, J.G.C.M. and J.W. Porter (1969): Evaporite formations and petroleum reservoirs in Devonian and Mississippian of Alberta, Saskatchewan and North Dakota; American Association of Petroleum Geologists Bulletin, v. 53, pp. 909-926.

Gloyna, E.F. and T.D. Reynolds (1961): Permeability measurements of rock salt; Journal of Geophysical Research, v. 66, pp. 3913-3921.

Grayston, L.D., D.F. Sherwin and J.F. Allan (1964): Middle Devonian; in Geological history of western Canada (R.G. McCrossan and R.P. Glaister, editors), Alberta Society of Petroleum Geologists, pp. 49-59.

Gross, A.A. (1980): Mannville channels in east-central Alberta; in Lloydminster and beyond: geology of Mannville hydrocarbon reservoirs (L.S. Beck, J.E. Christopher and D.M. Kent, editors), Saskatchewan Geological Society, Special Publication 5, pp. 33-63.

Gupta, S.K., C.R. Cole, F.W. Bond and A.M. Monti (1984a): Finite-element three-dimensional groundwater (FE3DGW) flow model formulation, program listings and users' manual; Pacific Northwest Laboratory, Richland, Washington.

Gupta, S.K., C.R. Cold and G.F. Pinder (1984b): A finite-element three-dimensional groundwater (FE3DGW) model for a multiaquifer system; Water Resources Research, v. 20, no. 5, pp. 553-563.

Hamilton, W.N. (1971): Salt in east-central Alberta; Bulletin 29, Alberta Research Council.

Harrison, D.B., R.P. Glaister and H.W. Nelson (1981): Reservoir description of the Clearwater oil sand, Cold Lake, Alberta, Canada; in The future of heavy crude and tar sands; New York: McGraw Hill, pp. 264-297.

Hill, G.A., W.A. Colburn and J.W. Knight (1961): Reducing oil-finding costs by use of hydrodynamic evaluations; in Economics of Petroleum Exploration, Development and Property Evaluation, Prentice-Hall Inc., Englewood Cliffs, New Jersey, pp. 38-69.

Hitchon, B. (1964): Formation fluids; in Geological History of Western Canada (R.G. McCrossan and R.P. Glaister, editors), Alberta Society of Petroleum Geologists, pp. 201-217.

Hitchon, B. (1969a): Fluid flow in the Western Canada Sedimentary Basin. 1. Effect of topography; Water Resources Research, v. 5, pp. 460-469.

Hitchon, B. (1969b): Fluid flow in the Western Canada Sedimentary Basin. 2. Effect of geology; Water Resources Research, v. 5, pp. 460-469.

Hitchon, B. (1984): Geothermal gradients, hydrodynamics and hydrocarbon occurrences, Alberta, Canada; American Association of Petroleum Geologists Bulletin, v. 68, no. 6, pp. 713-743.

Hitchon, B. and M.E. Holter (1971): Calcium and magnesium in Alberta brines; Alberta Research Council, Economic Geology Report No. 1, 39 pp.

Hitchon, B., A.A. Levinson and M.K. Horn (1977): Bromide, iodide and boron in Alberta Formation waters; Alberta Research Council, Economic Geology Report No. 5, 25 pp.

Hitchon, B., C.M. Sauveplane, S. Bachu, E.H. Koster and A.T. Lytviak (1987): Hydrogeology of the Swan Hills area, Alberta: evaluation for deep waste injection. Alberta Research Council Bulletin. (in preparation).

Hubbard, R.J., J. Pape and D.G. Roberts (1985): Depositional sequence mapping as a technique to establish tectonic and stratigraphic framework and evaluate hydrocarbon potential on a passive continental margin; in Seismic stratigraphy II: an integrated approach (O.R. Berg and D.G. Woolverton, editors), American Association of Petroleum Geologists Memoir 39, pp. 79-92.

Jackson, P.C. (1984): Paleogeography of the Lower Cretaceous Mannville Group of western Canada; in Elmworth - Deep basin gas field (J.A. Masters, editor), American Association of Petroleum Geologists Memoir 38, pp. 49-77.

Kansas Geological Survey (1978): Surface II graphics system.

Kertin, J., H. Khalifa Ezzat and R.J. Correia (1981): Tables of the dynamic and kinematic viscosity of aqueous NaCl solutions in the temperature range 20-150'C and the pressure range 0.1-35MPa, Journal of Physical Chemistry, v. 10, no. 1, pp. 71-87.

Lusczynsky, N.J. (1961): Head and flow of ground water of variable density. Journal of Geophysical Research, v. 54, no. 12, pp. 4247-4256.

Matheron, G. (1967): Elements pour une theorie des milieux poreux, Masson et Cie (ed.), p. 166.

McCrossan, R.G. and R.P. Glaister (1964): Geological history of western Canada; Alberta Society of Petroleum Geologists.

Mossop, G.D., J.W. Kramers, P.D. Flach and B.A. Rottenfusser (1981): Geology of Alberta's oil sands and heavy oil deposits; in The future of heavy crude and tar sands; New York: McGraw Hill, pp. 197-207.

O'Connell, S.C. (1985): The geology of resource characterization of the lower and mid Mannville Formations of the south Lloydminster heavy oil trend, Alberta; Alberta Research Council Publication.

Parsons, W.H. (1973): Alberta; Canadian Society of Petroleum Geologists Memoir 1, Future petroleum provinces of Canada, pp. 73-120.

Peaceman, D.W. (1983): Interpretation of well-block pressures in numerical reservoir simulation with nonsquare grid blocks and anisotropic permeability. Society of Petroleum Engineers Journal, v. 23, no. 3, pp. 541-543.

Porter, J.W., R.A. Price and R.G. McCrossan (1982): The Western Canada Sedimentary Basin; Philosophical Transactions of the Royal Society of London, Series A, v. 305, pp. 169-192.

Pugh, D.C. (1973): Subsurface Lower Paleozoic stratigraphy in northern and central Alberta; Geological Survey of Canada, Paper 72-12.

Putnam, P.E. (1982): Aspects of the petroleum geology of the Lloydminster heavy oil fields, Alberta and Saskatchewan; Bulletin of Canadian Petroleum Geology, v. 30, no. 2, pp. 81-111.

Rudkin, R.A. (1964): Lower Cretaceous; in Geological History of Western Canada (R.G. McCrossan and R.P. Glaister, editors), Alberta Society of Petroleum Geologists, Calgary, pp. 156-168.

Simpson, F. (1975): Marine lithofacies and biofacies of the Colorado Group (middle Albian to Santonian) in Saskatchewan; in The Cretaceous system in the western interior of North America (W.G.E. Caldwell, editor), Geological Association of Canada, Special Paper 13, pp. 553-588.

Stelck, C.R. (1975): Basement control of Cretaceous and sequences in western Canada; in The Cretaceous system in the western interior of North America (W.G.E. Caldwell, editor), Geological Association of Canada, Special Paper 13, pp. 427-440.

Stoakes, F.A. (1982): Evolution of the Frasnian regressive phase of western Canada (abstract); in Major controls on Devonian stratigraphy and sedimentation: Conference Proceedings; Canadian Society of Petroleum Geologists.

Tilley, B.J. (1984): Cold Lake south - heavy oil deposits; in Oil sands geology studies of the Alberta Research Council, Internal Report, pp. 59-75.

Wendte, J.C. (1982): Evolution of the Frasnian transgressive phase of western Canada; Conference abstract, Canadian Society of Petroleum Geologists.

Wightman, D.M. and T. Berezniuk (1985): Resource characterization of the Clearwater Formation Cold Lake oil sands deposits, east-central Alberta; Alberta Research Council Publication.

Williams, G.D. (1963): The Mannville Group (Lower Cretaceous) of central Alberta; Bulletin of Canadian Petroleum Geology, v. 11, pp. 350-368.

Williams, G.D. and C.R. Stelck (1975): Speculations on the Upper Cretaceous paleogeography of North America; in The Cretaceous system in the western interior of North America (W.G.E. Caldwell, editor), Geological Association of Canada, Special Paper 13, pp. 1-20.

APPENDIX A

DATA BASE AND DATA PROCESSING

Stefan Bachu, Andre T. Lytviak and Claude M. Sauveplane

INTRODUCTION

In general, there is a great wealth of data regarding the subsurface environment in the Western Canada Sedimentary Basin, and in the Cold Lake study area in particular, due to the exploration and exploitation of hydrocarbon resources. The data are very diverse, and sometimes even the form of presentation varies for the same type of information.

In the Cold Lake study area, as defined for the purpose of this study, there are about 2200 wells in Saskatchewan, and more than 12 000 wells in Alberta. The examination and processing of the information at these wells cannot be performed manually. The acquisition and handling of all the pertinent information requires an automatic system for data management and data processing. This system has to be integrated in such a way as to provide synthesized information needed by the numerical model for the simulation of injection. A diagrammatic representation of the data processing system is shown in figure A1. Basically, the system has at its core a data base for the storage and management of all pertinent information. The large volume of data involved in this type of work requires a systematic, consistent, and ongoing commitment to the acquisition and management of raw data, as well as retention and management of the results of some standard initial calculations, interpretations and syntheses.

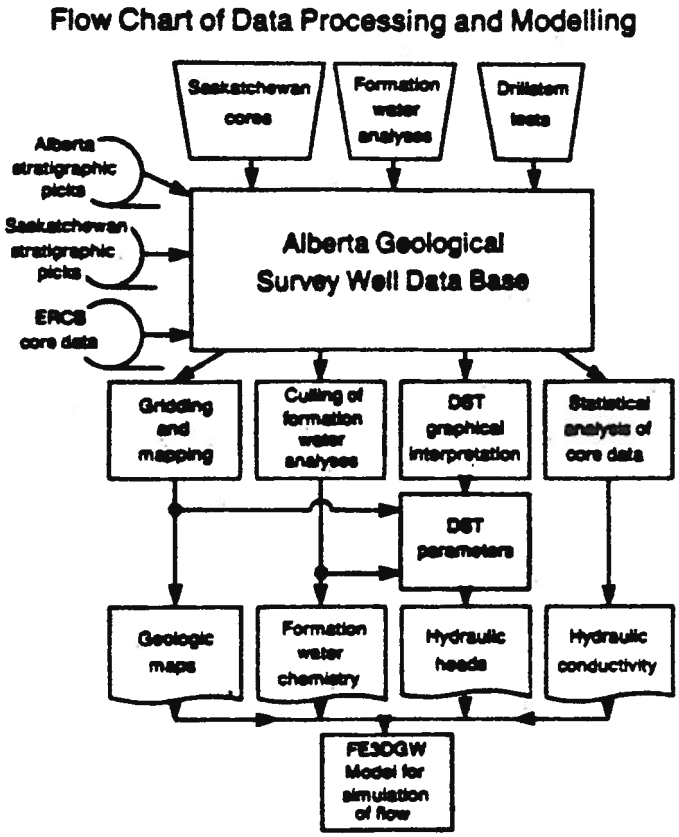

Figure A1. Flow chart of the data processing system used to process the hydrogeological information in the Cold Lake area

There are various inputs into the the data base, depending not only on the type of information but also on its source. Though much information is available from provincial regulatory agencies, such as the Energy Resources Conservation Board (ERCB) and Saskatchewan Energy and Mines (SEM), there are many differences in data from these sources. These differences can be in definitions and units of measure of data elements, in the parameters available, in the storage and distribution media, in currency, or in methods of parameter determination. For example, the ERCB electronic data bases contain core analysis results, whereas these analyses are available from SEM only on microfiche. Some elements of ERCB drillstem test data such as tested interval, recovered fluids, and total test length, are available in electronic form; other elements, such as the time-pressure curves, are available only in hardcopy. ERCB formation water chemistry is available only in paper copy. The SEM data may be given in either SI or British units. SEM codes for stratigraphic units are different from those of the ERCB. Further, the list of possible units in the two data bases is different.

Different types of data are extracted from the data base on sequential files using various criteria for screening and selection. The information contained in these files is processed into a synthesized form to provide a base for an analysis of the natural flow regime and as input into the numerical model FE3DGW. The development and set-up of this automatic system for data management and data processing allows the examination and interpretation of almost all the pertinent information extant in the study area. Figure A2 presents, as bar charts, the amounts of data processed for this study.

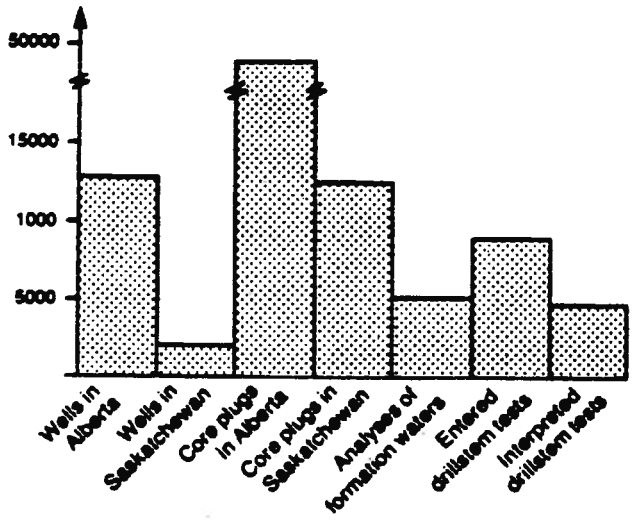

Figure A2. Diagrammatic representation of the amount of data processed to define the natural hydrogeological regime in the Cold Lake area

DATA BASE

Prior to this study, the management, standardization, analysis and access to this type of data was performed by software designed and written by the Basin Analysis Group using the FORTRAN programming language as implemented on VAX/VMS. This system was designed to support the initial Cold Lake project (Basin Analysis Group, 1985). It was, however, sufficiently general and flexible that it was applied to studies in other areas of Alberta, Saskatchewan, and the Beaufort-Mackenzie Basin.

With the increasingly multidisciplinary nature of many projects undertaken by the Alberta Geological Survey (AGS) it became imperative to be able to interrelate data collected or generated for purposes other than that of the syntheses or studies currently at hand. To maximize the applicability of the tools and expertise developed for the storage, analysis and display of information, as well as to enhance the utility of currently collected data for future purposes, AGS undertook to make the data holdings more compatible among its various groups and programs. In order to facilitate this task, a commercially available data base management system, INGRES, was purchased. The Alberta Geological Survey Well Data Base (AGSWDB) is designed and implemented on INGRES. The purchase of this system and the reimplementation of the well data base has an immediate advantage over the previous system, in that users willing to learn INGRES control languages have access to sophisticated data retrieval and reporting facilities independent of, and in addition to, those implemented by the computing support people. An obvious disadvantage of this reimplementation is that a number of specialized tools, for example the interactive drillstem test evaluation and reporting software, needed to be redesigned and rewritten.

Data base management systems such as INGRES, which implement a relational model, are particularly well suited for the ad hoc exploration of interdependencies among data. This is especially the case where these were not explicitly recognized at the time the data were collected or generated. In order to do this in the case of spatially distributed data, such as well information, it is important to be able to identify and locate each site at which data are collected using a unique identifier. Moreover, the identifiers and locations should be mappable across all the wells, for all data types, from all sources. Thus, one of the very important aims of AGSWDB is to provide a mechanism whereby the data acquired or produced by various groups, programs and projects within AGS can be so interrelated. This mechanism rests on the two central relations: MASTER and LOCATION.

The purpose of the MASTER table is to relate well identifications used by primary data sources to those used in AGSWDB. Most agencies have some method of uniquely identifying a specific well, for example, each well is usually given a name; in addition, some combination of characters and/or digits is assigned to each well as a unique well identifier. AGSWDB uses integer values as a unique identifier. This allows in excess of four billion wells to be identified. In order to avoid complications with record normalization, this identifier was given no inherent physical meaning.

The purpose of the LOCATION table is to locate the well site on the surface of the Earth. The geographic system of latitude and longitude is used for horizontal positioning, and metres above sea level for vertical. Each record also contains an estimate of the resolution of these values.

No other record in AGSWDB contains references to well ID or positional data except relative to that given in the MASTER and LOCATION tables. This allows proper registry of any data records which adhere to this system. In addition to these relations, stratigraphic pick, drillstem test and formation water chemistry data have been implemented in AGSWDB. Each of these is represented by more than one table. The stratigraphic pick data are represented by two kinds of relations. The first is basically a catalog of all the supported stratigraphic units, their various names, as well as their identifiers for AGSWDB purposes. The second type is repeated once for each unit and contains the actual depths at which that unit was picked in a well.

In the previous data base, stratigraphic markers and units were implemented as linked lists reflecting the serial penetration of strata by a well. This record structure implicitly models wells. As the Basin Analysis Group used this information to construct a three-dimensional model of the geological framework, this data was then manipulated to define a series of surfaces. These surfaces, taken together, not only reflect a generally accepted conceptual model of the geological framework (earth model), but are more useful for purposes of the kind of simulations currently done by the Basin Analysis Group. AGSWDB implements the earth rather than the well model for markers and units, in that each unit is stored in a separate table. This makes areal manipulations of stratigraphic information much more straight forward, at the expense of manipulations which depend on downhole relations.

A potential advantage of the AGSWDB model for stratigraphic information is that the "above", "below", and "between" relations are much more straight forward to implement than is the case with the well

model. This arises from the fact that in many wells only some stratigraphic units have actually been picked. Thus, though the subject unit is present, if the reference unit is not picked in the specific well being examined, then these relations cannot be determined.

Drillstem test (DST) data are maintained in 15 types of tables. This makes DST data the most complex type implemented to date. This complexity arises from the fact that the relational model implements variable occurrence one-to-many relations in a less straight forward way than a hierarchical model. DST data contain numerous and nested one-to-many relations. For example, a well may contain any number of DST's, each of which may contain one or more phases, and each of which may again contain one or more measurements of pressure and fluid flow. To complicate matters further, the fluids recovered during the test may vary, and if some of these fluids have been analysed this will be represented in an additional set of relations.

Formation water chemistry data, like DST data, contain one-to-many relations, and thus must be represented by four types of tables. More than one fluid sample may occur per well, more than one constituent may be determined per sample, some constituents can be determined by more than one method, or in the case of total dissolved solids, at more than one temperature.

Though many desirable record types have not yet been implemented in AGSWDB, those which represent a large proportion of the possible relations may be encountered. Implementation of a new record type is relatively straight forward, because in most cases an existing record type can be used as a template.

GENERAL DATA PROCESSING

The point-related information stored in the data base has to be processed at higher levels of knowledge in a synthesized form in order to be able to describe and analyse the fluid flow phenomena in a sedimentary basin. Automatic data processing is "blind" and, therefore, it is very important to have a clear understanding and definition of the algorithms used and of the criteria for selection and/or error detection (Bachu et al., 1987). Manual examination of data is done only when and where possible errors are flagged for checking. As a result, the processing of data from point-value to synthesized information is an iterative hybrid loop. Only a brief outline of the methods and techniques used to process large amounts of data are presented here; a more detailed description can be found in Bachu et al. (1987).

In order to analyse fluid flow in a sedimentary basin, the physical frame has to be described first, that is, the geometry and stratigraphy of the subsurface environment. Therefore, the processing of the stratigraphic data has to precede the processing of the fluid flow data. A series of programs allow for interactive examination of stratigraphic picks on a record-by-record basis, addition or deletion of picks, and correction of formation codes and/or depths. For any rectangular area defined by its coordinates, another series of programs report the stratigraphic picks of any particular group of units, hydraulic data in the area (permeabilities, hydraulic heads, porosities, storativities), measured temperatures and chemical components of formation waters (total dissolved solids, Na (diff.), Ca, Mg, Cl, Br, I, HCO_3, CO_3 SO_4, density, pH). The stratigraphic tops are converted at the same time to

elevations relative to sea level, in order to have a constant reference and to avoid the influence of present topography. The data reported in the sequential files have to pass different culling criteria and logical filters for completeness and consistency.

In conjunction with AGSWDB, a new software package, GEOCRT, is being written. Its purpose is to provide user-friendly, transparent access to AGSWDB for some standard types of queries. GEOCRT presently also processes data into a form suitable for input to the cartographic software, GEOPLTR, and thus suitable for input to the SURFACE II display and manipulation package. Development is currently underway to make GEOCRT itself perform the cartographic, surface display and manipulation functions.

The irregular distribution of points which defines each top or thickness of a formation is then transformed into a regular grid of values and contoured using the SURFACE II software package (Kansas Geological Survey, 1978). Manual examination of the maps allows the detection of possible errors and anomalies in the original data. These data are checked by examination of the well logs and corrected back in the data base if necessary. Usually, there is need for a few passes through all this processing loop before the grids and maps present a satisfactory degree of confidence.

The regular grids of values for stratigraphic surfaces and isopachs are produced automatically by the computer using interpolation and extrapolation techniques, and are based solely on the data distribution. A software package for grid manipulation was designed in order to be able to process the grids according to known information about the subsurface environment. The grids can be interactively accessed and

modified, prescribed by boundaries, and combined through different arithmetic and logical operations. The final result of this data processing procedure is a set of stratigraphic surfaces and isopachs stored on magnetic devices and represented graphically as contour maps, isopachs and cross-sections.

The flow data are processed in a similar way to the processing of stratigraphic data, except that they have to be first assigned to stratigraphic units. This is done using an automatic procedure for interpolation of the point data through the three-dimensional stratigraphic grid structure. After allocation and sorting by stratigraphic units, the point data characterizing flow phenomena are analysed and synthesized to describe the processes in the sedimentary basin. Parameters such as permeability and porosity depend on the solid matrix and are represented by statistical distributions. The variables related to fluid and heat flow, such as hydraulic heads, solute content or temperature, have a continuous variation. For each hydrostratigraphic unit, the point data distribution of variables with continuous variation was converted into a regular grid distribution using the kriging spatial interpolation scheme and analysed for trends.

In the end, all important hydrostratigraphic units were characterized by their position, geometry (isopachs), hydraulic parameters, and chemistry and hydrodynamics of formation waters.

TREATMENT OF HYDRODYNAMIC DATA

Introduction

The treatment of the hydrodynamic data comprises selection, and two levels of processing. This study is based solely on existing information from two sources: the drillstem test and the core analyses results. These results are the raw information to be selected and processed. Little can be done about the three-dimensional distribution of this raw information, nor about its intrinsic quality (deficient measurement or reporting).

The data selection and processing techniques, on the contrary, can have a significant impact on the quality of the final data to be used in the flow analysis. For example, one could (erroneously) use the last shut-in pressure of a drillstem test to calculate hydraulic heads leading to incorrect potentiometric surfaces and a distorted flow analysis. Refinements of the data processing techniques may substantially enhance the quality of the flow regime analysis and, consequently, one should not really separate these aspects from the flow analysis itself. Because of the degree of dependence between the treatment of the data and the end results (potentiometric surfaces, regional values of hydraulic parameters) these should always be presented with a clear explanation on how they have been obtained.

In a gravity-driven and three-dimensional flow system, such as the one prevailing in the considered block of sediments, the natural (steady-state) configuration of the flow is governed by contrasts of hydraulic heads and hydraulic conductivities between hydrogeological

units and by the boundary conditions. If the system is perturbed by injection, its unsteady response cannot be analysed without the knowledge of an additional parameter, namely, the specific storage.

None of these three types of variables/parameters are directly accessible by drillstem test interpretation or core data analysis, that is, further processing is required. Also, they are not intrinsic to the rock but represent characteristics of the (rock+fluid) system and the necessary evaluation of the in situ values of formation water density and dynamic viscosity requires data about the salinity of the formation waters, the pore pressure, and the temperature at the point of interest. The dynamic viscosity is also needed to calculate the permeability from the slope of the Horner straight line.

A computer-based methodology for hydrodynamic data processing needs to be: (1) accurate in its relation to the physico-chemical processes of the flow; (2) consistent so that only comparable interpreted information is generated and used; and (3) efficient because of the sheer size of the data bases of raw information. Such a methodology has been developed and is described in detail in Basin Analysis Group (1985).

The purpose of this part of Appendix A is to describe the main changes that have been made to this prior methodology in order to overcome some of its inherent problems and inaccuracies. Such changes were conducted together with the change of the data base management system; the areas where the modifications are significant comprise the selection of raw data and the evaluation of missing parameters.

It is possible to define two levels of interpretation: the localized or point level, and the regional or synthetic level. For each

of these levels, the hydrodynamic data must be carefully screened in order to eliminate erroneous data and, in some instances, to reduce the amount of unnecessary data processing.

Processing of Point Information

Data Selection

Because the major portion of the core data was available in electronic form, it was not possible to conduct a preselection for units where the data are too densely distributed in order to limit the data entry. Typically, a core analysis determines three components of permeability -- maximum horizontal; at 90 degrees with the maximum in the same horizontal plane; and vertical; porosity is also commonly determined. Thus, at most, one can expect four values of hydraulic parameters measured on an individual plug. Some values of permeability reported are below the threshold of routine laboratory measurements, that is 9.8×10^{-18} m^2 (0.01 md) and were removed as unreliable. Similarly, values of porosity greater than 50 percent were judged too high and removed. These two operations have been the only culling done on the core plug data. For the entire study area, the amount of core plugs considered and effectively used is 46 700.

For some hydrostratigraphic units of the Cretaceous (Upper Mannville and Clearwater aquifers), the amount of drillstem information is such that some culling for point level interpretation was necessary. It was based on two main criteria: (1) the three-dimensional location, and (2) the amount and nature of liquid recovered during the test which,

if abundant and mudless, is a good indication of a good quality drillstem test. Both criteria have been used simultaneously to cull out possible uninterpretable drillstem tests. Only 42 percent of the wells in the study area have drillstem test records; this represents 17 615 drillstem tests in 5945 wells. At the present moment, AGSWDB contains information for 53 percent of these, or 9323 drillstem tests. All drillstem test data for the Paleozoic has been entered, but the data entry has been only selective for the Cretaceous.

Point Data Processing

For the drillstem test data, the major change has been to use the interactive software package developed by the Basin Analysis Group (1985) for Phase I in an incomplete manner, that is, only the graphical interpretation is conducted yielding values of k/μ (or $k/[\mu zT]$ for gas) from the slope of the chosen straight line and after calculation of the flow rate; also, values of the extrapolated pore pressure (extrapolated Horner line for $\log[1+(t/t')]=1$ or for an infinite recovery time t') are obtained without any further processing.

These two interpreted data are the only ones kept in the INGRES data base. Each phase of the drillstem test is considered on its own merit in the newly interpreted data and the operator is not asked to make a judgement as to which of the first or second shut-in slope and intercept should be used in the subsequent calculations. This is made possible because of a new feature that enables one to calculate the flow rate corresponding to the preflow occurring before the first shut-in has

been introduced. The data which were interpreted with the old system have been kept as one value of slope and intercept per drillstem test, and not per phase of a drillstem test.

The point values of pore pressure and k/μ (or $k/[\mu zT]$) are reported from the data base before any further data processing is performed. Based on their three-dimensional location, these data are allocated to the various hydrostratigraphic units of the sedimentary block. Only then are point values of hydraulic head, hydraulic conductivity and specific storage calculated on the basis of the best estimate of fluid characteristics at that location and for that particular hydrostratigraphic unit. The algorithms of Kertin et al. (1981) are used to compute the density and viscosity of the produced liquid for a given set of estimated or measured pressure, temperature and salinity conditions; in the case of produced gas, the values of density and dynamic viscosity are either given, or average (default) values are used; the same is done for the supercompressibility factor z. The error is minimal because of the usually small range of variation for these three gas parameters.

For both formation water and gas, the temperature is estimated from a regular grid of geothermal gradients and the mid-depth of the tested interval. In the case of formation water, the salinity is represented by a regular grid of Cl concentrations for the considered hydrostratigraphic unit.

Hydraulic heads and pressure heads are calculated with the real water density whether the drillstem test produced water or gas; fresh water hydraulic heads are also calculated with a density of 1000 kg/m^3 and used to study the lateral flow in the aquifers (Lusczynsky, 1961).

The radial hydraulic conductivity is calculated from the permeabilities with the real density and dynamic viscosity of the produced formation water.

The point values of specific storage are calculated similarly from the given data of porosity and total compressibility in the drillstem test data base. The real formation water liquid density is obtained as indicated above. Default values (from grid or average) are used when porosity and compressibility are missing for the tested interval.

Two files are created for each hydrostratigraphic unit: one containing point values for hydraulic head, fresh water hydraulic head, pressure head and elevation, all at the depth of the tested interval; the other file contains the logarithm of the point values of permeability, hydraulic conductivity, and specific storage, all expressed in SI units.

In the previous study (Basin Analysis Group 1985), for the core analyses data, the weighted averages based on lengths of plugs analysed were calculated at a point level so that a cored interval was represented by its position and three parameters: (1) the horizontal permeability; (2) the vertical permeability; and (3) the porosity. In order to improve the method and to check if the discrepancies between these results and the drillstem test results observed during Phase I could be dependent on the data processing methodology, two new techniques were considered in this study: (1) the total information from the core plug data are allocated to the formations and processed as such on a regional basis without modifying the three components of permeability, and (2) the coring technique is considered. Tests were conducted on the core plug data of the Upper Mannville aquifer in search of a statistical dependence of the

measurements on the sampling method. The data were separated on the basis of the five categories: "vertical diamond", "unconsolidated", "side-wall", "wireline" and "unknown". The chosen Upper Mannville aquifer contains enough data of each category for a meaningful analysis. Both processing techniques are briefly discussed in the next section on the regional data processing.

Regional Data Processing of Hydraulic Parameters

Core Data

For the core plug data, the following regional statistics are determined for the tnree components of permeability: the minimum, the harmonic average, the geometric average, the 50 percent frequency value on a log-normal frequency plot, the arithmetic average, and the maximum; these regional values are determined for each hydrostratigraphic unit. Because the statistical distribution of permeability is commonly log-normal, both the 50 percent frequency value and the geometric average are usually very close; the more they differ, the less the distribution is log-normal. According to the work of Matheron (1967), the representative regional values are the geometric averages for log-normal distributions of permeability in steady-state two-dimensional (lateral) flow conditions; for three-dimensional flow, the representative regional value is at two-thirds of the distance between harmonic and arithmetic averages. In cases of poor log-normal distributions, one can use, as an approximation, the harmonic average for the low "side" and the arithmetic average for the high "side" of the regional permeability

components. Porosities usually follow a normal distribution; the arithmetic average is the best regional estimate within a given hydrostratigraphic unit; low and high "sides" are approximated by the minimum and maximum point-values, respectively.

Hydraulic conductivities and specific storages of the various units are "synthesized" from the regional values of permeability and porosity given by the above-mentioned statistical averages. Regional (grid) averages are used for the values of formation water density and viscosity to be used in the calculations of the three components of hydraulic conductivity and of the specific storage. These average formation water characteristics are obtained from the point-values determined for the drillstem test data. From the drillstem test raw data, an average value of total compressibility can be obtained for a given unit and these are used, together with the three values of porosity and the average density, to "synthesize" regional values of specific storage. When data on total compressibility are not sufficient, the correlations presented in Earlougher (1977) have been used to obtain literature estimates of this parameter.

The processing of core plug data, rather than weighted averages for cored intervals, has the advantage of being statistically more meaningful; also, cores are rarely cut in the same lithological unit and individual plug permeability and porosity can be more precisely allocated to a given hydrostratigraphic unit than if the entire cored interval as represented by its mid-elevation. The inconvenience of processing the core plugs is that it may require the manipulation of very large files (for example, 28 500 values of plug porosity were examined in the Upper Mannville aquifer). The regional results obtained

with both data processing techniques are compared in Table A1 for the Upper Mannville aquifer and in Table A2 for the more homogeneous Viking aquifer. Both tables indicate very little difference between the two methods used to compute the specific storage. For the hydraulic conductivities, the method of weighted averages often introduces overestimations by a factor of ten or more, especially for the harmonic average. These are related to the homogeneity of the rock material, as shown by the results for the Viking aquifer. In view of these results, it appears worthwhile to do the processing on the core plug data.

As illustrated by figure A3, parallel and not different statistical distributions are evidenced when the coring technique is taken into account. Unavoidable biases exist due to the uneven sizes of the populations; these, however, are not likely to change the overall picture which suggests that the data from different coring methods can be merged regionally.

Drillstem Test Data

Only one value of hydraulic conductivity (referred to as the bulk value) can be determined from drillstem test interpretation. For thick units, where the tested interval partially penetrates the aquifer, this bulk value corresponds roughly to the geometric mean of the three components obtained with the core data. In thinner units, where the flow may be assumed to be radial during the test, the radial hydraulic conductivity is computed as $Kr=(K^2_{max}+K^2_{90})^{1/2}$. These theoretical relations are the basis for a meaningful comparison of the two types of results on a regional scale. Preference is given when the data are

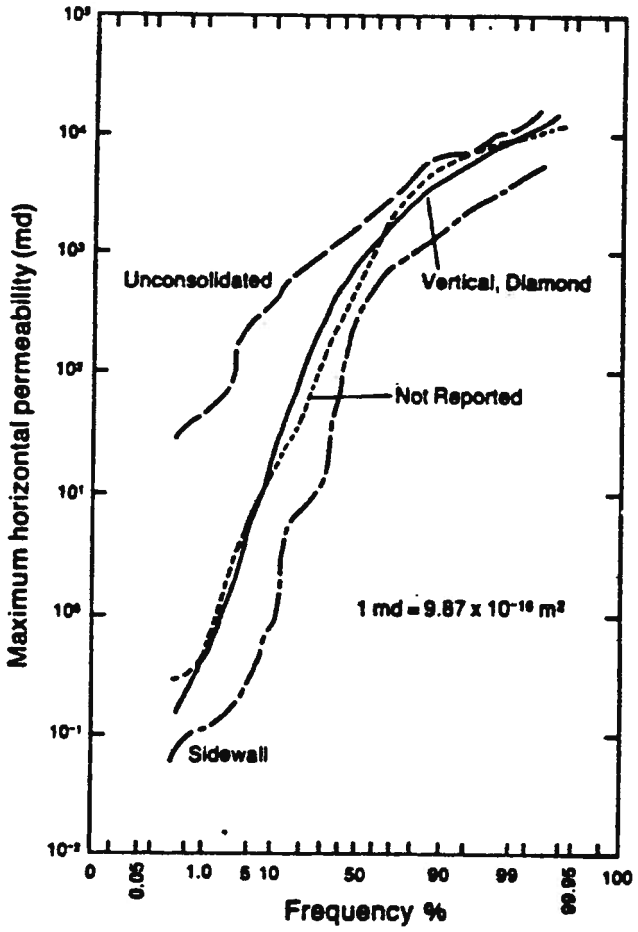

Figure A3. Comparison of the influence of the coring technique on the regional distribution of permeabilities for the Mannville aquifer system

Table A1. Comparison of regional characteristics with two methods of processing the core data for the Upper Mannville aquifer

		Number of Samples	Minimum	Harmonic Average	Geometric Average	50% value on Log-normal Plot	Arithmetic Average	Maximum
K_{max} (m/d)	(1)	8832	1.7×10^{-5}	6.9×10^{-3}	0.32	0.63	1.23	15.00
	(2)	523	6.4×10^{-4}	6.6×10^{-2}	0.87	1.26	2.44	9.10
K_{90} (m/d)	(1)	726	1.7×10^{-5}	3.6×10^{-4}	9.3×10^{-3}	1.7×10^{-2}	0.13	12.30
	(2)	137	6.7×10^{-5}	3.8×10^{-3}	0.61	1.28	1.57	6.40
K_{vert} (m/d)	(1)	657	1.7×10^{-5}	2.6×10^{-4}	3.9×10^{-3}	6.7×10^{-3}	5.7×10^{-2}	1.40
	(2)	39	1.7×10^{-5}	7.6×10^{-5}	4.7×10^{-4}	2.0×10^{-4}	3.7×10^{-2}	0.82
S_s (m^{-1})	(1)	28 504	3.0×10^{-3}	-	-	4.4×10^{-3}	5.5×10^{-3}	8.5×10^{-3}
	(2)	909	1.1×10^{-3}	-	-	5.5×10^{-3}	6.4×10^{-3}	8.0×10^{-3}

K_{max}: maximum horizontal hydraulic conductivity

K_{90}: horizontal hydraulic conducivity at 90° with K_{max}

K_{vert}: vertical hydraulic conductivity

S_s: specific storage

(1) from processing of individual core-plug data

(2) from processing the weighted values per cored interva; the number for S_s (e.g. 909) represents the total number of cored intervals used

* The 50% value is from the normal frequency distribution plot of porosity

Table A2. Comparison of regional characteristics with two methods of processing the core data for the Viking aquifer

		Number of Samples	Minimum	Harmonic Average	Geometric Average	50% value on Log-normal Plot	Arithmetic Average	Maximum
K_{max} (m/d)	(1)	158	4.2×10^{-5}	2.6×10^{-3}	0.28	0.84	1.30	8.32
	(2)	86	8.4×10^{-5}	2.9×10^{-3}	0.20	0.14	1.20	6.70
K_{90} (m/d)	(1)							
	(2)			Insufficient Data				
K_{vert} (m/d)	(1)							
	(2)			Insufficient Data				
S_s (m^{-1})	(1)	321	3.1×10^{-4}	-	-	4.7×10^{-3}	4.4×10^{-3}	6.6×10^{-3}
	(2)	103	7.5×10^{-4}	-	-	3.7×10^{-3}	3.7×10^{-3}	5.7×10^{-3}

(1) from processing of individual core-plug data

(2) from processing the weighted values per cored interval and number for S_s (e.g. 103) represents the total number of cored intervals used

abundant enough from the drillstem test results because they are more representative, less disturbed, and closer to well-injection conditions. The difference in both series of results (from drillstem test and from core) may be explained, in part, by the data processing technique. For the core data, permeabilities and porosities are processed first at the regional level; for the drillstem test, hydraulic conductivities and specific storages are obtained at the point level and then synthesized at the regional level. The processing of the core data in terms of hydraulic conductivity and specific storage is possible, in principle, but was not judged worth the data processing effort in the limited scope of this study.

Regional Data Processing of Hydraulic Heads

These are only obtained from drillstem test results; they are continuous variables and are treated at the regional level with contouring software already described in the previous study (Basin Analysis Group, 1985). Fresh water hydraulic heads are used to study the lateral flow in aquifers. Point water heads, rather than the difficult-to-evaluate "true environmental" head (De Wiest, 1969; Hitchon et al., in preparation), are used on cross-section profiles, together with the local pressure head versus depth plots, to study cross-formational flow. Specific discharges for lateral flow are computed on a regional scale as indicated in the previous study and the same trend analysis is conducted on the potentiometric surfaces.

Conclusion

Although new improvements have been brought to the methodology of data selection and processing, yielding more reliable and consistent results for regional hydrodynamic analysis, the quality of this analysis is still dependent on two crucial factors: the data distribution and density for each hydrostratigraphic unit. The analysis presented in the main text is based on 2951 selected drillstem tests and on effectively all the core-plug data.

APPENDIX B

REGIONAL HYDRODYNAMIC RESULTS

Claude M. Sauveplane

This appendix presents, in table and graph form without comments, the results of the regional data processing for the hydrodynamic data. The format is by hydrostratigraphic unit from the base to the top of the sedimentary block in the Cold Lake study area. Comments are found in the section of the report (main text) where the analysis of the natural flow regime is discussed. Only the aquifer units, for which the data are sufficient, have been considered. Reference is also necessary to the "Treatment of Hydrodynamic Data" in Appendix A.

Table B1.

Hydraulic parameters for hydrostratigraphic units in the Cold Lake area, Alberta, determined from core analyses

Hydrostratigraphic unit		No. of values	Minimum value	Harmonic average	Geometric average	Median value	Arithmetic average	Maximum value
Cambrian	K_M	200	0.000038	0.00200	0.1100	0.23000	1.11000	12.80000
	K_{90}	37	0.000085	0.00200	0.0150	0.01500	0.08400	0.83000
	K_v	22	0.000310	0.00160	0.0052	0.00470	0.02700	0.30000
	S_s	271	0.000017	-	-	0.00027	0.00028	0.00053
Red Beds	K_M	272	0.000017	0.00072	0.0840	0.21000	0.5200	5.30000
	K_{90}	11	0.000150	0.00130	0.0120	-	0.0420	0.13000
	K_v	8	0.000034	0.00017	0.0008	-	0.0002	0.00044
	S_s	299	0.000012	-	-	0.00020	0.0002	0.00044
Winnipegosis	K_M	77	0.000015	0.00007	0.0002	0.00015	0.0220	1.42000
	K_{90}	55	0.000015	0.00005	0.0001	-	0.0006	0.01200
	K_v	11	0.000015	0.00007	0.0003	-	0.0270	0.02400
	S_s	112	0.000019	-	-	0.00056	0.0007	0.00600
Beaverhill Lake	K_M	173	0.000017	0.00007	0.0002	0.00010	0.0023	0.07900
	K_{90}	145	0.000017	0.00006	0.0002	0.00010	0.0020	0.06600
	K_v	57	0.000017	0.00017	0.0005	0.00045	0.0020	0.03100
	S_s	222	0.000012	-	-	0.00040	-	0.00150
Camrose Tongue	K_M	38	0.000290	0.00410	0.1100	0.110000	2.060	26.20000
	K_{90}	43	0.000088	0.00130	0.0420	0.046000	0.590	9.98000
	K_v	36	0.000035	0.00038	0.0029	0.003300	0.033	0.66000
	S_s	44	0.000100	-	-	0.000440	-	0.00089
Grosmont	K_M	434	0.000025	0.00120	0.0460	0.05200	0.550	25.10000
	K_{90}	393	0.000017	0.00062	0.0230	0.02500	0.390	25.10000
	K_v	308	0.000017	0.00026	0.0053	0.00540	0.110	6.08000
	S_s	468	0.000095	-	-	0.00050	-	0.00138
McMurray	K_M	482	0.000110	0.00130	0.4700	0.91000	1.8900	9.90000
	K_{90}	37	0.000240	0.00420	0.0230	0.02500	0.2000	1.40000
	K_v	36	0.000067	0.00079	0.0074	0.00420	0.2400	1.67000
	S_s	1879	0.000360	-	-	0.00810	0.0077	0.01200
Clearwater	K_M	2549	0.000084	0.03200	1.5700	1.67000	2.7900	12.20000
	K_{90}	201	0.000017	0.00010	0.0002	0.00083	0.0340	1.55000
	K_v	261	0.000017	0.00008	0.0007	0.00083	0.3400	4.79000
	S_s	13776	0.000023	-	-	0.00082	0.0008	0.00110
Mannville	K_M	8832	0.000017	0.00590	0.3200	0.63000	1.2300	15.00000
	K_{90}	726	0.000017	0.00036	0.0093	0.01700	0.1300	12.30000
	K_v	657	0.000017	0.00026	0.0039	0.00670	0.0520	1.40000
	S_s	28504	0.003000	-	-	0.00440	0.0055	0.00850
Viking	K_M	158	0.000042	0.00260	0.2800	0.84000	1.3000	8.32000
	K_{90}	-	-	-	-	-	-	-
	K_v	3	0.00033	-	-	-	-	0.30000
	S_s	321	0.003100	-	-	0.00470	0.0044	0.006600

K_M - maximum horizontal hydraulic conductivity

K_{90} - horizontal hydraulic conductivity at 90° angle with K_M

K_v - vertical hydraulic conductivity

S_s - specific storage

Median - 50% value on the log-normal frequency plot for K and on the normal frequency plot for S_s

Permeability values given in (m/d), and specific storage values given in (m^{-1})

Hydraulic parameters for hydrostratigraphic units in the Cold Lake area, Alberta, determined from drillstem tests

Hydrostratigraphic unit		No. of values	Minimum value	Harmonic average	Geometric average	Median value	Arithmetic average	Maximum value
Winnipegosis	K	27	0.000016	0.00030	0.0110	0.01100	0.210	3.46000
Beaverhill Lake	K	44	0.000014	0.00038	0.0073	0.00730	0.0770	0.86000
Camrose Tongue	K	39	0.000290	0.00340	0.0220	0.02200	0.137	1.12000
Grosmont	K	8	0.000200	0.00120	0.0140	0.07300	0.098	0.54000
McMurray	K	137	0.000056	0.00092	0.0300	0.01000	1.52	26.70000
	S_s	186	0.002000	-	-	-	0.0032	0.00430
Clearwater	K	96	0.000018	0.00038	0.0140	0.01000	0.150	0.950
	S_s	118	0.000440	-	-	-	0.00045	0.00047
Mannville	K	1497	0.0000009	0.00013	0.0023	0.00180	0.016	0.860
	S_s	1615	0.0000052	-	-	-	0.00045	0.00047
Viking	K	1167	0.0000010	0.00019	0.0213	0.03460	1.14000	69.1000
	S_s	1226	0.0000021	-	-	-	0.00226	0.03354

K - bulk (radial) hydraulic conductivity

S_s - specific storage

Median - 50% value on the log-normal frequency plot for K and on the normal frequency plot for S_s

Permeability values given in (m/d), and specific storage values given in (m^{-1})

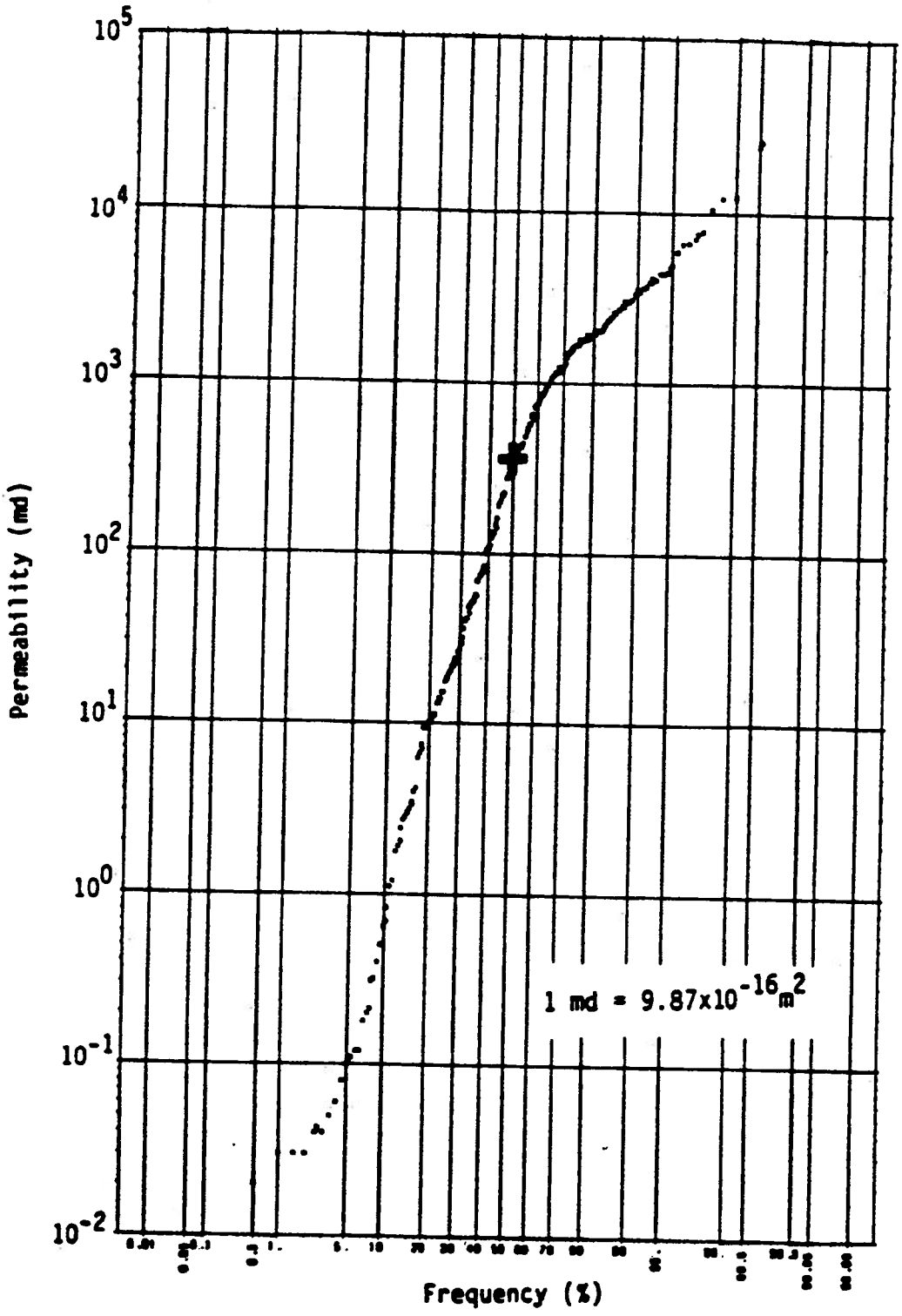

Figure B1 Log-normal cumulative frequency plot for maximum horizontal permeability as derived from core analyses, Basal Cambrian aquifer, Cold Lake study area

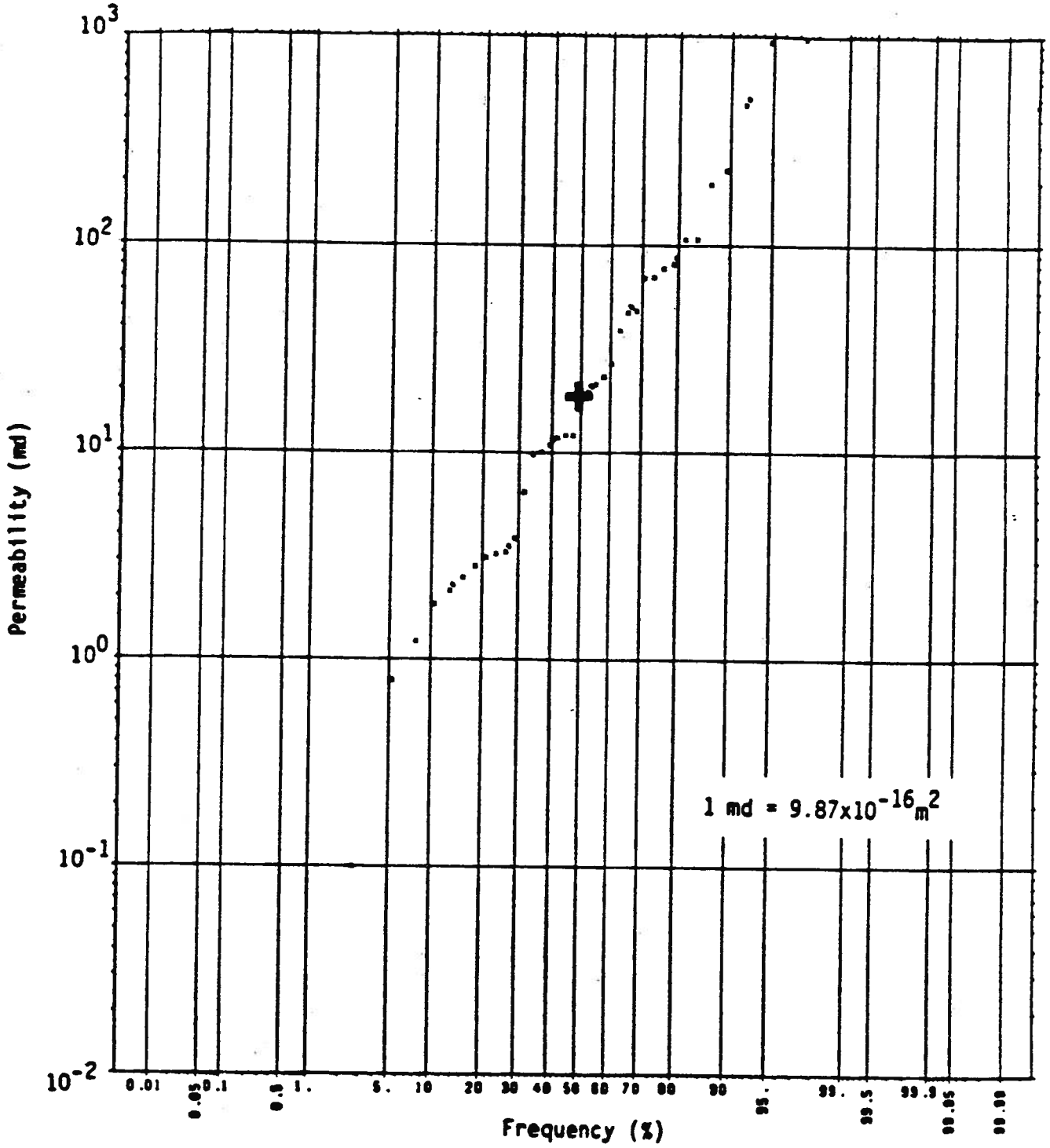

Figure B2 Log-normal cumulative frequency plot for horizontal permeability at 90° with the maximum horizontal as derived from core analyses, Basal Cambrian aquifer, Cold Lake study area

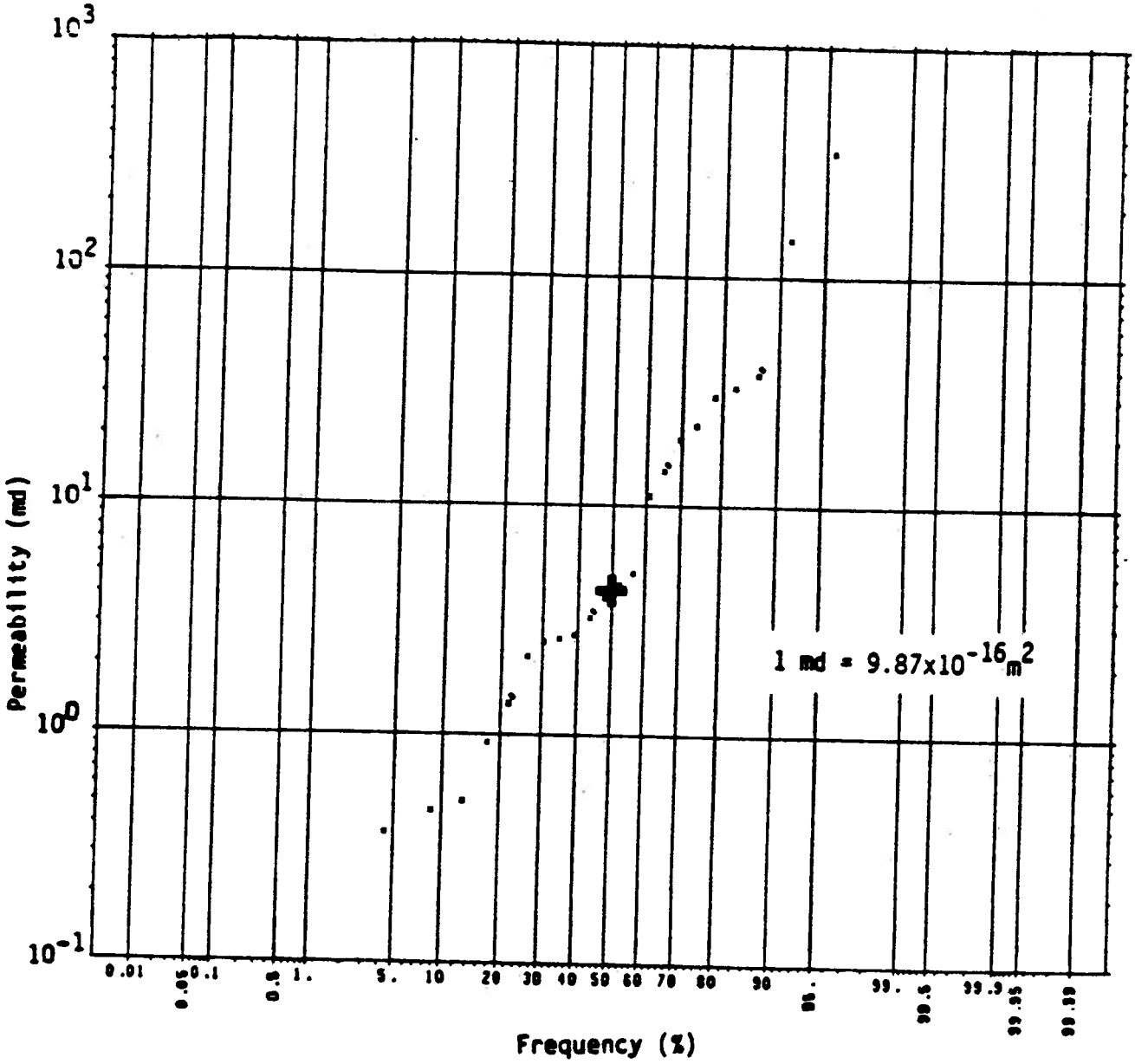

Figure B3 Log-normal cumulative frequency plot for vertical permeability as derived from core analyses, Basal Cambrian aquifer, Cold Lake study area

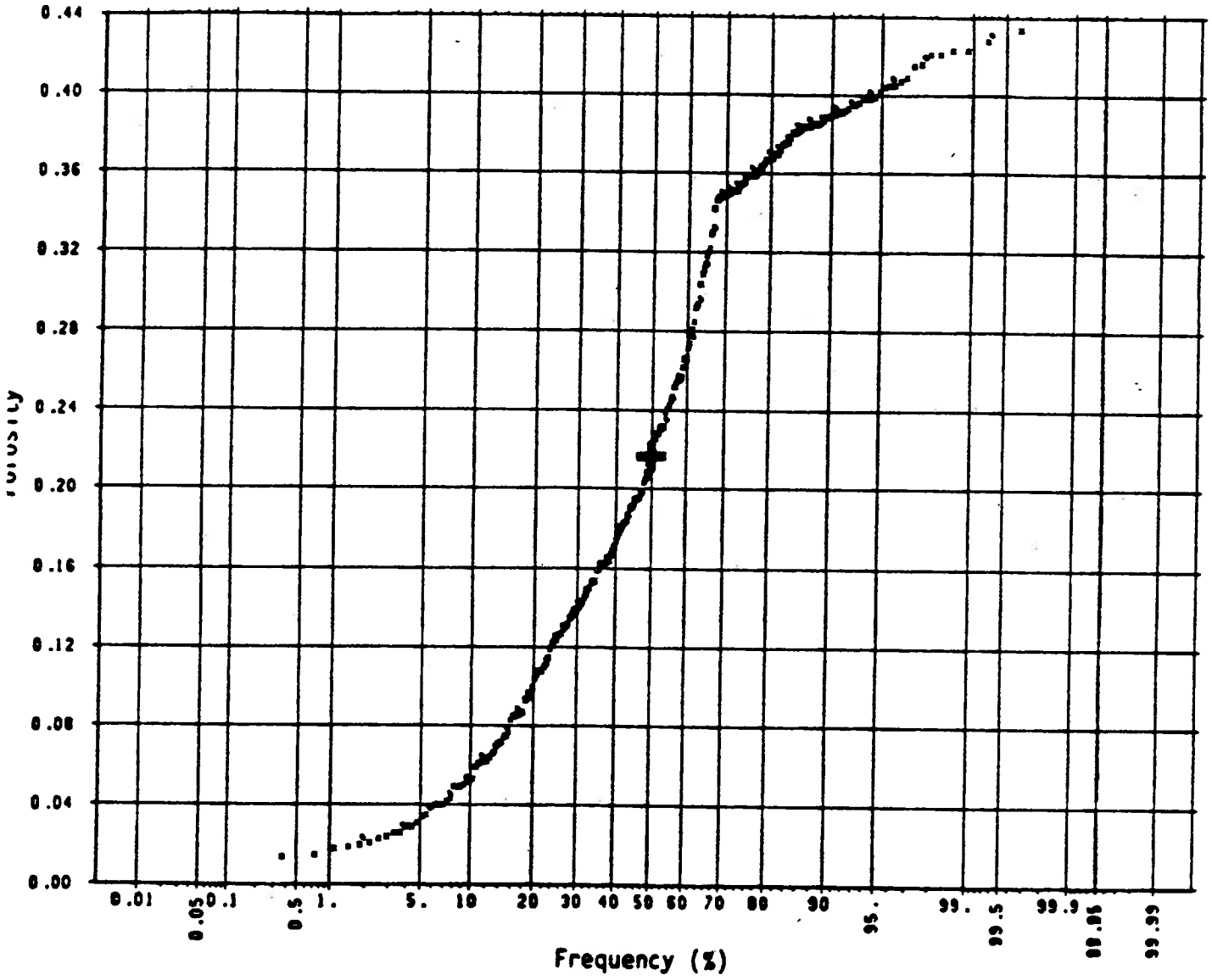

Figure B4 Normal cumulative frequency plot for porosity as derived from core analyses, Basal Cambrian aquifer, Cold Lake study area

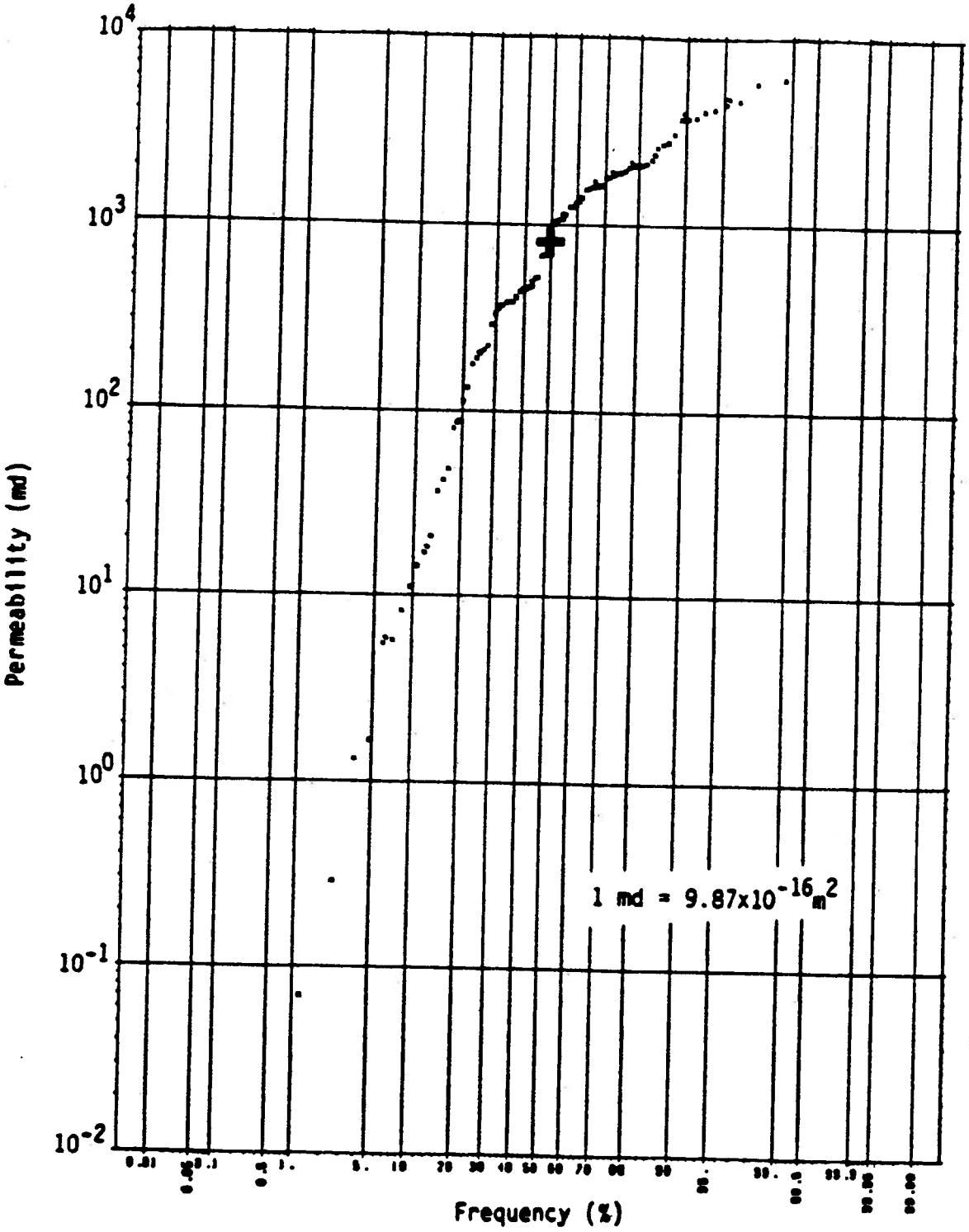

Figure B5 Log-normal cumulative frequency plot for maximum horizontal permeability as derived from core analyses, Cambrian aquifer, Cold Lake study area

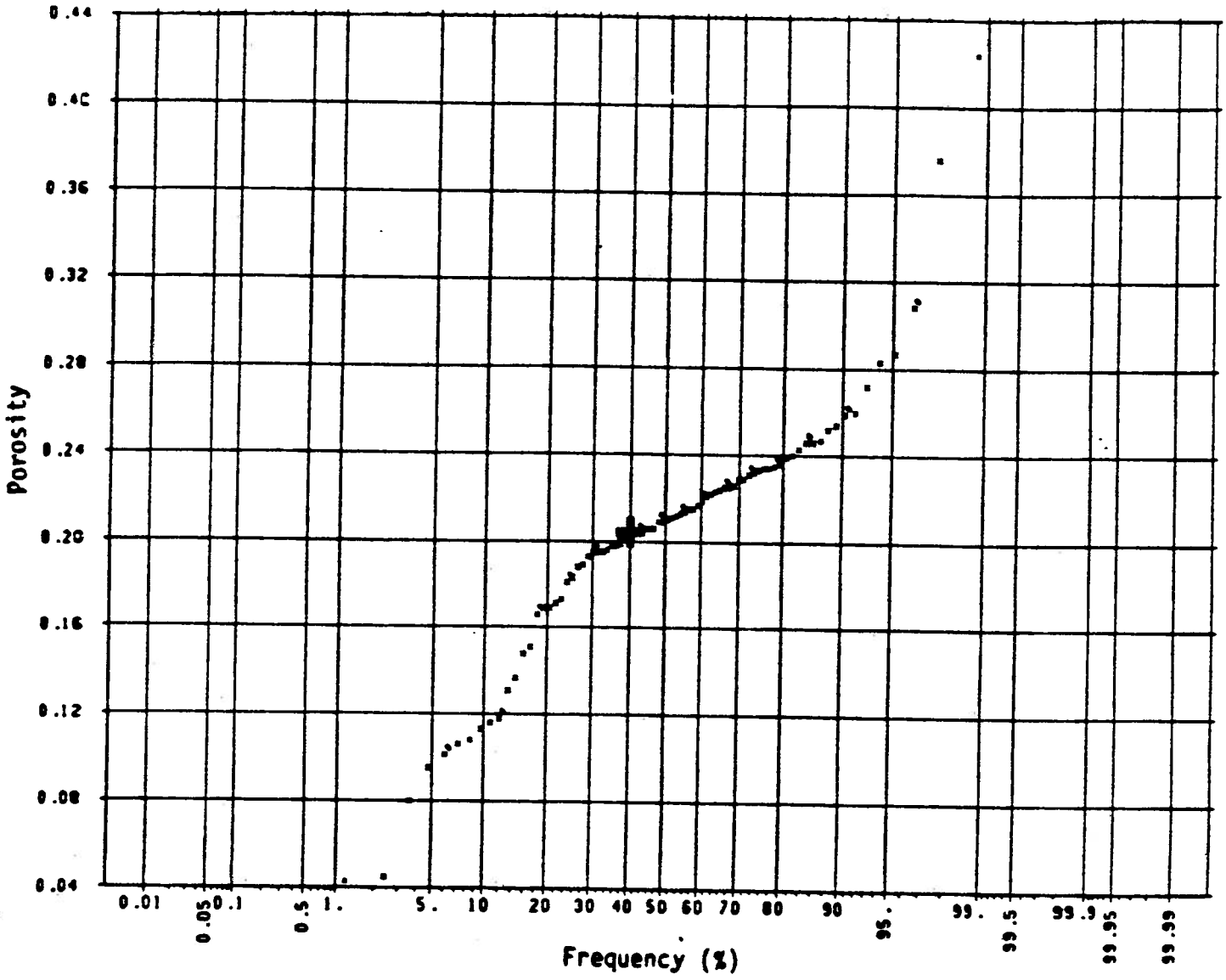

Figure B6 Normal cumulative frequency plot for porosity as derived from core analyses, Cambrian aquifer, Cold Lake study area

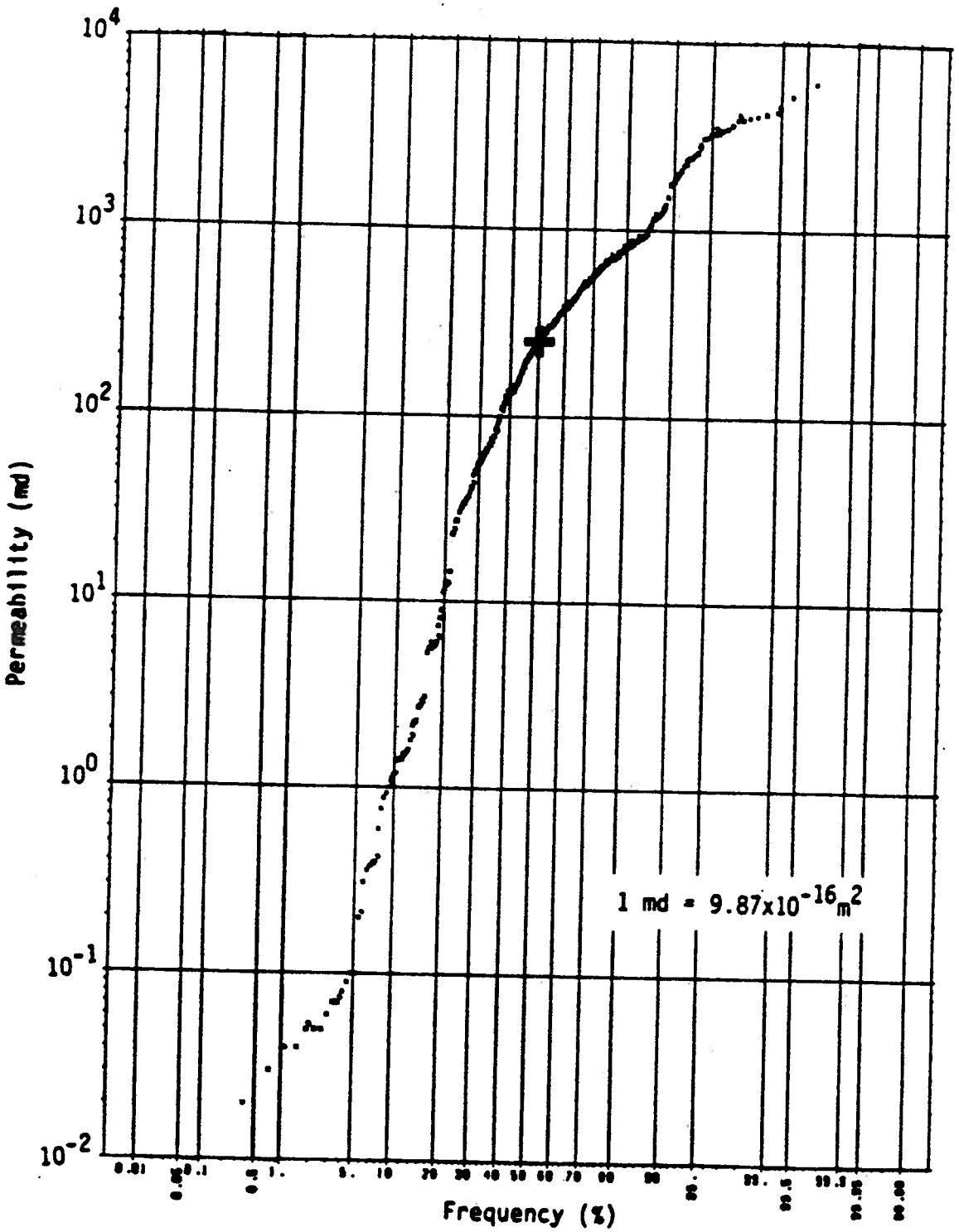

Figure B7 Log-normal cumulative frequency plot for maximum horizontal permeability as derived from core analyses, Basal Red Beds "aquifer", Cold Lake study area

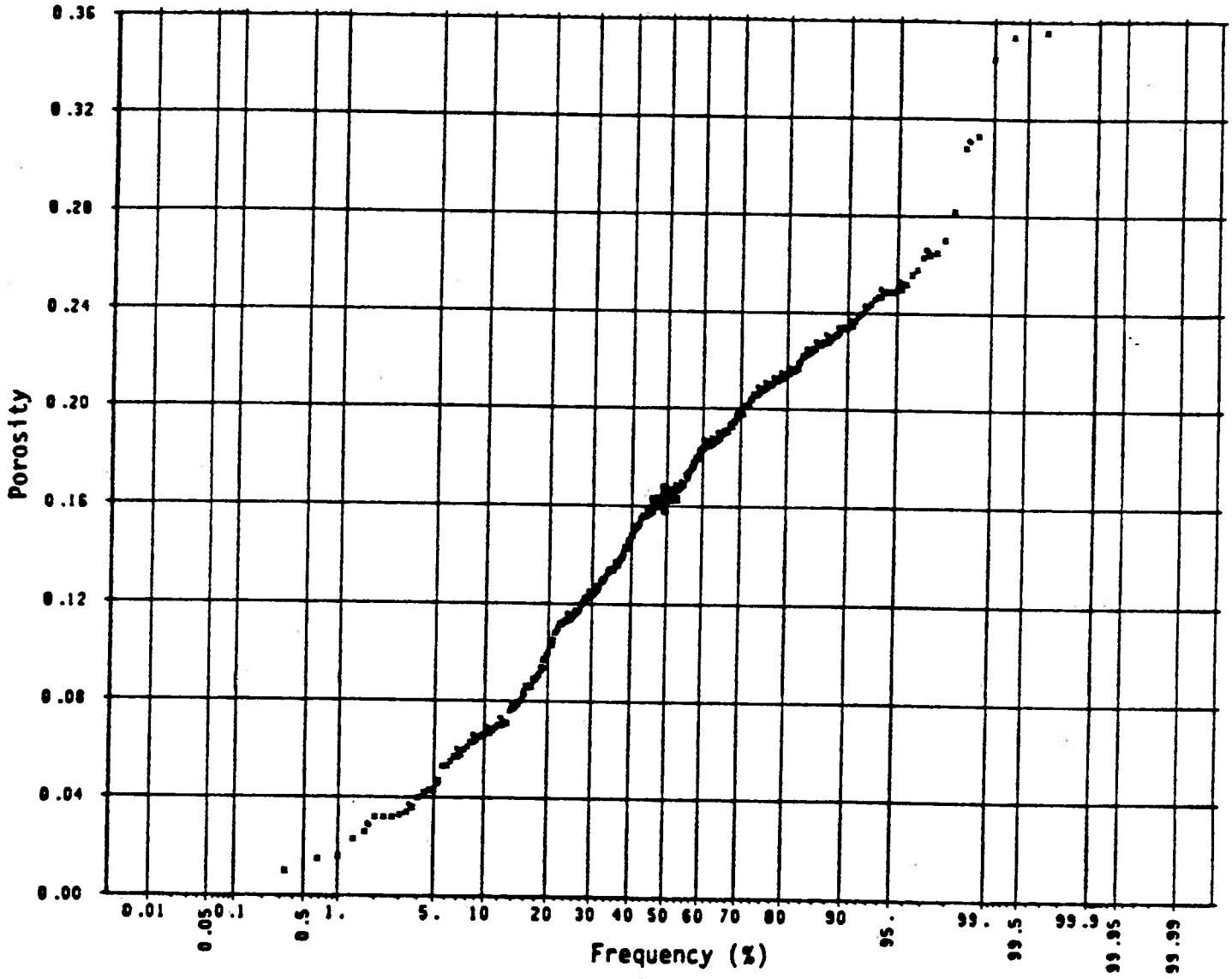

Figure B8 Normal cumulative frequency plot for porosity as derived from core analyses, Basal Red Beds "aquifer", Cold Lake study area

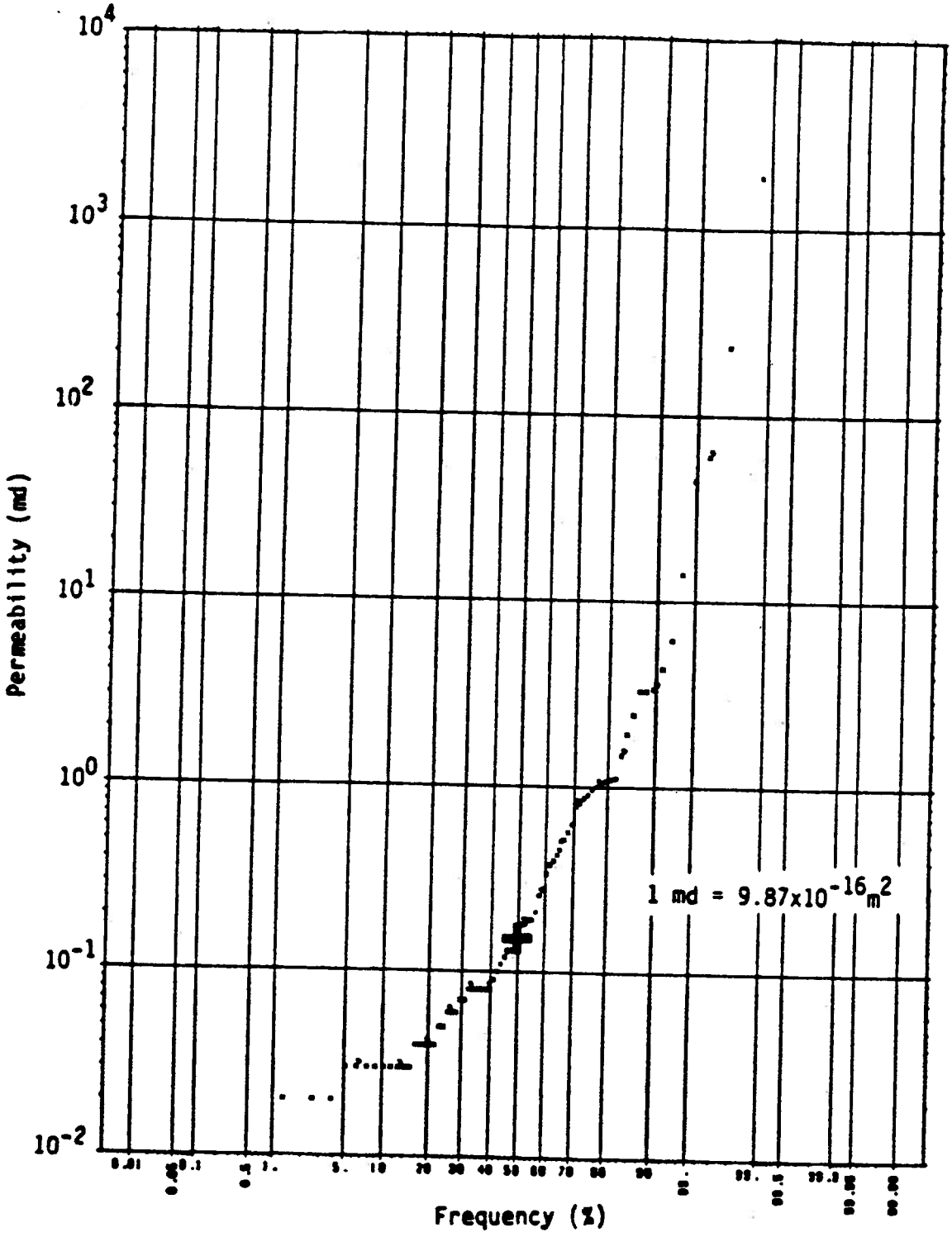

Figure 89 Log-normal cumulative frequency plot for maximum horizontal permeability as derived from core analyses, Winnipegosis aquifer, Cold Lake study area

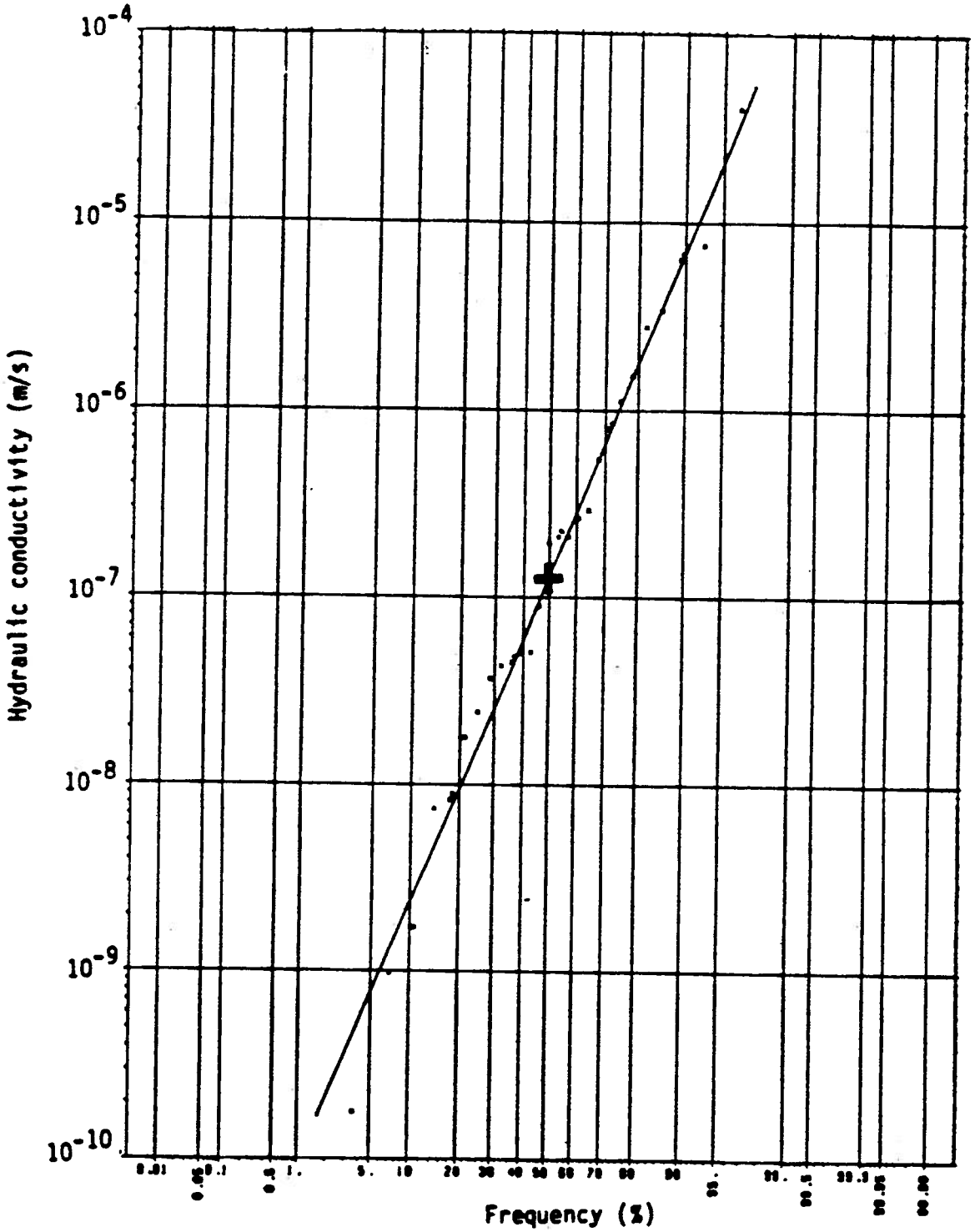

Figure B10 Log-normal cumulative frequency plot for hydraulic conductivity as derived from drillstem tests, Winnipegosis aquifer system, Cold Lake study area

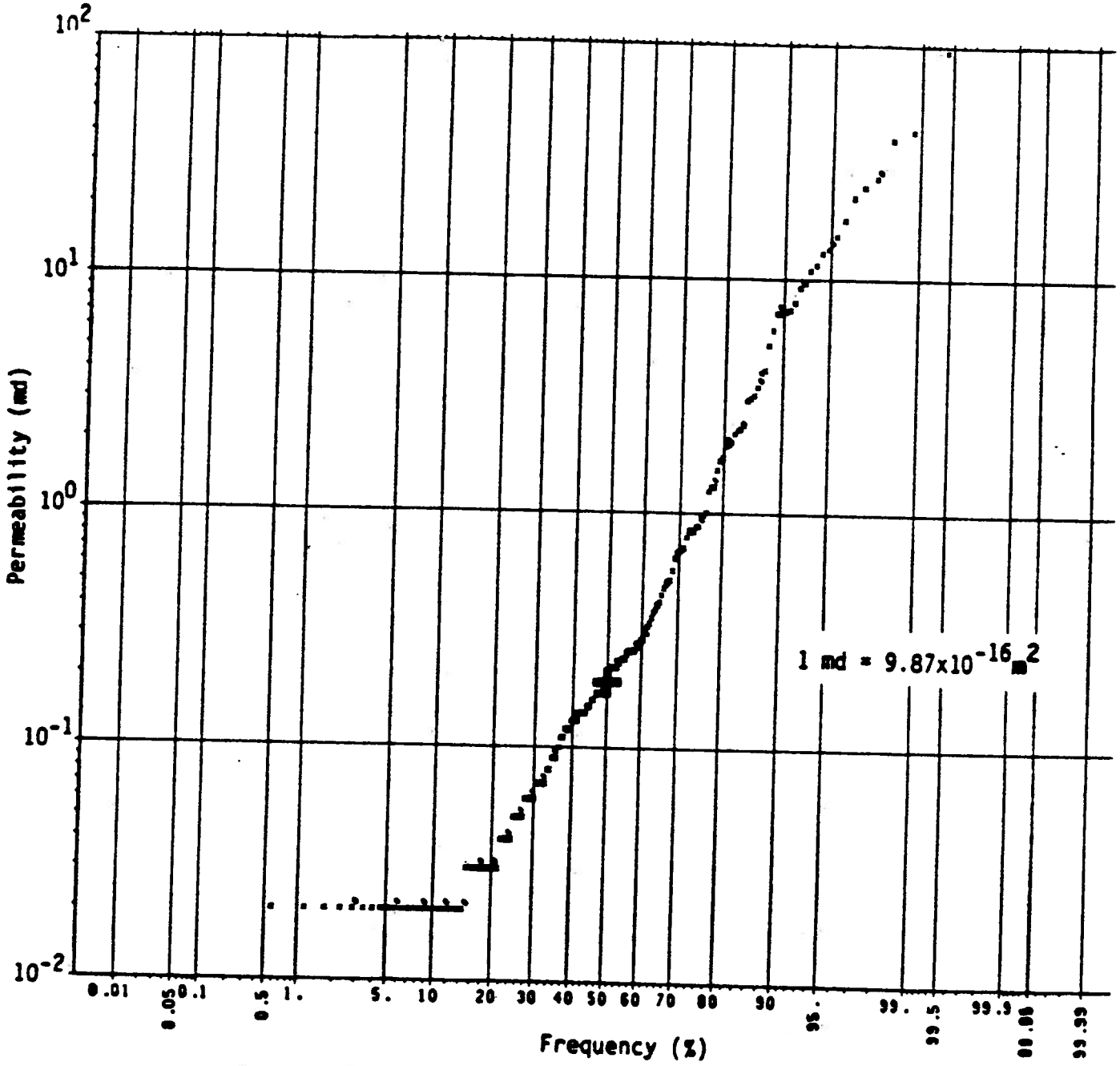

Figure B11 Log-normal cumulative frequency plot for maximum horizontal permeability as derived from core analyses, Beaverhill Lake aquifer, Cold Lake study area

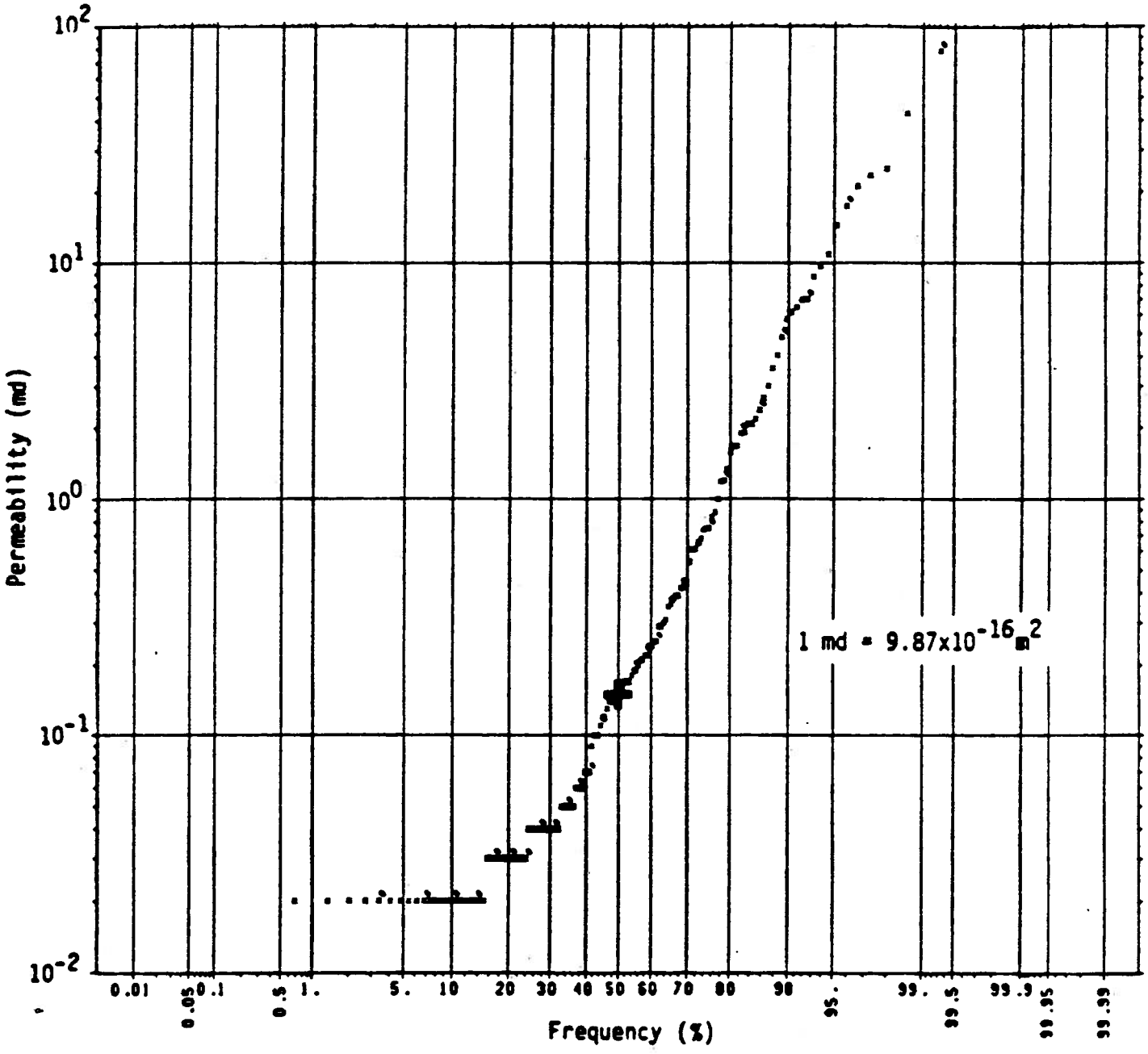

Figure B12 Log-normal cumulative frequency plot for horizontal permeability at 90° with the maximum horizontal as derived from core analyses, Beaverhill Lake aquifer, Cold Lake study area

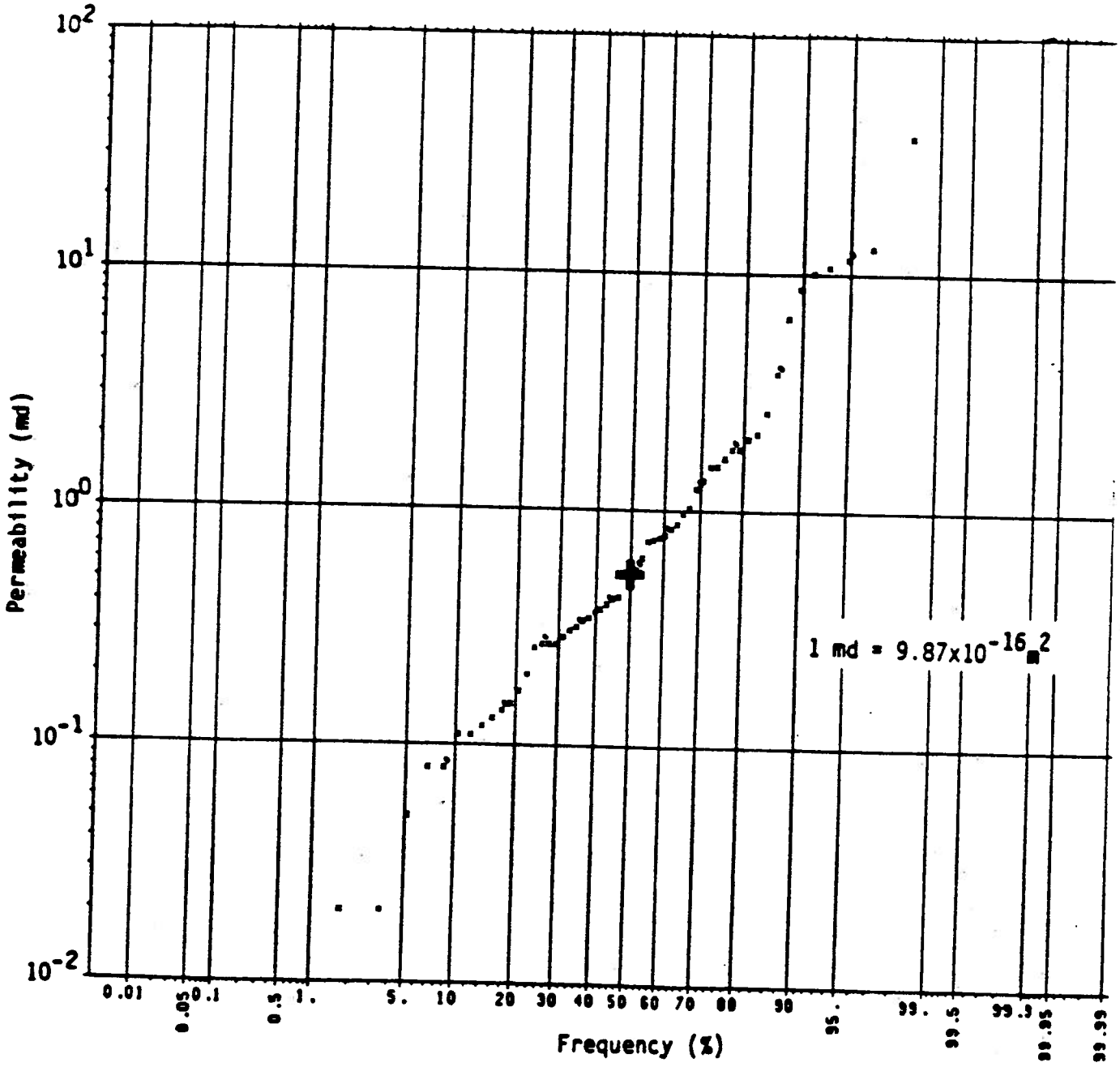

Figure B13 Log-normal cumulative frequency plot for vertical permeability as derived from core analyses, Beaverhill Lake aquifer, Cold Lake study area.

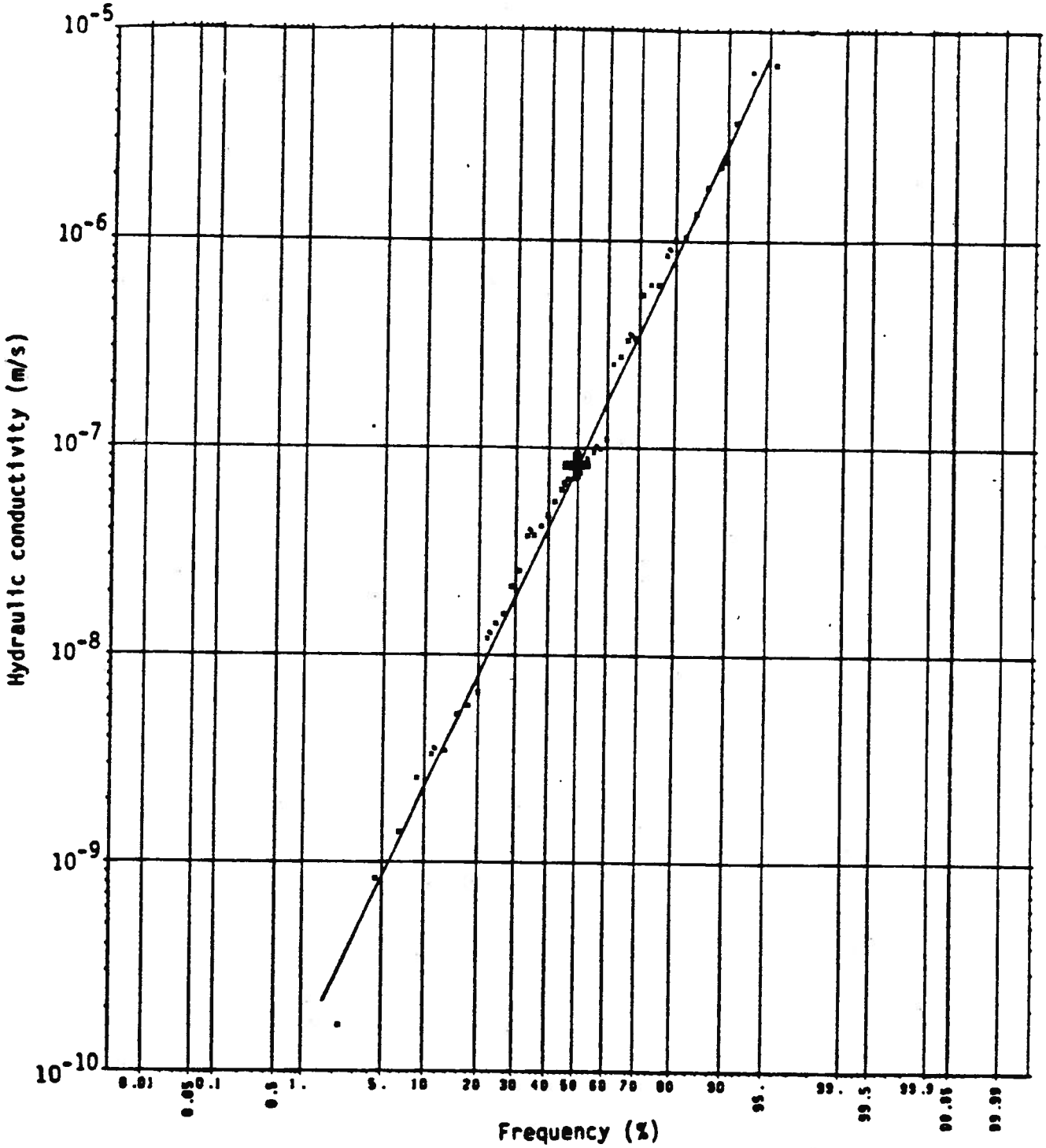

Figure B14 Log-normal cumulative frequency plot for hydraulic conductivity as derived from drillstem tests, Beaverhill Lake aquifer system, Cold Lake study area

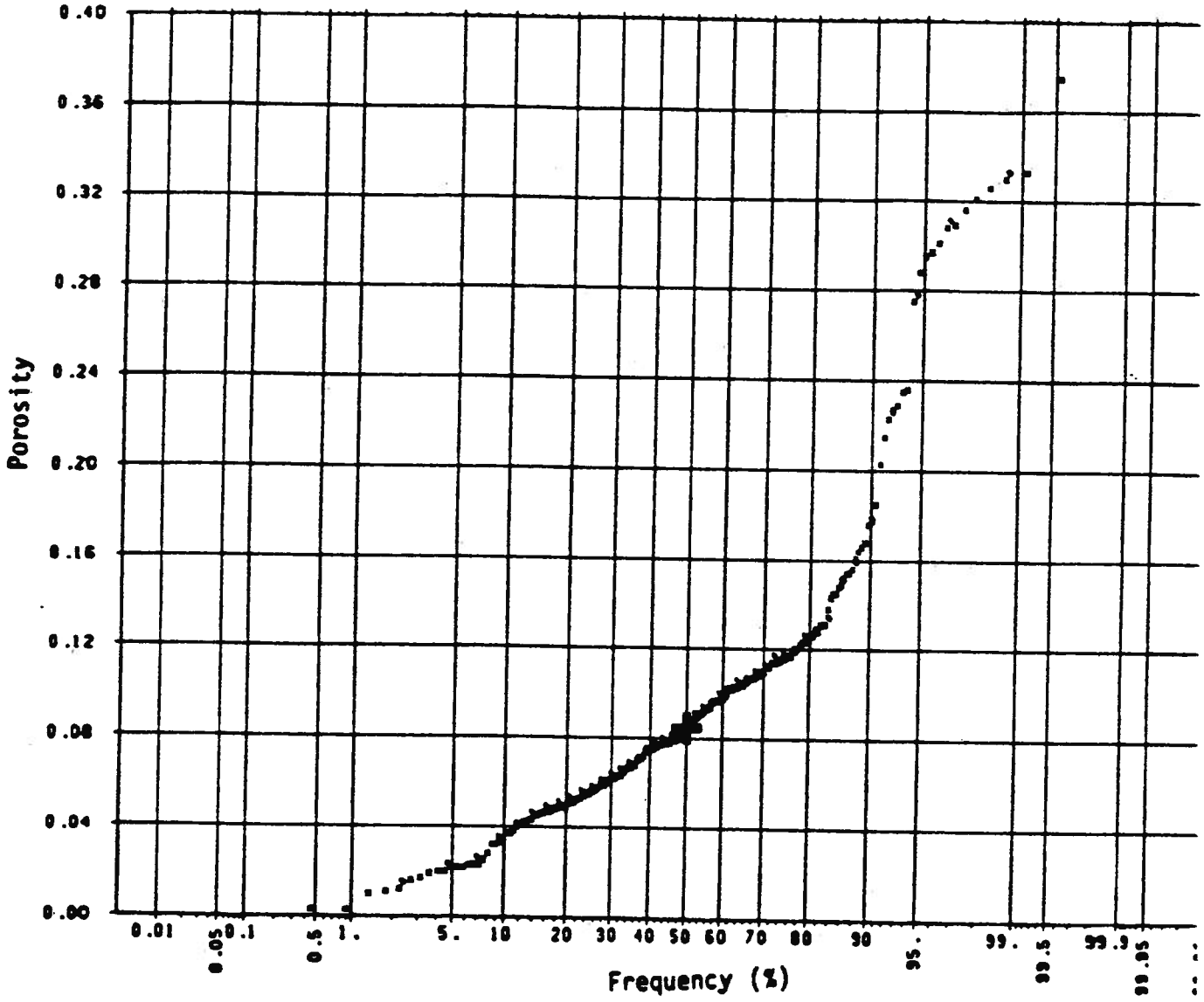

Figure B15 Normal cumulative frequency plot for porosity as derived from core analyses, Beaverhill Lake aquifer, Cold Lake study area

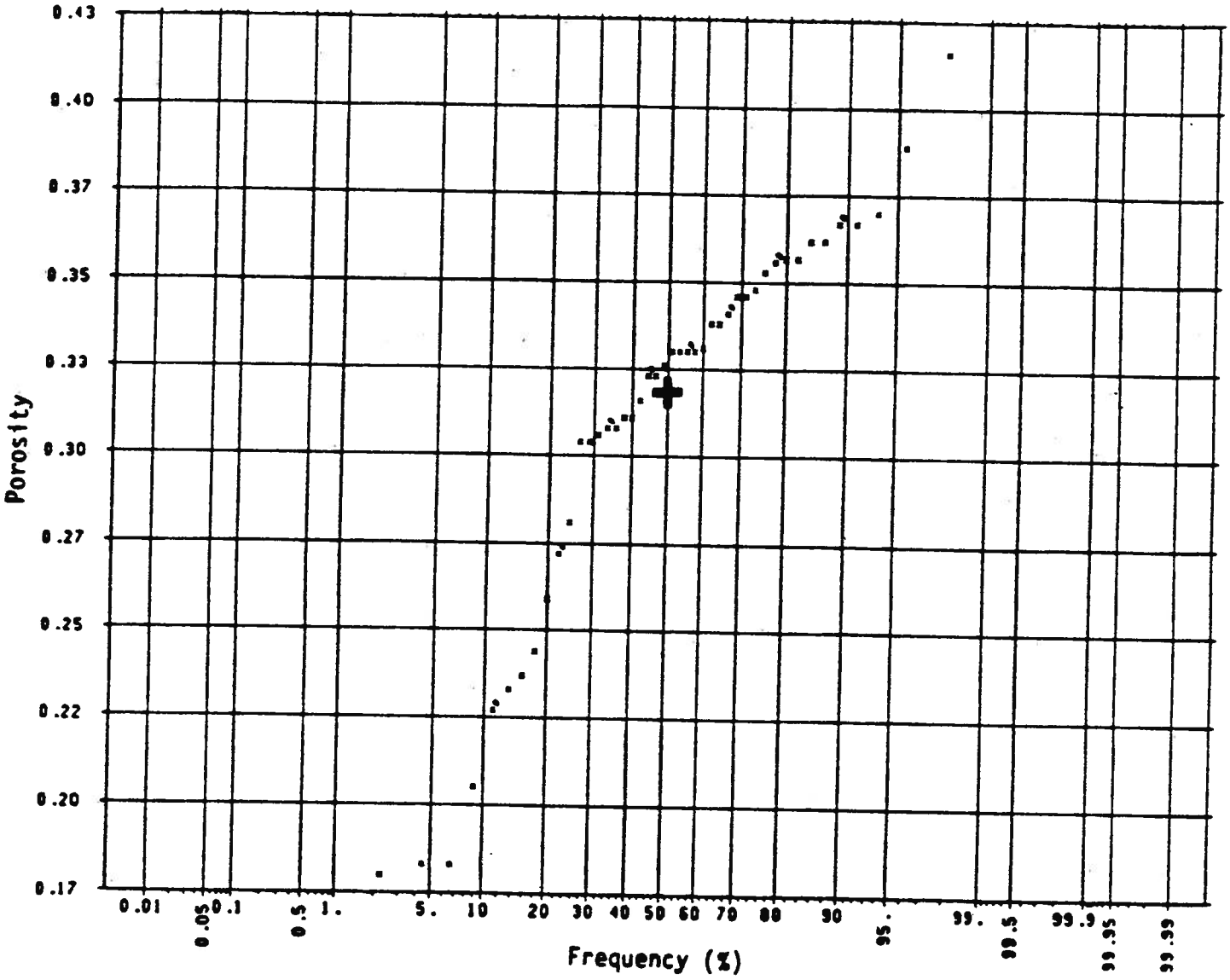

Figure B16 Normal cumulative frequency plot for porosity as derived from core analyses, Cooking Lake aquifer, Cold Lake study area

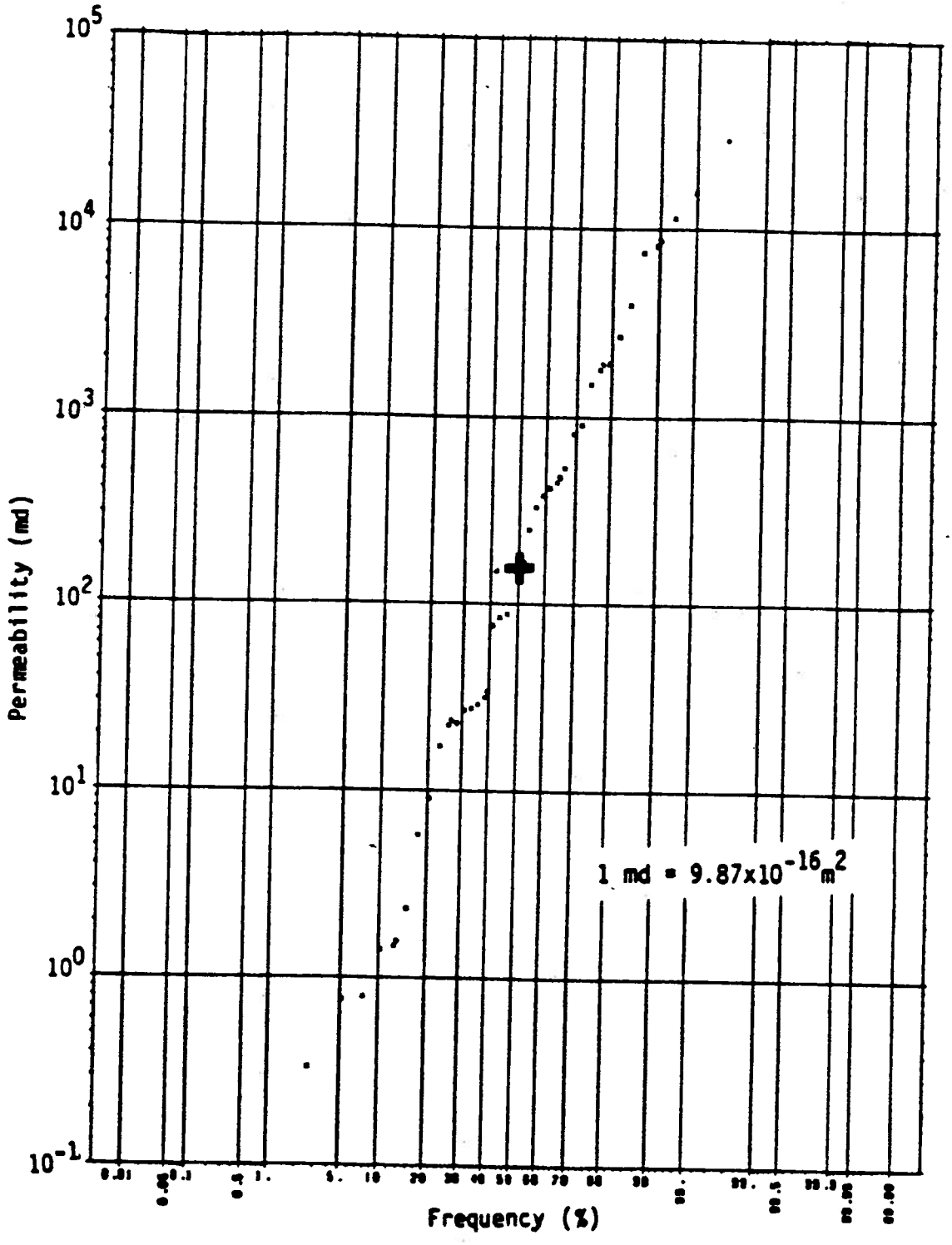

Figure B17 Log-normal cumulative frequency plot for maximum horizontal permeability as derived from core analyses, Camrose Tongue aquifer, Cold Lake study area

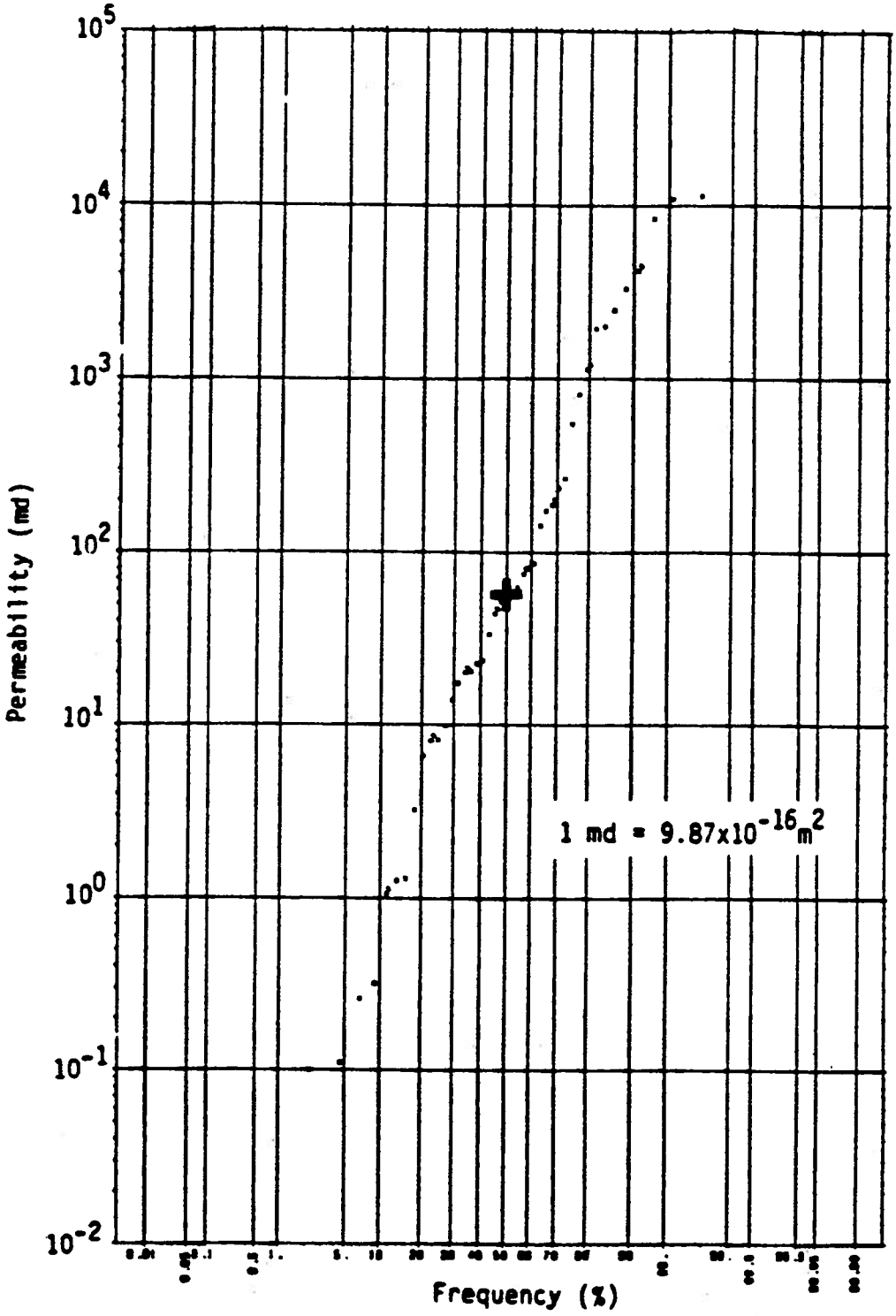

Figure B18 Log-normal cumulative frequency plot for horizontal permeability at 90° with the maximum horizontal as derived from core analyses, Camrose Tongue aquifer, Cold Lake study area

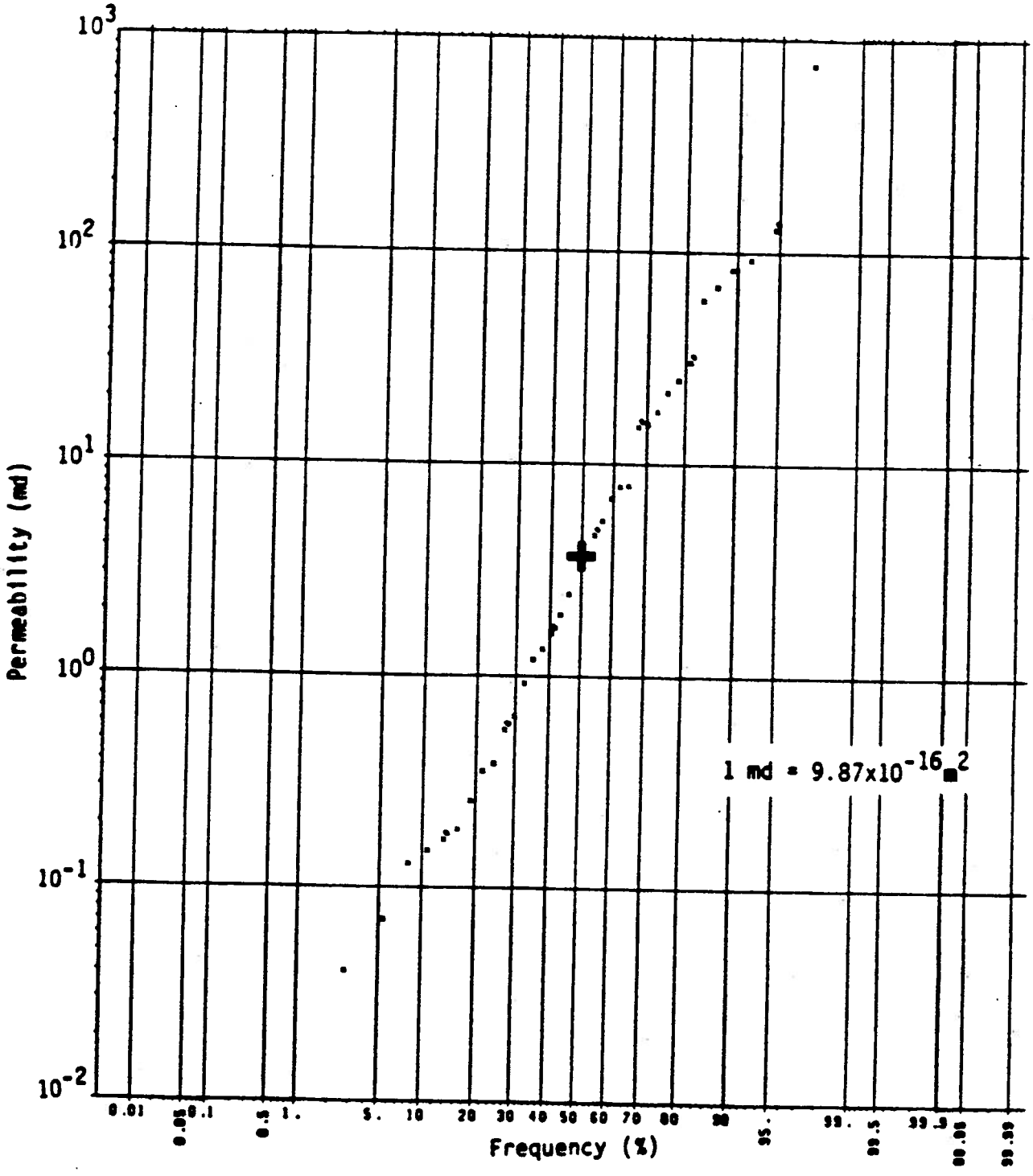

Figure B19 Log-normal cumulative frequency plot for vertical permeability as derived from core analyses, Camrose Tongue aquifer, Cold Lake study area

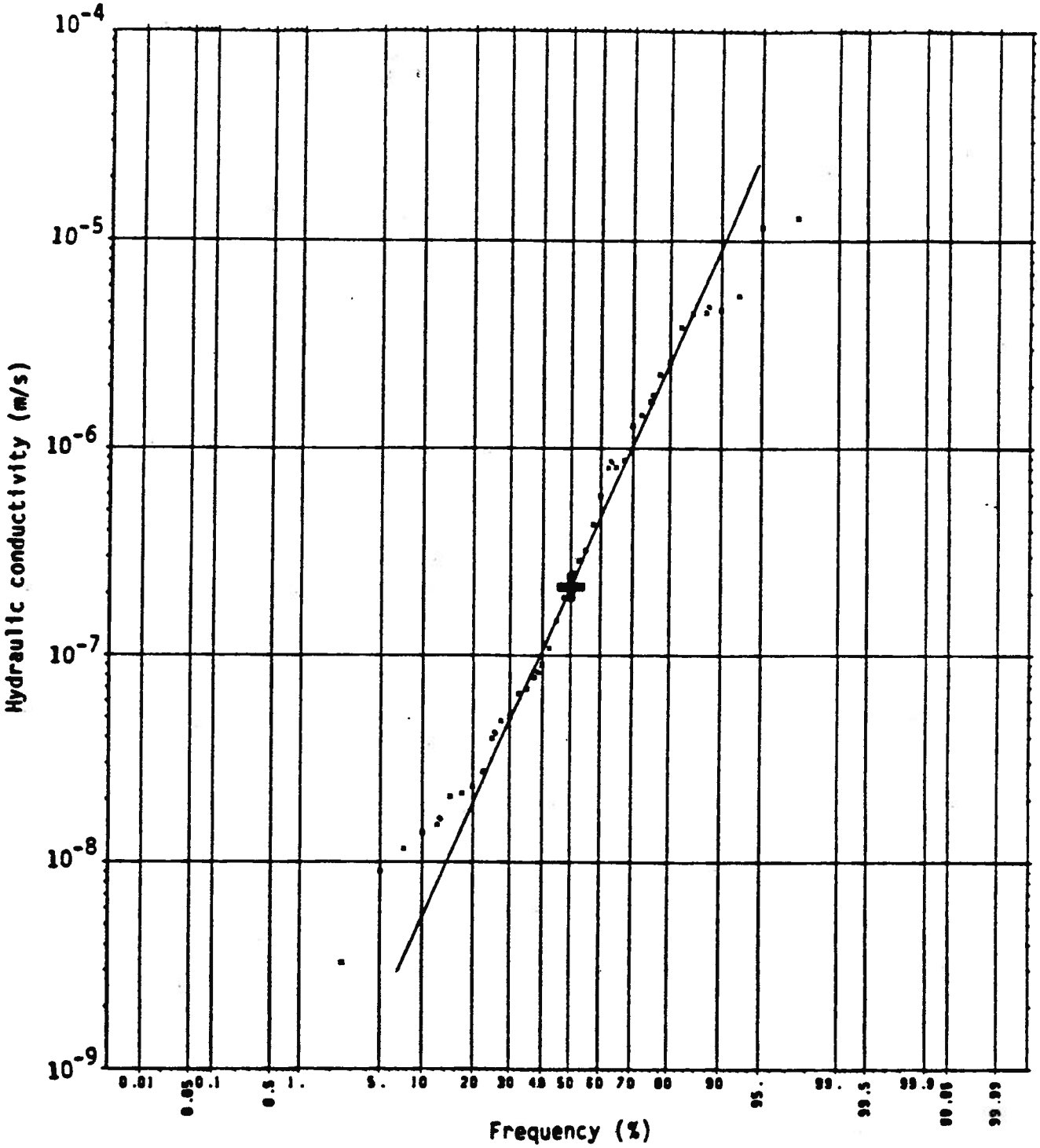

Figure B20 Log-normal cumulative frequency plot for hydraulic conductivity as derived from drillstem tests, Camrose Tongue aquifer, Cold Lake study area

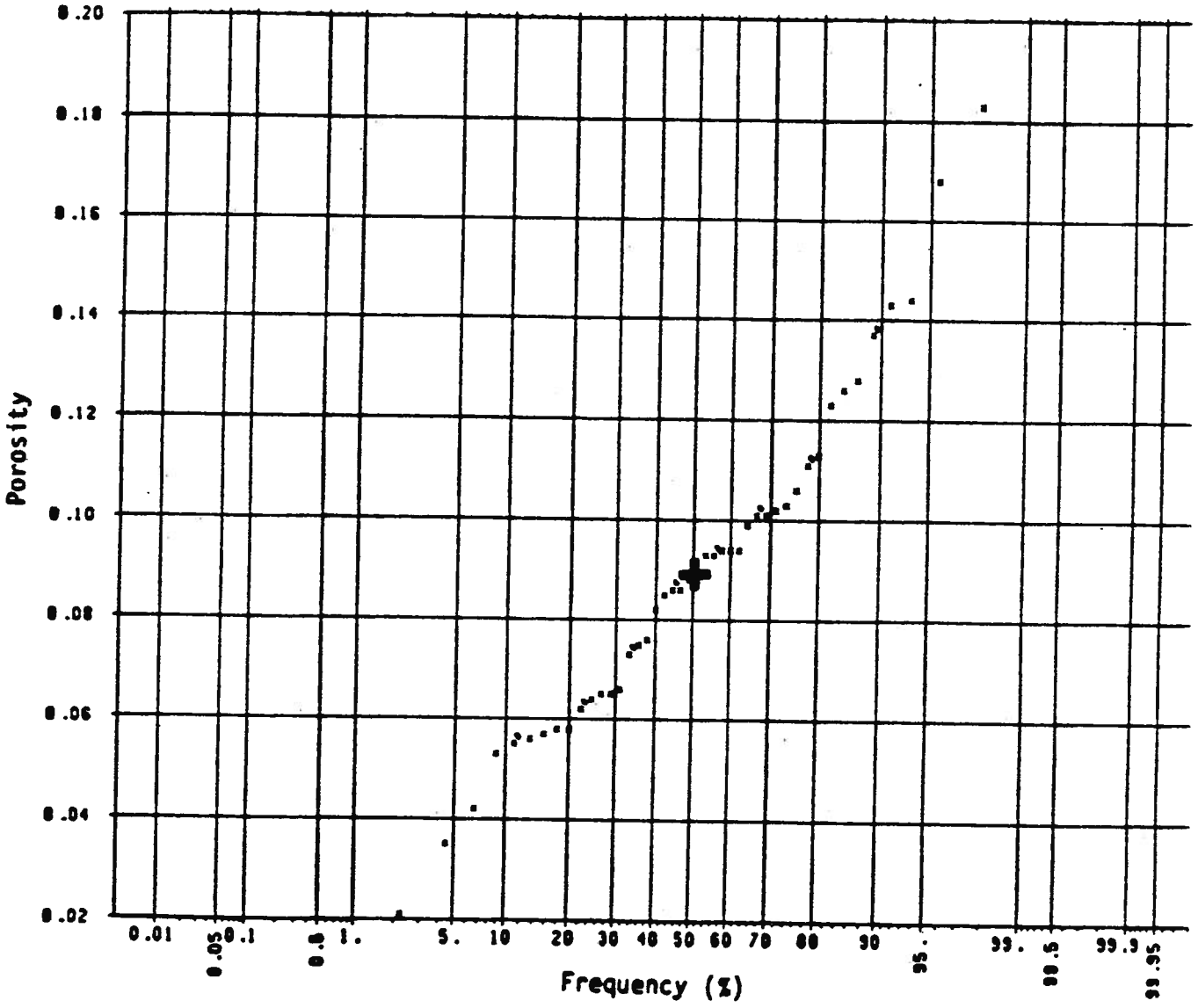

Figure B21 Normal cumulative frequency plot for porosity as derived from core analyses, Camrose Tongue aquifer, Cold Lake study area

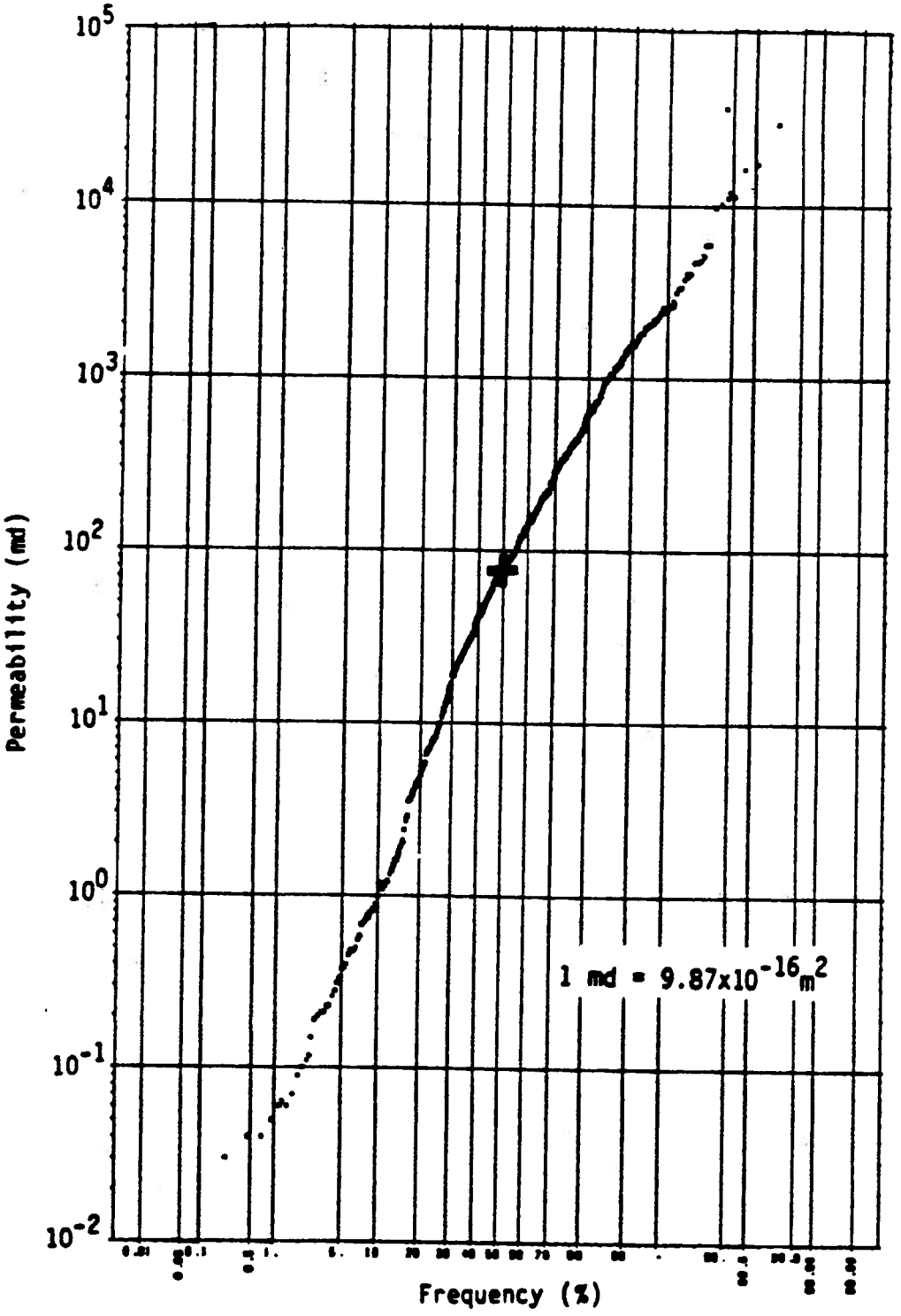

Figure B22 Log-normal cumulative frequency plot for maximum horizontal permeability as derived from core analyses, Grosmont aquifer, Cold Lake study area

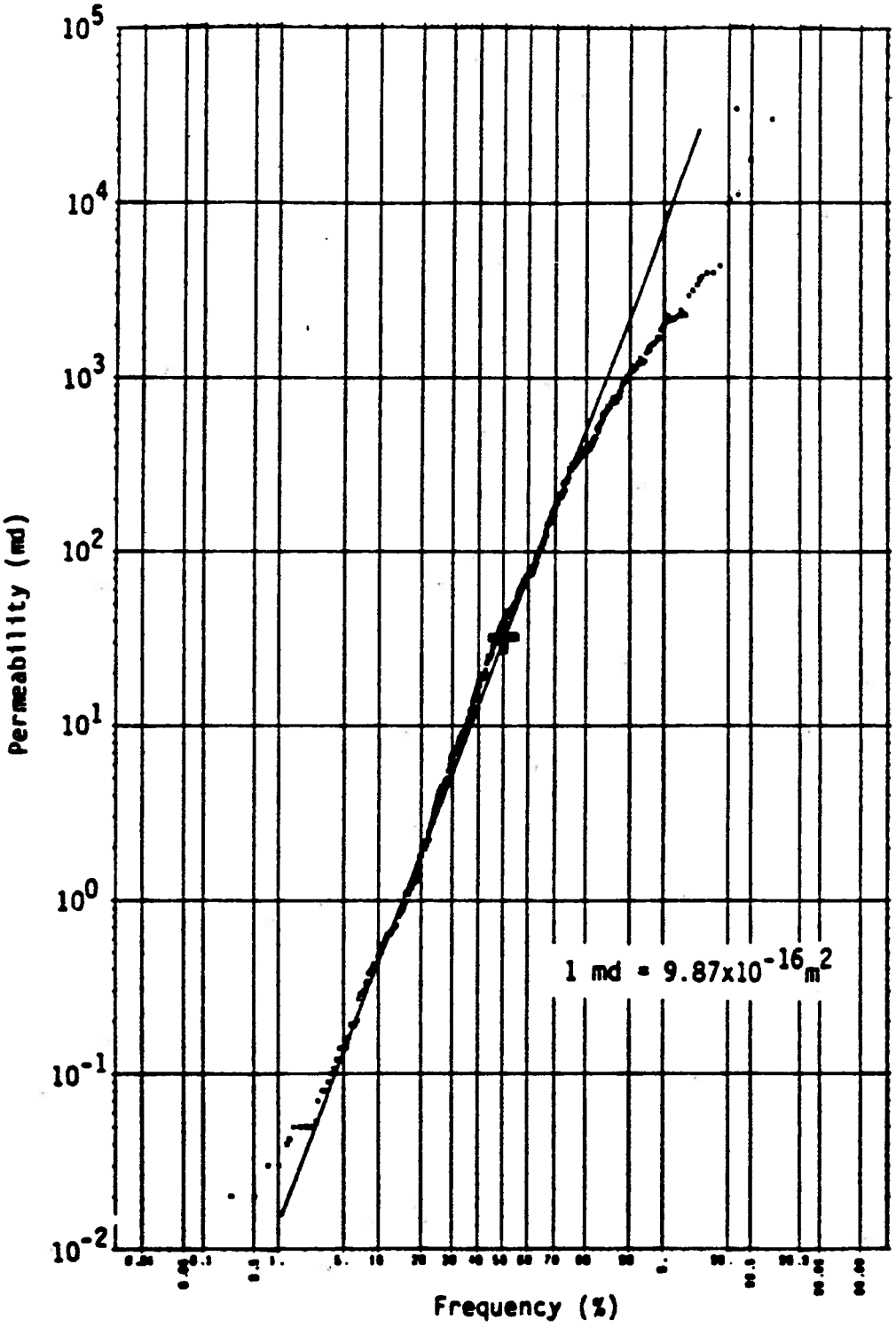

Figure B23 Log-normal cumulative frequency plot for horizontal permeability at 90° with the maximum horizontal as derived from core analyses, Grosmont aquifer, Cold Lake study area

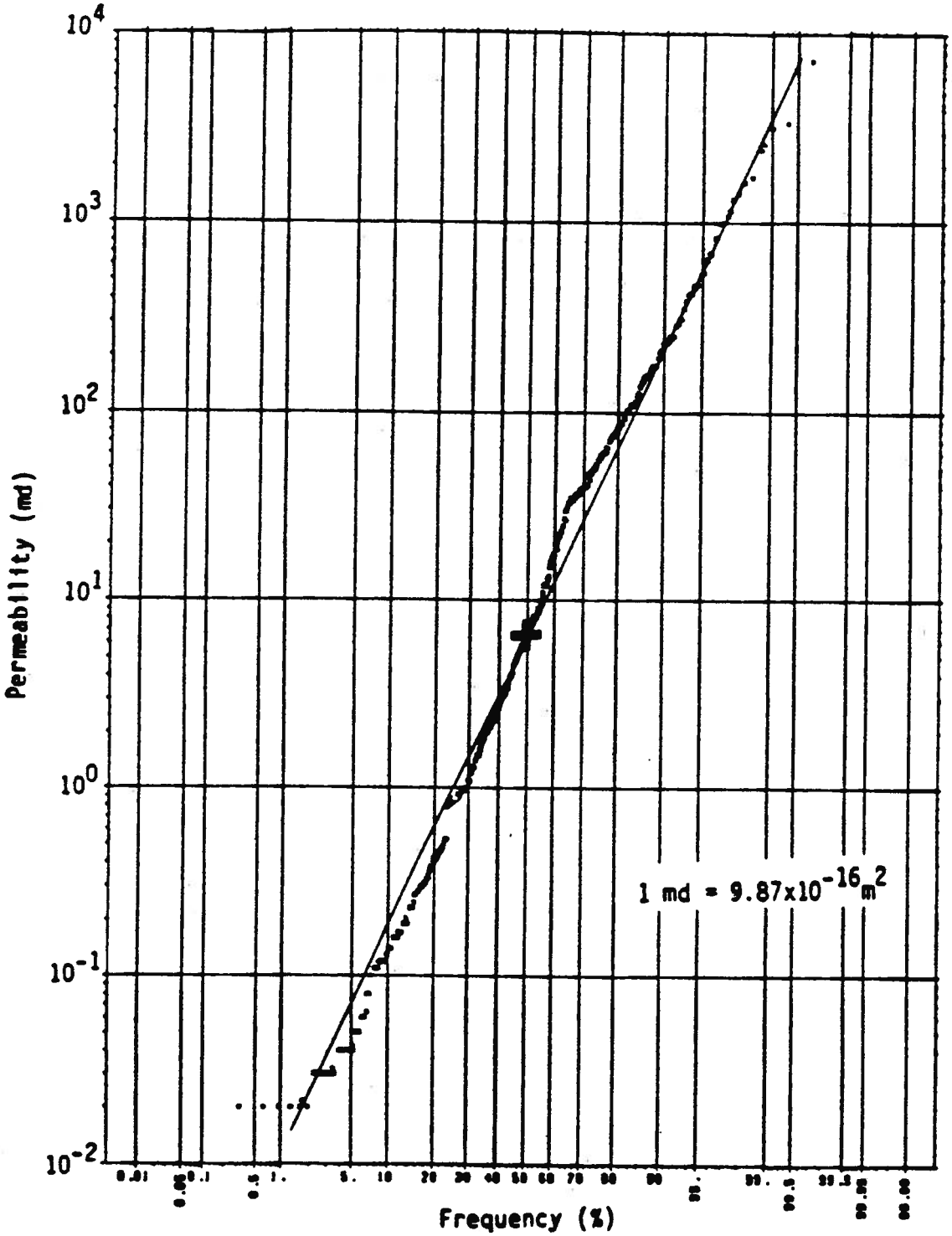

Figure B24 Log-normal cumulative frequency plot for vertical permeability as derived from core analyses, Grosmont aquifer, Cold Lake study area

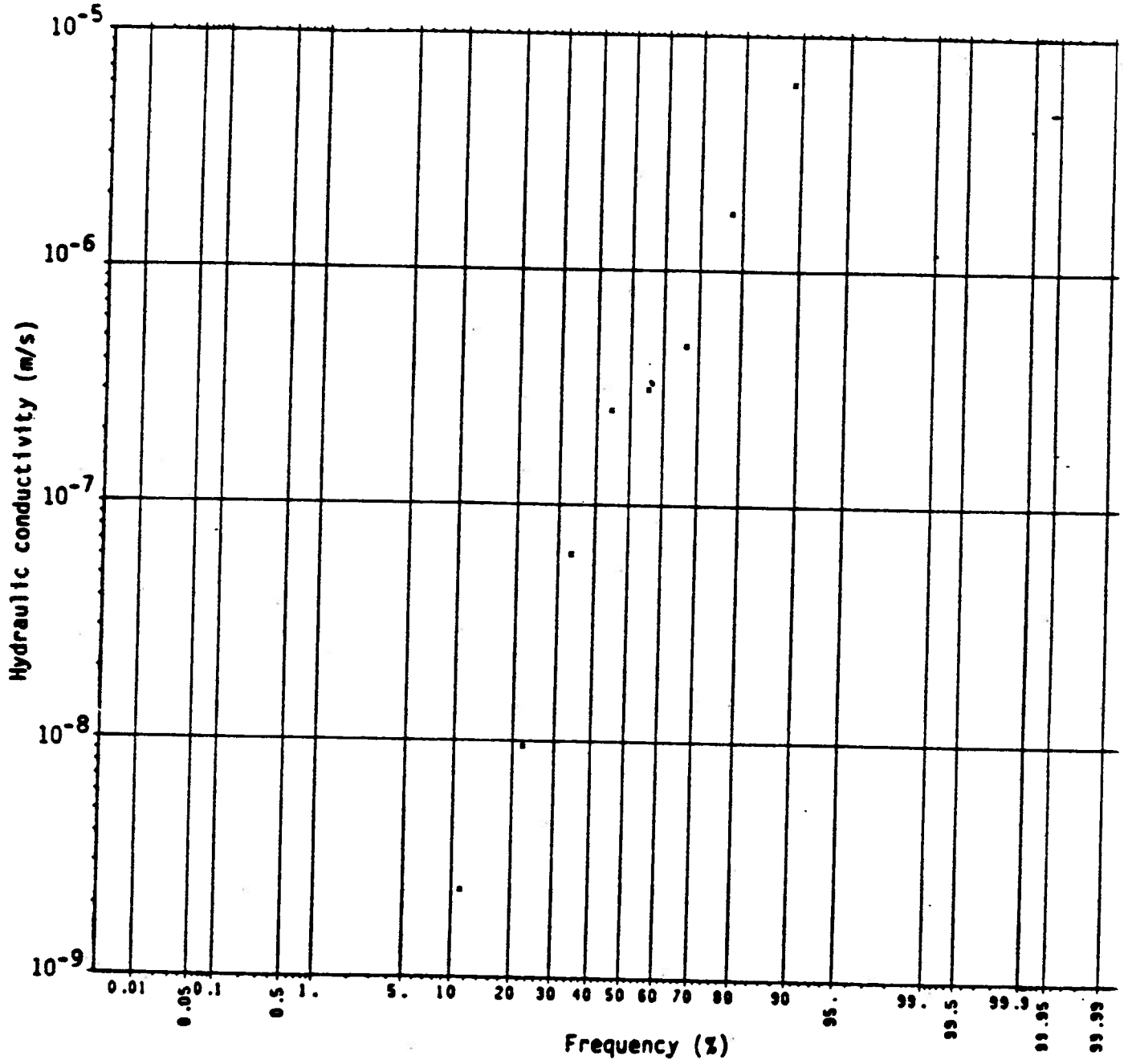

Figure B25 Log-normal cumulative frequency plot for hydraulic conductivity as derived from drillstem tests, Grosmont aquifer, Cold Lake study area

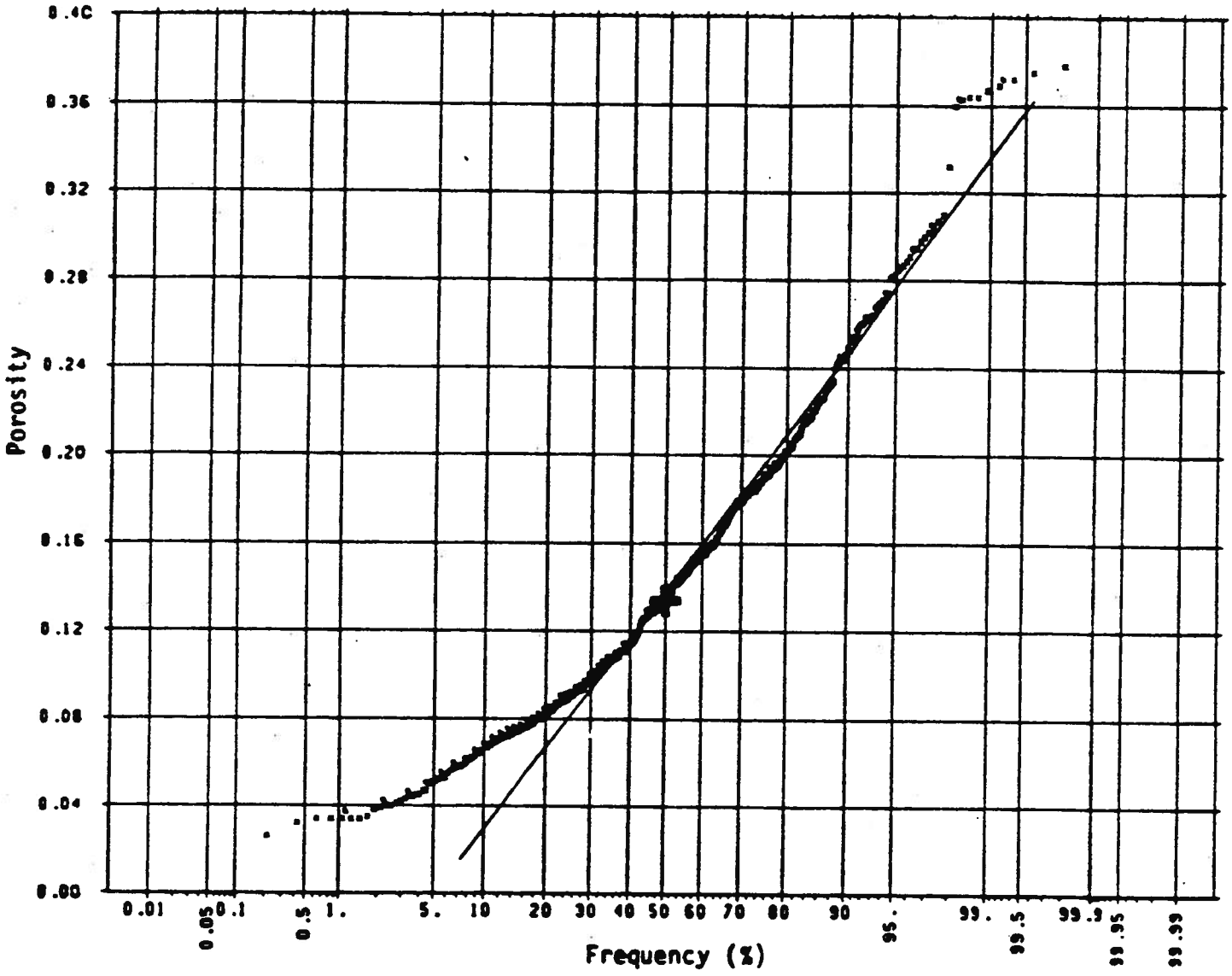

Figure B26 Normal cumulative frequency plot for porosity as derived from core analyses, Grosmont aquifer, Cold Lake study area

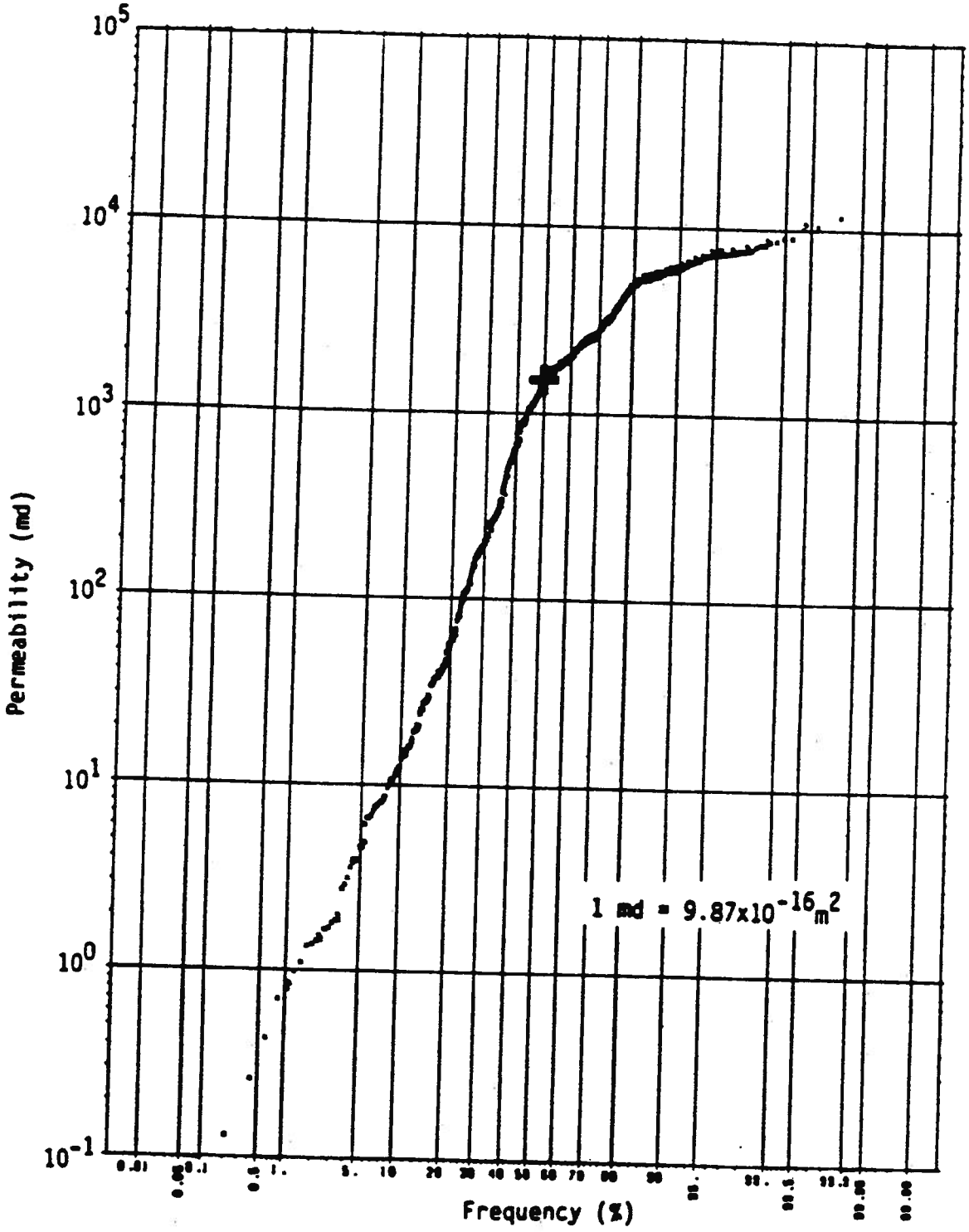

Figure B27 Log-normal cumulative frequency plot for maximum horizontal permeability as derived from core analyses, McMurray aquifer, Cold Lake study area

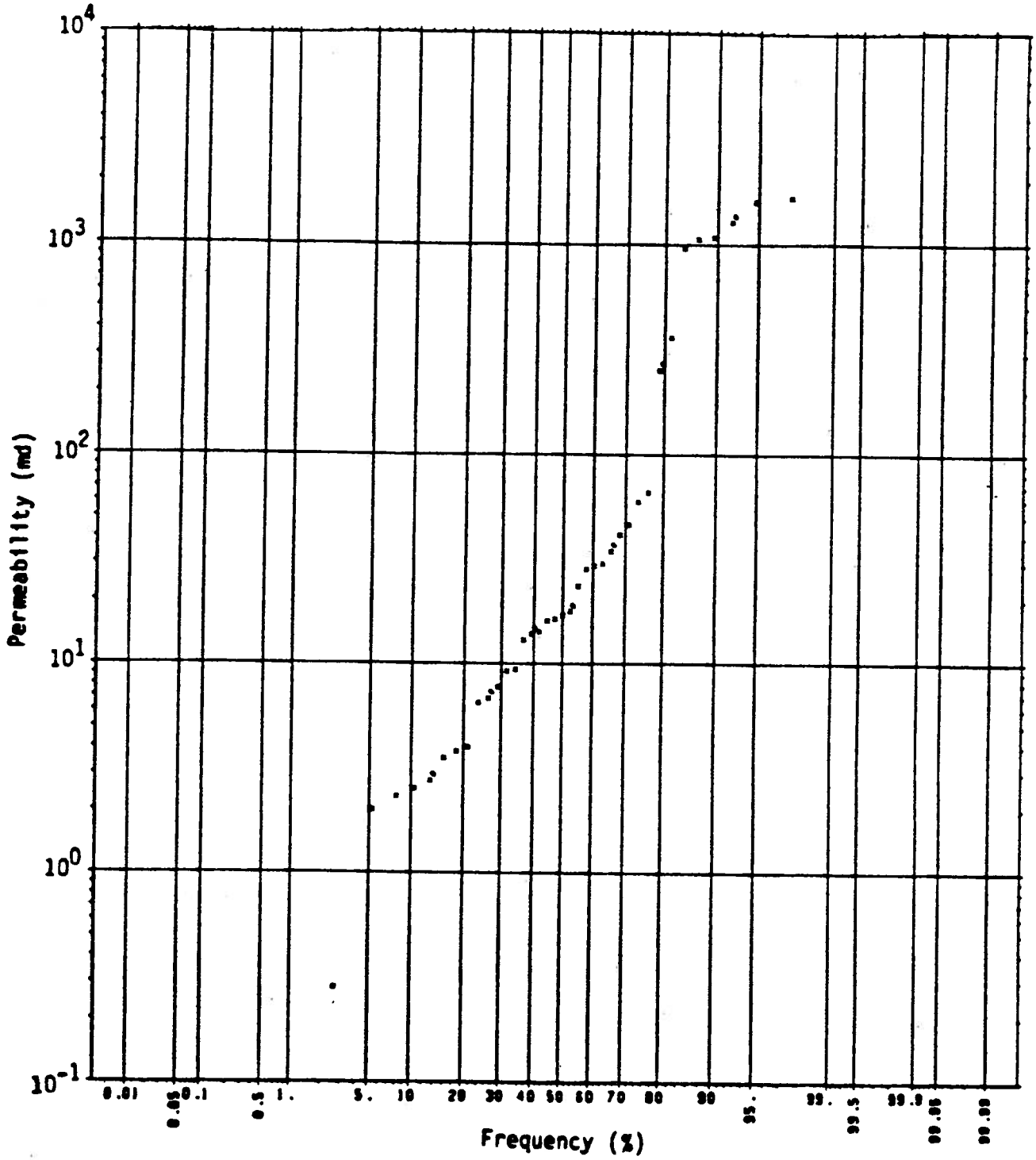

Figure B28 Log-normal cumulative frequency plot for maximum horizontal permeability at 90° with the horizontal as derived from core analyses, McMurray aquifer, Cold Lake study area

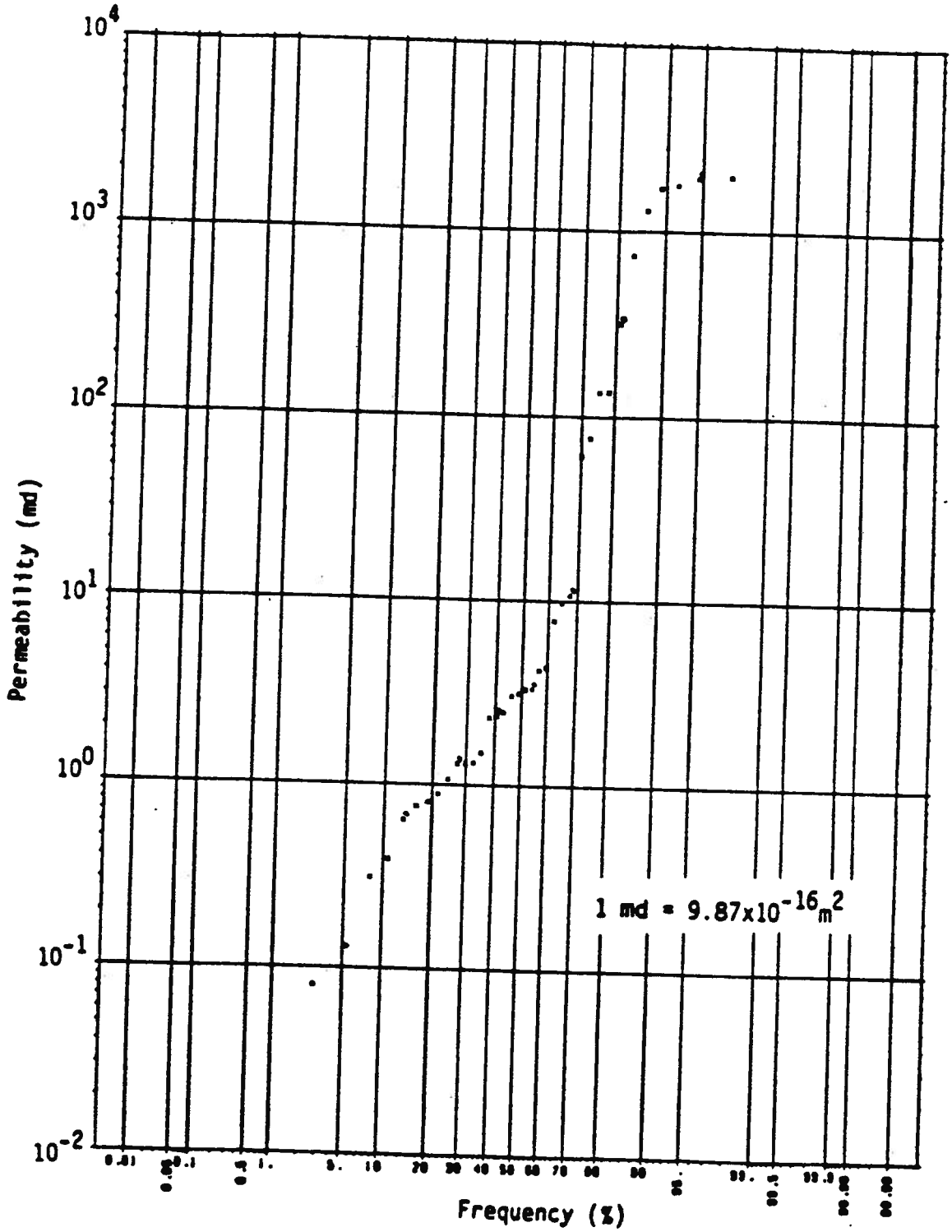

Figure B29 Log-normal cumulative frequency plot for vertical permeability as derived from core analyses, McMurray aquifer, Cold Lake study area

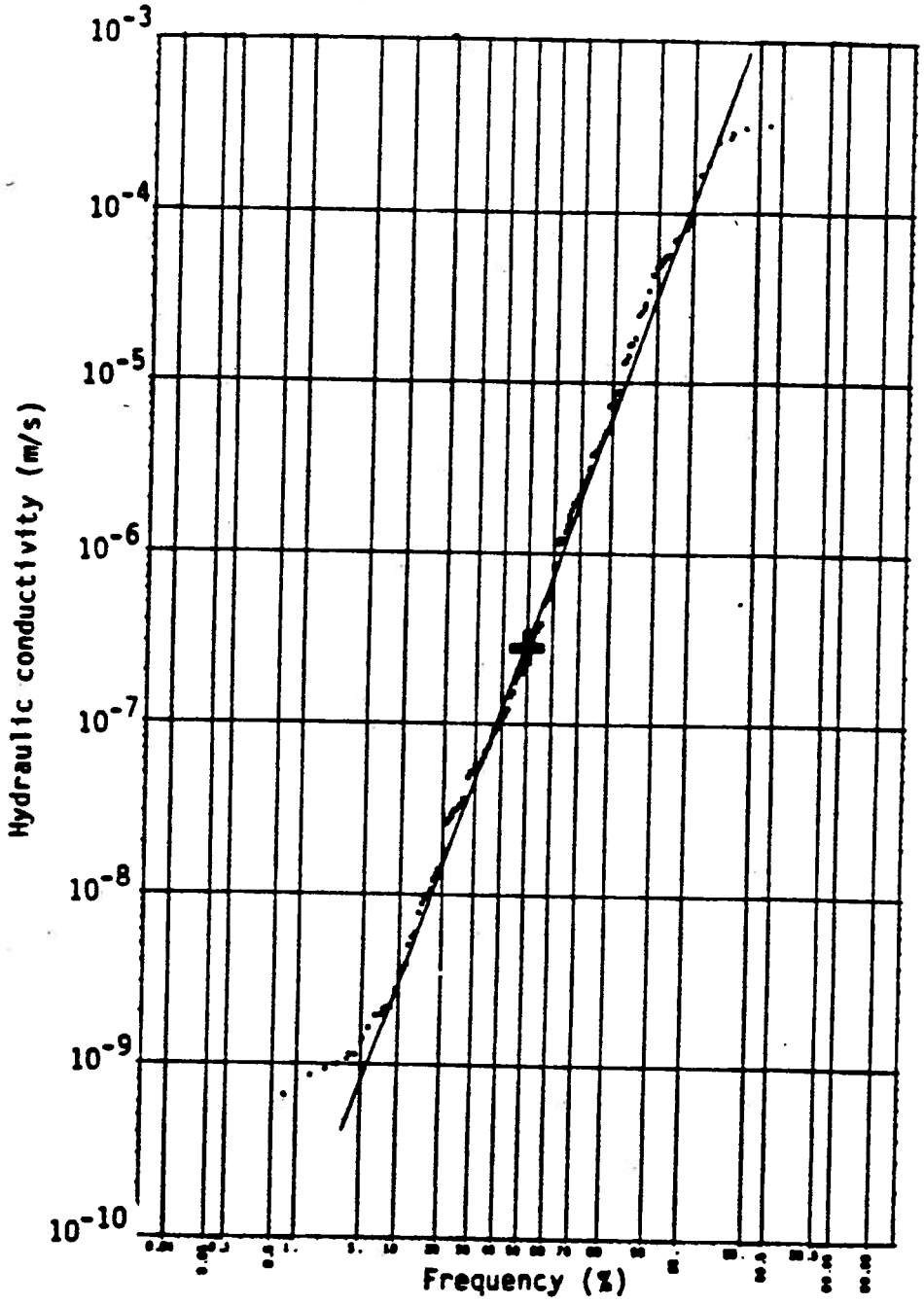

Figure B30 Log-normal cumulative frequency plot for hydraulic conductivity as derived from drillstem tests, McMurray aquifer, Cold Lake study area

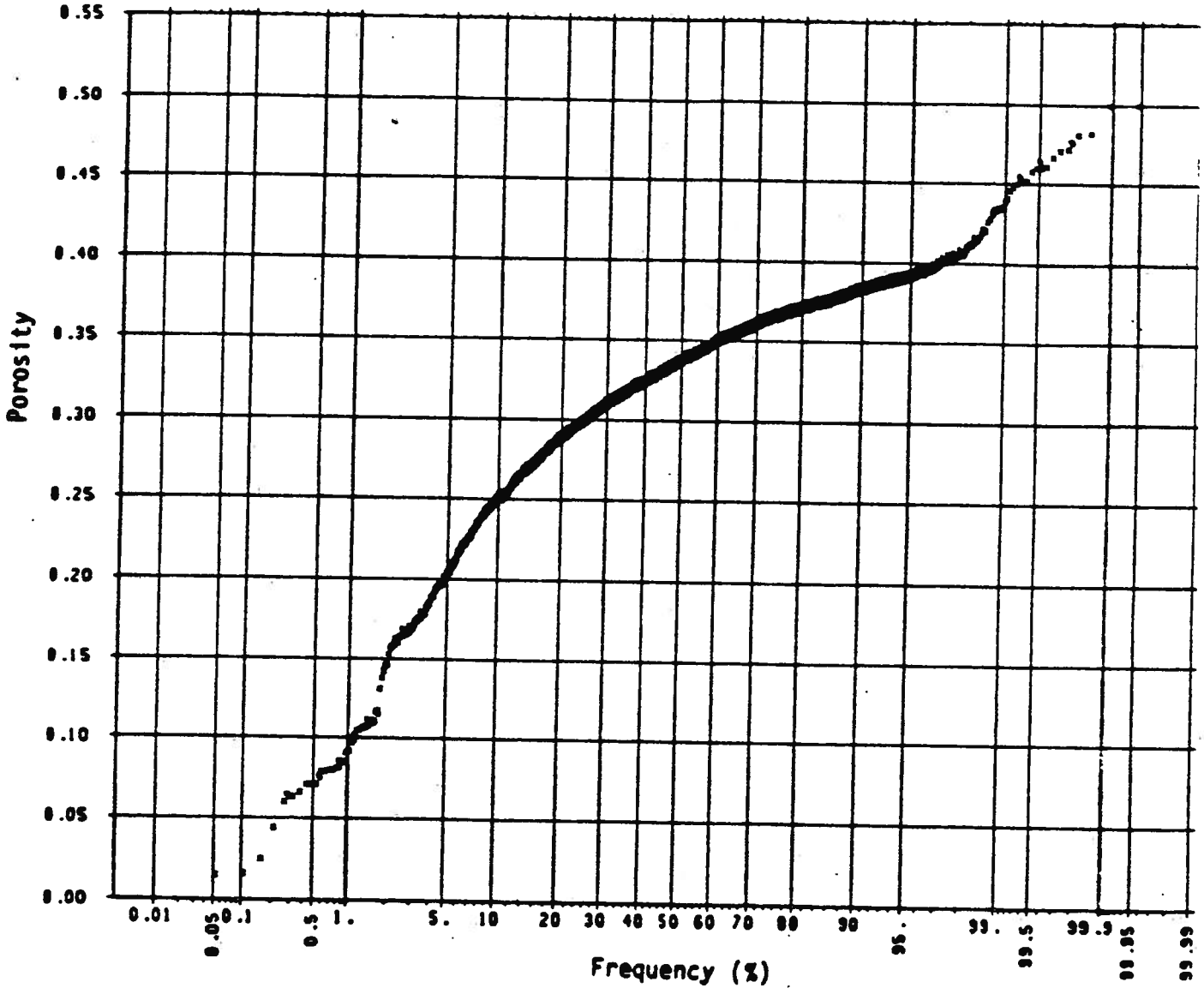

Figure B31 Normal cumulative frequency plot for porosity as derived from core analyses, McMurray aquifer, Cold Lake study area

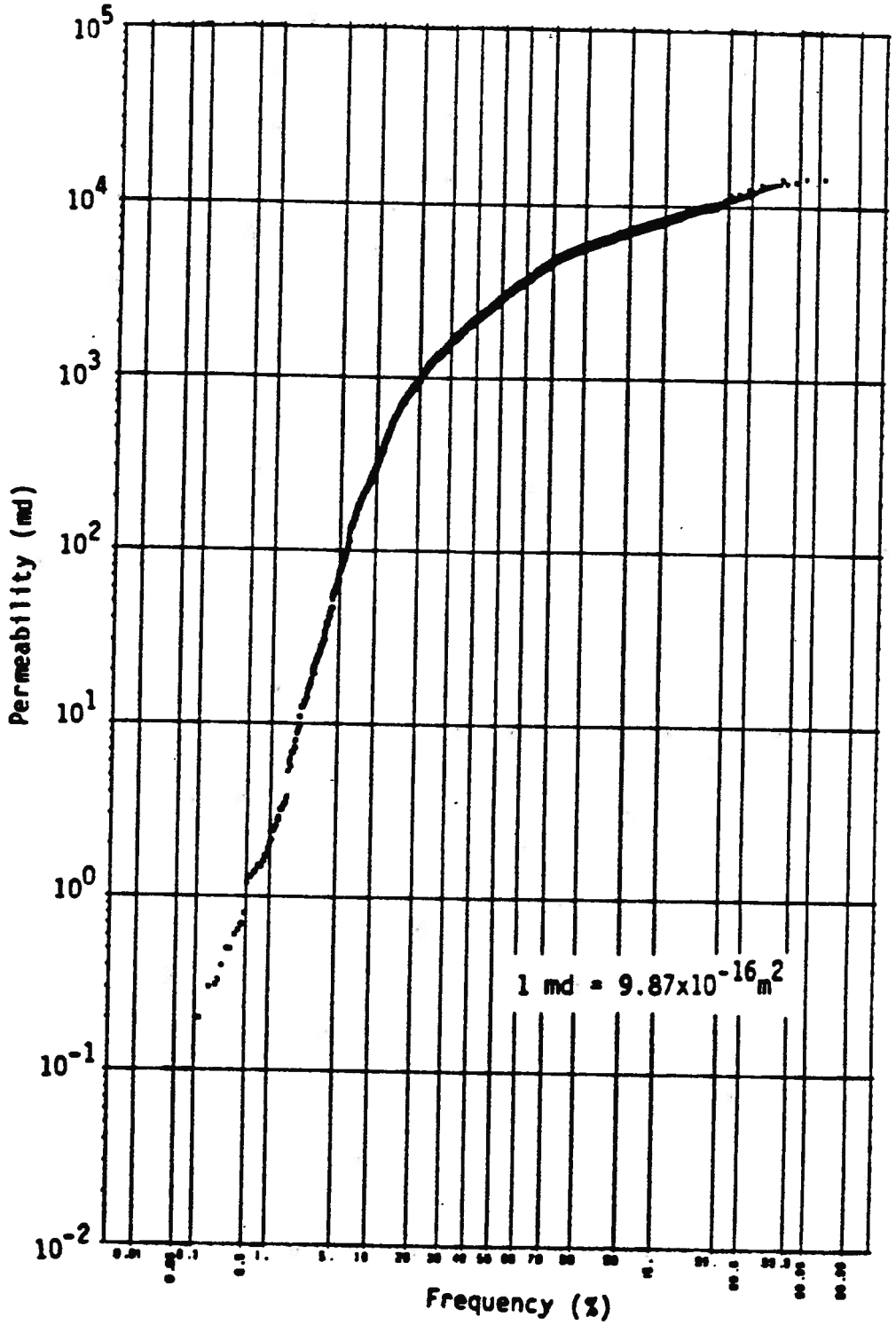

Figure B32 Log-normal cumulative frequency plot for maximum horizontal permeability as derived from core analyses, Clearwater aquifer, Cold Lake study area

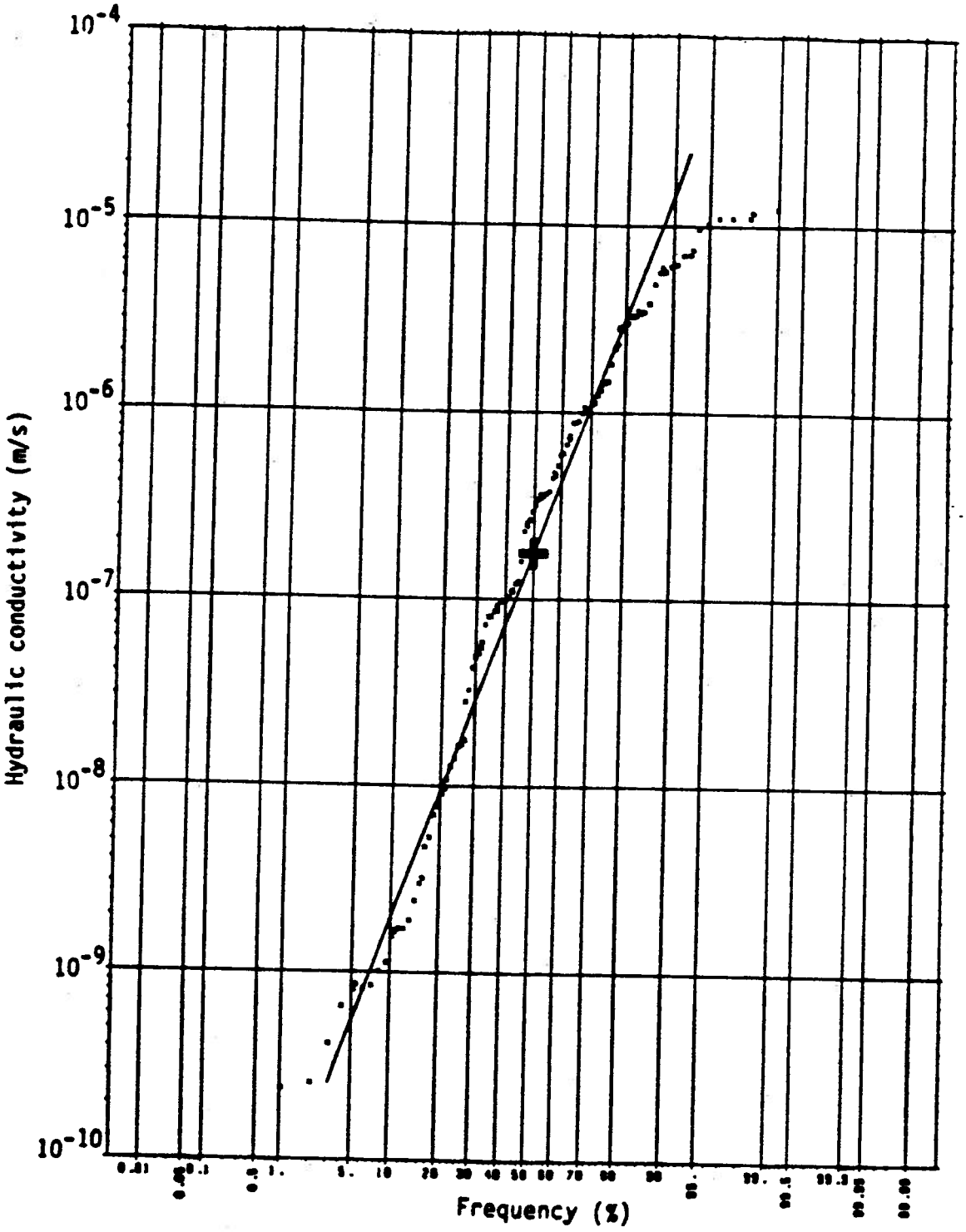

Figure B33 Log-normal cumulative frequency plot for hydraulic conductivity as derived from drillstem tests, Clearwater aquifer, Cold Lake study area

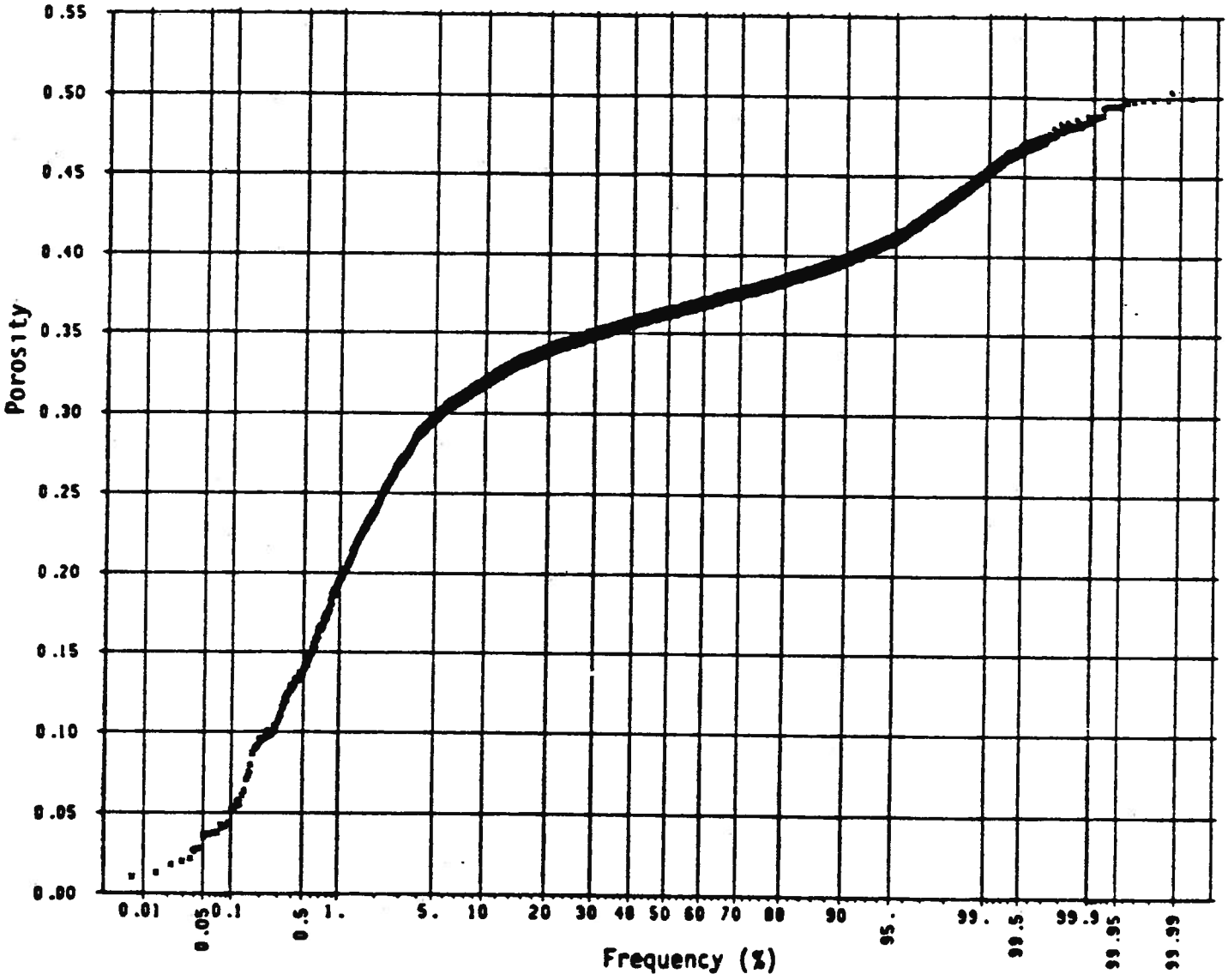

Figure B34 Normal cumulative frequency plot for porosity as derived from core analyses, Clearwater aquifer, Cold Lake study area

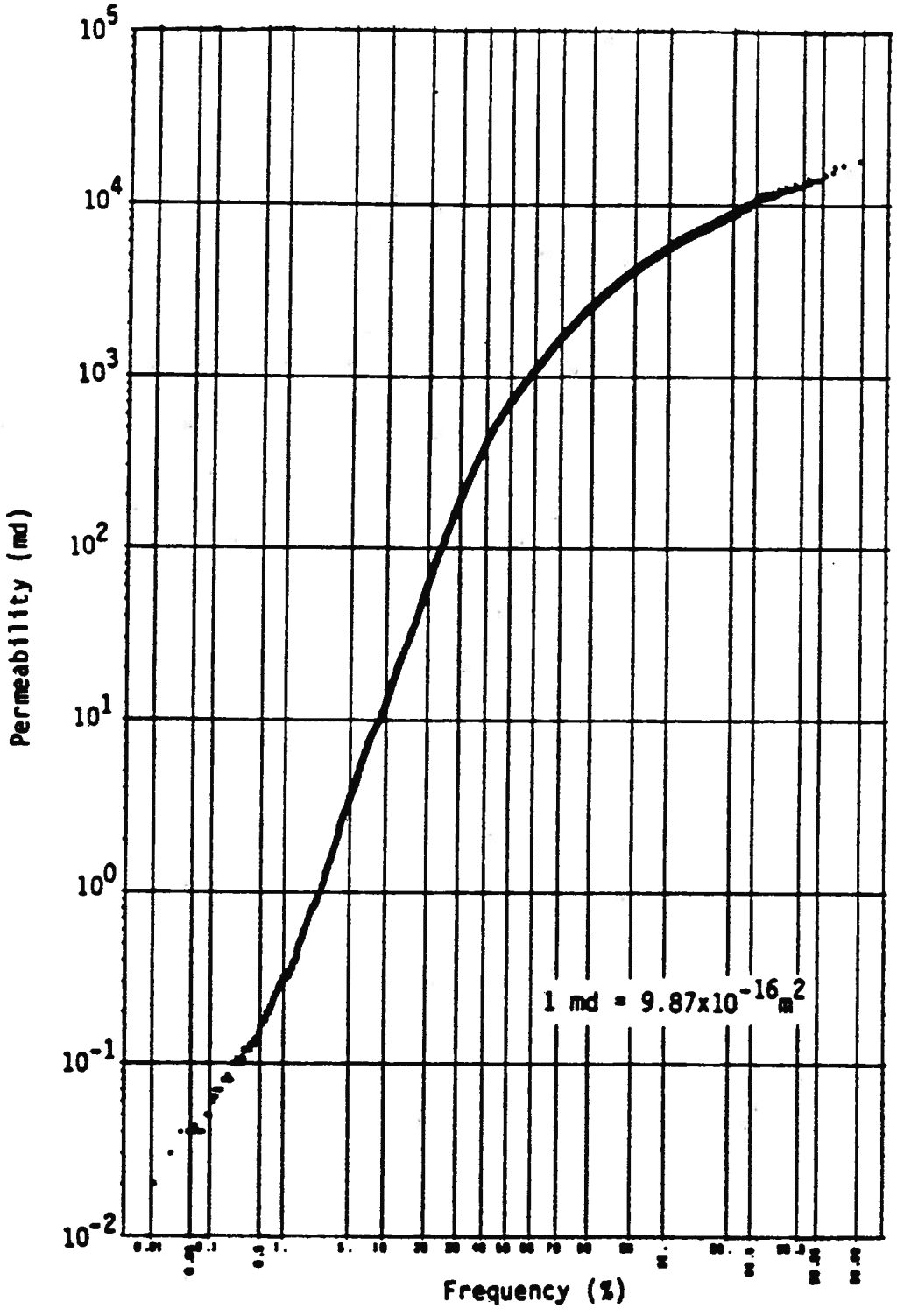

Figure B35 Log-normal cumulative frequency plot for maximum horizontal permeability as derived from core analyses, Mannville aquifer, Cold Lake study area

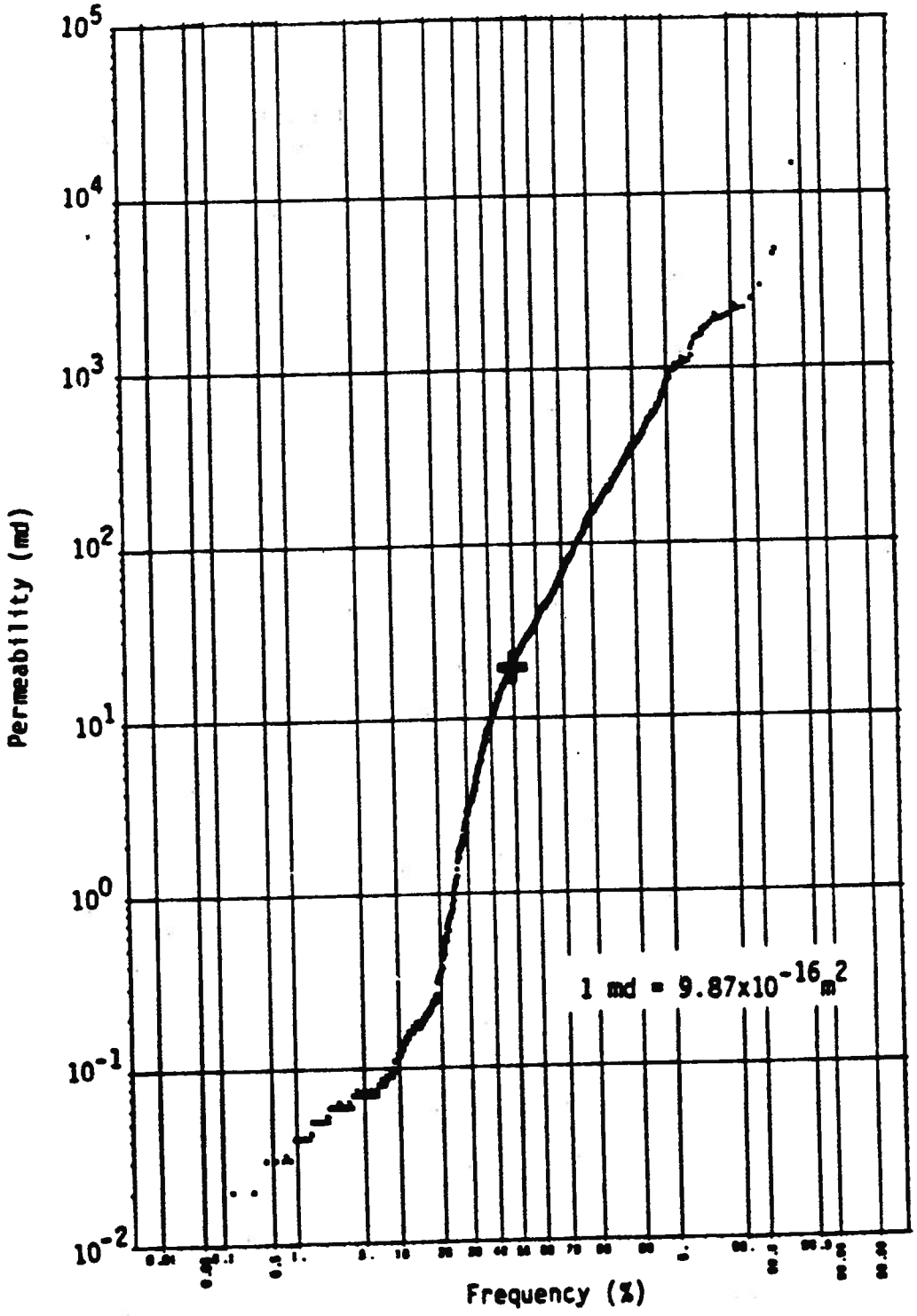

Figure B36 Log-normal cumulative frequency plot for horizontal permeability at 90° with the maximum horizontal as derived from core analyses, Mannville aquifer, Cold Lake study area

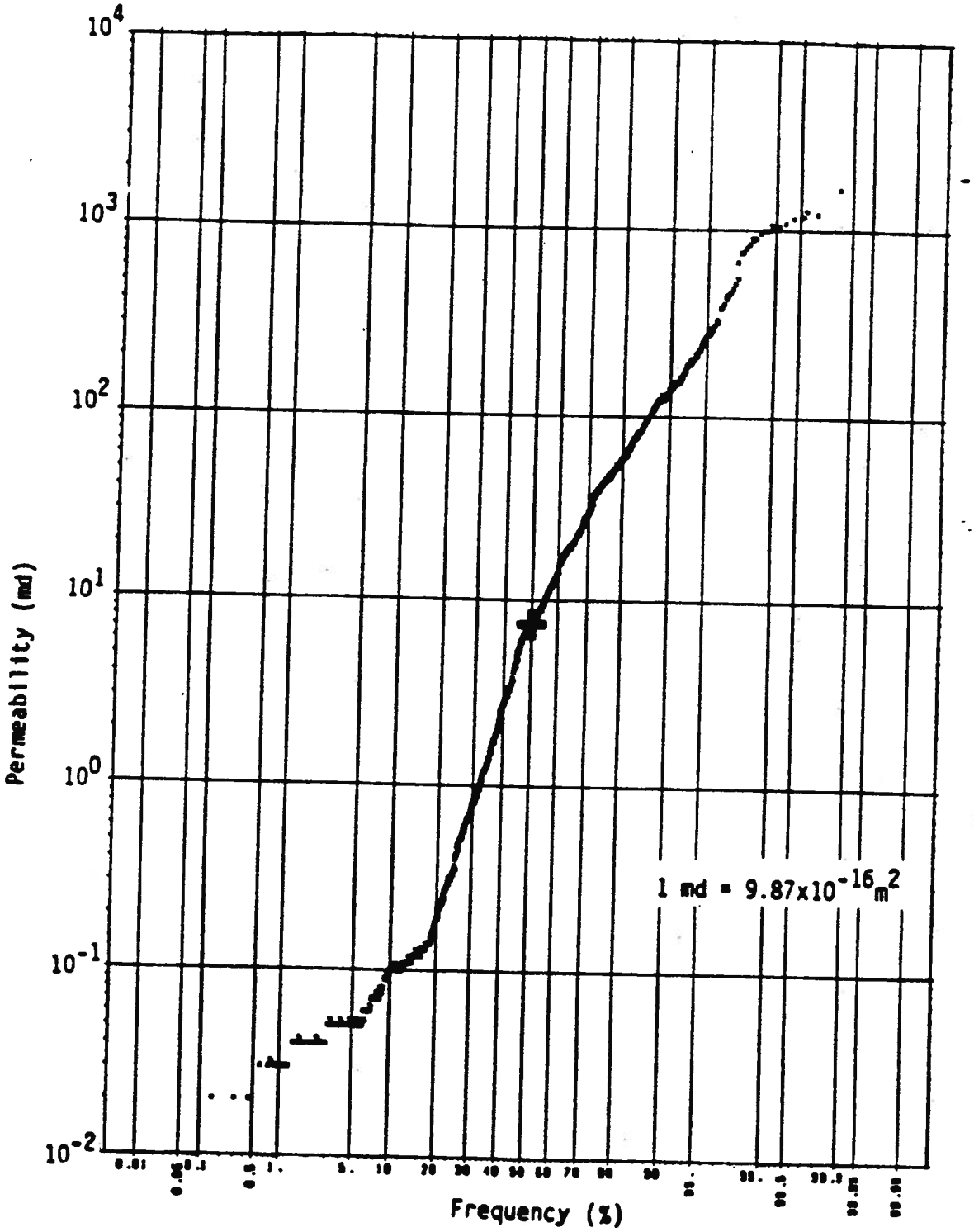

Figure B37 Log-normal cumulative frequency plot for vertical permeability as derived from core analyses, Mannville aquifer, Cold Lake study area

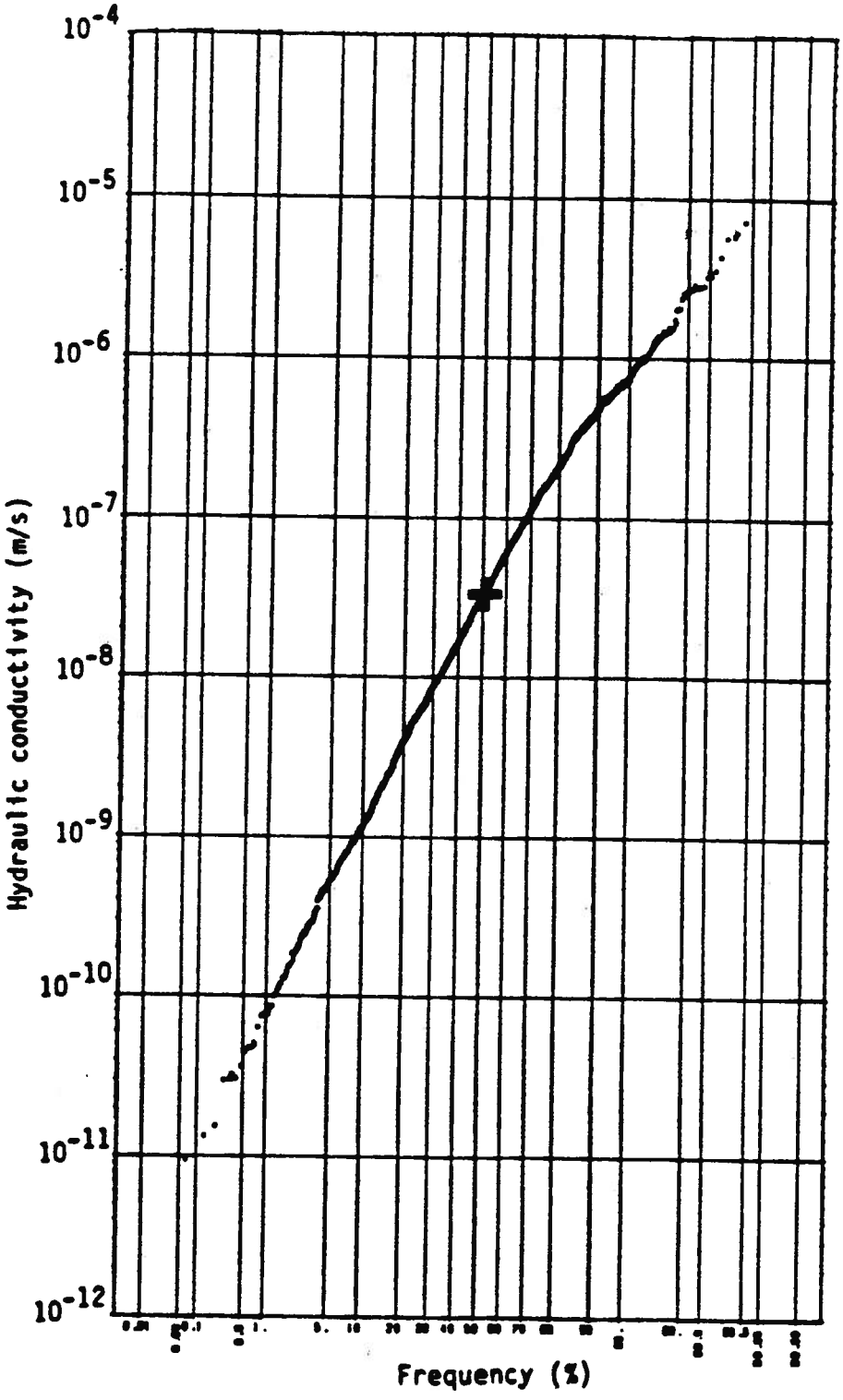

Figure B38 Log-normal cumulative frequency plot for hydraulic conductivity as derived from drillstem tests, Mannville aquifer, Cold Lake study area

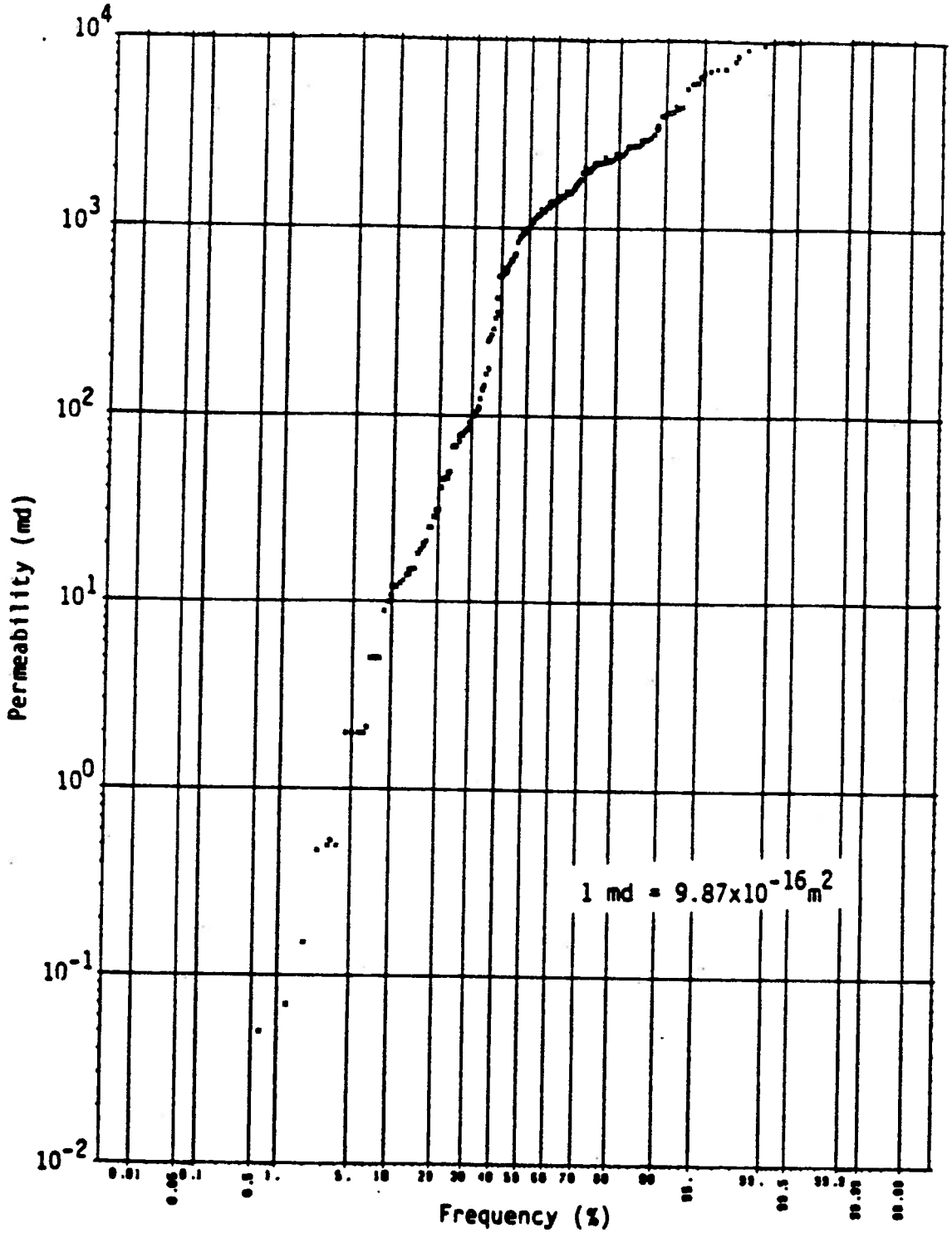

Figure B39 Log-normal cumulative frequency plot for maximum horizontal permeability as derived from core analyses, Viking aquifer, Cold Lake study area

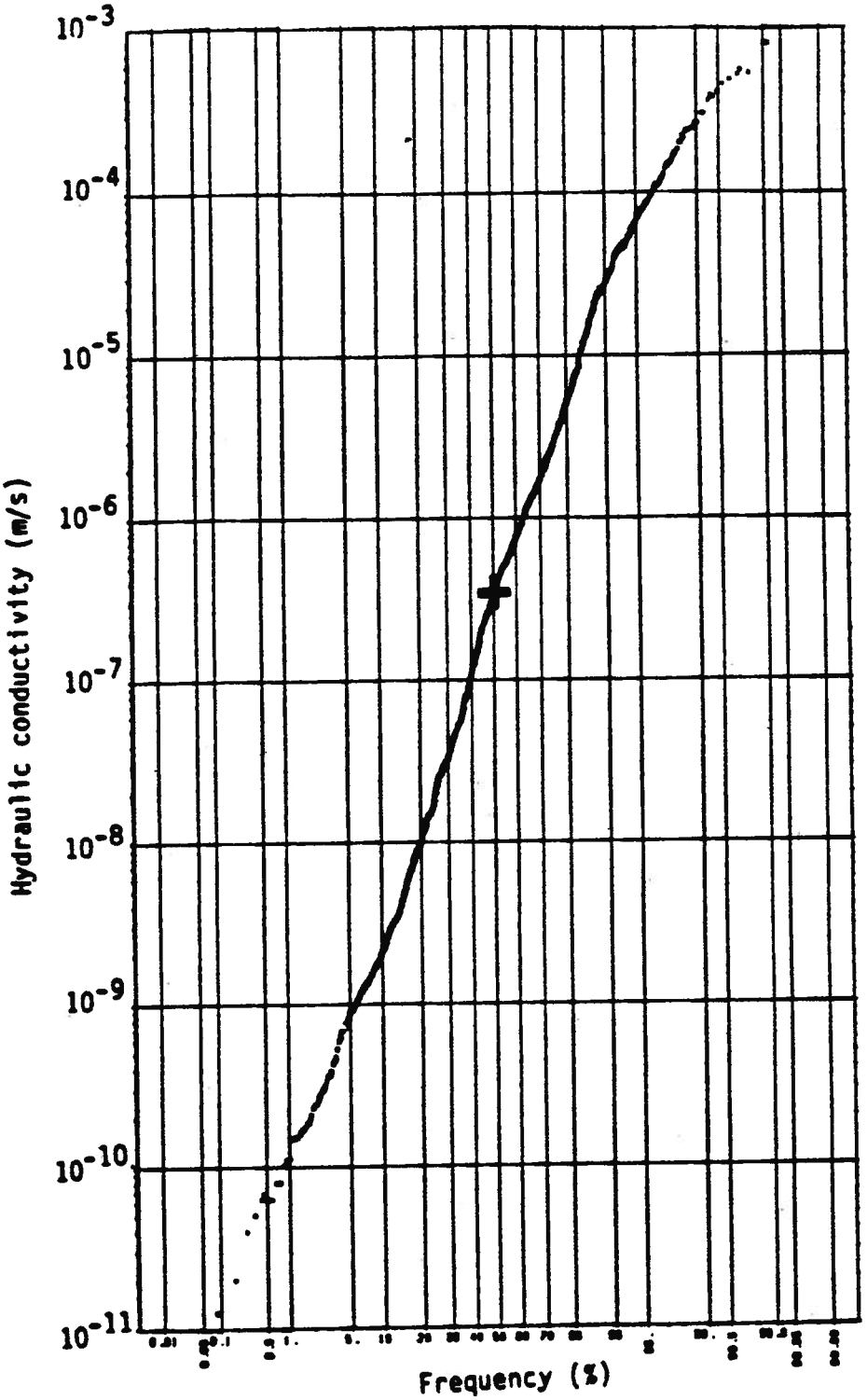

Figure B40 Log-normal cumulative frequency plot for hydraulic conductivity as derived from drillstem tests, Viking aquifer, Cold Lake study area

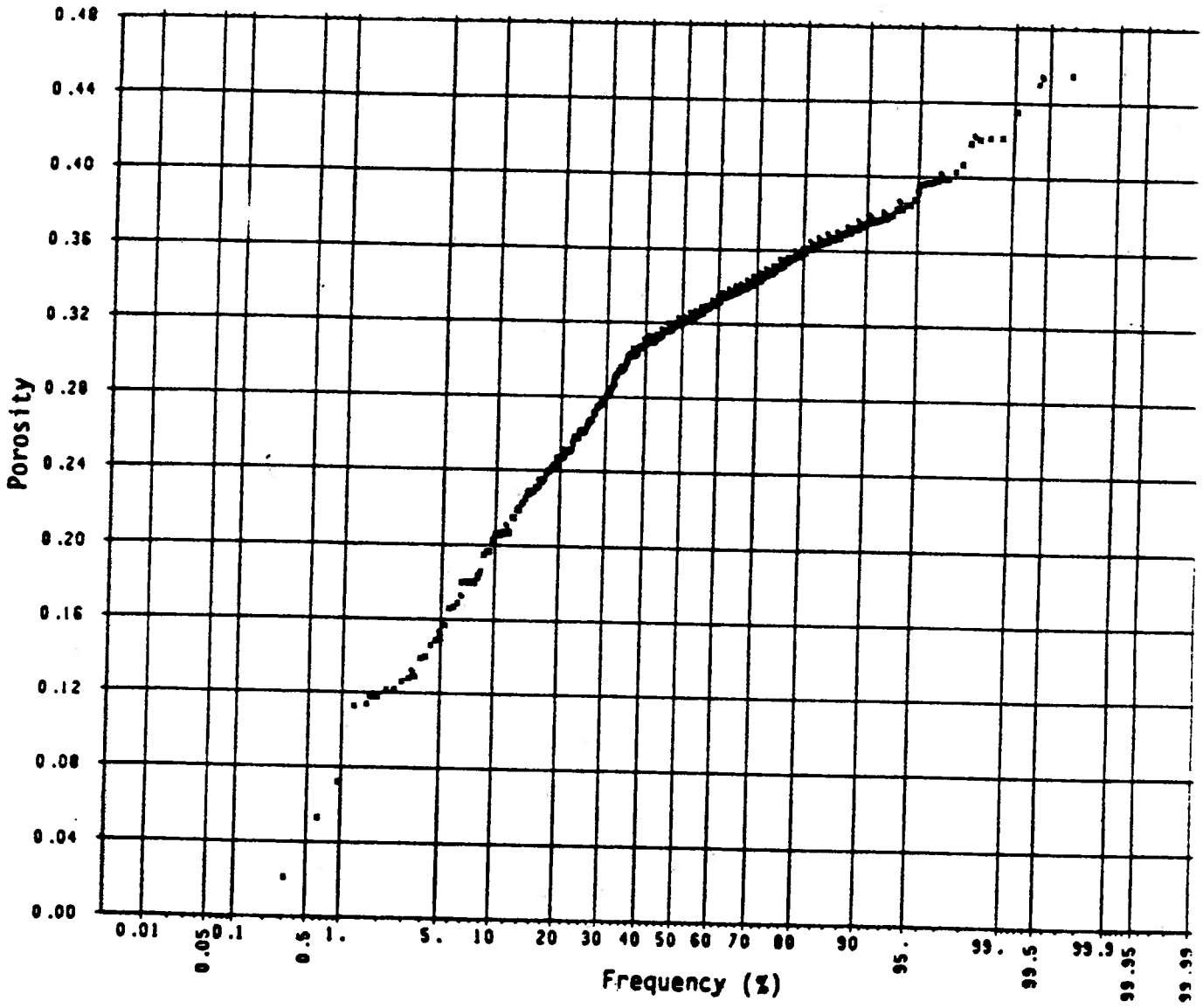

Figure B41 Normal cumulative frequency plot for porosity as derived from core analyses, Viking aquifer, Cold Lake study area